

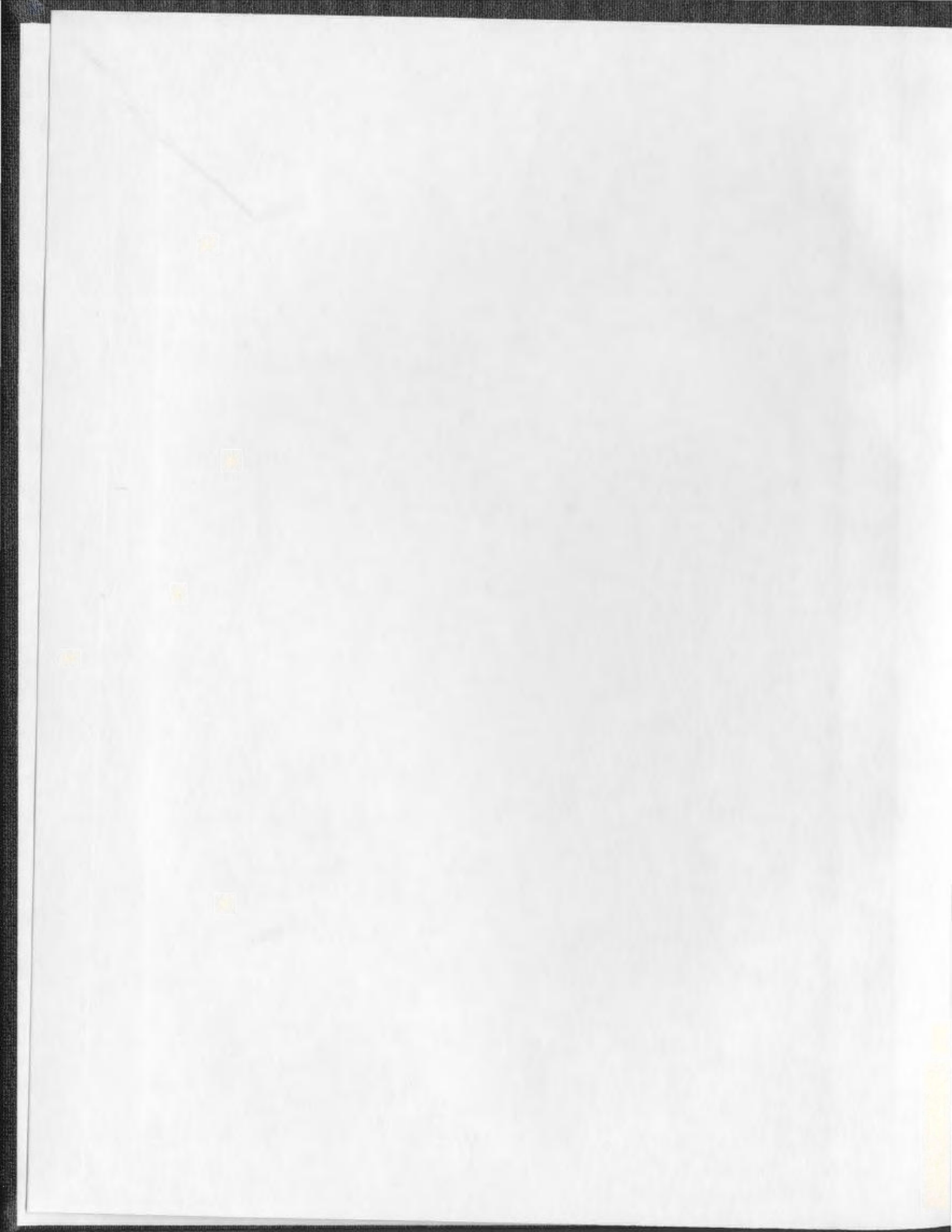
ECLOGITE FACIES METAMORPHISM OF MAFIC AND
ULTRAMAFIC ROCKS IN THE TSHENUKUTISH
TERRANE, MANICOUAGAN IMBRICATE ZONE,
EASTERN GRENVILLE PROVINCE

CENTRE FOR NEWFOUNDLAND STUDIES

**TOTAL OF 10 PAGES ONLY
MAY BE XEROXED**

(Without Author's Permission)

RICHARD ALEXANDER COX



INFORMATION TO USERS

This manuscript has been reproduced from the microfilm master. UMI films the text directly from the original or copy submitted. Thus, some thesis and dissertation copies are in typewriter face, while others may be from any type of computer printer.

The quality of this reproduction is dependent upon the quality of the copy submitted. Broken or indistinct print, colored or poor quality illustrations and photographs, print bleedthrough, substandard margins, and improper alignment can adversely affect reproduction.

In the unlikely event that the author did not send UMI a complete manuscript and there are missing pages, these will be noted. Also, if unauthorized copyright material had to be removed, a note will indicate the deletion.

Oversize materials (e.g., maps, drawings, charts) are reproduced by sectioning the original, beginning at the upper left-hand corner and continuing from left to right in equal sections with small overlaps.

Photographs included in the original manuscript have been reproduced xerographically in this copy. Higher quality 6" x 9" black and white photographic prints are available for any photographs or illustrations appearing in this copy for an additional charge. Contact UMI directly to order.

**Bell & Howell Information and Learning
300 North Zeeb Road, Ann Arbor, MI 48106-1346 USA
800-521-0600**

UMI[®]



National Library
of Canada

Acquisitions and
Bibliographic Services

395 Wellington Street
Ottawa ON K1A 0N4
Canada

Bibliothèque nationale
du Canada

Acquisitions et
services bibliographiques

395, rue Wellington
Ottawa ON K1A 0N4
Canada

Your file *Votre référence*

Our file *Notre référence*

The author has granted a non-exclusive licence allowing the National Library of Canada to reproduce, loan, distribute or sell copies of this thesis in microform, paper or electronic formats.

The author retains ownership of the copyright in this thesis. Neither the thesis nor substantial extracts from it may be printed or otherwise reproduced without the author's permission.

L'auteur a accordé une licence non exclusive permettant à la Bibliothèque nationale du Canada de reproduire, prêter, distribuer ou vendre des copies de cette thèse sous la forme de microfiche/film, de reproduction sur papier ou sur format électronique.

L'auteur conserve la propriété du droit d'auteur qui protège cette thèse. Ni la thèse ni des extraits substantiels de celle-ci ne doivent être imprimés ou autrement reproduits sans son autorisation.

0-612-54832-5

Canada

**Eclogite facies metamorphism of mafic and ultramafic rocks in the
Tshenukutish terrane, Manicouagan Imbricate Zone, eastern Grenville
Province.**

Richard Alexander Cox B.Sc. (Hons), M.Sc.

1999

Memorial University of Newfoundland

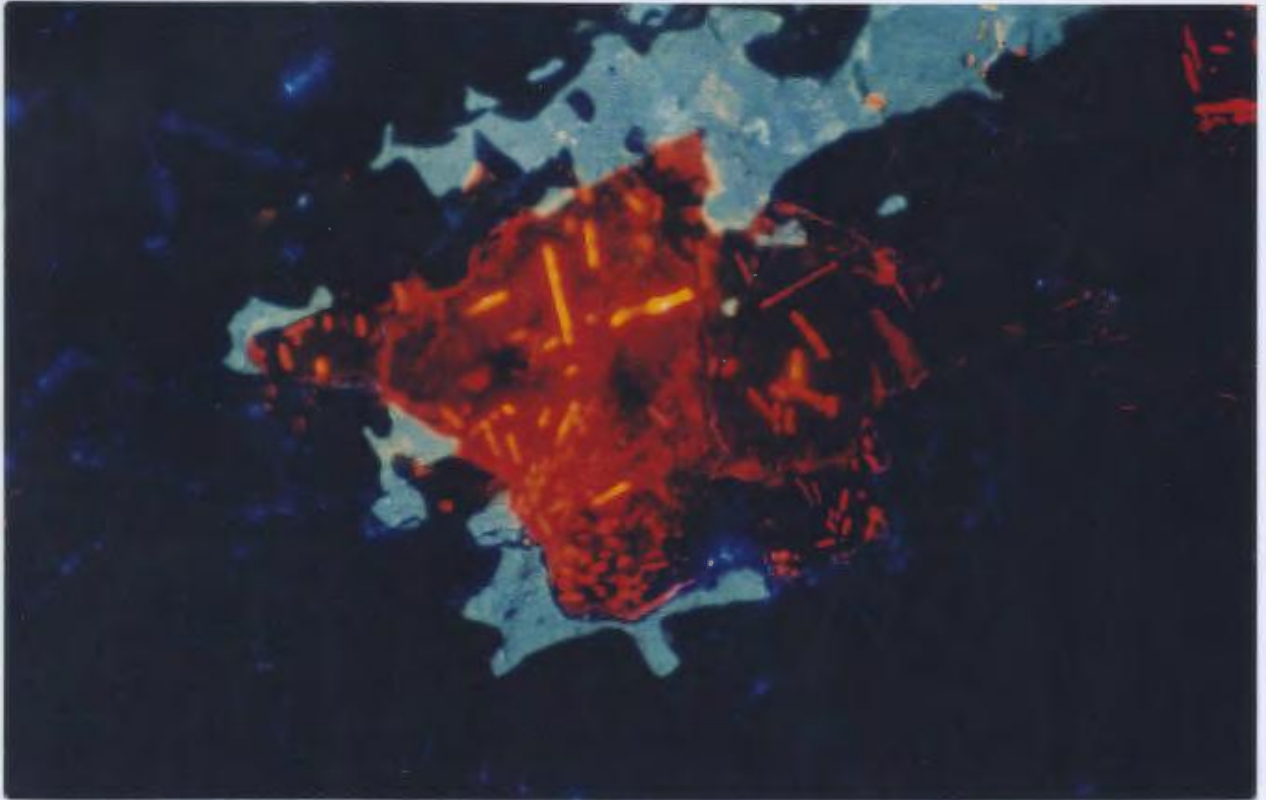
Department of Earth Sciences

A thesis submitted in partial fulfillment of the degree of Doctor of Philosophy.

Abstract

The Grenville Province of eastern Canada consists of a variety of lithotectonic units (terrane) which formed a large mountain chain along the margin of Laurentia at 1190-1000 Ma. The deepest crustal levels of the Grenvillian orogen are best exposed along a belt of high-PT terranes which form part of the parautochthonous belt. The best exposed section is the Manicouagan Imbricate Zone which contains rocks metamorphosed at conditions up to eclogite facies. The Tshenukutish terrane is the highest structural division of the Manicouagan Imbricate Zone and contains mafic and ultramafic rocks which characterise two distinct lithotectonic units. The structurally lower unit, the Baie du Nord segment, comprises granitic and dioritic country rocks intruded by Fe-Ti gabbro and anorthosite. The highest structural units in the Tshenukutish terrane belong to the Boundary zone, a complex series of tectonic slices, which include lenses of mafic and ultramafic rocks known as the Lac Espadon suite. Cumulate textures suggest that the Lac Espadon suite represents a layered, mafic and ultramafic complex. Geochemical analysis of the gabbroic end-members from both the Lac Espadon suite and the Baie du Nord segment indicate a within-plate tholeiite petrotectonic signature. REE-patterns of the gabbroic rocks and associated cumulates further suggest fractionation from a tholeiitic source and high-crustal level emplacement. U-Pb dating of igneous baddeleyite gives an age of 1170 \pm 5 Ma for emplacement of Fe-Ti gabbro in the Baie du Nord segment. In the Lac Espadon suite, U-Pb ages of igneous zircon and baddeleyite (ca. 1650-1630 Ma) suggest a Labradorian age of emplacement. The ages of zircon formed during anatexis (1046 \pm 3 Ma) and other metamorphic zircon ages (1042 \pm 22/-28 Ma, 1030 \pm 10/-7 Ma, 1030 \pm 12 Ma, 1012 \pm 12 Ma) show the timing of high-PT metamorphic overprint to be Grenvillian in age. The timing of retrogression and cooling is constrained by the ages of titanite (1006-997 Ma) and rutile (960-929 Ma). The Fe-Ti gabbroic rocks from the Baie du Nord segment display mineral assemblages which represent progressive stages of metamorphic transformation resulting in the formation of coronas, granoblastic pseudomorphs (transitional)

and eclogites. In addition, the transitional and eclogitic samples exhibit coronas developed locally around igneous xenocrysts. Maximum T-conditions recorded in the Baie du Nord segment are in the range 720-820 °C with recorded P-conditions reflecting increasing eclogitization (14 kbar in coronitic rocks and up to 17 kbar in eclogitic rocks). Estimates of peak PT-conditions recorded by massive corona-bearing rocks in the Lac Espadon suite are in the range 780-930 °C at 16-19 kbar. Reequilibration during the early stages of exhumation at high T-conditions (>700 °C) variably affected all samples in the Tshenukutish terrane. The PT-conditions recorded during retrogression (ca. 700-800 °C and 8-12 kbar) define segments of steep PT-paths and isothermal metamorphic (field) gradients, suggesting high heat flow through the lower crust. The presence of syn-metamorphic mafic dykes and granites further suggest heat input (including from the mantle) during exhumation. The rates of cooling and exhumation in the Manicouagan Imbricate Zone were modelled using all the available PT-data and U-Pb ages for zircon, monazite, titanite and rutile. The results indicate that the early stages of exhumation were characterized by near isothermal conditions. Uplift rates were relatively fast (>1 mm/yr) consistent with tectonic exhumation. Rates subsequently slowed, probably during thrust emplacement of the highest structural levels (the Boundary zone) over the rest of the Tshenukutish terrane. Differences between titanite and rutile cooling ages suggest that late-stage cooling and exhumation was slow, consistent with other high-P terranes. The PTt-evolution of the Tshenukutish terrane is compatible with models for tectonic exhumation by extrusion during northwest thrusting, with extension on top of the pile. Evidence for high heat flow and rapid uplift during the initial exhumation in the Manicouagan Imbricate Zone supports current models which suggest that asthenospheric upwelling immediately followed extensional collapse of the Grenville orogen.



"...man will occasionally stumble over the truth, but usually manages to pick himself up, walk over or around it, and carry on." ... Sir Winston Churchill.

Acknowledgements

Firstly, I would like to thank my supervisors Greg Dunning and Aphrodite Indares who have supported my work tirelessly, both through their NSERC and Lithoprobe grants, but also well beyond the financial sphere. Mark Wilson, who formed part of my supervisory committee, and Toby Rivers are thanked for their many contributions in the way of both technical advice and in philosophical points of view over the years as have many of the other faculty. I would like to thank them and the technical staff at Memorial University, in particular Pam King, Mike Tubrett, Pat Horan, Carolyn Emerson, Robbie Hicks, Rod Churchill and Maggie Piranian. It would be remiss of me not mention a few of the other people who have offered advice, help and friendship over the years. Pablo Valverde is gratefully acknowledged for his friendship during our time at Memorial. I thank Sandy Archibald who pressed many a Professor until a project for me was found. My thanks also go to Gary Thompson and his wife Sarah who have shown me that there is indeed a normal life to be had in research and beyond. Many other people including Paul and Dawn Lamswood, Theresa Fleming and Lisa Gardner have all made me feel a part of Newfoundland from the first day to the present. I thank them and all the others too numerous to mention. Finally, there is a phrase in Scotland, "you can choose your friends but you can't choose your family". I have to say that no one could chosen a more loving and supportive family. Without them I would not have reached this point in life. My only regret is that my father was not here to see my achievements over the years. It is to him and my mother that I dedicate this thesis.

Frontispiece (overleaf). Mineral assemblages in hornblendite from the Lac Espadon suite suggest low-P retrograde (mid-amphibolite facies) metamorphism. However, cathodoluminescence images such as the one shown here reveal kyanite inclusions (bright red) illuminating the surrounding garnet and also contained in the blue-luminescent plagioclase (the image is 0.5 mm across). The assemblage garnet-plagioclase-kyanite-corundum indicates high-P metamorphism. Indeed the PT-conditions recorded by the sample (maximum 920 °C and 19 kbar) are the among the highest documented in the Grenville Province.

Contents

Abstract	Page i-ii
Frontispiece	Page iii
Acknowledgements	Page iv
Contents	Page v
Table of contents	Page v-ix
List of figures	Page x-xiii
List of tables	Page xiii-xiv

Table of contents

General Introduction: Orogenic belts, the Grenville Province and Manicouagan Imbricate Zone

GI.1. Introduction	Page GI.1
GI.1.1. PTt-paths in orogenic belts	Page GI.1-GI.2
GI.1.2. The Grenville Province	Page GI.2
GI.1.3. The Manicouagan Imbricate Zone and the Tshenukutish terrane	Page GI.3-GI.4
GI.2. Thesis outline	Page GI.4
GI2.1. Aims and objectives	Page GI.4-GI.5
GI.2.2. Outline of techniques: petrologic investigations	Page GI.5
GI2.3. U-Pb dating	Page GI.6
GI2.4. Thesis format	Page GI.6-GI.7
Figures	Page GI.8-GI.10

Introduction: An introduction to the high pressure and temperature metamorphic transformation of mafic rocks in continental collisional orogens.

I.1. High-PT metamorphism of mafic rocks	Page I.1
I.1.1. Reactions and kinetics	Page I.1-I.4
I.1.2. Retrogression textures in high-PT rocks	Page I.4-I.5
I.1.3. PT-estimates using disequilibrium textures	Page I.5-I.6
I.2. Geochronology in high-PT terranes: dating of mafic rocks and metamorphism	Page I.6-I.7
I.2.1. Protolith ages	Page I.7
I.2.2. Metamorphic ages	Page I.7-I.8

I.3. Summary	Page I.8-I.9
Figures	Page I.10-I.13

Paper 1: Petrology and U-Pb geochronology of the mafic and ultramafic, high-pressure metamorphic coronites from the Tsheaukutish terrane.

Abstract	Page 1.1-1.2
1.1. Introduction	Page 1.2-1.3
1.2. Geological Setting	Page 1.3-1.6
1.3. Petrology of the Mafic Rocks	
1.3.1. Lac Espadon Suite (LES)	Page 1.6-1.8
1.3.2. Baie du Nord segment (BNS)	Page 1.8-1.10
1.4. Geochemistry	Page 1.10
1.4.1. Analytical techniques	Page 1.10
1.4.2. Tectonic discrimination of gabbros	Page 1.11-1.12
1.4.3. REE distribution	Page 1.12-1.15
1.5. U-Pb geochronology	Page 1.15
1.5.1. Sample selection	Page 1.15-1.16
1.5.2. U-Pb method	Page 1.16-1.17
1.5.3. U-Pb results: Lac Espadon suite (LES)	Page 1.17-1.19
1.5.4. U-Pb results: Baie du Nord segment (BNS)	Page 1.20-1.22
1.6. Discussion	Page 1.22
1.6.1. Intrusive relationships and protolith ages	Page 1.22-1.23
1.6.2. Grenvillian metamorphism of the TT	Page 1.23-1.25
1.7. Conclusions	Page 1.25-1.26
Figures	Page 1.27-1.40
Tables	Page 1.41-48

Paper 2: Transformation of Fe-Ti gabbro to coronite, eclogite and amphibolite in the Baie du Nord segment, Manicougan Imbricate Zone, eastern Grenville Province.

Abstract	Page 2.1-2.2
2.1. Introduction	Page 2.2-2.3
2.2. Geological Setting	Page 2.3-2.5
2.3. Petrography	Page 2.5
2.3.1. Coronitic metagabbros	Page 2.5-2.6
2.3.2. Transitional metagabbros	Page 2.6-2.7
2.3.3. Eclogites	Page 2.7-2.8
2.3.4. Migmatitic garnet amphibolites	Page 2.8-2.9
2.4. Mineral Chemistry	Page 2.9-2.10
2.4.1. Garnet	Page 2.10-2.12
2.4.2. Clinopyroxene	Page 2.12-2.13
2.4.3. Plagioclase and amphibole	Page 2.13-2.14
2.5. Reaction History	Page 2.14
2.5.1. Transition from Fe-Ti gabbro to eclogite	Page 2.14-2.15

2.5.1.1. Transformation from Stages I (igneous phases) to II (grt-opx corona)	Page 2.15-2.16
2.5.1.2. Transformation from Stages II (opx-grt corona) to III (cpx-grt corona)	Page 2.16
2.5.1.3. Transformation from Stages III (cpx-grt corona) to III (eclogite)	Page 2.17-2.18
2.5.2. Migmatite formation and amphibolite overprint	Page 2.18-2.19
2.5.2.1. Stages I (amphibolite) to II and III (cpx and garnet bearing leucosomes)	Page 2.19-2.20
2.5.2.2. Stages IV and V (amphibolite retrogression)	Page 2.20-2.21
2.6. Thermobarometry	Page 2.21
2.6.1. Point selection and general approach	Page 2.21-2.23
2.6.2. PT-determinations	Page 2.23-2.24
2.6.3 Interpretation of data	Page 2.24-2.26
2.7. Discussion and conclusions	Page 2.27-2.28
Figures	Page 2.29-2.38
Tables	Page 2.39-2.43

Paper 3: High pressure and temperature metamorphism of the mafic and ultramafic Lac Espadon suite, Manicouagan Imbricate Zone, eastern Grenville Province.

Abstract	Page 3.1-3.2
3.1. Introduction	Page 3.2-3.3
3.2. Geological Setting	Page 3.3-3.5
3.3. Petrography	Page 3.5
3.3.1. Sample selection and petrographic study	Page 3.5-3.6
3.3.2. Textures	Page 3.6-3.9
3.4. Mineral Chemistry	Page 3.9
3.4.1. Mineral analysis	Page 3.9
3.4.2. Garnet	Page 3.10-3.12
3.4.3. Clinopyroxene, plagioclase and amphibole	Page 3.12-3.13
3.5. Interpretation of textures and thermobarometry	Page 3.13
3.5.1. General approach	Page 3.13-3.14
3.5.2. Troctolite (sample 5a)	Page 3.14-3.17
3.5.3. Hornblendite (sample 3b)	Page 3.17
3.5.4. Olivine garnet amphibolite (sample 6am)	Page 3.18
3.5.5. Garnet amphibolite (sample 2b)	Page 3.19
3.5.6 Nelsonite (sample 9c)	Page 3.19-3.20
3.5.7 Olivine gabbro (sample 35b)	Page 3.20-3.21
3.6. Discussion and conclusions	Page 3.21-3.23
Figures	Page 3.24-3.33
Tables	Page 3.34-3.41

Paper 4: Temperature-time paths and exhumation rates in the high-P Manicouagan Imbricate Zone, eastern Grenville Province.

Abstract	Page 4.1-4.2
4.1. Introduction	Page 4.2-4.4
4.2. Geological Setting	Page 4.4
4.2.1. Regional context	Page 4.4
4.2.2. Lithotectonic framework of the MIZ	Page 4.5-4.6
4.3. High-PT metamorphism in the MIZ	Page 4.6
4.3.1. Lelukuau terrane (LT)	Page 4.6-4.7
4.3.2. Baie du Nord segment (BNS)	Page 4.7-4.8
4.3.3. Boundary Zone (BZ)	Page 4.8
4.4. The behaviour of accessory phases during high-PT metamorphism	Page 4.9
4.4.1. Summary of U-Pb data in the MIZ	Page 4.9-4.10
4.4.2. Zircon	Page 4.10-4.12
4.4.3. Monazite	Page 4.12-4.14
4.4.4. Titanite and rutile	Page 4.14-4.15
4.5. Tt-paths and exhumation rates	Page 4.15
4.5.1. Calculating closure temperatures	Page 4.15-4.16
4.5.2. Cooling rates in the Lelukuau terrane (LT-III)	Page 4.17
4.5.3. Cooling rates in the Baie du Nord segment (BNS)	Page 4.17-4.19
4.5.4. Cooling rates in the Boundary zone	Page 4.19-4.20
4.6. Discussion	Page 4.20
4.6.1. Models for tectonic exhumation of the MIZ	Page 4.20-4.22
4.6.2. Comparisons with other Grenville terranes	Page 4.22-4.24
4.7. Conclusions	Page 4.24
Figures	Page 4.25-4.34
Tables	Page 4.35-4.40

Discussion and Conclusions: The Manicouagan Imbricate Zone within the context of the Grenville**Province and orogenic belts.**

C.1. Terrane correlation	Page C.1
C.1.1. Protolith ages	Page C.1-C.2
C.1.2. Labradorian units: the Lelukuau terrane (LT) and Lac Espadon suite (LES)	Page C.2
C.1.3. Pinwarian and other Mid-proterozoic rocks	Page C.2-C.3
C.1.4. Syn-metamorphic intrusions	Page C.3-C.4
C.2. Grenvillian metamorphism	Page C.4
C.2.1. Timing of high-PT metamorphism	Page C.4
C.2.2. Conditions of metamorphism	Page C.5
C.3. Conclusions	Page C.6

References	Page R.1-R.24
------------	---------------

Appendix A: Polarizing microscopy, cathodoluminescence, scanning electron microscope techniques and photomicrographs.

A. 1. Polarized transmitted and reflected light microscopy	Page A. 1
A. 1.1. Sample preparation	Page A. 1
A. 1.2. Microscopy and photomicrography	Page A. 1
Plates A1.1-A1.11	Page A.1-A.16
A. 2. Cathodoluminescence (CL) microscopy	Page A. 17
A. 2.1. CL procedure	Page A. 17
A. 2.2. CL activators	Page A. 17-A. 18
Plates A2.1-A2.2	Page A. 19-A. 22
A. 3. Accessory mineral morphology	Page A. 23
A. 3.1. Sample preparation	Page A. 23
A. 3.2. Accessory mineral images	Page A. 23
Plates A3.1-A3.3	Page A. 24-A. 26

Appendix B: Analytical methods

B. 1. X-ray fluorescence (XRF) analysis of major and trace element concentrations	Page B. 1
B. 1.1. Sample preparation	Page B. 1
B. 1.2. Loss on ignition (LOI)	Page B. 1
B. 1.3. Disc and pellet preparation	Page B. 1-B. 2
B. 1.4. XRF analysis	Page B. 2
B. 2. Trace element analysis by Inductively coupled plasma mass spectrometry (ICP-MS)	Page B. 3
B. 2.1. Sample preparation and dissolution	Page B. 3
B. 2.2. ICP-MS analysis	Page B. 3-B. 4
B. 3. U-Pb isotopic analysis	Page B. 4
B. 3.1. Sample preparation	Page B. 4-B. 5
B. 3.2. Sample cleaning, weighing, spiking, dissolution and U-Pb separation	Page B. 5
B. 3.3. U-Pb isotopic analysis and age determination	Page B. 6
B. 4. Electron microprobe analysis	Page B. 7
B. 4.1. Sample preparation	Page B. 7
B. 4.2. Polished section analysis	Page B. 7-B. 8

List of figures

- Figure GI.1 (a-b). Two hypothetical PT-paths for rocks in collisional orogens (after England and Thompson 1984).
Page GI.8
- Figure GI.2. Map showing the location of the Manicouagan Imbricate Zone (MIZ) and adjacent terranes in the eastern Grenville Province.
Page GI.9
- Figure GI.3. Map showing the main lithotectonic units and structural boundaries within the MIZ.
Page GI.10
- Figure I.1. Generalised reaction pathways for the transformation from original gabbro, to coronitic and transitional rocks, and finally to eclogite (after Rubie 1990).
Page I.10
- Figure I.2. Two examples of progressive transformation of gabbro to eclogite (figure modified from Rubie 1990)
Page I.11
- Figure I.3. Simplified reaction pathway showing the retrogression of an eclogitic lens by hydration of the deformed margin and fluid infiltration from the surrounding country rock (after Heinrich 1982).
Page I.12
- Figure I.4. Representative U-Pb diagrams from mafic rocks showing simplified examples of typical sets of data in metamorphosed samples.
Page I.13
- Figure 1.1 (a-b). Maps of a) the general location of the MIZ and b) study area showing the main structural boundaries, lithological units and U-Pb sample localities in the TT.
Page 1.27-1.28
- Figure 1.2 (a-c). Tectonic discrimination plots showing the within-plate tholeiite nature of the gabbros from the TT, after a) Irvine and Baragar (1971), b) Meschede (1986) and c) Pearce and Cann (1973).
Page 1.29
- Figure 1.3 (a-d). Tectonic discrimination plots showing the within-plate tholeiite nature and apparent Zr and Ti fractionation within the gabbros from the TT, after a) Pearce and Norry (1979), b) Pearce and Cann (1973), c) Floyd and Winchester (1975) and d) Pearce (1982).
Page 1.30-1.31
- Figure 1.4 (a-f). Whole rock/primitive mantle normalized REE-patterns for a) Olivine gabbro and amphibolites (LES), b) Fe-Ti gabbros and migmatitic-garnet amphibolite (BNS), c) troctolite and dunite (LES), d) nelsonite and hornblendite (LES), e) marginal gabbros (BNS) and f) anorthosites (BNS).
Page 1.32-1.34

-
- Figure 1.5 (a-b). U-Pb concordia diagrams showing a) the igneous protolith age on the upper intercepts and b) metamorphic ages for the lower intercepts for two discordia lines defined by zircon and baddeleyite fractions from LES 1 (hornblendite).
Page 1.35
- Figure 1.6 (a-b). U-Pb concordia diagrams showing a) igneous protolith age for the upper intercept on zircon from LES 2 (olivine gabbro) and b) the cooling age for the upper intercept on rutile from both LES 1 and LES 2.
Page 1.36
- Figure 1.7 (a-b). U-Pb concordia diagrams for a) igneous zircon with metamorphic overgrowths found in LES 3 (nelsonite) giving an emplacement age at the upper intercept and b) concordant metamorphic titanite from LES 4 (garnet amphibolite).
Page 1.37
- Figure 1.8 (a-b). U-Pb concordia diagrams for a) BNS 1 (coronitic Fe-Ti gabbro), showing the protolith age with concordant baddeleyite and metamorphic ages with concordant zircon, and b) concordant metamorphic zircon from BNS 2 (re-equilibrated coronite).
Page 1.38
- Figure 1.9 (a-c). U-Pb concordia diagrams BNS 3 (migmatitic-garnet amphibolite) showing, a) concordant metamorphic zircon, b) two ages from concordant metamorphic titanite populations and c) cooling ages from both concordant, large grain size (R4, R5) and fine-grained (R1, R2, R3) rutile populations.
Page 1.39
- Figure 1.10. Summary diagram of U-Pb ages from the Manicouagan Imbricate Zone (MIZ).
Page 1.40
- Figure 2.1. Map of the eastern Grenville Province showing the location of the Manicouagan Imbricate Zone and surrounding terranes.
Page 2.29
- Figure 2.2. Simplified geological map of the Tshenukutish terrane and adjacent terranes with the locations of sample localities in the Baie du Nord segment (coronites, amphibolites and eclogites) used for thermobarometry in this study.
Page 2.30
- Figure 2.3. Garnet compositions plotted as Grs, Alm+Sp and Prp for the selected samples.
Page 2.31
- Figure 2.4 (a-c). Garnet zoning profiles for a) garnet corona between plagioclase and olivine (eclogite, sample 21), b) garnet coronas around plagioclase xenocryst in transitional metagabbro (sample 85) and c) garnet corona in a coronitic metagabbro (sample 123).
Page 2.32
- Figure 2.5 (a-b). Zoning profile for a large garnet poikiloblast in a migmatitic garnet-amphibolite (sample 313).
Page 2.33

- Figure 2.6. Clinopyroxene compositions plotted as Di+Hd, Ae and Jd measured in the selected samples as described in the text. Page 2.34
- Figure 2.7. Plagioclase compositions (relicts and collars) measured in the selected samples. Page 2.35
- Figure 2.8. Summary of reaction stages and pathway for the formation of the main textures during the transition from Fe-Ti gabbro to eclogite in the samples described in the text. Page 2.36
- Figure 2.9. Summary of reaction stages and pathway for the formation of the main textures during the anatexis and amphibolite overprinting of the migmatitic garnet amphibolite (sample 313). Page 2.37
- Figure 2.10. PT-conditions recorded by the samples from the BNS. PT-estimates shown in the diagram were calculated using the TWEEQU program. Page 2.38
- Figure 3.1 (a-b). Maps showing a) location of the Manicouagan Imbricate Zone in the eastern Grenville Province, and b) simplified lithotectonic framework of the Manicouagan Imbricate Zone. Page 3.24-3.25
- Figure 3.2. Map showing the main lithologies structures and sample localities of the Lac Espadon complex in the Boundary zone. Page 3.26
- Figure 3.3. Garnet compositions plotted as Grs, Alm+Sps and Prp for the selected samples from the LES. Page 3.27
- Figure 3.4 (a-h). Garnet zoning profiles for a) sample 5a (coronitic troctolite) amphibole-free corona and b) amphibole bearing corona, c) sample 3b (hornblendite) kyanite-bearing garnet corona around a plagioclase chadacryst, d), sample 6am (olivine amphibolite) zoning traverse across a garnet porphyroblast, e) sample 2b (garnet amphibolite) traverse across a subhedral porphyroblast, f) sample 9c (nelsonite) garnet corona with biotite inclusions, g) sample 35b (olivine gabbro) large garnet corona around a relict igneous clinopyroxene and h) small kyanite-bearing garnet. Page 3.28-3.29
- Figure 3.5. Compositional diagrams for clinopyroxene for the troctolite and olivine gabbro in the LES. Page 3.30
- Figure 3.6. Plagioclase compositions for samples in the LES. Page 3.31
- Figure 3.7. Ca-amphibole compositions for samples from the LES. Page 3.32

Figure 3.8 (a-b). PT-diagrams showing the maximum and minimum metamorphic conditions calculated partly using the analyses in Table 3.1.	Page 3.33
Figure 4.1. Map of the eastern Grenville Province showing the location of the Manicouagan Imbricate Zone and surrounding terranes.	Page 4.25
Figure 4.2. Simplified geological map of the MIZ with the locations of Figures 4.3a-b shown.	Page 4.26
Figure 4.3. Map of slice LT-III (south east LT) and TT with localities of samples used for PT-determinations (data in Table 4.1) and U-Pb ages (Table 4.2).	Page 4.27
Figure 4.4. Diagram showing a) temperatures and b) pressures recorded by rocks across the MIZ.	Page 4.28
Figure 4.5. Diagram showing the U-Pb ages from across the MIZ.	Page 4.29
Figure 4.6 (a-c). Graphs showing closure temperature versus cooling rates for different grain sizes of a) monazite, b) titanite and c) rutile.	Page 4.30
Figure 4.7. Tt-path for slice LT-III.	Page 4.31
Figure 4.8. Tt-path for the central and south-west BNS.	Page 4.32
Figure 4.9. Tt-path for the northern and southern BZ and the LES.	Page 4.33
Figure 4.10. Summary of the metamorphic and tectonic evolution of the MIZ.	Page 4.34
List of Tables	
Table 1.1. Major- and trace-element compositions of selected mafic samples from the TT obtained by XRF analyses.	Page 1.41-1.44
Table 1.2. REE-analyses and additional trace-element compositions of selected mafic samples from the TT obtained by ICP-MS analyses.	Page 1.45-1.46
Table 1.3. U-Pb isotope data for mineral fractions from the mafic rocks of the TT.	Page 1.47-1.48

Table 2.1. Representative analyses of garnet, plagioclase, clinopyroxene, pargasite (amphibole), spinel and ilmenite, in the eclogites, transitional metagabbros, coronites and amphibolites from the BNS.	Page 2.39-2.42
Table 2.2. PT-conditions recorded by the eclogites, transitional metagabbros, coronites and amphibolites from the BNS.	Page 2.43
Table 3.1. Representative analyses of garnet, plagioclase, clinopyroxene, amphibole, orthopyroxene and olivine and spinel, in the mafic samples from the LES.	Page 3.34-3.40
Table 3.2. PT-conditions recorded by the mafic sample of the LES.	Page 3.41
Table 4.1. Summary of PT-data from the MIZ.	Page 4.35-4.36
Table 4.2. Summary of U-Pb age determinations from the MIZ.	Page 4.37
Table 4.3. Diffusion data used to calculate the respective closure temperatures in Table 4.4.	Page 4.38
Table 4.4. Interpretation of zircon ages along with grain sizes and closure temperatures (T_c) at cooling rates of 1 °C/My and 100 °C/My for monazite, titanite and rutile.	Page 4.39-4.40
Table A.1. CL colours, textures revealed and possible activators in minerals examined in this study.	Page A.18

Orogenic belts, the Grenville Province and Manicouagan Imbricate Zone**GL1. Introduction***GL1.1. PTt-paths in orogenic belts*

Many orogenic (mountain) belts, e.g. Alps, Himalayas, are interpreted to be the result of continent-continent collision. This process produces an area of thickened continental crust which in turn leads to an increase in temperature (T) and pressure (P) resulting in metamorphic transformation of the rock types present. The petrologic responses to metamorphism are commonly diverse and are driven not only by PT-conditions attained, but also the time (t) over which the transformation processes operated. Metamorphism is therefore controlled by the extent of crustal thickening (i.e., the PT-conditions experienced) and by subsequent exhumation processes, which govern the duration of metamorphic (orogenic) events. Ideally, absolute dating of metamorphism can be combined with the PT-data to produce a metamorphic history. Thus, the PTt-history (or PTt-path) defined by rocks within a terrane can be used to elucidate the tectonic processes in operation during the orogenic event.

Several models have been suggested to explain the metamorphic processes caused by crustal thickening in continental collision zones (e.g. England and Thompson 1984; Thompson and England 1984; Davy and Gillet 1986; Thompson and Ridley 1987; Shi and Wang 1987; Bohlen 1987; Hodges 1991; Rupel and Hodges 1994). All of these models show that the shapes of the PT-paths followed by metamorphic rocks depend upon the relative rates of heat transfer during orogenic processes, and on the type of exhumation (tectonic versus erosional). Exhumation controlled by erosional denudation only (e.g. Thompson and England 1986) will follow long, slowly evolving PT-paths (Figure GL1a). Since reaction rates increase exponentially with T, rocks that follow this type of PT-path tend to lose the mineral

assemblages formed at maximum pressures. Alternative mechanisms controlling exhumation, e.g. tectonic uplift, will produce a different type of PT-path (e.g. Thompson and Ridley 1987). Because tectonic exhumation is faster than erosion, heat in the thickened crust has less time to accumulate. The maximum temperature attained will not only be lower, but both the P and T-conditions recorded are likely to be closer to the maximum burial depth (Figure GL1b). If we assume that the rate of heat transfer is constant, it will take longer for the peak temperatures to be attained by rocks following the first PT-path (erosional denudation) than in the second (tectonic exhumation). Thus, the relative lengths of the paths are broadly representative of the duration of the metamorphic events.

GL.1.2. The Grenville Province

The Grenville Province, located in the in the eastern Canadian Shield, represents the exposed roots of a collisional orogen. The Province comprises units accreted to the southeastern margin of Laurentia with the main accretion events occurring at ca. 1650 Ma (Labradorian), ca. 1450 Ma (Pinwarian) and ca. 1250 (Elzevirian). These units were subsequently involved in the Grenvillian orogeny which occurred in discrete pulses between 1190 and 990 Ma (Rivers 1997). Various supracrustal rocks and intrusions, from anorthosites and large gabbro bodies to smaller dyke swarms and granites, occur throughout the Grenville Province. Some of these rocks, the mafic units in particular, record PT-conditions up to eclogite facies (Grant 1988; Rivers and Mengel 1988; Indares 1993; Indares and Rivers 1995). The metamorphic conditions recorded by both the high-P assemblages in these rocks and by their retrogressed equivalents define very steep PT-paths (e.g. Indares 1993). These PT-paths support models which suggest rapid tectonic exhumation throughout much the of the orogen shortly after the high-P event (e.g. Rivers et al. 1989, 1993). Thus, the Grenville Province represents one of the few examples of a geological terrane where processes operating in deep orogens can be studied and where rapid tectonic exhumation may have preserved some record of these processes.

GI.1.3. The Manicouagan Imbricate Zone and the Tshenukutish terrane

Among the high-P lithotectonic units of the Grenville Province, the Manicouagan Imbricate Zone is the best exposed. The Manicouagan Imbricate Zone (MIZ) is a 70 km wide assembly of crustal slices which lie at the southern margin of the Parautochthonous Belt of the eastern Grenville Province (Indares 1994, Figure GL2). The MIZ is located at the western extension of the Molson Lake terrane and tectonically overlies the Gagnon terrane to the north and is in turn overlain by the Harte Jaune terrane to the south. Both the Molson Lake and Gagnon terranes contain eclogite facies rocks (Indares 1993; Indares and Rivers 1995). There are two domains identified within the MIZ, the Lelukuau terrane to the west and the smaller Tshenukutish domain to the east (Figure GL3). The Lelukuau terrane (LT) comprises a Labradorian anorthosite-mangerite-charnockite-granite (AMCG) suite intruded by 1040 Ma mafic dykes (Indares et al. 1998). The rocks in the LT occur as a stack of thrust slices with kinematic evidence of north-west directed movement. The Tshenukutish terrane (TT) tectonically overlies the LT (Indares 1994) and can be divided into two units (Figure GL3). The structurally lower unit, the Baie du Nord segment, comprises diotitic-granitic country rocks with rafts of metapelite. These are cross cut by mesocratic Fe-Ti gabbro sills which grade into more leucocratic rocks. The structurally higher unit, the Boundary zone, lies to the east and south of the TT (Figure GL3) and is represented by a complex assembly of tectonic slices and lenses. This area includes lenses of mafic and ultramafic rocks called the Lac Espadon suite, the Brien anorthosite, the Hart Jaune granite, various orthogneisses and metapelites and the lower-grade X-complex. The main boundaries in the TT show evidence for south-east directed extension (Indares et al. 1998).

Evidence for high-PT metamorphism is witnessed in the MIZ and is particularly well documented by the mafic rocks. The Fe-Ti gabbro and anorthosite bodies in the BNS show variable replacement of igneous minerals with high-P coronas and pseudomorphs. The margins of the Fe-Ti gabbros show evidence for deformation, fluid infiltration and partial melting. The mafic and ultramafic

rocks (LES) in the BZ also show evidence of high-PT corona development. In addition, the mafic rocks of both the BNS and LES have margins of amphibolite. The amphibolite margins are indicative of retrogression and may be used to constrain part of the PT-evolution. Therefore, the metagabbroic and metamorphosed ultramafic rocks from the TT show great potential for constructing segments of PT-paths. By applying U-Pb geochronology the timing of peak metamorphism and initial exhumation may also be constrained. The combination of detailed PT-history and U-Pb ages should prove to be of great benefit in understanding the high-PT processes in both the Grenville and in orogenic belts in general.

GL2. Thesis outline

GL.2.1. Aims and Objectives

The main aim of this project is to obtain a detailed metamorphic history of the Tshenukutish terrane (TT) by applying a number of techniques to the mafic and ultramafic rocks of the area. This is achieved by fulfilling the following objectives;

1) To broadly classify the parent rock types of the gabbroic bodies both in terms of emplacement ages and geochemistry. The ages are constrained by U-Pb geochronology carried out on igneous accessory phases such as zircon and baddeleyite. Petrologic investigations and geochemistry (XRF major and trace-element and ICP-MS rare-earth element) are used to characterize the geochemical signatures and tectonic setting of the protoliths. By combining these two approaches the diversity of the parent rock types can be well established. In addition, the geochemical composition of the rocks is used to clarify the potential relationships between whole-rock chemistry and metamorphic mineral assemblages.

2) To determine the PT-conditions experienced by the mafic rocks. This is done in two stages. First, the petrographic studies of the igneous precursor minerals, metamorphic textures and the composition and zoning trends obtained by electron microprobe analysis, are used to identify the mineral

reaction history. The second stage is to determine the range of PT-conditions which have been recorded. This is achieved by determining microdomains for which local equilibrium may be assumed and using selected mineral compositions for the application of thermobarometry.

3) To determine the age of metamorphism, exhumation and cooling rates recorded by the TT. This is achieved by combining the PT-data and high precision U-Pb dating of the mafic and ultramafic samples examined in this study, and associated rocks across the TT. Using well established U-Pb dating techniques on the accessory phases along with textural and PT-data for the main phase mineral assemblage, a detailed time-scale for the metamorphic processes is obtained.

Thus, both the parent rock types and the metamorphic history of the mafic and ultramafic rocks from the TT is determined. In addition, a comparison of the metamorphic history of these rocks with others in the Grenville Province and with other high-PT terranes can be made. The implications of the PTt-history of these rocks on models for the development of collisional orogens can then be considered.

GI.2.2. Outline of techniques: petrologic investigations

Much of the petrologic work carried out on the samples displaying both preserved high-PT textures and their amphibolite margins uses standard transmitted and reflected light microscopy along with cathodoluminescence and back-scattered scanning electron microscopy (CL and BS-SEM). The mineralogy and textures of a large number of the polished sections are characterized. Disequilibrium textures (essentially coronas) are very common in the mafic and ultramafic samples from the TT. The significance of these textures is discussed fully in the next section. In general, the least reequilibrated assemblages in appropriate microdomains can be used to determine the peak PT-conditions of metamorphism. The amphibolites and reequilibrated corona assemblages are used to obtain retrograde PT-conditions. Specific problems in applying thermobarometry in rocks with complex textures are discussed in each section.

GI.2.3. U-Pb geochronology

The U-Pb isotopic investigations were carried out to, a) place absolute ages on the protoliths and b) determine the timing of metamorphic event(s) and c) the rates of cooling. The latter two objectives are combined to give the relative time scale variations required to construct PTt-paths for the TT. Accessory minerals present in the samples include zircon ($ZrSiO_4$), both igneous and metamorphic, baddeleyite (ZrO_2), titanite ($CaTiSiO_5$) and rutile (TiO_2). Available U-Pb ages from other rocks within the MIZ (Indares et al. 1998; Indares and Dunning, in press) include further zircon, titanite and rutile ages from mafic rocks and granites, along with monazite ages from metapelitic samples. Due to the high closure temperature (T_c) of zircon and monazite (ca. 900 °C and ca. 750 °C, respectively) and somewhat lower T_c for titanite and rutile (ca. 650 °C and ca. 400 °C, respectively) the U-Pb age information can be used to determine cooling rates, and when combined with the PT-data, rates of uplift.

GI.2.4 Thesis format

This study involves metamorphism of mafic rocks at high-PT conditions and the resultant formation of coronitic textures. The current understanding about the formation and significance of coronitic textures and U-Pb dating of mafic rocks is discussed in some detail in the next section. The remainder of the thesis is presented as a series of four papers, which have been published or submitted for publication in international journals. The papers have been formatted to a standard style and all references are located at the end of the thesis rather than after each paper. Some changes were made to the thesis versions of the papers, such as standardizing the names of terranes and sub-units, and including expanded data sets which would have been too large for the submitted manuscripts. However, none of these changes alter the conclusions presented.

Paper 1 (Cox, R.A., Dunning, G.R. and Indares, A., *Precambrian Research*, 1998, volume 90, pages 59-83) deals with the general classification of the mafic and ultramafic rocks in the TT by using

petrologic and geochemical analysis and U-Pb dating to determine the protolith ages. The timing of metamorphism is also constrained and the results are discussed and compared with other available data in both the MIZ and in the Grenville Province.

Paper 2 (Cox, R.A. and Indares, A., *Journal of Metamorphic Geology*, 1999, volume 17, pages 537-556) examines in detail the metamorphism of the Fe-Ti gabbroic rocks in the BNS, western TT. The study characterizes the transformation from gabbro, to coronite and eclogite. Evidence for partial melting of the deformed and hydrated gabbro margins is examined along with the effects of retrogression to amphibolite. Thermobarometry has been applied to determine the PT-conditions of metamorphism recorded by these samples.

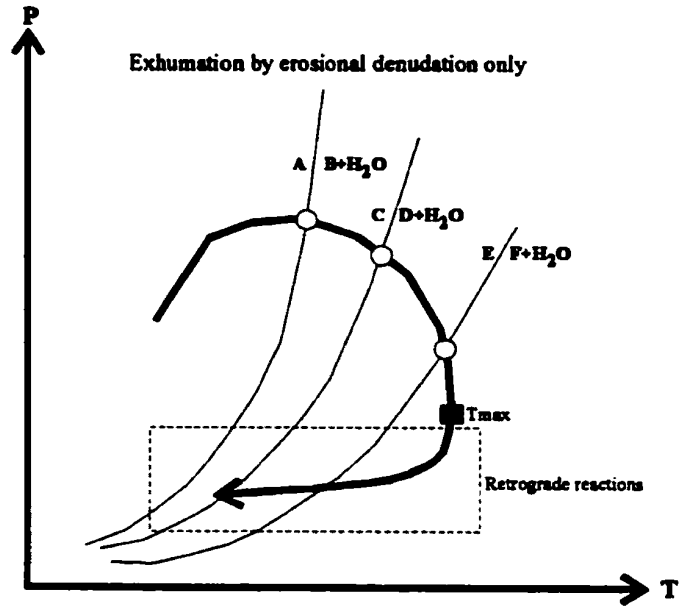
Paper 3 (Cox, R.A. and Indares, A., *Canadian Mineralogist*, 1999, volume 37, pages 335-357) deals with the metamorphism of the mafic and ultramafic rocks which comprise the LES, located in the BZ, eastern TT. These rocks display high-PT coronitic assemblages which require careful micro-scale characterization and detailed thermobarometry to elucidate peak metamorphic conditions. Retrogression has variably affected these rocks and the PT-data set produced by both peak and retrograde assemblages is used to characterize conditions of metamorphism during exhumation.

Paper 4 (Cox, R.A., Indares, A. and Dunning G.R., submitted to *Precambrian Research*) compiles the U-Pb and PT-data sets from the MIZ, including those presented in the preceding papers. The data are used to model cooling and exhumation rates for the TT and part of the underlying LT. The results from this study are compared with those from other areas of the Grenville and younger high-PT orogenic belts. The discussion points out the similarities and differences in the tectonic models suggested for the tectonic evolution of the Grenville with other orogens.

A section at the end of the thesis summarizes the conclusions from all four papers. The photomicrographs discussed in each paper are presented in Appendix A and more complete descriptions of the techniques and analytical methods are presented in Appendix B.

Figure GI.1 (a-b). Two hypothetical PT-paths for rocks in collisional orogens (after England and Thompson 1984). Note the difference in both the length and shape of the paths along with the difference in peak-T achieved in each case. Retrograde reactions due to water input may occur during exhumation but will affect the rocks following path (a) more than those in (b).

a)



b)

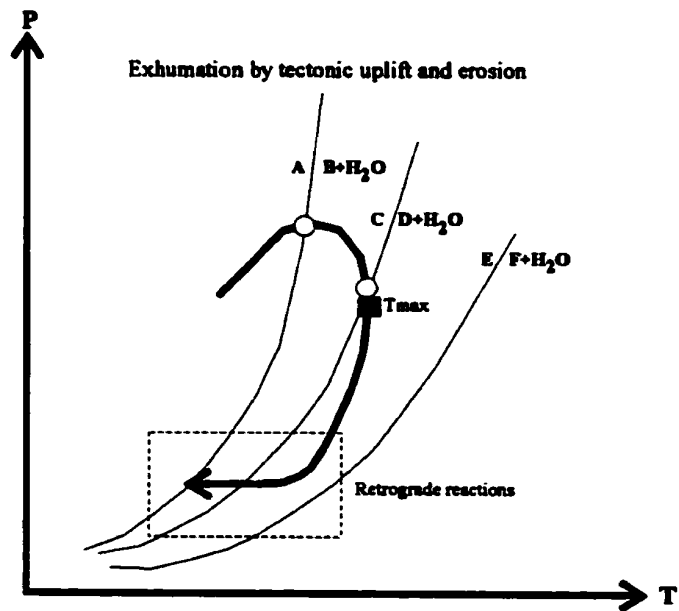


Figure GI.2. Map showing the location of the Manicouagan Imbricate Zone (MIZ) and adjacent terranes in the eastern Grenville Province.

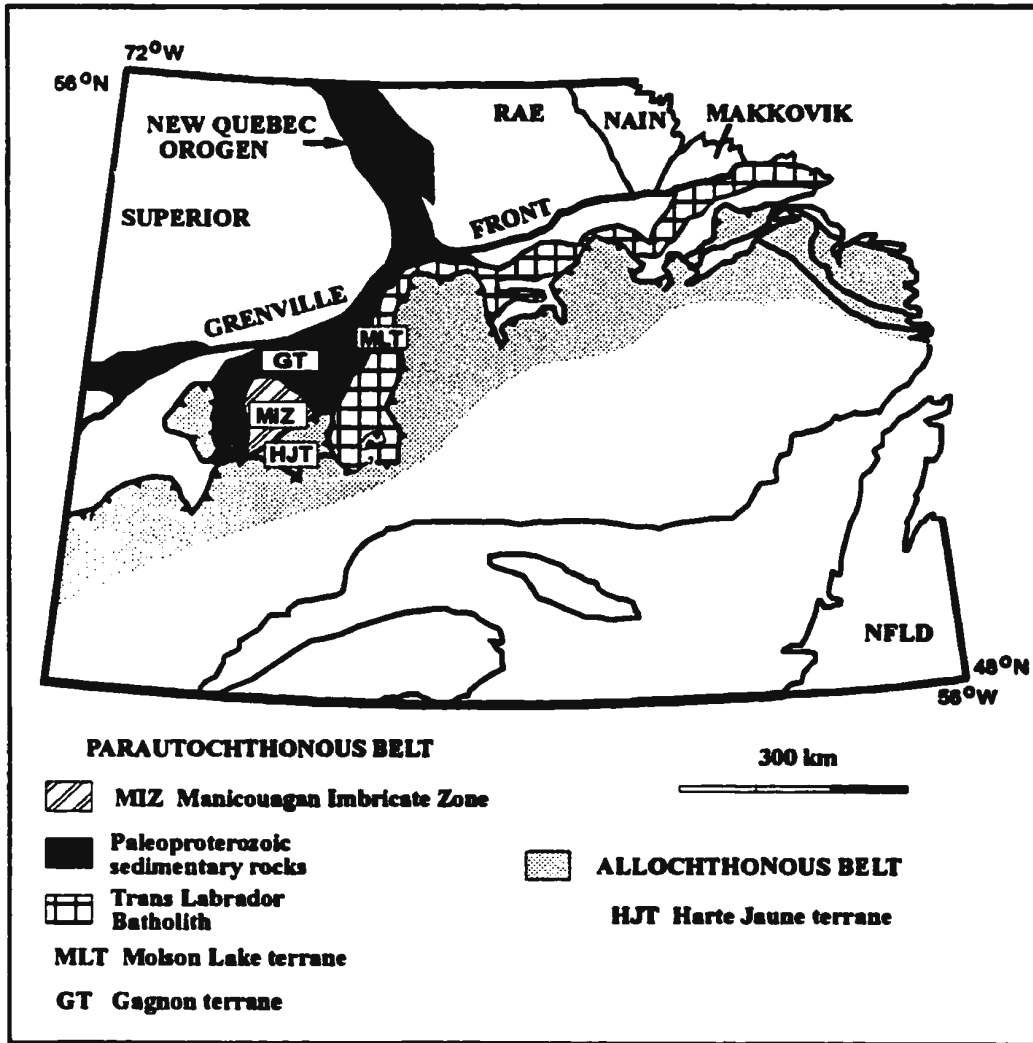
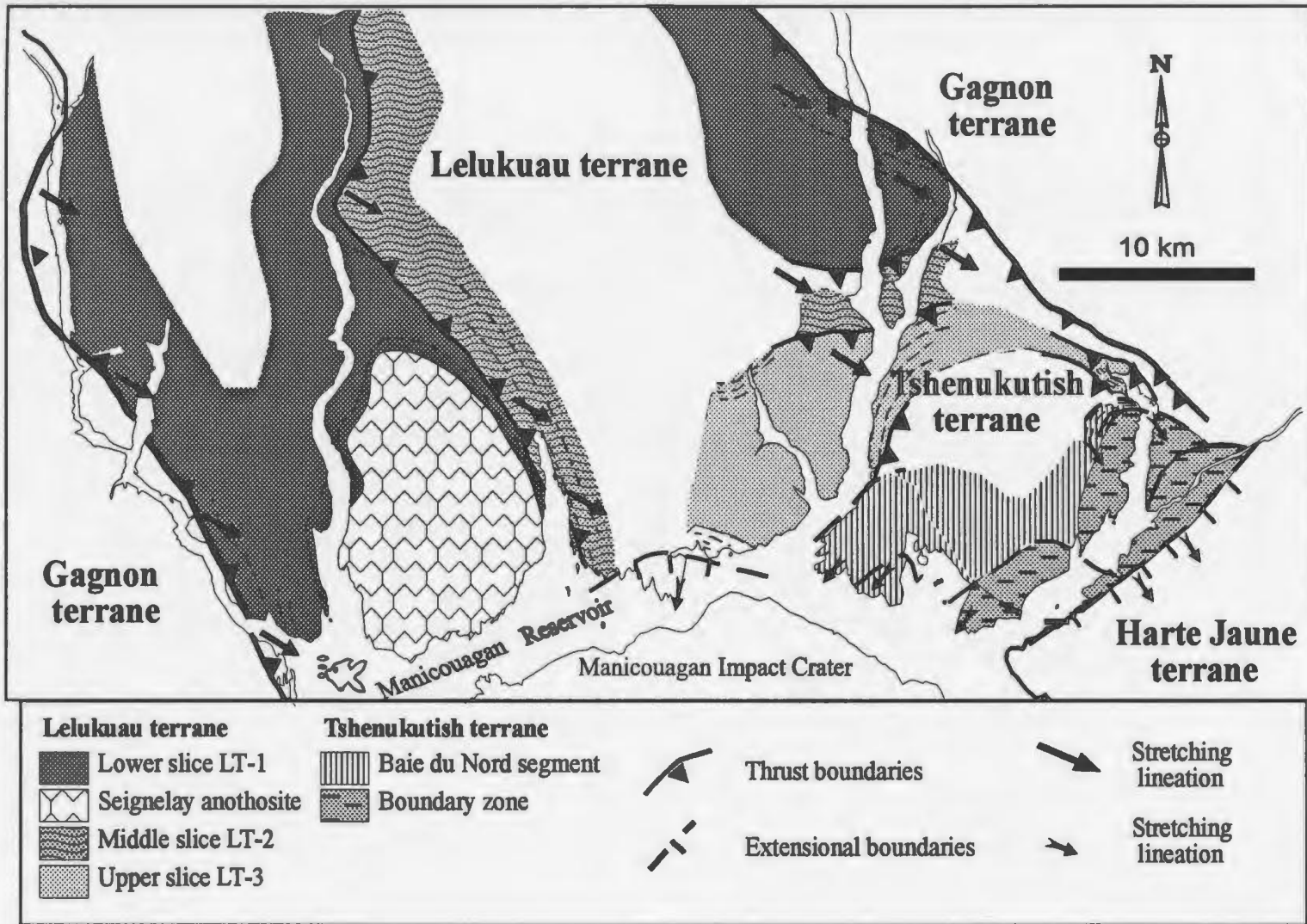


Figure GI.3. Map showing the main lithotectonic units and structural boundaries within the MIZ.



An introduction to the high pressure and temperature metamorphic transformation of mafic rocks in continental collisional orogens.

1.1. High-PT metamorphism of mafic rocks

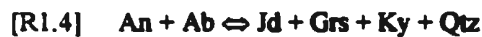
The study of high-P metamorphic rocks, such as eclogite, is of importance to the understanding of tectonic processes in deep crustal segments during orogenesis. As discussed in the Section GL.1 (and shown in Figure GL.1a-b), the preservation of high-PT assemblages requires that the rocks do not pervasively reequilibrate at lower PT-conditions or during retrogression. It has been suggested that this may happen for a variety of reasons such as rapid exhumation (e.g. Droop et al. 1990) or dry conditions (e.g. O'Brien 1999) limiting typical retrogression reactions. Undeformed, dry, mafic igneous rocks, which have been exhumed rapidly, are often the most likely to record peak-PT conditions.

1.1.1. Reactions and kinetics

Coarse grained, undeformed meta-igneous rocks such as metagabbros, where fluid has played a limited role in the reaction path, commonly display disequilibrium textures (e.g. Mørk 1985, 1986, Pognate 1985, Koons et al 1987, Johnson and Carlson 1990, Indares 1993). The coarse grain size and dry nature of metagabbros results in slow diffusion despite large chemical gradients between igneous phases such as olivine and plagioclase, which in turn leads to the formation of corona assemblages. During eclogite facies metamorphism of a typical metagabbro with original mineral domains of olivine, plagioclase and augite, a first corona stage produces orthopyroxene around olivine, garnet around the plagioclase and an increase in the Na-content of augite (Figure L1). Increasing eclogitization leads to formation of omphacite, while orthopyroxene and garnet tend to develop pseudomorphs after olivine and plagioclase. Commonly Al in the remaining plagioclase forms high Al phases such as kyanite, corundum or spinel (e.g. Mørk 1985, Indares

1993). The last stage of eclogitization results in the loss of the corona texture and the production of a granoblastic, omphacite/jadeite and garnet assemblage, i.e. a "true" eclogite (Carswell 1990).

There are many reactions described for this general transformation process, some of which are illustrated in Figure L.2. The resulting high-P phases are controlled by the kinetics of these breakdown reactions. Plagioclase breakdown reactions under high-PT metamorphic conditions can occur by either a migration of elements out of the plagioclase site to form new minerals or the production of new mineral assemblages inside the plagioclase domains. In the latter case, the initial reactions involve the anorthite component and fluid to produce a number of products. One such transformation involves the production of zoisite, kyanite, quartz and more albitic plagioclase by the breakdown of the anorthite component of the plagioclase and H₂O. In the absence of H₂O, the initial anorthite-consuming reaction produces grossular garnet, kyanite and quartz (Wayte et al. 1989). At about 17 kbar and 600 °C the albitic component of the plagioclase begins to react to produce jadeite, kyanite and/or quartz. These reactions are summarized below (after Wayte 1989 et al. and Rubie 1990).



Detailed studies of the textures related to plagioclase breakdown reactions (Wayte et al. 1989) show that even at an advanced state of reaction during metamorphism the plagioclase is not consumed completely and that the Na-component is stable until 17 kbar when reactions [R1.2] and [R1.4] begin.

The breakdown of augite involves the replacement of Ca, Mg and Fe by Na and Al from plagioclase. Ca and Al diffuse extremely slowly in pyroxene (Brady and McCallister 1983). In Figures L.1

and L2 it was shown that, in the first stage of eclogitization under high-PT conditions, the formation of a Na-augite is part of the usual assemblage. Therefore, there must be some diffusion of Na from the plagioclase to the clinopyroxene site at this stage. Otten and Buseck (1987) carried out a detailed study of the transformation of clinopyroxene to omphacite. The main reaction involved the formation of very fine Na-augite lamellae along pre-existing crystal structures (i.e. cleavage and lattice defects) and the presence of these allowed more rapid growth of Na-clinopyroxene at later stages. Thus, only a very small amount of Na migration was necessary to produce the Na-bearing clinopyroxene compositions often observed during the early stages of the eclogitization of metagabbroic rocks. In addition, increased albite breakdown at higher pressures produces Na-clinopyroxene pseudomorphs after plagioclase (Wayte et al. 1989).

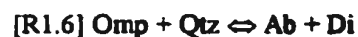
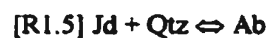
Olivine breakdown usually involves progressive development of orthopyroxene coronas and eventually pseudomorphs which are contemporaneous with the breakdown of anorthite then albite in plagioclase. These solid-solid reactions usually occur at high temperatures (>750 °C) in the absence of any fluid. Where fluids are present, the breakdown of olivine can take place at temperatures well below those encountered in high-PT metamorphic conditions, i.e. <600 °C. The resulting reactions with the fluid and surrounding phases in such cases produce talc, chlorite and other hydrous products. Thus, the composition, fluid activity, PT-conditions and kinetic factors all control the breakdown of original mineral domains and the formation of the resulting coronas and pseudomorphs.

The distribution of the minerals in the coronas and possible chemical zoning trends depend upon the type of chemical gradient between adjacent igneous phases. For example, plagioclase is poor in Fe and Mg and olivine is poor in Al and Ca. Diffusion of Fe and Mg towards the plagioclase and Al and Ca towards the olivine leads to the typical corona assemblage of orthopyroxene (surrounding olivine), clinopyroxene in the middle and garnet around plagioclase (e.g. Grant 1988; Johnson and Carlson 1990). The composition of the garnet changes from Fe and Mg-rich (almandine and pyrope) on the olivine side of the corona to Ca-rich (grossular) on the plagioclase side of the corona, thus reflecting the element/mineral relationships in each domain. Excess Al in the plagioclase site may lead to the development of kyanite

and/or corundum inclusions, whereas in more mafic rocks, excess Mg and Fe diffusing into the plagioclase site may result in spinel inclusions (Indares 1993; Indares and Rivers 1995). Due to the slow rates of diffusion in undeformed gabbroic rocks, textures will often not evolve past corona formation stages. Thus, in many cases the transformation from coronite to eclogite will be “frozen” and the PT-conditions recorded will likely be close to the metamorphic peak.

1.1.2. Retrogression textures in high-PT rocks

The preservation of disequilibrium textures in high-PT rocks such as those described above can persist for tens of millions of years (Rubie 1990). However, deformation of high-PT rocks greatly increases reaction rates. As a result deformed mafic rocks tend to experience more pervasive development of high P-mineral assemblages but are also more prone to retrogression (e.g. Mørk 1985; Koons et al 1987). This is because deformation not only enhances mineral diffusion by grain size reduction but also increases the susceptibility of the rock to fluid infiltration which in turn facilitates retrograde reactions. Deformed rocks are therefore much more likely to reequilibrate to produce lower grade metamorphic assemblages upon uplift and cooling than those which display incomplete prograde transformation to eclogite. Some of the reactions involved during re-equilibration of high-PT rocks upon cooling and decompression are listed below.



Reactions [R1.5] and [R1.6] are solid-solid reactions which require no input of fluid. The rate of these reactions is usually very slow. Under fluid poor (or absent) conditions the time to replace a 10 μm

jadeite with albite is >40 Ma (Rubie 1986). In this case, only in extremely slow cooling terranes will retrogression pervasively affect the high-P assemblage. On the other hand the same reaction, fluid assisted, can take place in a few tens of years at only 550 °C (Rubie 1986). The injection of fluid, or the presence of existing fluid bearing minerals, will invariably induce reactions [R1.7] and [R1.8]. These reactions are considerably more likely to occur in deformed high-PT rocks, partly due to enhanced rates of fluid migration, due to reduced grain size and the development of strongly directional fabrics. Reaction [R1.7] will take place due to the presence of some hydrous phases which are often found in deformed eclogitic rocks (Koons et al. 1987). However, the preservation of eclogitic rocks as undeformed lenses within deformed and retrogressed high-PT terranes is not uncommon (e.g. Heinrich 1982). The deformation and subsequent re-hydration and retrogression of many such lenses can be seen to be restricted to the outer edge of the eclogite body (Figure L3). H₂O is consumed in reactions along the outer edges of the body which generally preserves the core of the lens through the uplift and cooling path of the rock.

1.1.3. PT-estimates using disequilibrium textures

PT-conditions in coronitic rocks can be determined using microdomains which can be regarded as displaying local equilibrium. For example, garnet and orthopyroxene or garnet and omphacite can be regarded as in equilibrium at their respective grain boundaries where Fe-Mg exchange reactions occur. By applying Fe-Mg exchange thermometry (e.g. Carswell and Harley 1990; Ellis and Green 1979; Krogh 1988) the T-conditions of these equilibrated contacts can be established. To determine the P-conditions a similar approach can be applied using an appropriate net transfer reaction. For instance, kyanite and corundum bearing plagioclase in contact with garnet can be used to determine the P-conditions (e.g. Ky-Crn-Pl-Grt barometer, Indares and Rivers 1995). A drawback with this method is that T-conditions are calculated in a different microdomain than P-conditions. For example the garnet in contact with the plagioclase is usually more grossular-rich than at the pyroxene contact. In such cases the assumption has to be made that the temperatures and pressures were recorded simultaneously. In any microdomain

equilibrium is likely achieved at the highest temperatures, and therefore this assumption is often correct. Calculation of both peak-P and T in coronitic rocks obviously requires that retrogression has not occurred. Retrogression may be indicated by the presence of lower grade minerals in the corona assemblage (e.g. biotite and hornblende) or by chemical reequilibration of mineral compositions. In strongly zoned minerals such as garnet, coronas in contact with plagioclase will tend to show a decrease in Ca-content if they have undergone reequilibration during cooling and exhumation. Similarly the Fe/Mg ratio in the garnet will tend to increase at the contact with pyroxene. Ca diffuses much more slowly than Fe or Mg in garnet, especially at temperatures below 700 °C (e.g. Cygan and Lasaga 1985; Loomis et al. 1985; Chakraborty and Ganguly 1992; Schwandt et al. 1996). In other words, Ca exchange between plagioclase and garnet (recording pressures) will cease before Fe-Mg exchange between garnet and pyroxene (recording temperatures). If the recorded T-conditions are below 700 °C, and there is no textural evidence for reequilibration, the combined PT-estimates for the corona assemblage are likely to be erroneous. Thus, only when a) textural evidence suggests local equilibrium, b) balanced reactions for the minerals present in the microdomain can be written, and c) chemical zoning profiles indicate no major reequilibration, can the independently derived pressures and temperatures be combined to give accurate PT-estimates for the formation of a corona assemblage. On the other hand, retrograde conditions can be calculated using domains where retrogression is evident. The estimation of both peak and retrograde conditions allows segments of PT-paths to be determined.

L.2. Geochronology in high-PT terranes: dating of mafic rocks and metamorphism

Accurately determined mineral ages are a prerequisite for placing PT-data in a temporal context. The U-Pb method often allows for both protolith and metamorphic ages to be calculated using a variety of accessory minerals. Concentrations of magmatic zircon may be as high as 35 mg/kg in gabbros, but the actual amount seems to bear little relation to the Zr-content of the protolith (Gebauer 1990). Zircon can also

occur as a metamorphic phase. Other primary igneous phases such as baddeleyite are also suitable for dating, but are not found as metamorphic crystals in mafic rocks. Thus, only after mineral separation and accessory mineral identification can a sample be deemed suitable for U-Pb geochronology.

1.2.1. Protolith ages

Zircon, baddeleyite and titanite have been used to constrain protolith ages for a variety of mafic rocks (e.g. Rogers and Dunning 1991; Lanyon et al. 1993). The temperature at which Pb-diffusion is negligible, known as the closure temperature (T_c) after Dodson (1979) is high for zircon and baddeleyite (>900 °C) and lower for titanite (ca. 650 °C). In addition, baddeleyite and titanite commonly react to form secondary metamorphic minerals. On the other hand, mafic rocks which have undergone metamorphism may still record protolith ages where primary magmatic zircon and/or baddeleyite can be recovered (e.g. Davidson and van Breemen 1988; Paquette et al 1989; Dudás et al. 1994). U-Pb ages, plotted on a concordia diagram, commonly show one of four different patterns in metamorphosed rocks (Figure L4). In the first scenario the protolith age would be reliably determined. In the other three cases the age given by the upper intercept may or may not be the true age for the protolith. Mixtures between Pb-loss ages, metamorphic diffusion and overgrowths and even new grown minerals may all be present in a suite of accessory phases. Thus, the careful characterization of the morphologies of igneous accessory minerals (essentially zircon and baddeleyite) is a prerequisite in the determination of reliable protolith ages.

1.2.2. Metamorphic ages

Metamorphic ages require the same careful characterization of the mineral phases to be dated and indeed are often more complex to determine reliably. Two basic approaches can be used to calculate the timing of metamorphism; a) indirect dating of metamorphism using the ages of cross-cutting intrusions such as dykes, pegmatites and granites, or b) direct dating of metamorphic minerals in the mafic rocks and in related supracrustal rocks (e.g. metasediments). In the former case the ages will essentially be those of

the igneous protoliths and thus, will give only minimum and/or maximum estimates for the age of metamorphism. Only rarely (e.g. syn-metamorphic intrusions) will these data be useful in determining metamorphic ages or cooling and exhumation rates. Direct dating of metamorphism can be constrained by lower intercepts on discordia lines produced by Pb-loss, metamorphic overgrowths or by new grown minerals (Figure L4) or indeed by a combination of these patterns. Metamorphic overgrowths (commonly on zircon) can produce discordia lines which constrain ages indicative of both metamorphism and protolith ages. Nonetheless, apparently simple discordia lines produced by metamorphic Pb-loss often produce lower intercept ages which are geologically meaningless (Mezger and Krogstad 1997). This is due to the fact that secondary Pb-loss from subsequent thermal events or recent Pb-loss can be superimposed onto metamorphic discordia lines. The most reliable ages for metamorphism result from dating of newly grown metamorphic minerals which have concordant ages. In addition, minerals with concordant metamorphic ages can be used to constrain discordia lines (Figure L4). The processes involving the formation of metamorphic accessory minerals are generally poorly understood and difficult to determine. However, some accessory phases grow as a result of reactions which can be constrained (e.g. titanite replacing rutile) or during anatexis (e.g. zircon) which can give reliable PT-estimates. The growth of the relevant phase may occur above its closure temperature (T_c) in which case the age will represent cooling and not growth. On the other hand, if a sufficient number of accessory phases with different closure temperatures can be dated, then the data can be used to determine peak metamorphism and also cooling rates.

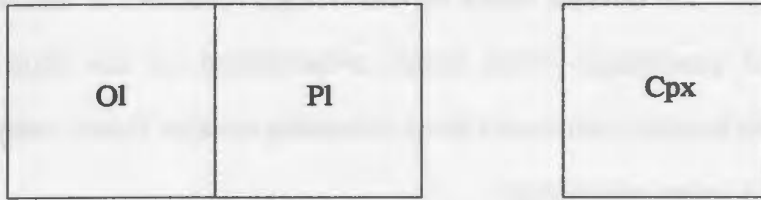
1.3. Summary

Mafic igneous rocks offer the most promising targets for deciphering the PT-history of the crust beneath orogenic belts. Rocks which display coronitic to granoblastic textures are particularly important as they tend to preserve a record of both the peak pressure and peak temperature conditions even at the highest grades of metamorphism. Deformed mafic rocks will typically be retrogressed and by combining the PT-

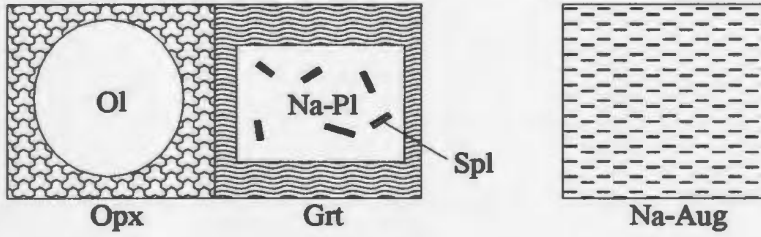
conditions recorded by these rocks with those from undeformed coronite and eclogite, PT-paths from the deepest crustal segments of metamorphic terranes can be established. These PT-paths in turn allow a greater understanding of the tectonic processes operating in collisional orogens. Modern U-Pb geochronology can be applied to mafic rocks and their metamorphosed equivalents. Thus, both the PT-history and the absolute time scales can be determined. The set of four papers which follows deals with a suite of metamorphosed mafic rocks from the Tshenukutish terrane in the Manicougan Imbricate Zone which is one of the best exposed high-P terranes in the Grenville Province.

Figure I.1. Generalised reaction pathways for the transformation from original gabbro, to coronitic and transitional rocks, and finally to eclogite (after Rubie 1990).

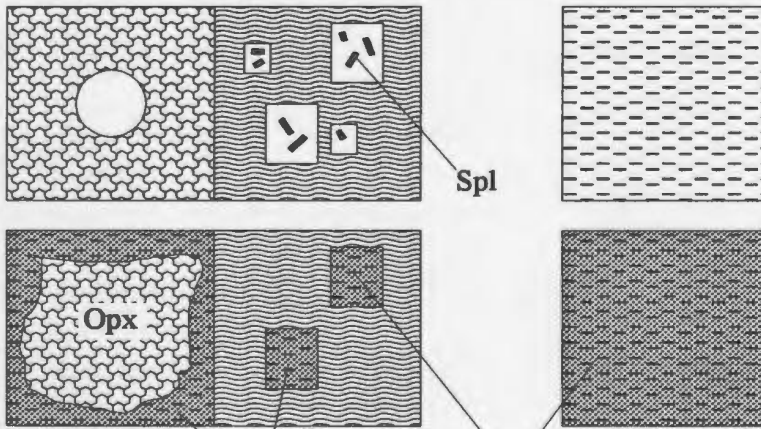
Original Mineral Domains



Corona Stage



Transitional Stage



Increasingly more Na in Cpx

Eclogite

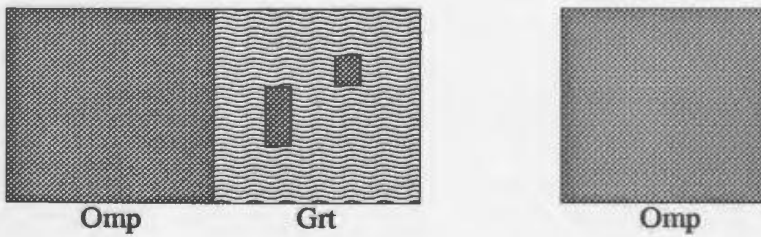
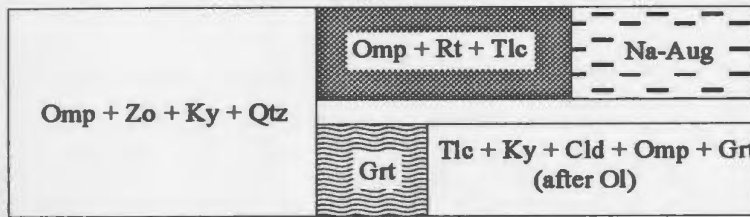
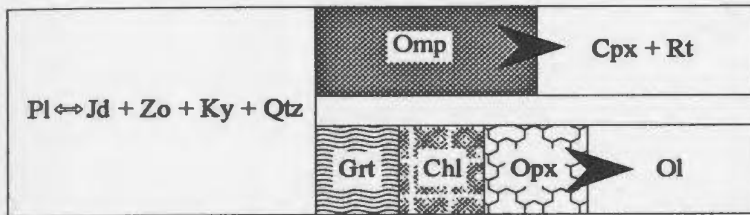


Figure I.2. Two examples of progressive transformation of gabbro to eclogite (figure modified from Rubie 1990). Individual microdomains (and coronas) within the assemblages are shown as separate shaded areas. The reactions and/or mineral assemblages within certain microdomains are also shown. Short arrows represent the direction of grain boundary movement along consuming reaction fronts. Long arrows indicate the prograde transition to the a corona assemblage.

Allalin Gabbro (Western Alps)

ca. 600 °C >20 kbar (Meyer 1983)

Corona Stage



Flemsoy (Western Norway)

ca. 700-800 °C 15-20 kbar (Mork 1986)

Corona stage

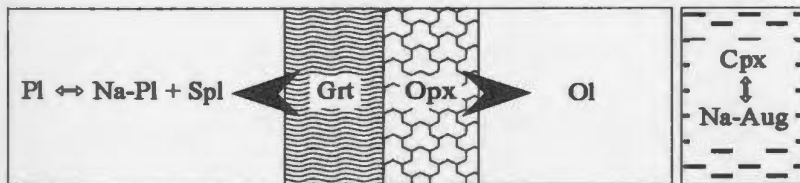


Figure I.3. Simplified reaction pathway showing the retrogression of an eclogitic lens by hydration of the deformed margin and fluid infiltration from the surrounding country rock (after Heinrich 1982).

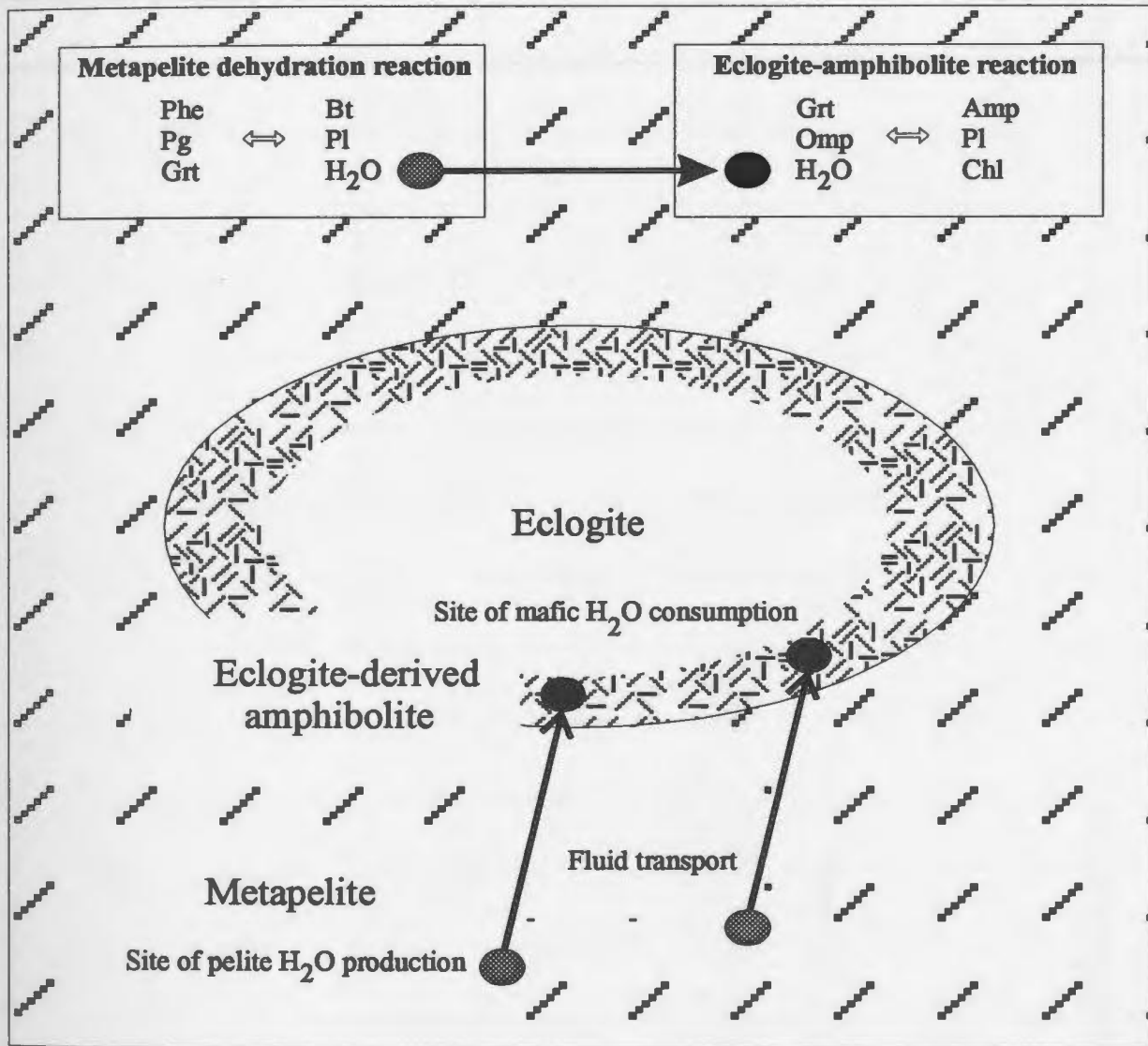
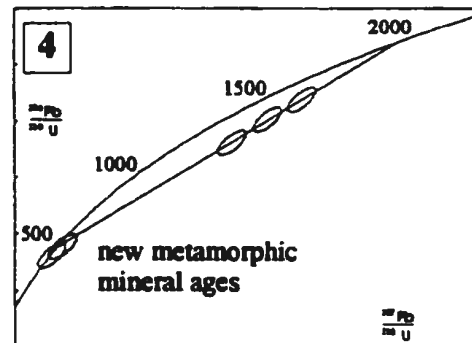
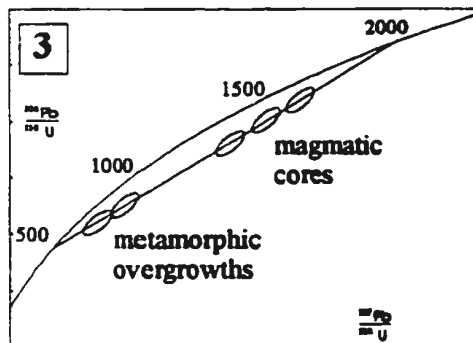
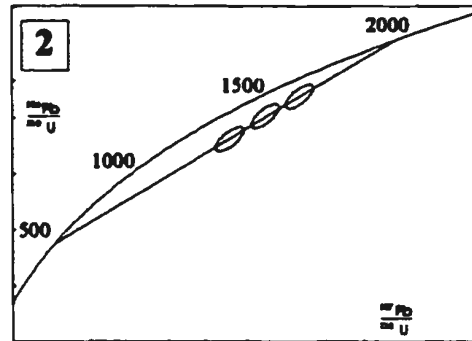
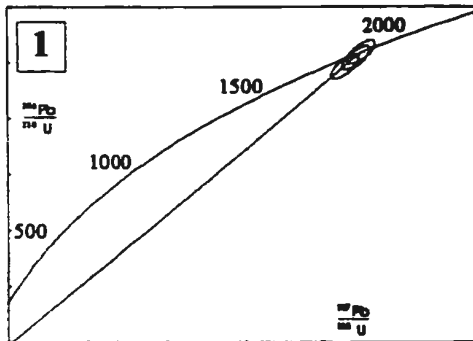


Figure I.4. Representative U-Pb diagrams from mafic rocks showing simplified examples of typical sets of data in metamorphosed samples. Clearly, the example 1 will represent the best case for determining a protolith age. The data in example 4 will most likely give a reliable age for the metamorphic event. The four examples are not mutually exclusive and combinations are possible.



- 1) concordant or near concordant ages with negligible, unspecified (often recent) Pb-loss.
- 2) discordant ages with an ancient Pb-loss event.
- 3) discordant ages with an overprint defined by magmatic zircons with metamorphic overgrowths.
- 4) discordant ages with an overprint defined by ancient Pb-loss possible metamorphic overgrowths and other new (metamorphic) mineral ages.

Petrology and U-Pb geochronology of the mafic and ultramafic, high-pressure metamorphic coronites from the Tshenukutish terrane.

Abstract

Two suites of mafic and ultramafic rocks from the Tshenukutish terrane, eastern Grenville Province, have been the subject of a detailed petrographic and geochemical study combined with U-Pb geochronology. The Tshenukutish terrane is the highest tectonic level in the eclogite-bearing, Manicouagan Imbricate Zone and is divided into two tectonic units, the Baie du Nord segment and the Boundary zone. A suite of mafic and ultramafic rocks, the Lac Espadon suite, forms part of the Boundary zone. The Lac Espadon suite comprises a diverse range of rock types, such as dunite, troctolite, hornblendite and olivine gabbro. Cumulate textures and geochemical characteristics suggest that the Lac Espadon suite represents a layered, mafic and ultramafic complex. In the Baie du Nord segment the mafic rocks sampled comprised of gabbro and anorthosite intrusions, along with smaller, coarse-grained gabbroic intrusions. In contrast to the Lac Espadon suite, the mafic rocks from the Baie du Nord segment represent a fairly homogeneous group of Fe-Ti gabbros and related anorthosites. Rocks of gabbroic composition from both suites have within-plate tholeiite, petrotectonic signatures. Furthermore, REE-patterns of gabbro and associated cumulate rocks in both suites suggest fractionation from a tholeiitic source. All the rocks show abundant petrographic evidence for high-pressure metamorphism, including the widespread development of garnet, clinopyroxene and kyanite-bearing metamorphic assemblages. Estimates of the conditions of high-pressure metamorphism in previous studies and melting textures in deformed and hydrated gabbro margins are in the range 750-900 °C and 16-18 kbar. In the Lac Espadon suite U-Pb ages of igneous zircon and baddeleyite are in the range 1643-1629 Ma for the emplacement of

the layered complex. In the Baie du Nord segment baddeleyite gives an age of 1170 \pm 5 Ma for emplacement of the Fe-Ti gabbros. Ages of high-P metamorphism are constrained by zircon formed during anatexis of deformed and hydrated Fe-Ti gabbro margins at 1046 \pm 3 Ma. Other metamorphic ages include zircons with (metamorphic) overgrowths (1042 \pm 22/-28 Ma), saccharoidal zircon replacing baddeleyite (1030 \pm 10/-7 Ma and 1030 \pm 12 Ma) and new growth of equant zircon (1012 \pm 12 Ma) from the undeformed interiors of samples in both suites of rocks. These ages indicate that the high-P metamorphism of the Tshenukutish terrane occurred during the Grenvillian (Ottawan) event. Retrogression to amphibolite facies is constrained by the ages of titanite (1006-997 Ma) in deformed gabbro margins. Rutile ages range between 960-929 Ma and are interpreted as cooling ages. The difference between the ages of titanite and rutile suggest slow cooling of the Tshenukutish terrane after initial high-pressure and temperature metamorphism and exhumation.

Keywords: Grenville Province, mafic rocks, high-pressure, coronas, U-Pb geochronology

1.1. Introduction

The Grenville Province of the Canadian Shield was formed by continental collision that affected the margin of Laurentia in the interval between 1200-1000 Ma (Grenvillian orogeny, Baer 1981; Windley 1986; Rivers et al. 1989). There is growing evidence that parts of the southern margin of the parautochthonous belt of the Grenville Province experienced eclogite facies metamorphism at 1100-1000 Ma. Evidence of this event has been particularly well preserved in massive and relatively dry coronitic metagabbros (Indares 1993; Indares and Rivers 1995; Indares and Dunning 1997). Textural evidence of the various stages of metamorphic evolution, along with information about the protoliths, tend to be best

preserved in undeformed mafic rocks (Rubie 1990). For these reasons, metagabbros are suitable targets for geochronological studies, since together with their amphibolite margins, they are likely to preserve a variety of accessory minerals with different growth and closure temperatures. Therefore they can be used for both the determination of the age of the protoliths and the timing of metamorphism. To date, the age of Grenvillian metamorphism has been investigated in the western Grenville (e.g. Mezger et al. 1991, 1993; Haggart et al. 1993; van der Pluijm et al. 1994; Jamieson et al. 1995; Friedman and Martignole 1995; Martignole and Reynolds 1997) and chiefly from Labradorian rocks of the eastern Grenville (e.g. Schärer et al. 1986; Schärer and Gower 1988; Phillippe et al. 1993; Connelly et al. 1995; Wasteneys et al. 1997). However, so far very few examples of high pressure (high-P) metagabbros or ultramafic rocks have been dated (e.g. Indares and Dunning 1997).

The aim of this contribution is to document a newly discovered occurrence of high-P, coronitic metagabbros and ultramafic rocks from the Tshenukutish terrane of the Manicouagan Imbricate Zone. These rocks are discussed in terms of their general petrographic and geochemical characteristics, protolith ages and the timing of metamorphism established by U-Pb geochronology.

1.2. Geological Setting

The Manicouagan Imbricate Zone (MIZ) is a 2000 km² stack of high-P crustal rocks recently discovered along the shores of Manicouagan Reservoir in eastern Quebec (Indares 1997). The MIZ is located at the same structural level, but a few tens of km west of the Molson Lake terrane, which contains 1450 Ma gabbros (Shabogamo gabbro, Connelly and Heaman 1993) partially transformed to eclogite during the Grenvillian orogeny (Indares 1993; Indares and Rivers 1995). To the north, both MIZ and Molson Lake terrane overlie the parautochthonous Gagnon terrane along a thrust contact (Figure 1.1a). The Gagnon terrane is a northwest-verging, Grenvillian fold-thrust and nappe belt, with metamorphic

grade increasing from greenschist facies in the north, to high-P amphibolite and locally, eclogite facies in the south. At its southeast margin, the MIZ is truncated by an extensional detachment (Hart Jaune fault, Eaton et al. 1995) which separates it from the overlying 1467 Ma granulites of the allochthonous Hart Jaune terrane. The latter rocks are characterized by a mid-amphibolite facies Grenvillian overprint (Scott and Hynes 1994).

The MIZ consists of two contrasting, fault-bounded lithotectonic units. The lower unit, known as the Lelukuau terrane (LT), is a thrust stack largely composed of anorthosite, olivine-gabbro and granitoid rocks, Labradorian in age and younger leucogranites and related rocks (1648±11/-10 Ma and 1298±8/-5 Ma, igneous zircon, Gale et al. 1994). The LT experienced high-P metamorphism during the Grenvillian orogeny as indicated by U-Pb ages of metamorphic zircon and monazite along with cooling recorded by titanite and rutile (Gale et al. 1994; Indares et al. 1998). Phase relationships in the upper levels of the LT are consistent with P-conditions of 16-18 kbar, at temperatures between 850-900 °C, indicating burial in excess of 50 km under a high thermal regime (Indares 1997). The structurally overlying Tshenukutish terrane (TT) comprises a variety of lithotectonic suites that occur between the LT and Harte Jaune terrane and are bounded by extensional shear zones (Figure 1.1b), the Baie du Nord segment (BNS) in the west, and the Boundary zone in the southeast. The structurally lower BNS is composed of migmatized orthogneiss, locally grading to diorite, which contains rafts of supracrustal rocks. These units have been intruded by Fe-Ti gabbros. Anorthosite has been observed as tectonic layers and lenses within shear zones. The interior of the BNS is variably affected by an early phase of deformation predating the intrusion of the Fe-Ti gabbro, and a later phase that caused boudinage of the gabbro bodies and development of shear zones with evidence of northwest-directed tectonic transport.

The Boundary zone contains mafic and ultramafic rocks known collectively as the Lac Espadon suite (LES), the Hart Jaune granite (1017 Ma, Indares et al. 1998) with rafts of metapelite and the Brien anorthosite (1169 Ma, Scott and Hynes 1994), which occurs as large tectonic lenses (Figure 1.1b). To the

southeast, the Boundary zone is tectonically overlain by the Hart Jaune terrane along the southeast-dipping Hart Jaune extensional shear zone (stage 2 extension, Eaton et al. 1995, Indares 1997) which consists of tectonic layers of granite and amphibolite. The LES is mainly composed of orthogneiss with tectonic enclaves of troctolite, dunite and hornblende, mesocratic olivine-gabbro and also Fe-Ti mafic pegmatite (nelsonite). The latter is restricted to the northern part of the suite and its relationship with the rest of the LES is unclear. The LES is characterized by L-dominant deformation with lineations plunging moderately to the southeast. Shear zones at the boundaries of BNS and LES display evidence of top-to-the-south extension (stage 1 extension, Indares 1997) which truncate earlier thrust related fabrics in the overlying LT as well as the L-fabric in the LES (Indares 1997).

Evidence of high-P metamorphism is mainly indicated by extensive replacement of igneous phases by garnet, clinopyroxene and subordinate kyanite in the mafic rocks of both the BNS and LES, and in the anorthosites of the BNS and the Boundary zone. The margins of the Fe-Ti gabbros of BNS are commonly transformed to granulitic amphibolite. In addition, the amphibolite margins contain up to 20% leucosomes with garnet porphyroblasts which are often several cm in diameter. Conditions of partial melting of amphibolite and associated production of garnet have been experimentally investigated (e.g. Wolf and Wyllie 1994; Senn and Dunn 1994) and documented in naturally occurring samples (Williams et al. 1995). According to these studies, the presence of mafic migmatite, with less than 20% melt in association with large garnet porphyroblasts, suggests fluid assisted melting under PT-conditions of 10-20 kbar and 750-900 °C. In addition, metapelitic rafts in the BNS are extensively migmatized and contain garnet, kyanite and K-feldspar restite, indicative of vapor absent partial melting under P-conditions in excess of 17 kbar at 800-900 °C. Similar PT-conditions are also recorded by rocks in the upper levels of the LT (Indares et al. 1995; Indares 1997). In stage 1 extensional shear zones of the southern BNS, asymmetric rotation of leucosomes and garnet porphyroblasts in the amphibolite margins of the Fe-Ti gabbros, is consistent with the top-to-the-south tectonic transport. This indicates that stage 1 extension

postdated the high-PT metamorphism and associated melting. The orthogneisses of the BNS and LES do not preserve diagnostic high-P mineral assemblages. In the Boundary zone, the Hart Jaune granite postdated the peak of metamorphism, but is deformed by the Hart Jaune shear zone. The metapelites and margins of the Brien anorthosite in the Boundary zone are highly retrogressed and characterized by widespread development of chlorite and epidote.

1.3. Petrography of the Mafic Rocks

1.3.1. Lac Espadon suite (LES)

The coronitic troctolites of the LES preserve relict igneous assemblages represented by olivine, plagioclase, and minor ilmenite. Metamorphic coronas of orthopyroxene, clinopyroxene, pargasitic amphibole and garnet are developed between the olivine and plagioclase (Appendix A, Plate A1.1a-c). Plagioclase has numerous crystallographically oriented inclusions of kyanite and corundum, consistent with metamorphism under high-P conditions (Indares 1993). Coronas of intergrown brown pargasitic amphibole and biotite are found around ilmenite. The presence of both clinopyroxene and pargasite may indicate either incomplete prograde reactions or retrogression of the clinopyroxene by fluid infiltration under high-P conditions. Coronitic troctolites grade into coarse-grained dunite, implying igneous layering. The dunites are dominated by fosterite-rich olivine with orthoamphibole (Appendix A, Plate A1.1d) and serpentine (antigorite), as well as minor opaques. Adjacent to shear zones troctolites grade into granoblastic amphibolites with relict olivine, and metamorphic garnet porphyroblasts, orthopyroxene and hornblende.

Small pods of coarse-grained, poikilitic hornblendite are found in close association with dunite and troctolite in the LES. Hornblendites are a feature of many intrusive complexes (eg. Muir et al. 1997; Sisson et al. 1997). Hornblende occurs as oikocrysts up to 10 cm in diameter that, in association with

large 2 cm phlogopitic micas, form subhedral, high-relief plates in thin section and comprise over half these rocks. Clinopyroxene crystals, 5 cm in diameter, locally reach high concentrations, (i.e. pyroxene hornblendite). Chadacrysts of olivine and plagioclase with minor opaque minerals and apatite are identifiable within hornblende oikocrysts. Chadacryst populations vary from high amounts of plagioclase to equal amounts of plagioclase and olivine (Appendix A, Plate A1.2a-b). Although there are no clear contacts between the hornblendites and other mafic units, the increase in modal plagioclase shown by the transition from dunite to troctolite, and the same trend in chadacryst populations within hornblendite, may reflect an increase in plagioclase formation in the magma. The hornblendites show abundant evidence of high-P metamorphism. Garnet forms coronas around plagioclase chadacrysts with both containing numerous inclusions of kyanite and corundum that are oriented parallel to cleavage in the plagioclase. Olivine chadacrysts have orthopyroxene and clinopyroxene coronas. Granoblastic clinopyroxene aggregates are randomly distributed, replacing plagioclase or primary clinopyroxene.

Small lenses of garnet amphibolite outcrop adjacent to the hornblendites. The garnet amphibolites are variably foliated, and are composed of euhedral to subhedral garnet porphyroblasts, plagioclase, hornblende and biotite with lesser amounts of rutile, titanite+/-ilmenite (Appendix A, Plate A1.4a-b). An outcrop of massive, coarse-grained, Fe-Ti mafic pegmatite occurs near the northern margin of the LES. The rock is characterized by large (1 to 5cm) apatite and ilmenite crystals. Similar rocks have been designated as nelsonite and have been reported from other Grenvillian terranes (e.g. Florence et al. 1995). Original pyroxene and plagioclase have been recrystallized, with clinopyroxene being replaced by hornblende. Plagioclase contains spinel-rich areas and sparse, cleavage-oriented corundum inclusions. Hornblende and garnet form irregular coronas between ilmenite and plagioclase (Appendix A, Plate A1.5a-b). Dark brown (Ti-rich) biotite occurs as inclusions in plagioclase and garnet, as intergrowths with hornblende, and in coronas around ilmenite. Small, clear plagioclase collars form between garnet

and hornblende. The relationship between this rock and the mafic and ultramafic rocks of the LES is not clear.

Olivine gabbros of the LES are coarse-grained and mesocratic. They show poikilophitic texture, with the original assemblage consisting of plagioclase, olivine, and interstitial clinopyroxene. Large (0.5 to 1 cm) apatites are common, with large rutile crystals and minor ilmenite also present (Appendix A, Plate A1.6a-b). Original plagioclase has been recrystallized and contains numerous kyanite and corundum plates. Olivine has been all but replaced by aggregates of orthopyroxene, surrounded by coronas of clinopyroxene and garnet. Locally plagioclase collars form in the coronas between garnet and clinopyroxene, commonly in association with pargasite. These may be the result of growth during decompression (Indares 1993). Pargasite also forms around original euhedral biotite, ilmenite and clinopyroxene.

The common occurrence of cumulate textures (dunites, troctolites and hornblendites) and the close association of the mafic to ultramafic units in the LES suggest that these rocks may represent dismembered portions of a layered intrusion.

1.3.2. Baie du Nord segment (BNS)

In the BNS, Fe-Ti gabbros show a range in both igneous and metamorphic mineralogy and textures. Igneous textures are variably preserved in the form of relict plagioclase and clinopyroxene and fine grained, rounded orthopyroxene aggregates after olivine (Appendix A, Plate A1.7a). Ilmenite and apatite are common constituents of the original igneous assemblage. Coronas of pargasite, with intergrown biotite/phlogopite around ilmenite, are present in many samples. Orthopyroxene aggregates are surrounded by clinopyroxene and garnet coronas. Garnet locally pseudomorphs the lath shape of the igneous plagioclase. Plagioclase collars between garnet and clinopyroxene (Appendix A, Plate A1.7b-d) are common and are evidence of decompression (Indares 1993). These are most common in samples

where garnet forms pseudomorphs after plagioclase (Appendix A, Plate A1.8a), indicating extensive re-equilibration following high-P garnet growth. Other samples are more granoblastic, with coronas less well preserved. Relict clinopyroxene and plagioclase contain numerous inclusions of an opaque phase, which leads to a distinctive clouded appearance and locally plagioclase also contains corundum. In addition, the northern margin of the BNS contains gabbros with assemblages dominated by omphacite-garnet and only sparse (less than 5%) relics of plagioclase containing high concentrations of spinel and corundum inclusions (Appendix A, Plate A1.9a). These represent rocks which are closest to "true" eclogites (Carswell 1990). Large plagioclase and olivine crystals occur in some of the Fe-Ti gabbros and are interpreted to be xenocrysts (Appendix A, Plates A1.8b and A1.9b). The Fe-Ti gabbros grade into more leucocratic varieties with a higher plagioclase/ilmenite ratio and are considered to be leucocratic portions of zoned intrusions, as opposed to true anorthosite bodies. However, the North Bay anorthosite is different, being granoblastic, with strongly recrystallized plagioclase and minor hornblende, garnet, biotite, ilmenite and rutile (Appendix A, Plate A1.10a). The North Bay anorthosite may be correlated with the Brien anorthosite.

Coarse-grained Fe-Ti gabbros also occur in the western and northern margins of the BNS (marginal gabbros). These gabbros display relicts of clinopyroxene, plagioclase and lesser amounts of olivine, ilmenite and large, 1-2 cm crystals of apatite (Appendix A, Plate A1.10b). Olivine is variably replaced by orthopyroxene. Plagioclase is strongly recrystallized and displays cleavage-oriented spinel and corundum inclusions. Extensive collars of plagioclase with pargasite, are present between garnet and clinopyroxene, implying decompression and hydrous retrogression.

In the leucosome-bearing, amphibolite margins of the Fe-Ti gabbros, primary textures are overprinted by granoblastic assemblages. The large garnet poikiloblasts occur within the leucosomes (Appendix A, Plate A1.11a) with cores rich in inclusions of quartz, plagioclase, ilmenite and rutile and inclusion-free rims (Appendix A, Plate A1.11b). Inclusions form sigmoidal trails indicating rotation of

the garnet poikiloblasts during growth. Titanite occurs mainly in the rims and along cracks in the garnet and is concentrated around rutile, and thus, post-dated rotation (Appendix A, Plates A1.11c-d). The matrix assemblage consists of hornblende, plagioclase, quartz, ilmenite, biotite and titanite+/-rutile. Titanite in the matrix is less abundant and smaller in grain-size than within the garnet, probably reflecting the involvement of rutile and garnet during the titanite-forming reaction.

1.4. Geochemistry

1.4.1. Analytical techniques

Geochemical analysis of representative rock samples was carried out at the Department of Earth Sciences, Memorial University of Newfoundland. XRF-elemental analysis was performed using a Fisons/ARL 8420+ sequential wavelength dispersive X-ray spectrometer on pressed pellets (5 g of fine, dried rock powder and 0.7 g of phenolic resin) for trace-elements and major-elements in samples with high Fe-content. Major-element compositions on the majority of samples were determined using fused beads (1.5 g of rock powder, 6 g of lithium metaborate and 1.5 g of lithium tetraborate). Detection limits for pressed pellets range from 0.7 ppm (Nb) to 41 ppm (Ce) with precision around 0.2% to 3.1%. Fused beads have detection limits of 0.006% (K₂O and TiO₂) to 0.079% (Al₂O₃) with precision ranging from 0.2% to 3.2%. Samples are compared with Govindaraju-1989 and 1 internal standard. Loss on ignition (LOI) was determined by weighing powders before and after drying at 1050 °C.

REE-concentrations were determined by Na-sinter analysis with a Perkin-Elmer SCIEX ELAN model 250 ICP-mass spectrometer. Detection limits range from 0.001 ppm for Lu to 0.015 ppm for Yb. Samples are compared with Chondrite, Govindaraju DNC-1, MRG-1, BR-688 and W-2 standards as well as 4 internal standards and blank solutions. Mean precision is better than 10%.

1.4.2. Tectonic discrimination of gabbros

Table 1.1 shows major and trace-element compositions of representative mafic rocks from the TT. In general, the major-element compositions mirror the major mineralogy with the troctolites, dunites and hornblendites being more Mg-rich than other gabbroic rocks in the TT (Table 1.1) in accordance with their ultramafic nature. Similarly, the olivine gabbros (LES) and Fe-Ti gabbros and anorthosites (BNS) are more plagioclase rich and consequently higher in Ca and Na. However, there is considerable overlap in the overall variation displayed by the major-element compositions of the rocks.

The troctolites, dunites and hornblendites of the LES and the anorthosite intrusions (BNS) have cumulate textures and therefore do not represent liquid compositions. Only the olivine gabbros from the LES and Fe-Ti and marginal gabbros from the BNS are likely to be representative of magmatic liquid compositions and thus, can be used in tectonic discrimination diagrams. All these samples show a tholeiitic trend using the classification diagram of Irvine and Baragar (1971) for major-element data (Figure 1.2a). However, the Fe-Ti gabbros (BNS) are the only group which display a within-plate tholeiitic character (Figure 1.2b-c) using the classification diagrams of Meschede (1986) and Pearce and Cann (1973). The olivine gabbros from the LES and the marginal gabbros of the BNS are not well constrained to any particular field and in particular seem to show a depletion in Zr. A further suite of diagrams (Figure 1.3a-d) show a general within-plate tholeiitic signature for the samples but there is a spread in both the Zr and Ti-contents. For example, in Figure 1.3a although the Y/Zr ratios are similar for all samples there is considerable variation in Zr-concentrations leading to samples which plot outside the fields defined. In Figure 1.3c-d a similar pattern exists with Ti-contents lying outside the petro-tectonic fields defined (Floyd and Winchester 1975; Pearce 1982) but displaying restricted Y/Nb and Nb/Y ratios. This is most likely due to fractionation of both Zr and Ti-bearing phases during

crystallization. The abundance of ilmenite in the BNS samples and the presence of both zircon and baddeleyite in several of the mineral separates (see *Section 1.5*) supports this interpretation. The LES olivine gabbros are probably petrogenetically related to the cumulates (dunites, troctolites and hornblendites) of the LES. Similarly, although the marginal gabbros of the BNS may be related to the main Fe-Ti gabbros (BNS), the coarse grain size and spread of some of the trace-element data points to either open system behavior, fractionation, or the possibility that these analyses may not represent liquid compositions.

1.4.3. REE distribution

REE-concentrations for selected samples are shown in **Table 1.2**. REE-fractionation was modeled for the LES ultramafic samples, nelsonite and the BNS anorthosites and marginal gabbros. All the fractions were assumed to have resulted from cumulate formation which is represented by the following formula;

$$C_r/C_o = (1 - F)^{(D-1)}$$

where,

C_r represents the concentration of a REE in the cumulate,

C_o represents the concentration of the REE in the parent liquid,

F is the fraction of melt remaining and,

D is the bulk distribution coefficient.

Bulk distribution coefficients were calculated using the mineral data from Arth (1976) for phlogopite, Schock (1979) for magnetite/ilmenite, Fujimaki et al. (1984) for olivine, plagioclase, clinopyroxene and hornblende and Fujimaki (1986) for apatite. For samples which contained biotite instead of phlogopite an average K_d using the data from Mahood and Hildreth (1983) and Arth (1976) was taken. Starting compositions were assumed to be of a within-plate tholeiite character with REE-fields defined by data in Dostal et al (1984).

The primitive-mantle normalized REE-patterns for the gabbroic rocks of the LES and BNS are shown in Figure 1.4a-b. In general, the variations between the gabbro HREE-patterns in each individual suite probably reflect variation in modal igneous olivine and clinopyroxene which have distribution coefficients an order of magnitude greater for HREE over plagioclase (e.g. Fujimaki et al. 1984; Messiga et al. 1995). The differences in MREE and LREE are likely controlled by apatite and plagioclase (e.g. Fujimaki et al. 1984; Fujimaki 1986). The patterns for both the BNS and LES gabbros correspond well to within-plate REE-signatures (Dostal et al. 1983, shaded field in Figure 1.4a-b).

The cumulates in the LES show significant fractionation of REE which reflect the mineral compositions and textures. The dunites are generally REE-poor with some HREE-enrichment whereas the troctolites are more light REE-enriched and have large, positive Eu-anomalies (Figure 1.4c) reflecting the increased plagioclase content. REE-fractionation was modeled assuming a 20% fractionation of cumulate material with 30% olivine and 70% plagioclase using the starting composition of the within-plate field (Figure 1.4a-b). The resulting field (shaded area) corresponds well to the overall patterns of the troctolites, although one rather REE-poor sample lies outside the modeled concentrations. Hornblendites show LREE and MREE-enrichment over the dunites and troctolites (Figure 1.4d), directly reflecting the hornblende (MREE) and to a lesser extent phlogopite (LREE), which comprise the bulk of these samples. Modeled compositions assuming a 20% fractionate with 2.5% plagioclase, 2.5% olivine, 15% phlogopite and 80% hornblende show a less satisfactory fit however. The MREE and HREE show a reasonably

similar trend, albeit with the modeled field narrower than the samples themselves. In contrast, the Eu and LREE-concentrations are higher in the hornblendites than in the modeled samples. This may be due to underestimation of the plagioclase contents, or the influence of apatite which is present in trace amounts in all the rocks. Alternatively the starting compositions or indeed the distribution coefficients may not be accurate.

The nelsonite (LES) is LREE-enriched (Figure 1.4d), similar to the gabbros from both the LES and BNS, and it is likely the abundance of apatite (ca. 5-10%) which produces a strong enrichment in LREE and MREE. The modeled REE-compositions were calculated assuming 30% fractionation of cumulate material with 50% plagioclase, 25% biotite, 10% clinopyroxene, 10% ilmenite and 5% apatite. The modeled results and the single REE-pattern obtained on the nelsonite are very similar (Figure 1.4d). Given the reasonable agreement between the modeled REE-fractionation patterns and the measured REE-concentrations in the rocks themselves, it is interpreted that the ultramafic samples in the LES represent cumulates fractionated from tholeiitic magmas similar to those which formed the olivine gabbros. The origin of the nelsonite remains enigmatic. Nelsonites are associated with anorthositic magmas (e.g. Florence et al. 1995). The sample displays a highly LREE-enriched pattern and thus, either the source of the melt was correspondingly enriched in LREE and/or the parent melt experienced a high degree of fractionation and HREE-depletion during high-level, crustal emplacement. Given the evidence displayed by the intrusions in the LES for tholeiitic within-plate magmatism and strong fractionation, the second scenario is favored. In conclusion, the LES represents rocks which all crystallized or fractionated from continental tholeiitic magmas.

The marginal gabbros in the BNS (Figure 1.4d) show similar patterns to the Fe-Ti gabbros. However, the marginal gabbros do show significant variation in MREE and HREE even between the two sample analysed. This, along with the trace-element patterns (Figure 1.2 and 1.3), strongly suggests some kind of fractionation. The modeled REE-patterns (Figure 1.4e) were calculated assuming a within-plate

tholeiitic parent melt and 30% fractionation of 25% plagioclase, 50% clinopyroxene, 10% ilmenite, 10% phlogopite/biotite and 5% apatite. Although the patterns overlap there is clearly a difference in the shapes of the patterns overall and one marginal sample shows significantly higher HREE-contents. This may be explained by enrichment in HREE by the presence of zircon, or that the modeled fields are unrealistic based on the starting melt compositions and the distribution coefficients used. The anorthosite samples in the BNS show the same overall REE-pattern as the Fe-Ti gabbros (Figure 1.4a and d). However, the lower LREE and HREE along with the positive Eu-anomalies in the anorthosites reflect the lower ilmenite, clinopyroxene and olivine, and the higher plagioclase contents. The modeled REE-patterns were calculated assuming 30% fractionation of 80% plagioclase, 10% ilmenite, 5% clinopyroxene and 5% phlogopite/biotite. The measured and modeled REE-patterns are in excellent agreement.

An interesting point to note is that, despite the textural evidence for fluid-assisted partial melting and retrogression, the major and trace-element compositions (sample 313, Table 1.1) and REE-pattern (Figure 1.4c) of the subordinate, migmatitic garnet amphibolite margin is identical to the main Fe-Ti gabbros in the BNS. Thus, despite melting and retrogression the chemical composition of the rock was not significantly changed, suggesting that the leucosomes and garnet poikiloblasts, which form part of the rock sample are indeed a localized phenomenon and unlikely to be the product of magma mixing or later melt injection.

1.5. U-Pb geochronology

1.5.1. Sample selection

Seven representative samples were chosen for U-Pb geochronology (Figure 1.1b) in order to establish the age of the protoliths and constrain the age of metamorphism. Samples of hornblendite (LES 1) and olivine gabbro (LES 2) were collected from the LES, representing the ultramafic and mafic units

respectively. The nelsonite (LES 3) was sampled to determine the temporal relationship between this intrusion and the rest of the TT. Garnet amphibolite (LES 4) was also sampled in order to constrain the timing of metamorphism and retrogression. Two representative Fe-Ti gabbros (BNS 1 and BNS 2) were selected. Sample BNS 1 is coronitic with high-P assemblages well preserved and limited secondary plagioclase/pargasite collars. Sample BNS 2 (transitional metagabbro) shows complete replacement of the igneous mineralogy by high-P assemblages but also extensive secondary plagioclase growth. Migmatitic-garnet amphibolite (BNS 3) from the Fe-Ti gabbro margins was sampled to determine the age of melting and also amphibolite retrogression. The large size of the garnets (5-10 cm) in sample BNS 3 enabled the extraction of mineral separates from garnet poikiloblasts and matrix independently. This was done to examine the effects of armoring by the garnets and evaluate any age difference between the inclusion assemblages and the matrix assemblages.

Individual zircon and baddeleyite grains were mounted on stubs and gold-coated. The grain mounts were examined using a Hitachi S-570 scanning electron microscope (SEM) with an accelerating voltage of 20 kV and a beam current of 100 μ A. Selected zircon grains were also mounted in resin, polished, carbon coated and examined using the same SEM in back-scattering mode. Cathodoluminescence (CL) images were obtained on a number of zircons using a Cambridge Instruments CL-unit on the SEM housed in the Physical Sciences Unit at the University of Glasgow. These grains were examined using an accelerating voltage of 20 kV and beam currents of between 0.1-0.01 mA.

1.5.2. U-Pb method

Accessory mineral fractions were obtained from the samples described above by Wilfley table, Frantz magnetic separator and heavy liquid separation. Fractions were picked under ethanol and air-abraded which has been shown to improve concordance (Krogh 1982), except the very smallest fractions (indicated in Table 1.3.) Fractions were then cleaned with 4N HNO₃, doubly distilled H₂O and distilled

acetone, then weighed and spiked with mixed $^{205}\text{Pb}/^{235}\text{U}$ tracer solution and dissolved with 8N HNO_3 and conc. HF for 5 days at 210 °C in teflon bombs. Ion exchange chemistry (after Krogh 1973) used DOWEX analytical grade AG1-X8 anion exchange resin in chloride form. The purified U and Pb were mounted together on single Re-filaments with silica gel and H_3PO_4 . Isotopic ratios were determined using a Finnigan-MAT 262 thermal ionization mass spectrometer in static mode, with faraday cups calibrated against NBS 981. The ^{204}Pb signal and both U and Pb isotope compositions for small samples were measured by peak jumping in the secondary electron multiplier-ion counter, which was calibrated using known faraday data. Ratios are corrected for U and Pb fractionation at 0.1%/AMU using repeated measurements of NBS standards and for laboratory blanks (2-12 pg Pb, 1 pg U). Composition of common-Pb above procedure blanks was estimated using the model of Stacey and Kramers (1975). Uncertainties on isotopic ratios were determined using an unpublished error propagation program and linear regressions follow the method of Davis (1982). Uncertainties in final age determinations are reported at the 95% confidence interval. Further details of the method are reported in Dubé et al. (1996).

1.5.3. U-Pb results: Lac Espadon suite (LES)

Sample LES 1 (hornblendite): Irregular zircons up to 400 μm in diameter, with some euhedral faces were recovered from sample LES 1 (Appendix A, Plate A3.1a). The presence of irregular zircon produced in the later stages of mafic crystallization has been documented in other Grenvillian gabbros (e.g van Breemen et al. 1986). CL and BS-SEM images (Appendix A, Plate A3.1b-c) show oscillatory zoning which is usually only associated with crystals of igneous origin. No metamorphic overgrowths or inherited segments were observed. Zircons with the same morphology, but showing a brown, turbid appearance indicative of α -particle damage in the crystal, are also present. The turbid appearance may indicate higher U-content and metamict structure. Two populations of baddeleyite were present in the sample. These consisted of small (50 μm), clear, pale brown blocks and prisms with cleavage parallel to

faces (Appendix A, Plate A3.1d) and small, brown to green, elongated crystals (Appendix A, Plate A3.1e). In addition sample LES 1 contained saccharoidal zircons, forming 20-200 μm , clear, rounded prisms and a second population of elongate, brown, sugary zircons (Appendix A, Plate A3.1f-g). Both saccharoidal zircon populations typically contained small baddeleyite inclusions. Thus, saccharoidal zircon populations appear to represent pseudomorphs after baddeleyite. This type of zircon replacement of baddeleyite is documented elsewhere (Davidson and van Breemen 1988; Heaman and LeCheminant 1993; Dudás et al. 1994) with extensive replacement of baddeleyite requiring, in general, much higher grades of metamorphism than partial replacement (Davidson and van Breemen 1988; Patterson and Heaman 1991). The U-Pb isotope data (Table 1.3) from zoned, irregular zircon prisms (Z1 and Z2), saccharoidal zircon (Z4 and Z5) and baddeleyite (B1, B2 and B3) define a discordia line (Figures 1.5a and 1.5b). The upper intercept gives an age of 1643 \pm 5 Ma and a lower intercept age of 1030 \pm 12 Ma (20% probability of fit). These ages are interpreted as the age of the igneous protolith and high-grade metamorphism respectively. The line omits the high-U and Th igneous zircons (Z3), and colored saccharoidal zircon (Z6, Z7) which have apparently undergone Pb-loss after metamorphism. The metamorphic zircon fractions (Z4 and Z5) have preserved some inherited component from the baddeleyite, and the lower intercepts are likely to represent growth ages for these populations. Sample LES 1 also contained one fraction of small, clear, bright yellow and red rutile prisms, the analysis of which is discussed with sample LES 2 below.

Sample LES 2 (olivine gabbro): Irregular, zircon crystals (Appendix A, Plate A3.2a), similar to those found in sample LES 1, were also recovered from the olivine gabbro (LES 2). BS-SEM images show oscillatory zoning likely of igneous origin and no metamorphic overgrowths, although the grains are clearly fragmented (Appendix A, Plate 2b). The sample also contained abundant large, dark, red/brown prisms and fragments of rutile (three fractions). In sample LES 2 the four zircon fractions give an upper intercept age of 1629 \pm 17/-11 Ma and a poorly constrained lower intercept of 854 \pm 111/-103 Ma with a 13% probability of fit (Figure 1.6a). This age is within error of the cumulate hornblendite (LES 1) age

and thus, interpreted as the protolith age of the later stages of magmatic activity which formed the mafic and ultramafic rocks of the LES. In addition, the lower intercept of the discordia line suggests Pb-loss at the later stages of post-metamorphic cooling, the age of which is more precisely constrained by the rutile populations. Rutile from both samples LES 1 and LES 2 define a discordia line which gives an upper intercept age of 929 ± 4 Ma (73% probability of fit, Figure 1.6b) with recent Pb-loss.

Sample LES 3 (nelsonite): In sample LES 3 zircons ranged from 100–400 μm in diameter, with rounded overgrowths on irregular crystals which occasionally display euhedral, prismatic faces (Appendix A, Plate A3.2c). Similar zircon morphologies have been reported from metamorphosed mafic rocks in the Grenville (e.g. van Breemen et al. 1986; Pehrsson et al. 1996). These have been interpreted as irregular, igneous zircons with rounded overgrowths which result from partial resorption and new crystallization during metamorphism. CL images reveal that these grains contain large cores with complex zonation and irregular overgrowths (Appendix A, Plate A3.2d). The four analysed fractions lie on a discordia with a 17% probability of fit, giving ages of $1042 \pm 22 \text{--} 28$ Ma with a poorly constrained upper intercept at $1596 \pm 129 \text{--} 99$ Ma (Figure 1.7a). These ages suggest that the zircons in LES 3 are indeed strongly affected by metamorphism (in the form of overgrowths) but still contain an inherited igneous component. The igneous age while poorly constrained suggests nelsonite emplacement at a similar time to the other mafic and ultramafic rocks of the LES.

Sample LES 4 (garnet amphibolite): Titanite was found in sample LES 4 forming light colored fragments of prisms which range in diameter from 0.5–0.25 mm, often with small rutile inclusions. The rutile inclusions were removed before or after air abrasion. All three fractions are concordant with fraction T2, the most precise (-0.25% discordant) giving an age of 1004 ± 4 Ma (Figure 1.7b). This age represents the time of retrograde metamorphic growth of titanite replacing rutile, or the age of cooling though the closure temperature of titanite.

1.5.4. U-Pb results: Baie du Nord segment (BNS)

Sample BNS 1 (coronitic Fe-Ti gabbro): In sample BNS 1 small amounts of brown, 20-40 μm blocks of baddeleyite and clear, saccharoidal prisms of zircon were recovered. Baddeleyite gives an igneous protolith age of 1170 \pm 5 Ma (Figure 1.8a) based on the concordant fraction (B2). Three analyses of saccharoidal zircon are closely clustered and Z2 overlaps concordia with $^{206}\text{Pb}/^{238}\text{U}$ age of 1023 Ma and a $^{207}\text{Pb}/^{206}\text{Pb}$ age of 1030 Ma. Analysis Z3 is less reliable due to a higher proportion of common-Pb but the $^{206}\text{Pb}/^{238}\text{U}$ is 1032 Ma. An age of 1030 \pm 10/-7 Ma is based primarily on Z2, but overlaps the most reliable data from the three fractions analysed. These ages are interpreted as the age of magmatic emplacement of the Fe-Ti gabbro and high-P Grenvillian metamorphism respectively.

Sample BNS 2 (transitional metagabbro): Sample BNS 2 (transitional metagabbro) contained angular zircon fragments (Appendix A, Plate A3.2e) which revealed rather irregular zones in CL, indicative of metamorphic growth (Appendix A, Plate A3.2f). The sample also contained rounded multifaceted grains (Appendix A, Plate A3.2g). Similar rounded zircon morphologies have been documented in several high-grade metamorphic terranes (e.g. Peucat et al. 1982; Paquette et al. 1989, 1995; Kalt et al. 1994; Creaser et al. 1997; Jeackel et al. 1997). Both fractions analysed are nearly concordant but with large uncertainties and gave $^{206}\text{Pb}/^{238}\text{U}$ ages of 1012 \pm 12 Ma and 988 \pm 12 Ma. Both analyses are sensitive to the common-Pb correction applied. The age of 1012 \pm 12 Ma may be valid for both populations (Figure 1.8b) if Z1 experienced some Pb-loss. This age overlaps those of the saccharoidal zircons in samples LES 1 and BNS 1 and is interpreted as dating high-P metamorphism although not precisely.

Sample BNS 3 (migmatitic-garnet amphibolite): From this sample two populations each of zircon, titanite and rutile were recovered. The first population of zircon consisted of small, multi-faceted, equant grains recovered from the matrix (Appendix A, Plate A3.2g). The second population of subhedral, elongated zircons with prismatic faces (Appendix A, Plate A3.2h) was found in both the matrix and

garnet porphyroblast separates. The equant, multi-faceted zircon morphology is typical of high-grade sub-solidus growth, whereas the elongated prismatic nature of the second population is more typical of those formed in magmatic liquids (e.g. Peucat et al. 1982; Paquette et al. 1989, 1995; Kalt et al. 1994; Jeackel et al. 1997). Thus, the analysis of these populations may permit determination of the timing of melting and sub-solidus development of the dominant textures in the sample. Titanite forms pale brown prisms replacing garnet and rutile, which are typically found as large inclusions (Appendix A, Plate A3.3c). Inclusions were removed before dissolution of the titanites. The crystals extracted from the matrix were smaller (0.25 mm) than those in garnet poikiloblasts (1 mm). Matrix and poikiloblast fractions were analysed separately. Rutile from sample BNS 3 was also analysed. In the matrix separates rutile forms elongated, yellow to dark brown prisms. These show a large variation in grain size (0.2-3 mm). Rutile from the garnet porphyroblasts is more angular but has similar color and grain size variations. Fractions were analysed as large and small grain sizes (Appendix A, Plate A3.3a-b) independently from each of the garnet and matrix separates.

Sample BNS 3 yields the most information in terms of metamorphic history. One zircon fraction (Z3) is concordant at 1041 Ma and is overlapped by three other fractions, two of elongated zircons from garnet and one abraded equant fraction from the matrix (Figure 1.9a). Two further fractions are discordant (Z1 and Z4, Figure 1.9a). Although the morphologies suggest that elongated and equant zircons may be different in origin, any age difference between the two populations in the sample is not resolvable. The best fit line for five of the six zircon fractions gives an age of 1046 ± 3 Ma (21% probability of fit). The Z1-population (Figure 1.9a) is an unabraded, equant fraction from the amphibolite matrix, and lies above this line. This may indicate later metamorphic growth which was either not present in the other fractions or may have been removed by abrasion. Large, 1 mm titanite inclusions from the garnets in sample BNS 3 give an age of 1006 ± 5 Ma (T4, -0.05% discordant). The smaller, 0.25 mm matrix titanite (T1 and T2, stipple pattern) give an age of 997 ± 3 Ma (T1, 0.2% discordant, Figure

1.9b). These ages, while very close, may reflect the closure temperatures for the different titanite grain sizes, or different growth events. Similarly, larger (4 mm) and smaller (0.25 mm) grain-size fractions of rutile give ages of 960 ± 6 Ma (R4 and R5, 0.04% discordant) and 946 ± 2 Ma (R1, R2 and R3, discordia line with 94% probability of fit), respectively (Figure 1.9c). The ages are independent of whether the rutiles were separated from the garnet poikiloblasts or matrix. Interestingly, the U-contents of the matrix titanite and rutile are significantly higher than for the garnet-hosted grains. However, the reason for this is not clear, although low U-contents in the garnet and the partial breakdown of U-bearing minerals in the matrix are possible explanations.

1.6. Discussion

1.6.1. Intrusive relationships and protolith ages

The mafic units of the TT have a similar petrotectonic setting (i.e. tholeiites and within-plate tholeiites) to many of the gabbros from the eastern Grenville Province (Gower et al. 1991a). The gabbroic rocks and cumulates from the LES are coarse grained and represent extensively fractionated magmas. The density of tholeiitic magma varies with pressure from 2.6 gm/cm^3 at surface conditions to 3.4 gm/cm^3 at 20-30 kbar (Kushiro 1980). The hornblende and olivine fractionation recorded in the LES mafic intrusions could have occurred over a wide range of crustal depths. The Fe-Ti gabbros from the BNS are dominated by plagioclase fractionation which occurs in tholeiitic melts at ca. 5 kbar (15 km) or less. Thus, these rocks were probably emplaced at higher crustal levels than those in the LES. The marginal gabbros from the BNS and the nelsonite from the LES represent melts which are the most enriched in LREE. The BNS marginal gabbros and LES nelsonite contain xenocrysts and inherited zircon respectively. This strongly suggests a high crustal level of emplacement.

The current available U-Pb ages from the Manicouagan Imbricate Zone are summarized in Figure 1.10. The ca. 1643-1629 Ma (Labradorian) age range for the most precisely dated mafic and ultramafic rocks from the LES is similar to the age for the anorthosite complex in the tectonically underlying LT (Gale et al. 1994; Indares et al. 1998). Mafic rocks from the two areas also have similar general characteristics (e.g. troctolites, fractionated mafic units) suggesting that the mafic rocks in the LES may be dismembered parts of the anorthosite complex of the LT. Labradorian anorthosites and mafic complexes also occur elsewhere in the eastern Grenville Province (e.g. Phillippe et al. 1993; Gower 1996), but they were not previously known to extend this far west. Thus, the Labradorian igneous activity which is characteristic of many parts of the eastern Grenville can now be seen extending west to the MIZ.

The 1170 \pm 5 Ma age for the Fe-Ti gabbros from the BNS is identical to the Brien anorthosite in the Boundary zone (1169 \pm 2 Ma, Scott and Hynes 1994) but is somewhat younger than the North Bay anorthosite (ca. 1250-1200 Indares et al. 1998). Fe-Ti gabbros with the same age are also found in the Wakeham terrane to the south (Martignole et al. 1994) and across western Grenville (e.g. Davidson and van Breemen 1988; Heaman and LeCheminant 1993; Indares and Dunning; 1997). Mafic rocks of this general age (1250-1160 Ma) in the Grenville are thought to be related to extension, removal of mantle lithosphere and asthenospheric up welling that occurred after the Elzevirian, crustal-thickening event (Corrigan and Hanmer 1997, Rivers 1997). Thus, ages of the Fe-Ti gabbros and anorthosites may represent similar magmatic activity in the BNS.

1.6.2. Grenvillian metamorphism of the TT

Textures in the mafic and ultramafic rocks of the TT are likely the result of high-P metamorphism. Crustal thickening, which led to the development of the high-P assemblages, must have begun after the emplacement of the Fe-Ti gabbros (BNS 1, 1170 \pm 5 Ma), which are the youngest pre-metamorphic intrusions in the TT. The U-Pb zircon ages of the nelsonite (LES 3), and ages of partial

melting and metamorphism in the migmatitic-garnet amphibolite (BNS 3) constrain the ages of peak metamorphism to ca. 1046-1042 Ma. These ages correspond to the Ottawa phase of the Grenvillian orogeny. During the early stages of decompression, temperatures above the blocking temperature of titanite (ca. 600 °C, Cherniak 1993) contributed to the breakdown of baddeleyite to form saccharoidal zircon and promoted new metamorphic zircon growth, along with reequilibration of some of the high-P textures. The ages of saccharoidal metamorphic zircon (1030 \pm 12 Ma, LES 1; 1030 \pm 10/-7 Ma BNS 1) and metamorphic zircon (1012 \pm 12 Ma, BNS 2) overlap. Similarly, titanite ages (1004 \pm 4 Ma; LES 4; 1006 \pm 5 Ma, BNS 3) are virtually identical. Thus, high-P metamorphism and the initial stages of cooling appear to be contemporaneous across the TT. In addition, metamorphic ages (Figure 1.10) and field relationships indicate that the TT and LT were in close association both during the late-Grenvillian (Ottawa) event and during subsequent exhumation. The reason for variation in rutile cooling ages from the units in the TT (960 \pm 6 Ma and 946 \pm 2 Ma, BNS 3; 929 \pm 4 Ma, samples LES 1 and LES 2) is not well understood. Regardless of these local variations, the difference between the youngest titanite (997 \pm 3 Ma, sample BNS 3) and rutile ages in the TT show that cooling down to ca. 400 °C, the average blocking temperature for rutile (Mezger et al. 1989), occurred over a fairly long period of time, at least 30 Ma.

It is noteworthy that pre-Ottawan metamorphic events are not recorded in the mafic rocks of the TT, as for instance the ca. 1450-1400 Ma metamorphism documented in some terranes in the eastern and southwestern Grenville (Tucker and Gower 1994; Ketchum et al. 1994) or the earlier Grenvillian event recorded at 1190-1160 Ma (e.g. van Breemen et al 1986; Mezger et al 1993; McEachern and van Breemen 1993). Saccharoidal zircon ages from the western Grenville Province, in particular the eclogite-bearing areas studied by Indares and Dunning (1997) are significantly older (1069 \pm 3 Ma) than those in the TT. U-Pb ages of rounded metamorphic zircons from retrogressed eclogites also in the western Grenville (Ketchum and Krogh 1998) range from 1090-1060 Ma. The ages of post-peak metamorphic pegmatites from the western Grenville (ca. 990-1050, Ketchum et al. 1997) overlap the age of high-P metamorphism

in the TT. Zircon ages of peak metamorphism from the eastern Grenville are very similar to those in the TT (e.g. Phillippe et al. 1993; Wasteneys et al. 1997). The older ages of high-P metamorphism in the western Grenville imply that the high-P Grenvillian event may show a younging trend from west to east.

The relatively prolonged period of later stage cooling recorded in the TT is consistent with studies of cooling in other Grenvillian terranes (e.g. Friedman and Martignole 1995; Martignole and Reynolds 1997; Mezger et al. 1991, 1993; van der Pluijm et al. 1994; Jamieson et al. 1995). The similarity between the cooling ages recorded by the terranes in these studies and the ages recorded by titanite and rutile in the TT metagabbroic rocks suggests that a process of slow cooling following tectonic exhumation may be rather widespread across the Grenville Province.

1.7. Conclusions

The cumulates, gabbros and nelsonite in the TT comprise parts of two igneous associations that formed during Labradorian magmatic activity (LES) and post-Elzevirian gabbro emplacement (BNS). The units have within-plate tholeiite chemical signatures, with textures, trace-element and REE-patterns suggesting a high crustal level of emplacement. During the late-Grenvillian (Ottawan) orogeny crustal-thickening led to high-P metamorphism at ca. 1046-1042 Ma in the TT, forming high-P assemblages in the gabbroic rocks. Evidence for an earlier metamorphism has not been detected in the gabbroic rocks of the TT. Exhumation and decompression at high temperatures probably continued for some time, producing both a variety of zircon morphologies and recording the age differences between zircon, titanite and rutile. The cooling ages indicated, in conjunction with decompressional metamorphic textures within the samples, suggests that the TT was most likely exhumed between 1046 Ma and 997 Ma at high temperatures, to amphibolite facies. The TT then experienced slow cooling, thus recording the large difference between the titanite and rutile ages. Metamorphic terranes in the other areas of the Grenville

Province show a similar trend. Thus, the processes controlling these exhumation paths may be rather widespread across the Grenville Province.

Figure 1.1 (a-b). Maps of a) the general location of the MIZ and b) study area showing the main structural boundaries, lithological units and U-Pb sample localities in the TT.

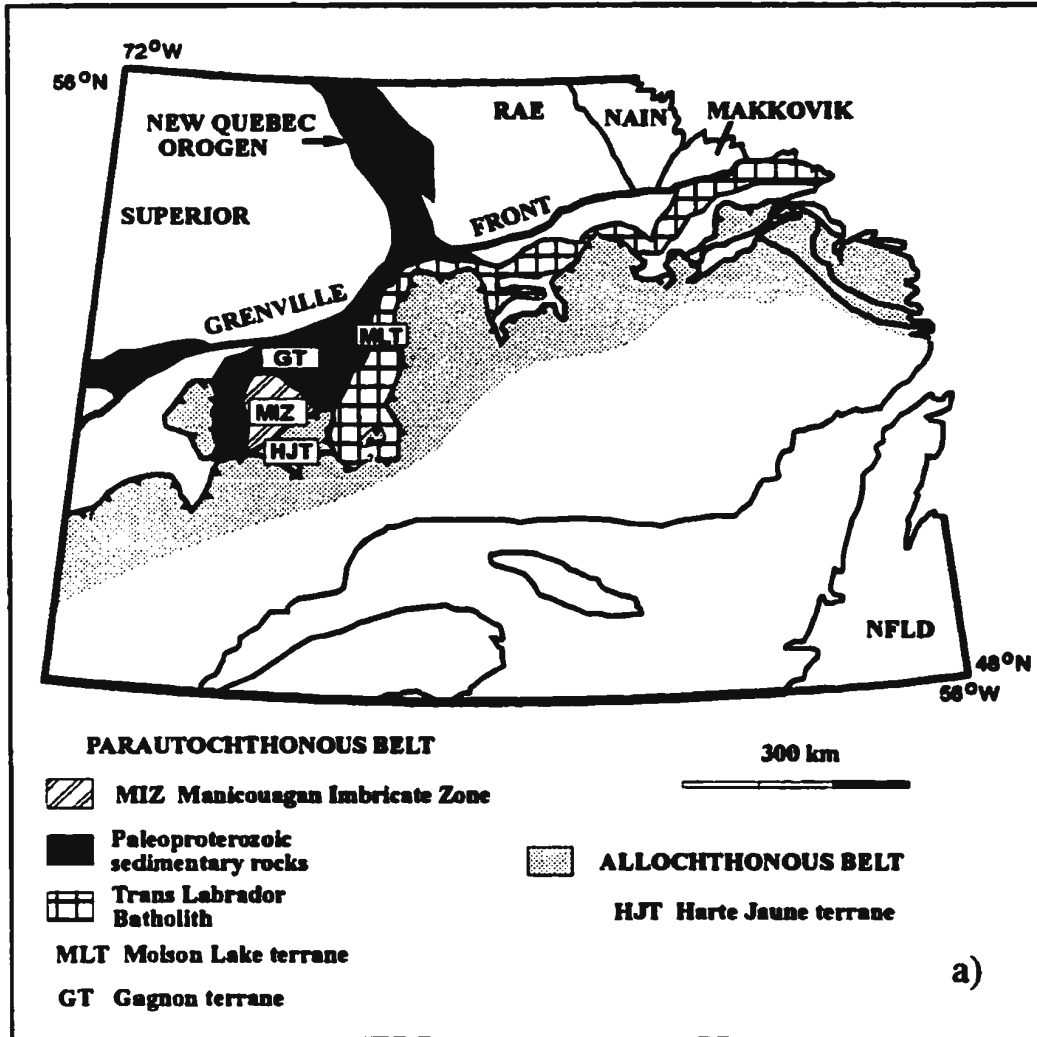


Figure 1.1 (continued).

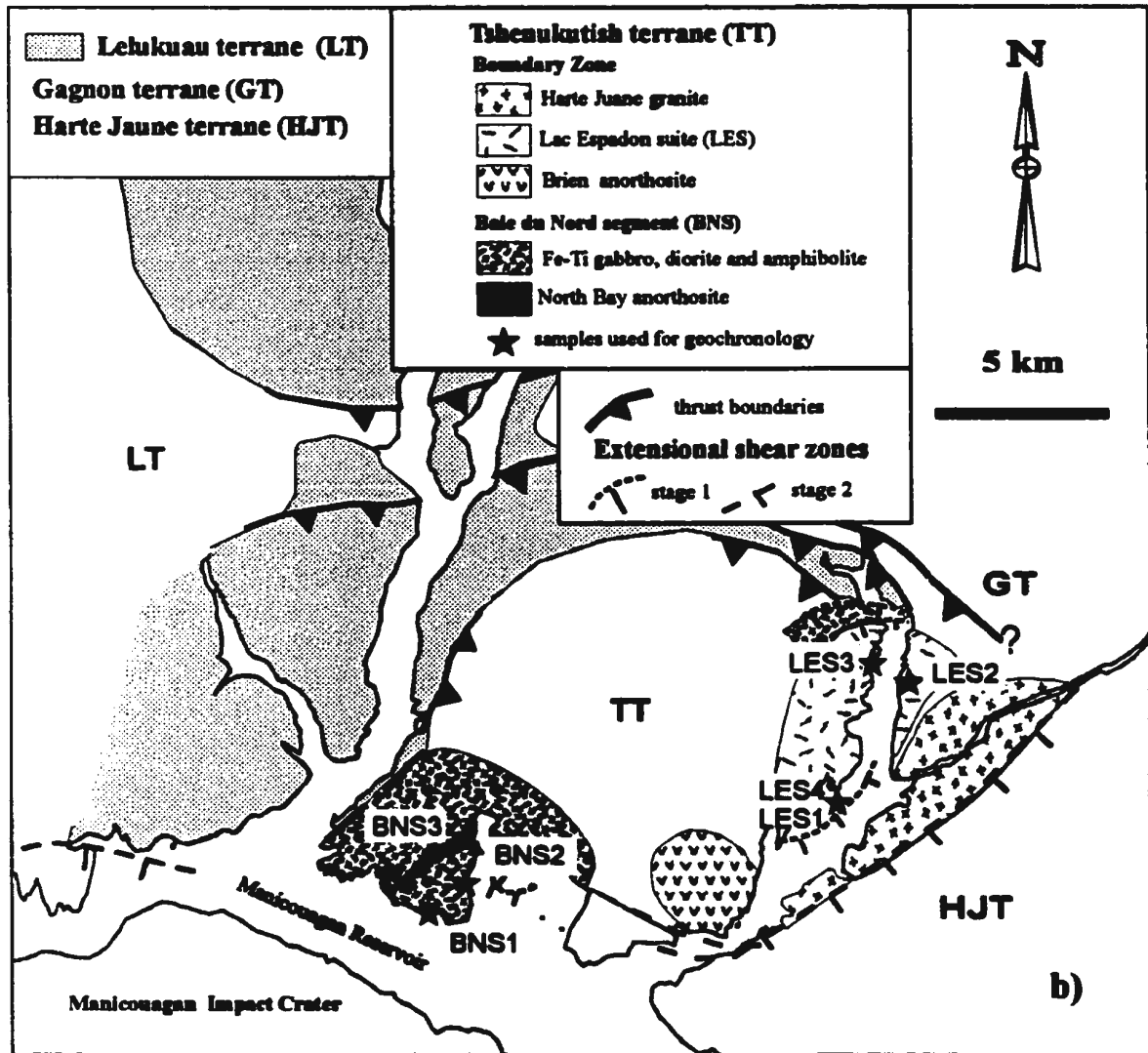


Figure 1.2 (a-c). Tectonic discrimination plots showing the within-plate tholeiite nature of the gabbros from the TT, after a) Irvine and Baragar (1971), b) Meschede (1986) and c) Pearce and Cann (1973).

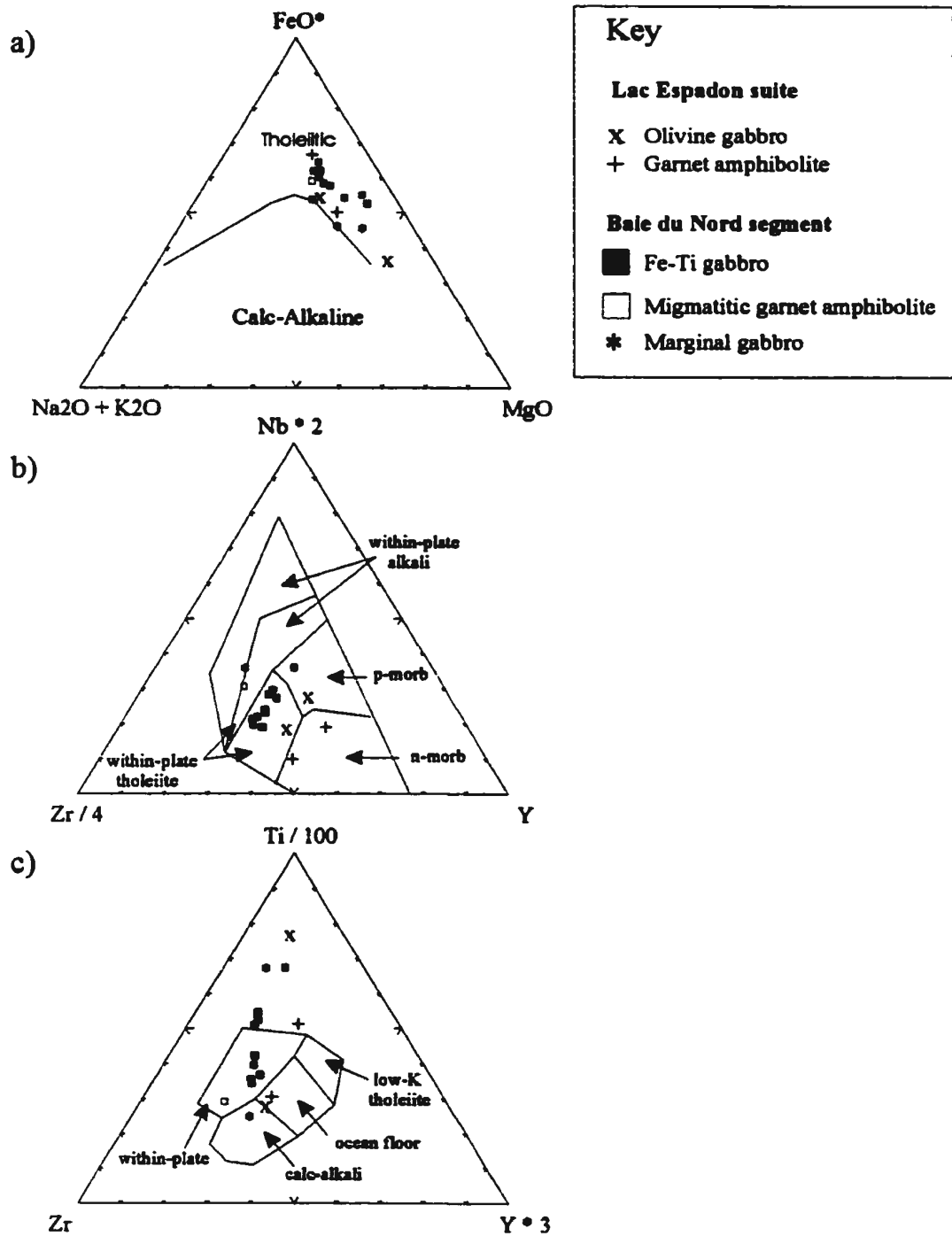


Figure 1.3 (a-d). Tectonic discrimination plots showing the within-plate tholeiite nature and apparent Zr and Ti fractionation within the gabbros from the TT, after a) Pearce and Norry (1979), b) Pearce and Cann (1973), c) Floyd and Winchester (1975) and d) Pearce (1982).

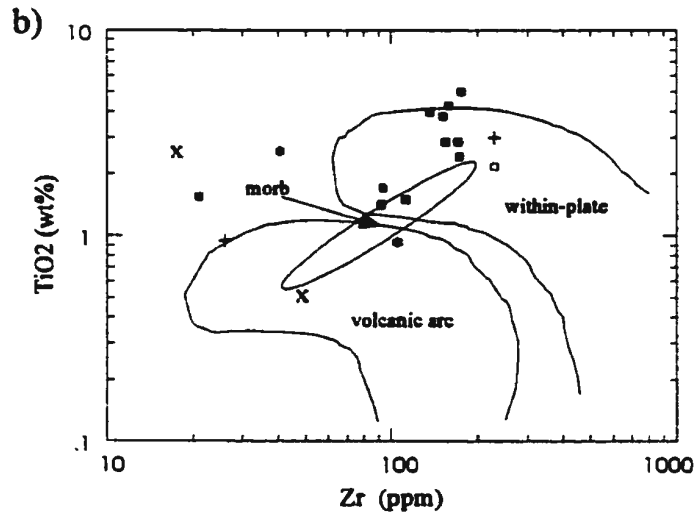
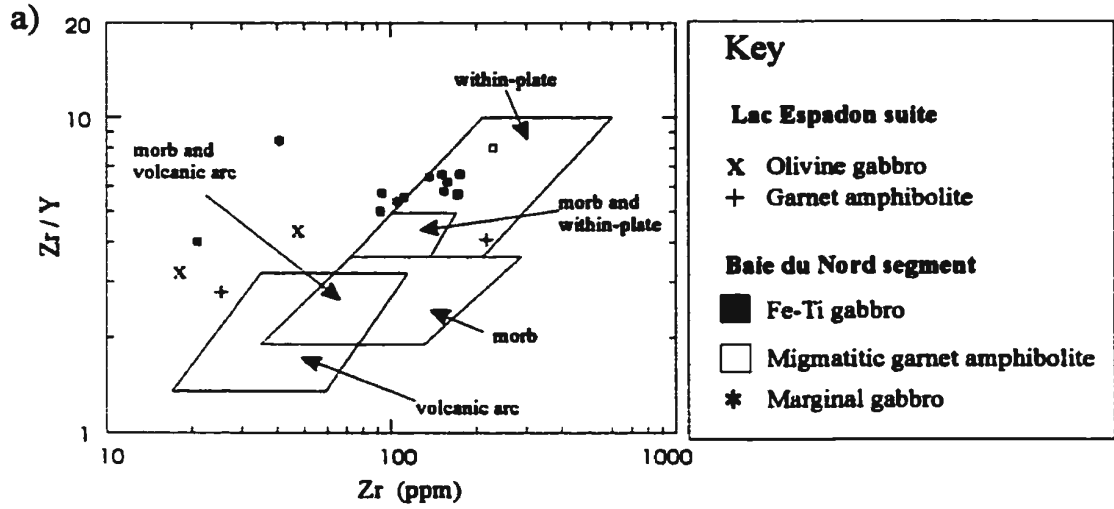


Figure 1.3 (continued).

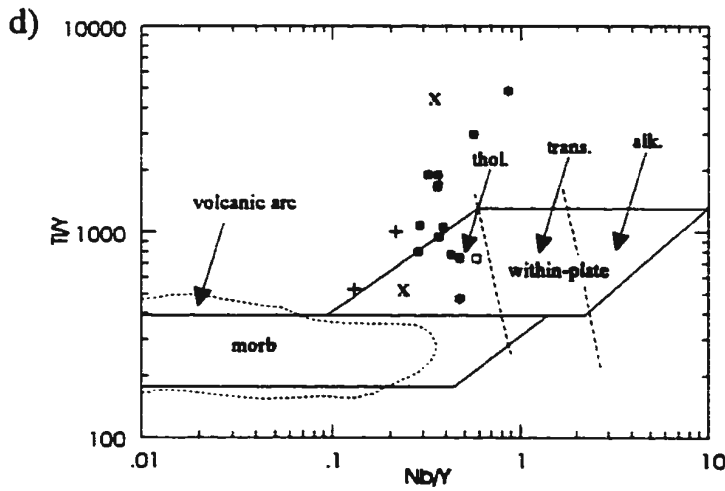
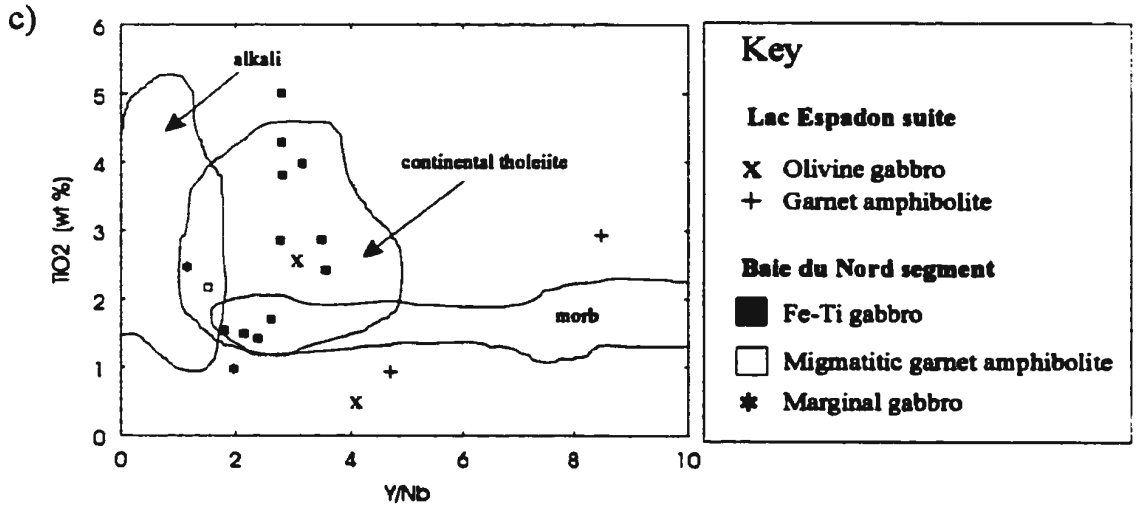


Figure 1.4 (a-f). Whole rock/primitive mantle normalized REE-patterns for a) Olivine gabbro and amphibolites (LES), b) Fe-Ti gabbros and migmatitic-garnet amphibolite (BNS), c) troctolite and dunite (LES), d) nelsonite and hornblendite (LES), e) marginal gabbros (BNS) and f) anorthosites (BNS). The dark field plotted represents "model" within-plate tholeiites (a and b) from data in Dostal et al (1984) or fractionates from this assumed starting composition (d-f). See text for discussion.

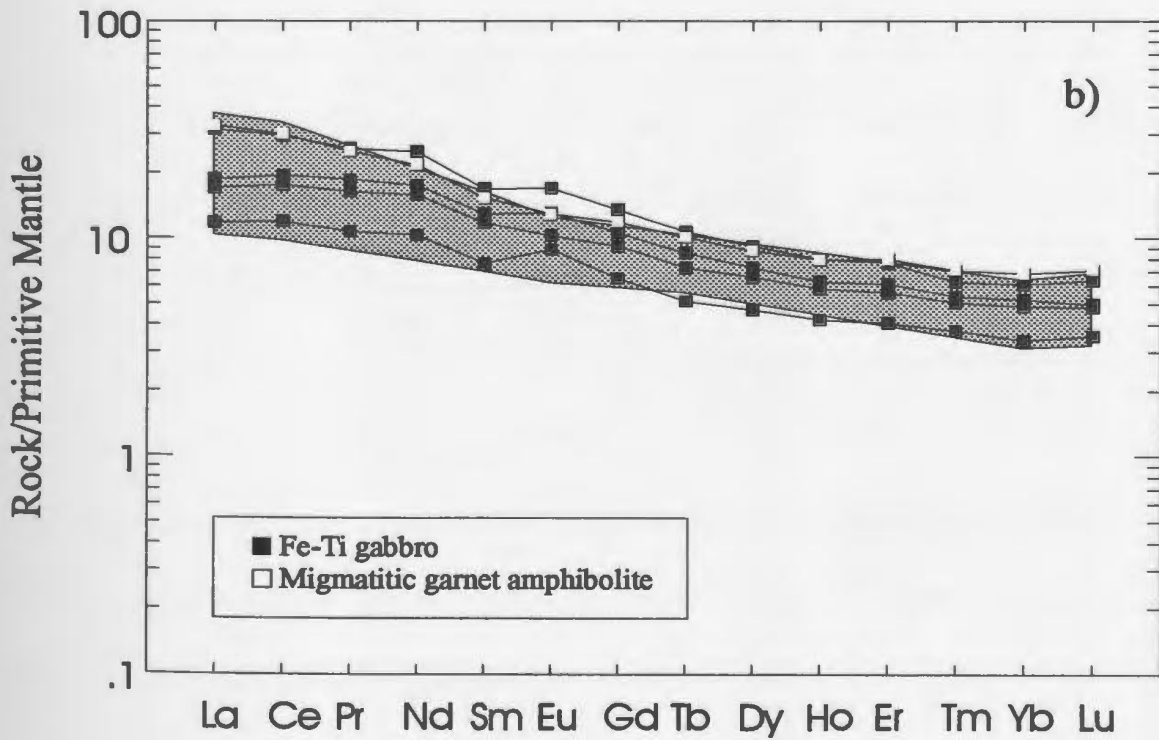
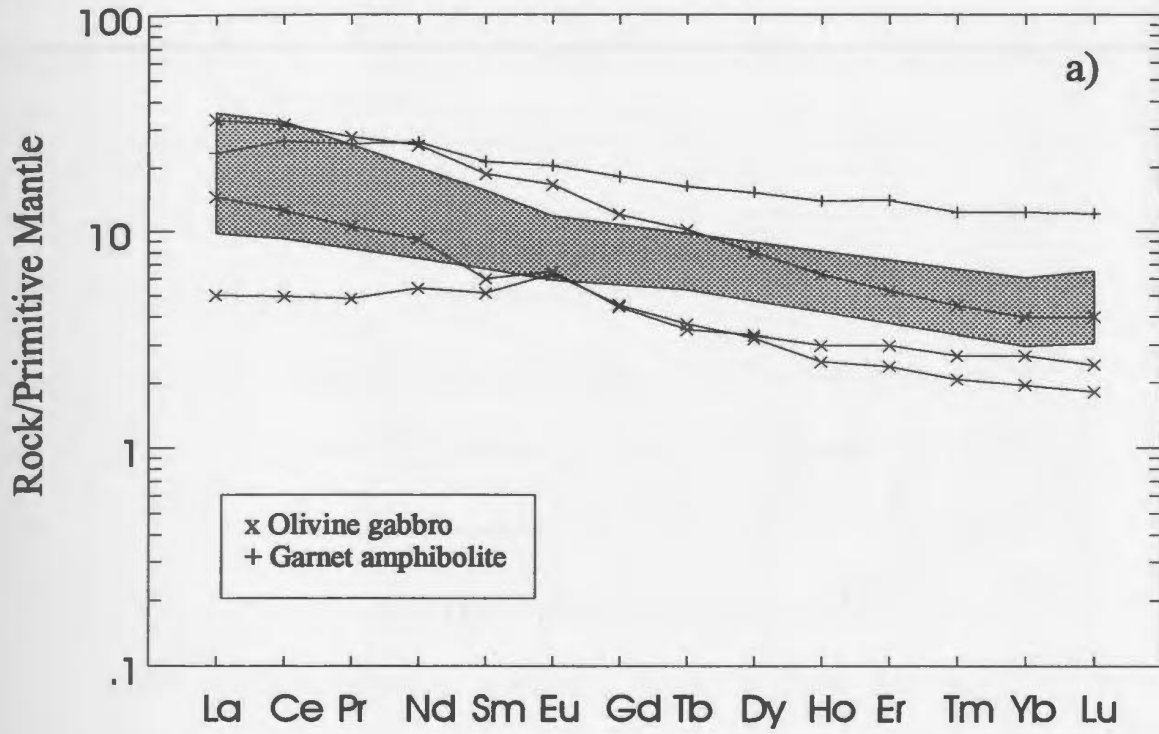


Figure 1.4 (continued).

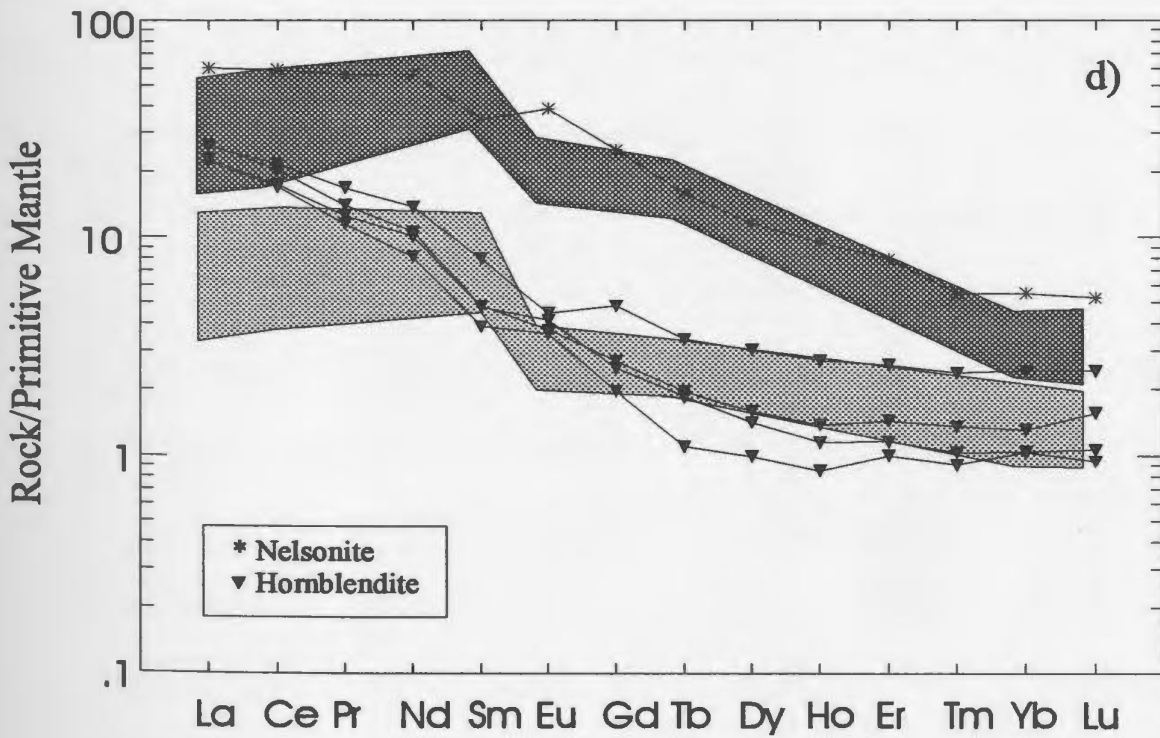
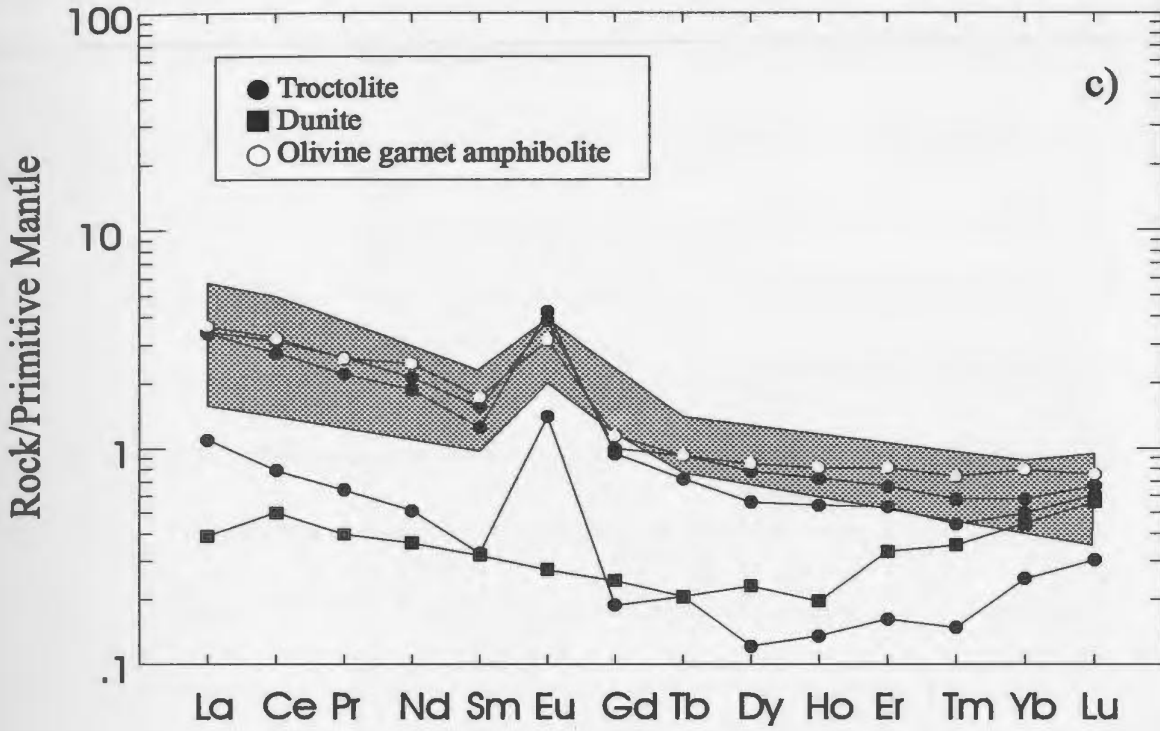


Figure 1.4 (continued).

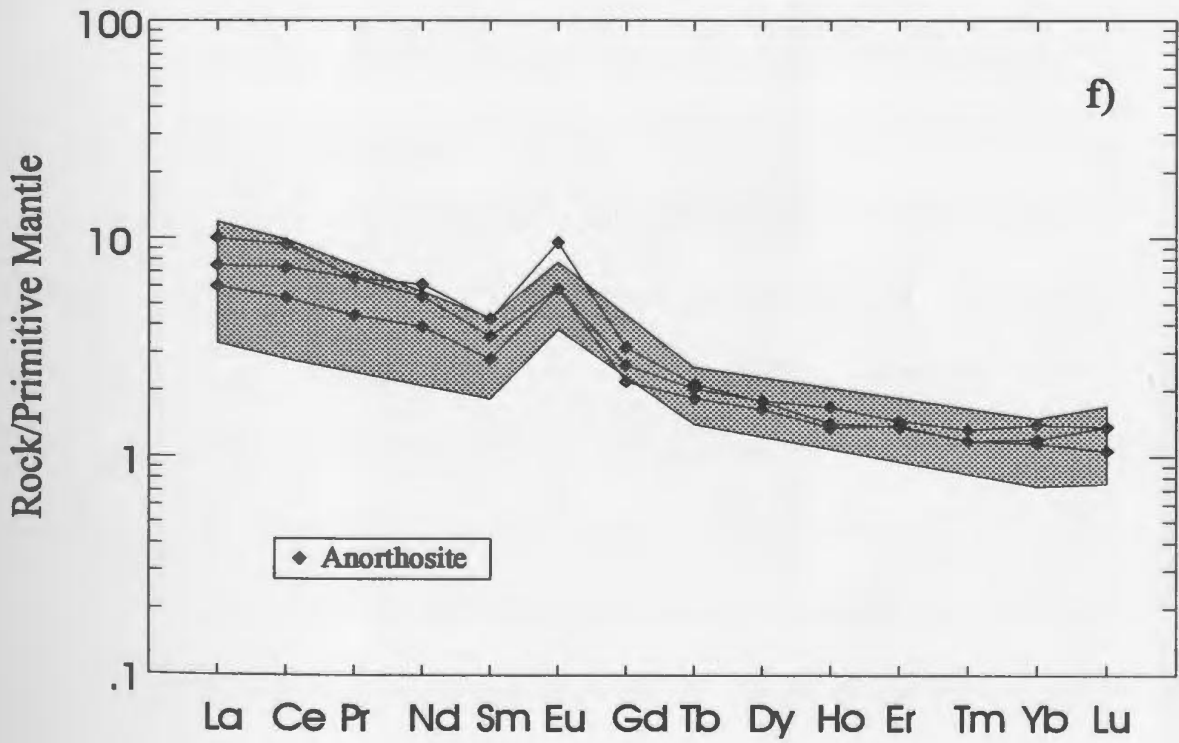
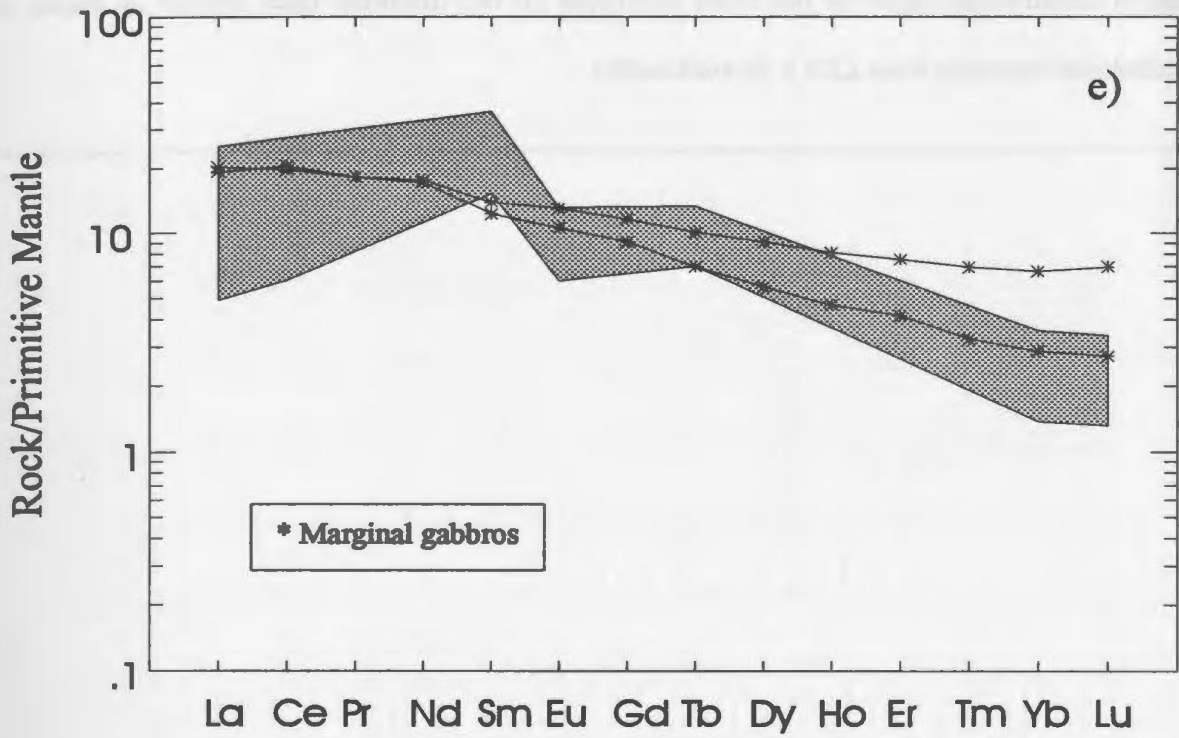


Figure 1.5 (a-b). U-Pb concordia diagrams showing a) the igneous protolith age on the upper intercepts and b) metamorphic ages for the lower intercepts for two discordia lines defined by zircon and baddeleyite fractions from LES 1 (hornblendite).

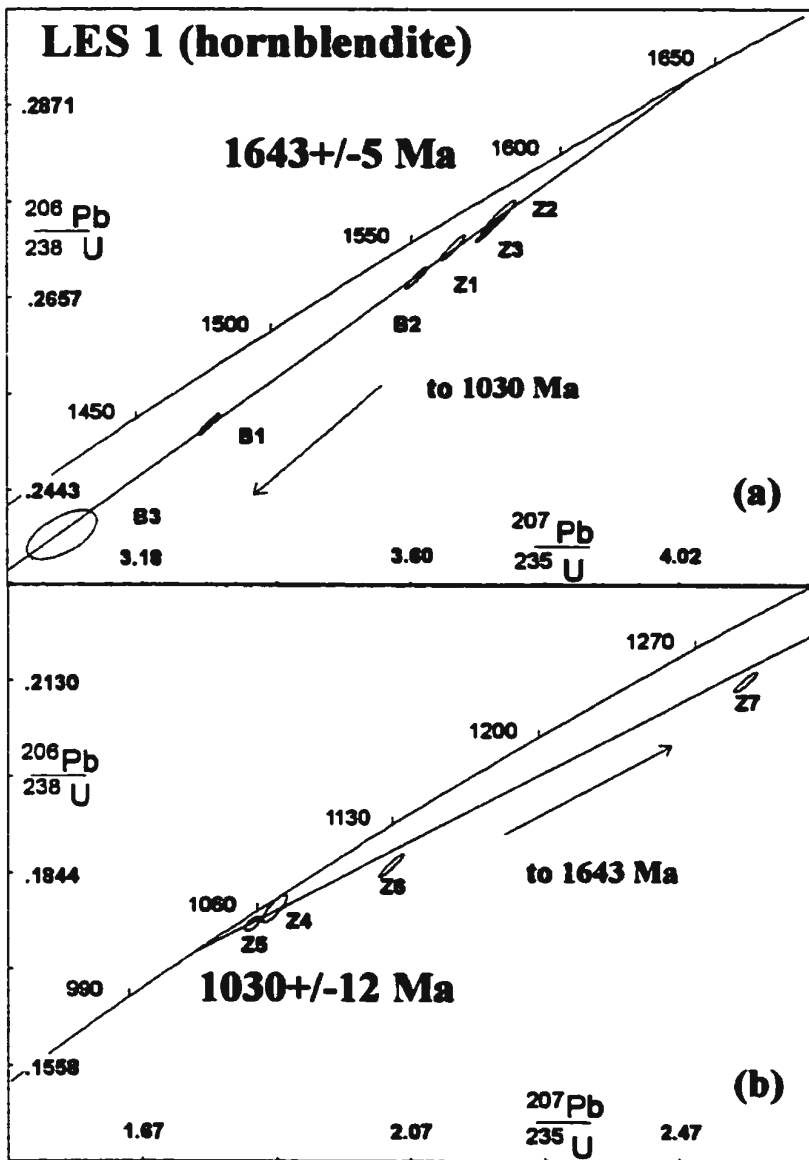


Figure 1.6 (a-b). U-Pb concordia diagrams showing a) igneous protolith age for the upper intercept on zircon from LES 2 (olivine gabbro) and b) the cooling age for the upper intercept on rutile from both LES 1 and LES 2.

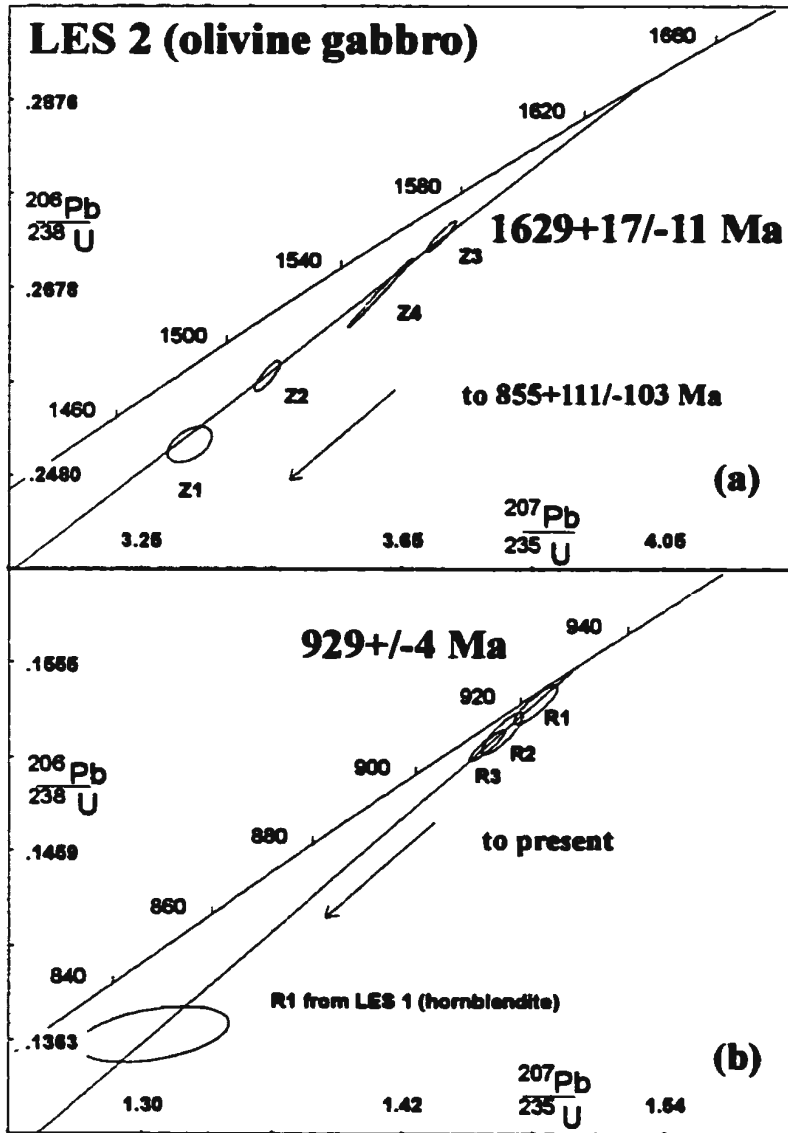


Figure 1.7 (a-b). U-Pb concordia diagrams for a) igneous zircon with metamorphic overgrowths found in LES 3 (nelsonite) giving a emplacement age at the upper intercept and b) concordant metamorphic titanite from LES 4 (garnet amphibolite).

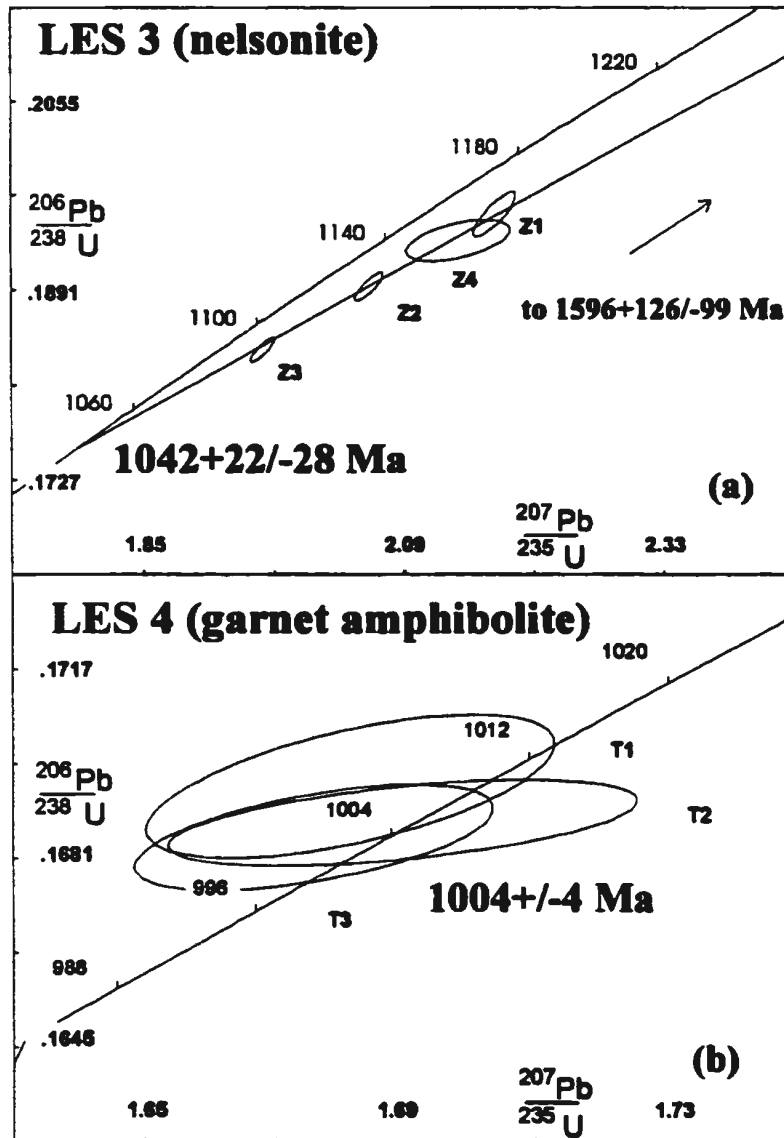


Figure 1.8 (a-b). U-Pb concordia diagrams for a) BNS 1 (coronitic Fe-Ti gabbro), showing the protolith age with concordant baddeleyite and metamorphic ages with concordant zircon, and b) concordant metamorphic zircon from BNS 2 (re-equilibrated coronite).

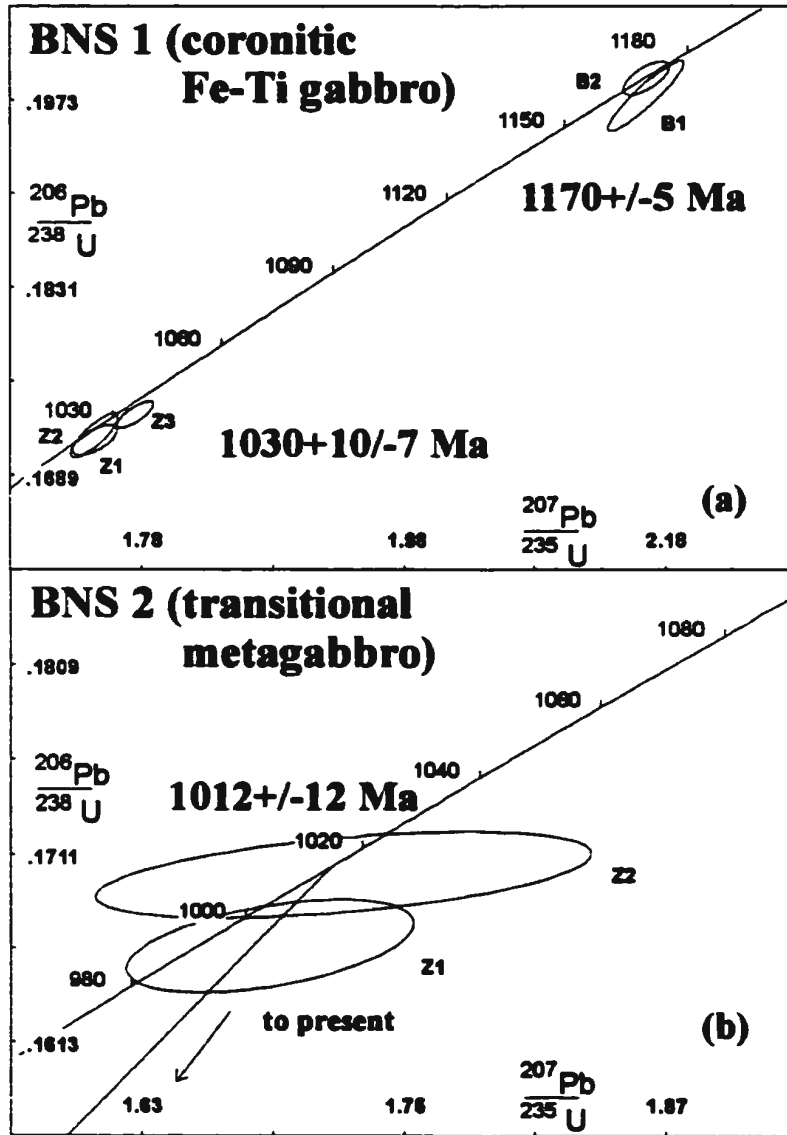


Figure 1.9 (a-c). U-Pb concordia diagrams BNS 3 (migmatitic-garnet amphibolite) showing, a) concordant metamorphic zircon, b) two ages from concordant metamorphic titanite populations and c) cooling ages from both concordant, large grain size (R4, R5) and fine-grained (R1, R2, R3) rutile populations.

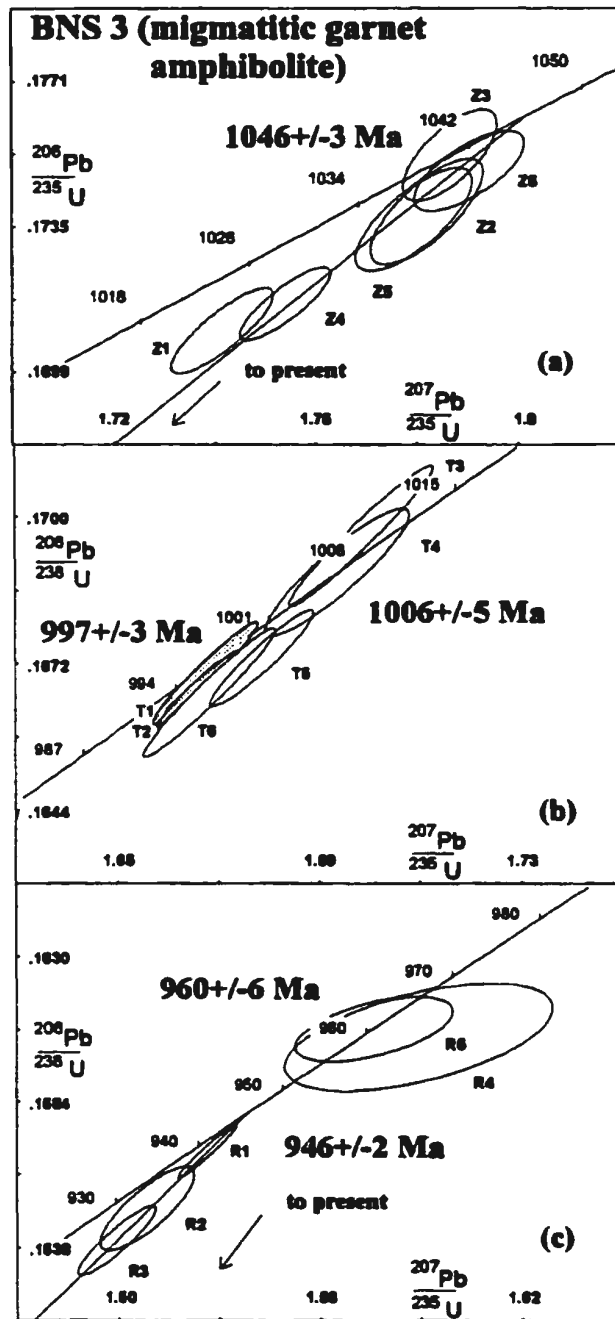


Figure 1.10. Summary diagram of U-Pb ages from the Manicouagan Imbricate Zone (MIZ). Ages in the LT are from Gale et al. (1994) and Indares et al (1998). Ages in the TT are from this study, Indares et al. (1998) and Indares and Dunning (in press). The Brien anorthosite age (Boundary zone) is from Scott and Hynes (1994). Note: Zi = igneous zircon, Bi = igneous baddeleyite, Zm = metamorphic zircon, Mm = metamorphic monazite, Tm = metamorphic titanite, Rm = metamorphic rutile (cooling ages).

Table 1.1. Major- and trace-element compositions of selected mafic samples from the TT obtained by XRF analyses. Note: * = analysis of major-elements by pressed pellet only, due to high Fe₂O₃.

Ultramafic rocks (Lac Espadon suite)												
	Troctolite			Dunite	Olivine amphibolite		Hornblende					
	5a	5b	5c*	6*	6am1*	6am2*	3b1	3b4	3b6	3b7	4	137
SiO ₂	42.94	44.57	32.17	30.23	35.15	35.07	45.53	44.64	44.32	44.06	44.1	44.65
TiO ₂	0.3	0.26	0.1	0.09	0.55	0.46	0.2	0.18	0.39	0.29	0.24	0.2
Al ₂ O ₃	12.98	16.25	4.52	0.43	7.05	7.07	14.06	11.88	11.27	10.81	12.31	12.73
Fe ₂ O ₃	18.01	14.74	25.21	30.97	21.83	22.28	12.52	13.75	14.08	14.2	13.71	13.3
MgO	17.77	14.8	22.36	22.94	19.36	19.78	18.18	21.45	22.54	22.4	21.97	21.29
CaO	5.81	7.07	3.45	0.65	5.52	5.46	6.23	5.02	5.6	4.93	5.86	5.34
MnO	0.2	0.17	0.27	0.36	0.22	0.24	0.18	0.19	0.19	0.2	0.18	0.19
K ₂ O	0.16	0.19	0.09	0.02	0.12	0.17	0.69	0.66	0.53	0.65	0.49	0.76
Na ₂ O	1.31	2.08	0.84	0.16	1.14	1.32	1.49	1.08	1.05	1.29	1.26	0.77
P ₂ O ₅	0.08	0.06	0.04	0.06	0.08	0.11	0.23	0.16	0.22	0.2	0.18	0.13
Total	99.56	100.19	89.05	85.91	91.02	91.96	99.31	99.01	100.19	99.03	100.3	99.36
LOI	1.25	2.87	0.13	0.72	0.58	0.27	0.86	1.02	0.53	2.58	2.08	1.94
Sc	12	10	0	12	0	0	12	11	17	12	16	0
V	33	29	17	19	105	89	50	49	90	64	52	56
Cr	40	50	87	115	732	617	468	699	750	708	465	698
Ni	496	445	835	1146	664	664	681	768	781	836	645	752
Ga	12	13	6	0	10	9	11	11	10	8	11	10
Rb	1.8	1.8	1	0.01	1.5	0.7	24.2	21.5	13.9	17.8	12.5	25.9
Sr	414.1	559.2	218.1	8.9	318.7	231.7	923.8	708.3	733	713.1	848.3	732.6
Y	2.1	1.5	1	1	2.9	1.9	4.9	2.8	7.7	10.2	4.2	4
Zr	11.9	4.7	1	2.5	15.6	13.3	61.5	53.6	70.1	66.8	48.2	43.7
Nb	2	1	0.8	1	1.6	1.3	4.1	2.7	4.3	4.3	3.2	3.6
Ba	187	214	96	0	134	42	662	698	570	634	545	596

Table 1.1 (continued).

Gabbroic rocks (Lac Espadon suite)					
	Olivine gabbro		Garnet amphibolite		Nelsonite
	35	35c	2b	2a	9c
SiO₂	46.1	47.26	47.72	48.8	39.77
TiO₂	0.52	2.6	2.96	0.97	4.72
Al₂O₃	16.83	16.02	12.07	17.45	15.36
Fe₂O₃	9.92	14.13	17.98	12.09	15.77
MgO	13.01	6.53	5.21	7.72	4.51
CaO	8.94	8.3	8.53	8.35	9.98
MnO	0.15	0.19	0.28	0.15	0.25
K₂O	0.53	0.97	1.68	0.28	0.91
Na₂O	1.81	3.06	1.35	3.27	3.12
P₂O₅	0.11	0.37	0.64	0.1	3.87
Total	97.92	99.43	98.42	99.18	98.26
LOI	0.16	0.78	0.51	0.91	1.44
Sc	43	20	15	6	19
V	444	115	147	67	134
Cr	54	65	147	62	7
Ni	19	503	150	115	0
Ga	22	15	22	21	18
Rb	56.6	8.6	6.6	6.2	7
Sr	249	652	513.3	446.6	997.8
Y	55.1	10.5	9.4	5.7	38.7
Zr	223.4	47.4	26	18.1	82.9
Nb	6.5	2.6	2	1.9	8.8
Ba	1737	656	235	160	2379

Table 1.1 (continued).

Fe-Ti Gabbros (Bale du Nord segment)												
	Coronitic and transitional metagabbro									Eclogite		Migmatitic garnet amphibolite
	85b1	85b2	110	113	118d	123b	124a1	124a2*	124b*	21	21c	313
SiO2	45.7	43.98	44.35	46.13	45.45	44.79	42.26	40.63	41.67	44.38	42.95	47.05
TiO2	2.85	1.47	4.29	2.42	1.5	2.86	5.01	3.98	3.81	1.55	1.71	2.17
Al2O3	15.8	15.47	15.39	16.35	16.43	15.76	14.57	14.63	11.67	16.21	13.27	17.2
Fe2O3	17.12	15.56	17.29	16.07	15.66	16.2	18.52	18.69	18.3	16.45	19.04	14.56
MgO	5.78	6.45	6.5	6.76	8.89	7.36	6.58	6.01	6.55	10.16	13.11	5.39
CaO	8	8.4	7.52	8.01	8.34	7.92	7.33	6.84	7.07	8.26	6.74	9.12
MnO	0.23	0.21	0.19	0.21	0.2	0.2	0.2	0.19	0.18	0.2	0.23	0.24
K2O	0.69	0.88	0.52	0.73	0.49	0.51	0.52	0.47	0.55	0.36	0.35	0.76
Na2O	3.04	5.01	3.25	2.83	2.55	2.84	3.11	2.89	3.15	1.58	2.03	2.97
P2O5	0.57	0.21	0.53	0.41	0.18	0.52	0.49	0.37	0.66	0.22	0.25	0.28
Total	99.78	97.64	99.83	99.92	99.69	98.96	98.59	94.7	93.61	99.37	99.68	99.74
LOI	0.94	0.06	0.05	0.83	0.03	0.13	0.66	0.65	0.12	0.31	0.51	1.64
Sc	25	37	25	28	24	24	30	21	27	6	20	24
V	275	302	356	2323	193	150	392	538	994	77	177	185
Cr	54	93	52	158	184	165	126	120	341	50	55	75
Ni	71	103	85	11	178	145	94	88	158	94	260	84
Co	26	25	22	23	21	22	24	26	20	22	17	27
Rb	11.6	9.8	5.1	13.6	12.7	5.5	6.2	4.7	4.3	2.7	5.2	13.6
Sr	634.5	714.8	483.7	293	300.2	493.1	467.2	501	292.3	453.8	367.7	481.9
Y	30.1	18.3	25.4	30.2	20.1	26.5	26.5	21.1	23	5.2	16.2	28.5
Zr	171	91.8	158.4	172.6	111.8	154.2	175	136.2	151.5	20.9	93.1	228.9
Nb	10.9	7.7	9.1	8.5	9.4	7.6	9.5	6.7	8.2	2.9	6.2	18.8
Ba	1226	683	305	333	179	340	356	311	254	118	356	163

Table 1.1 (continued).

Anorthosites and Marginal Gabbros (Bale du Nord segment)						
	Anorthosite				Marginal Gabbro	
	302	311b	316	317	268a	268b
SiO ₂	44.76	45.88	48.47	48.51	52.71	44.29
TiO ₂	1.47	2.45	0.5	0.62	0.92	2.37
Al ₂ O ₃	15.58	16	23.87	24.39	12.35	13.78
Fe ₂ O ₃	16.19	15.8	7.08	6.72	12.04	13.87
MgO	10.4	6.6	5.04	4.46	8.26	11.72
CaO	8.14	8.72	10.63	10.92	9.03	9.35
MnO	0.21	0.2	0.09	0.08	0.18	0.19
K ₂ O	0.42	0.71	0.4	0.3	0.37	0.52
Na ₂ O	1.84	2.65	3.25	3.15	3.84	2.5
P ₂ O ₅	0.18	0.37	0.06	0.08	0.15	0.25
Total	99.19	99.38	99.39	99.23	99.85	98.84
LOI	0.05	0.14	0.39	0.29	2.55	1.95
Sc	24	22	14	25	115	14
V	235	267	190	323	165	52
Cr	161	34	54	820	96	15
Ni	104	73	225	275	262	62
Co	26	28	17	22	20	20
Rb	16.4	19.5	6.4	3.1	10.6	1
Sr	285.7	760.5	412.9	544.9	287.3	753.6
Y	32.2	20.5	13.3	16.6	19.6	4.8
Zr	179.1	187.2	66.2	176.1	104.8	40.5
Nb	9.1	23.3	5.4	11.4	9.8	4.2
Ba	347	408	245	61	230	246

Table 1.2. REE-analyses and additional trace-element compositions of selected mafic samples from the TT obtained by ICP-MS analyses.

Ultramafic rocks (Lac Éopeden suite)								
	Troctolite			Dunite	Olivine amphibolite	Hornblende		
	5a	5b	5c	6	6sm1	3b4	3b7	4
La	2.14	2.12	0.69	0.25	2.27	13.92	16.34	14.23
Ce	4.92	4.34	1.25	0.80	5.05	26.98	34.22	27.66
Pr	0.65	0.55	0.16	0.10	0.65	2.88	4.21	3.14
Nd	2.55	2.25	0.62	0.44	2.96	9.84	16.67	12.16
Sm	0.62	0.5	0.13	0.13	0.69	1.54	3.18	1.9
Eu	0.57	0.63	0.21	0.04	0.47	0.54	0.67	0.62
Gd	0.53	0.5	0.1	0.13	0.61	1.05	2.56	1.33
Tb	0.09	0.07	0.02	0.02	0.09	0.11	0.33	0.18
Dy	0.52	0.37	0.08	0.15	0.56	0.65	2	0.94
Ho	0.11	0.08	0.02	0.03	0.12	0.13	0.4	0.17
Er	0.29	0.23	0.07	0.14	0.35	0.43	1.11	0.5
Tm	0.04	0.03	0.01	0.02	0.05	0.06	0.16	0.07
Yb	0.25	0.22	0.11	0.20	0.35	0.45	1.07	0.46
Lu	0.04	0.04	0.02	0.04	0.05	0.06	0.16	0.07
Hf	0.38	0.24	0.26	0.09	0.43	1.28	1.42	1.19
Ta	2.05	0.76	0.4	0.36	1.03	0.72	1.08	0.89
Th	0.11	0.08	0.05	0.02	0.1	0.68	0.72	0.46

Gabbroic rocks (Lac Éopeden Suite)					
	Olivine gabbro		Amphibolite		Nelsonite
	35	35c	2b	2a	9c
La	9.14	20.75	3.15	14.64	37.86
Ce	19.88	49.97	7.85	41.72	94.19
Pr	2.64	6.88	1.21	6.38	14.06
Nd	11.07	30.44	6.5	31.39	68.49
Sm	2.37	7.41	2.04	8.42	13.92
Eu	0.97	2.48	0.94	3.04	5.83
Gd	2.35	6.38	2.4	9.6	13.36
Tb	0.34	0.99	0.36	1.58	1.54
Dy	2.18	5.27	2.11	10.03	7.68
Ho	0.44	0.93	0.37	2.05	1.40
Er	1.28	2.27	1.03	6.05	3.42
Tm	0.18	0.30	0.14	0.83	0.37
Yb	1.18	1.76	0.86	5.42	2.43
Lu	0.16	0.26	0.12	0.8	0.35
Hf	1.28	5.06	0.98	5.11	2.11
Ta	1.23	2.63	0.62	0.84	1.14
Tb	0.34	1.49	0.19	1.19	0.66

Table 1.2 (continued).

Fe-Ti Gabbros (Bale du Nord segment)					
	Coronitic and transitional metagabbros			Eclogite	Migmatitic garnet amphibolite
	85b1	110	124a1	21c	313
La	19.96	11.74	10.70	7.40	20.7
Ce	46.99	30.86	27.83	18.97	47.86
Pr	6.47	4.66	4.11	2.68	6.28
Nd	30.12	21.14	19.11	12.42	26.28
Sm	6.72	5.13	4.68	3.04	6.09
Eu	2.54	1.96	1.54	1.32	1.922
Gd	7.17	5.6	4.88	3.47	6.3
Tb	1.04	0.83	0.71	0.50	0.98
Dy	6.05	4.82	4.37	3.09	5.76
Ho	1.18	0.93	0.87	0.63	1.17
Er	3.31	2.66	2.43	1.76	3.44
Tm	0.43	0.36	0.34	0.25	0.48
Yb	2.70	2.31	2.15	1.50	3.02
Lu	0.42	0.33	0.32	0.23	0.47
Hf	3.89	3.66	3.28	2.22	5.36
Ta	1.31	1.92	1.79	0.95	1.61
Th	1.10	0.41	0.38	0.38	3.72

Aenorthosites and Marginal Gabbros (Bale du Nord segment)					
	311b	Aenorthosite		Marginal gabbro	
		316	317	268a	268b
La	4.72	6.3	3.79	12.1	12.7
Ce	11.71	14.93	8.48	32.41	31.17
Pr	1.65	1.64	1.11	4.56	4.55
Nd	7.43	6.54	4.77	20.77	21.34
Sm	1.7	1.42	1.12	4.87	5.54
Eu	1.43	0.88	0.88	1.58	1.95
Gd	1.69	1.4	1.18	4.86	6.18
Tb	0.21	0.2	0.18	0.68	0.98
Dy	1.18	1.19	1.09	3.73	6.01
Ho	0.21	0.25	0.2	0.69	1.2
Er	0.59	0.63	0.6	1.8	3.26
Tm	0.08	0.09	0.08	0.22	0.47
Yb	0.51	0.62	0.53	1.27	2.94
Lu	0.07	0.09	0.09	0.18	0.46
Hf	1.31	0.59	0.7	4.29	4.05
Ta	1.67	1.39	2.02	1.57	1.66
Th	0.17	0.47	0.27	0.53	1.06

Table 1.3. U-Pb isotope data for mineral fractions from the mafic rocks of the TT.

Note:

- 1) Z = zircon, B = baddeleyite, R = rutile, T = titanite (sphene).
 - 2) Final Frantz magnetic separation ,where sample size allowed, was done with 5°, 3°, 1°, and 0° side tilts and 30° forward slope after methyl iodide separation.
 - 3) Measured $^{206}\text{Pb}/^{204}\text{Pb}$ ratios are corrected for fractionation, blank and spike.
 - 4) Other atomic ratios are also corrected for initial common Pb, using the model of Stacey and Kramers (1975).
 - 5) Errors are quoted at 2σ for measured ratios. Errors on sample weights due to balance fluctuations are $\pm 0.0010\text{mg}$.
-

Frac.	General Description	Wt mg	Model Th/U	U ppm	Pb rad ppm	Pb com. pg	^{235}Pb	^{235}Pb	^{235}Pb	^{237}Pb	^{237}Pb	Apparent ages (Ma)		
							^{235}Pb	^{235}Pb	^{235}U (+/-)	^{237}U (+/-)	^{237}Pb	^{237}Pb	^{237}Pb	^{235}Pb
LES 1 (hornblende UTM 5544 57268)														
Z1	Lge. frags prisms	0.1688	1.422	90	33	28	16411	0.4606	0.2713 (12)	3.6671 (146)	0.09804 (102)	1587	1547	1564
Z2	Lge. frags prisms	0.1611	1.509	90	34	42	8270	0.4830	0.2746 (16)	3.7284 (214)	0.09872 (16)	1600	1564	1579
Z3	Lge. prisms, turbid	0.0923	2.406	876	387	27	90763	0.7737	0.2733 (12)	3.7239 (172)	0.09884 (10)	1602	1558	1576
Z4	Saccharoidal	0.0388	0.137	161	28	15	21173	0.0687	0.1791 (16)	1.8660 (152)	0.07557 (40)	1083	1062	1069
Z5	Saccharoidal	0.1290	0.186	209	37	12	31763	0.0934	0.1767 (8)	1.8330 (88)	0.07523 (28)	1076	1049	1057
Z6	Saccharoidal, not abr	0.0685	0.772	142	30	11	10439	0.2271	0.1855 (14)	2.0410 (152)	0.07980 (18)	1190	1097	1129
Z7	Saccharoidal, not abr	0.0384	0.206	44	46	25	8372	0.0892	0.2128 (12)	2.5692 (142)	0.08755 (18)	1373	1244	1292
B1	Brown blocks	0.0156	0.007	784	186	16	55866	0.0026	0.2516 (10)	3.2848 (134)	0.09470 (10)	1522	1447	1478
B2	Brown blocks	0.0128	0.007	848	215	15	57897	0.0029	0.2679 (10)	3.6095 (140)	0.09773 (10)	1581	1530	1552
B3	Green needles, not abr	0.0083	0.061	25	6	28	202	0.2001	0.2380 (22)	3.0635 (550)	0.09334 (110)	1490	1377	1424
R1	Small angular prisms	0.0125	0.026	33	4	31	205	0.0093	0.1366 (12)	1.3059 (282)	0.06936 (132)	909	825	848
LES 2 (olivine gabbro UTM 5572 57327)														
Z1	Small, multi-fac'd	0.0153	0.738	87	26	86	300	0.2583	0.2513 (16)	3.3239 (278)	0.09594 (72)	1547	1445	1487
Z2	Elongated, cracks	0.0218	0.808	138	42	13	44442	0.2748	0.2585 (12)	3.4426 (158)	0.09658 (26)	1559	1482	1514
Z3	L. prisms, euhedral	0.0585	0.835	143	46	31	7853	0.2686	0.2732 (14)	3.7100 (180)	0.09850 (16)	1596	1557	1574
Z4	L. prisms, euhedral	0.1391	1.016	209	69	31	24974	0.3354	0.2672 (30)	3.6162 (402)	0.09815 (10)	1589	1527	1553
R1	L. dark brown	1.1260	0.021	14	2	247	662	0.0624	0.1534 (8)	1.4815 (82)	0.07006 (20)	930	920	923
R2	L. dark brown	0.6889	0.009	13	2	60	1822	0.0230	0.1519 (8)	1.4660 (76)	0.06999 (20)	928	912	917
R3	L. bright red/brown	1.0265	0.100	16	2	170	995	0.0686	0.1513 (6)	1.4590 (66)	0.06994 (12)	926	908	914
LES 3 (nepheline UTM 5563 57339)														
Z1	V. large, prisms	0.1386	0.668	18	4	12	3051	0.2908	0.1956 (16)	2.1723 (160)	0.08061 (34)	1211	1152	1173
Z2	Prisms, small size	0.1265	0.593	19	4	10	3094	0.2657	0.1898 (10)	2.0582 (523)	0.07863 (210)	1163	1121	1135
Z3	V. large, crack'd, prisms	0.1638	0.436	27	5	21	5725	0.2020	0.1836 (8)	1.9570 (89)	0.07729 (10)	1087	1101	1129
Z4	Small, clear, equant	0.0116	0.429	21	4	58	81	0.1890	0.1933 (14)	2.1402 (390)	0.08030 (126)	1204	1139	1162
LES 4 (garnet amphibolite UTM 5546 57269)														
T1	Pale brown	0.7709	1.593	16	4	2860	62	1.1907	0.1695 (12)	1.6817 (256)	0.07197 (10)	985	1009	1002
T2	Small, pale brown	0.4178	1.656	14	4	1117	70	1.1736	0.1688 (6)	1.6897 (296)	0.07261 (10)	1003	1005	1005
T3	Small, pale brown	0.6453	1.498	18	5	1862	80	1.0690	0.1685 (8)	1.6761 (226)	0.07215 (10)	990	1003	1000

Table 1.3 (continued).

Frac	General Description	Wt. (mg)	Model Th/U	U ppm	Pb rad ppm	Pb com. pg	$^{207}\text{Pb}/^{235}\text{Pb}$			$^{207}\text{Pb}/^{238}\text{U}$			Apparent ages (Ma)		
									(+/-)			(+/-)	$^{207}\text{Pb}/^{235}\text{Pb}$	$^{207}\text{Pb}/^{238}\text{U}$	$^{207}\text{Pb}/^{235}\text{U}$
BNS 1 (coronitic Fe-Ti gabbro UTM 5352 57224)															
B1	Blocks, not abr	0.0056	0.046	246	46	10	41719	0.0148	0.1976 (22)	2.1652 (234)	0.07946 (34)	1184	1163	1170	
B2	Blocks, not abr	0.0031	0.051	182	34	31	386	0.0156	0.1990 (10)	2.1655 (142)	0.07894 (38)	1171	1170	1170	
Z1	Saccharoidal	0.0147	0.338	102	18	38	640	0.1079	0.1709 (8)	1.7424 (110)	0.07394 (36)	1040	1017	1025	
Z2	Saccharoidal	0.0133	0.298	71	12	4	10545	0.0946	0.1719 (14)	1.7439 (146)	0.07359 (34)	1030	1025	1023	
Z3	Saccharoidal, not abr	0.0173	0.243	125	22	97	293	0.0861	0.1736 (8)	1.7770 (114)	0.07424 (30)	1048	1032	1037	
BNS 2 (transitional Fe-Ti gabbro UTM 5352 57224)															
Z1	Equant, not abr	0.0025	0.096	42	7	17	232	0.0355	0.1659 (20)	1.6742 (638)	0.07319 (208)	1019	990	999	
Z2	Angular, not abr	0.0029	0.443	45	8	45	59	0.1603	0.1700 (18)	1.7223 (932)	0.07346 (364)	1027	1012	1017	
BNS 3 (migmatitic grt amphibolite UTM 5326 57233)															
Z1	Equant, not abr	0.0330	0.298	81	14	8	11811	0.0961	0.1708 (8)	1.7416 (82)	0.07393 (20)	1040	1017	1024	
Z2	Equant, not abr	0.0241	0.242	83	14	7	3248	0.0872	0.1739 (10)	1.7821 (90)	0.07433 (30)	1050	1034	1039	
Z3	Equant	0.0476	0.245	84	15	10	4218	0.0881	0.1753 (10)	1.7866 (80)	0.07393 (28)	1040	1041	1041	
Z4	Elongate fm/matrix	0.0374	0.236	62	11	7	9110	0.0760	0.1715 (8)	1.7541 (74)	0.07417 (18)	1046	1020	1029	
Z5	Elongate fm/garnet	0.0210	0.210	42	7	8	6276	0.0668	0.1736 (10)	1.7796 (94)	0.07434 (70)	1049	1034	1042	
Z6	Elongate fm/garnet	0.0120	0.187	100	17	11	15040	0.0588	0.1748 (8)	1.7904 (90)	0.07428 (28)	1051	1032	1038	
R1	Small fm/matrix	1.8619	0.017	69	10	546	2396	0.0053	0.1568 (6)	1.5264 (72)	0.07060 (10)	946	939	941	
R2	Small fm/garnet	1.7002	0.172	17	3	369	812	0.0552	0.1540 (8)	1.4993 (96)	0.07060 (18)	946	923	930	
R3	Small fm/garnet	0.7031	0.035	16	2	311	374	0.0113	0.1550 (10)	1.5084 (116)	0.07058 (30)	945	929	934	
R4	L. prisms fm/matrix	1.4001	0.126	70	11	1688	76	0.0395	0.1604 (14)	1.5891 (326)	0.07184 (124)	981	959	966	
R5	L. prisms fm/garnet	0.4272	0.124	13	2	812	87	0.0389	0.1607 (8)	1.5760 (192)	0.07113 (72)	961	960	960	
T1	Brown fm/matrix	1.0253	1.845	108	26	840	1415	0.5788	0.1670 (8)	1.6674 (86)	0.07241 (10)	998	996	996	
T2	Brown fm/matrix	0.6802	2.002	190	23	616	1131	0.6296	0.1667 (6)	1.6664 (70)	0.07251 (10)	999	994	996	
T3	L. brown fm/garnet	1.4336	4.554	62	23	1319	743	1.4068	0.1696 (6)	1.6984 (116)	0.07261 (12)	1003	1010	1008	
T4	L. brown fm/garnet	0.8387	2.735	75	21	2566	279	0.8483	0.1690 (10)	1.6938 (114)	0.07271 (22)	1006	1006	1006	
T5	L. brown fm/garnet	0.4509	2.669	76	21	535	705	0.8361	0.1673 (8)	1.6787 (84)	0.07278 (12)	1008	997	1000	
T6	L. brown fm/garnet	0.6926	4.549	92	33	888	776	1.4308	0.1666 (10)	1.6682 (54)	0.07261 (12)	1003	994	997	

Transformation of Fe-Ti gabbro to coronite, eclogite and amphibolite in the Baie du Nord segment, Manicouagan Imbricate Zone, eastern Grenville Province.

Abstract

Fe-Ti gabbros from the Baie du Nord Segment of the Manicouagan Imbricate Zone, metamorphosed under high-PT conditions during the Grenvillian orogeny, have been the focus of a detailed micropetrological study. Textures and mineral chemistry suggest that the mineral assemblages represent progressive stages of metamorphic transformation resulting in the formation of coronas, pseudomorphs after igneous phases (transitional) and true, granoblastic eclogites. The transitional and eclogitic samples also have coronas which are developed locally around igneous xenocrysts of plagioclase and olivine. The deformed margins of coronitic Fe-Ti gabbros are transformed to amphibolite and contain clinopyroxene-bearing leucosomes with garnet poikiloblasts that are indicative of high-PT, dehydration melting. Interpretation of garnet zoning and thermobarometry suggest that the highest PT-conditions are recorded by coronas around xenocrysts (ca. 720–800 °C at 14–17 kbar) and garnet-clinopyroxene cores in granoblastic assemblages (ca. 740–820 °C at 13–17 kbar) in the eclogitic samples. Reequilibration during the early stages of exhumation at high T-conditions (>700 °C) affected all samples, and is evidenced by the widespread development of pargasite-bearing plagioclase collars in the coronitic and transitional metagabbros and by widespread reequilibration of the eclogites giving lower PT-estimates at grain boundaries. However, the difference in calculated P-conditions between coronite and eclogite samples is consistent with increasing pressure (depth) from the coronites (11–13 kbar) to the eclogites (13–17 kbar).

The PT-conditions recorded by these rocks define an apparent isothermal PT-path. In fact, this is a steep metamorphic field gradient indicating that all the samples experienced temperatures in excess of 800 °C both during and shortly after peak metamorphism over a range of depths (ca. 65-35 km). This in turn suggests high heat flow through this segment of the lower crust during the Grenvillian orogeny.

Key words: Grenville Province, coronitic metagabbro, eclogite, amphibolite, anatexis, garnet zoning, thermobarometry.

2.1. Introduction

The study of the formation of coronitic metagabbros and eclogites has contributed to the understanding of the metamorphic processes in deep crustal levels during continental collision. This is in part due to the fact that rocks which have undergone high-PT metamorphism offer the opportunity to study, model and deduce the metamorphic evolution over a wide range of PT-conditions and on timescales which can be resolved using modern geochronological methods. The validity of this statement depends on the effective preservation of high-PT assemblages. High-PT conditions are usually regarded as the high-T amphibolite (>600 °C) to eclogite facies classifications (e.g. Mørk 1985; 1986; Carswell 1990). At these temperatures and over "normal" metamorphic timescales, in the tens of millions of years, (e.g. England & Thompson 1984; Thompson & Riddley 1987; Ruppel & Hodges 1994) undeformed and dry mafic rocks will tend to preserve best high-PT assemblages (e.g. Mørk 1985; 1986; Pognante 1985; Grant 1988; Zhang & Liou 1997). Deformed mafic rocks will equilibrate faster at high-PT conditions (e.g. Austrheim & Griffen 1985; Pognante 1985; Koons 1987; Rubie 1990; Austrheim et al. 1998) but will also be more easily retrogressed during exhumation and cooling due to enhanced rates of diffusion and fluid infiltration (Heinrich 1982; Koons 1987). Coronitic gabbros from the Molson Lake terrane in the southern part of the

parautochthonous belt of the eastern Grenville Province have been shown to record PT-conditions up to eclogite facies (e.g. Indares 1993; Indares & Rivers 1995). Here we provide new data from west of the Molson Lake terrane in the Manicouagan Imbricate Zone (MIZ). The MIZ contains a variety of mafic rocks, metamorphosed at high-P conditions (Indares 1994; Indares et al. 1994) between 1050-1000 Ma during the Grenvillian orogeny (Cox et al. 1998). The Baie du Nord segment, located in the south-eastern Manicouagan Imbricate Zone, contains Fe-Ti gabbros that have been variably transformed to coronite and eclogite. The gabbro margins have been transformed to amphibolite with garnet and clinopyroxene-bearing leucosomes. The aim of this study is to describe the transition of the Fe-Ti gabbros to eclogite and amphibolite in the Baie du Nord segment and determine the PT-conditions under which the metamorphic textures developed. The results are discussed in terms of the implications for the metamorphism of gabbroic rocks in general, and also the regional tectonic context of the Baie du Nord segment.

2.2. Geological Setting

The Manicouagan Imbricate Zone is a 2000 km² stack of high-P crustal rocks exposed along the shores of Manicouagan Reservoir in eastern Quebec (Figure 2.1). It occurs at the same structural level as the Molson Lake terrane to the east, in which high-P rocks were discovered for the first time in the eastern Grenville Province (Indares & Rivers 1995). To the north, both the Manicouagan Imbricate Zone and Molson Lake terrane tectonically overlie the Gagnon terrane, a Grenvillian fold-thrust and nappe belt, along a thrust contact. To the south, the Manicouagan Imbricate Zone is overlain by the allochthonous Harte Jaune terrane along an extensional shear zone. The Harte Jaune terrane experienced medium-P metamorphism during the Grenvillian orogeny (Hynes & St. Jean 1997).

The Manicouagan Imbricate Zone consists of two, fault-bounded lithotectonic units. The lower unit, known as the Lelukuau terrane (Figure 2.2), is a thrust stack, largely composed of Labradorian rocks that are thought to represent an AMCG suite. The terrane has experienced high-PT metamorphism (up to 16-18 kbar and 850-900 °C, Indares 1997) between 1050 and 1000 Ma (Gale et al. 1994; Indares et al. 1998) which was coeval with emplacement of mafic dykes.

The tectonically overlying Tshenukutish Terrane comprises two lithotectonic segments, the structurally lower Baie du Nord segment and the overlying Boundary zone. Both units are transected and bounded by extensional shear zones with evidence for top-to-the-southeast or southwest transport in two separate stages (Indares et al. 1998). The Boundary zone (Figure 2.2) contains igneous rocks ranging in age from Labradorian (Lac Espadon suite, 1650-1600 Ma, Cox et al. 1998) to Grenvillian, e.g. the Brien anorthosite (1169 \pm 3 Ma, Scott & Hynes 1994) and the Hart Jaune Granite (1017 \pm 2 Ma, Indares et al. 1998) and subordinate metasedimentary units. The Lac Espadon suite is composed of troctolite, ultramafic rocks (dunite, hornblendite, nelsonite) and mesocratic olivine-gabbro, that are interpreted to represent parts of a mafic to ultramafic complex. High-P metamorphism recorded by coronitic troctolite and ultramafic rocks (hornblendite) indicates peak conditions of 800-920 °C at 17-19 kbar (Cox & Indares, in press). U-Pb ages of metamorphic zircon and titanite (ca. 1040-1000 Ma) suggest that high-P metamorphism in the Lac Espadon Suite and the Lelukuau terrane was synchronous (Cox et al. 1998; Indares et al. 1998).

The Baie du Nord segment (BNS) is mainly composed of megacrystic diorite (ca. 1450 Ma, Indares et al. 1998) intruded by Fe-Ti gabbro (1170 \pm 5 Ma, Cox et al. 1998). Locally Fe-Ti gabbro grades into anorthosite. Based on petrography and geochemistry, we suggest that these rocks represent within-plate tholeiites emplaced at a high crustal-level. The Fe-Ti gabbros show a transition from coronite in the

southwest to eclogite in the northeast. These studies also show that metamorphism in the BNS was contemporaneous with the rest of the Manicouagan Imbricate Zone, occurring ca. 1050-1000 Ma.

2.3. Petrography

Samples were studied using standard micropetrographic techniques and using cathodoluminescence (CL) microscopy (a Nuclide Luminoscope CL-unit with accelerating voltages of 10-15 kV and beam currents of 0.1-2 mA) to reveal plagioclase growth textures and to identify mineral inclusions. Samples are discussed below in order of increasing metamorphic transformation. Recent investigations of metagabbros have shown that igneous precursor minerals can preserve their magmatic compositions even at high PT-conditions (e.g. Hartel & Pattison 1996). However in this study igneous precursor minerals preserve original crystal shapes but not necessarily their chemical composition and forthwith we refer to these crystals as relict.

2.3.1. Coronitic metagabbros

The coronitic Fe-Ti gabbros, from the south-western part of the BNS (Figure 2.2) show a limited range in igneous textures, variably preserved in the form of relict plagioclase laths (Appendix A, Plate A1.7a), interstitial clinopyroxene and sparse olivine (Appendix A, Plate A1.7b). Ilmenite and apatite are also common constituents of the original igneous assemblage. Metamorphism of the Fe-Ti gabbros has resulted in the growth of coronas and partial replacement of original igneous phases. Among the metamorphic minerals orthopyroxene occurs as aggregates, interpreted as pseudomorphs after olivine (Appendix A, Plate A1.7c-d). These are surrounded by clinopyroxene and garnet coronas. Clinopyroxene

crystals, which preserve igneous shapes, display a strong green color, and are rich in rutile inclusions. Plagioclase relicts contain abundant spinel and locally, corundum inclusions, and are separated from ferromagnesian phases by garnet coronas. Thus, the metamorphic textures in these rocks suggest that the coronas are the result of diffusion of Ca, Na and Al from plagioclase sites and Fe and Mg from olivine sites (Mongkoltip & Ashworth 1983; Grant 1988). The resulting formation of the orthopyroxene, clinopyroxene and garnet coronas, inclusions in the plagioclase and the preservation of both olivine and clinopyroxene relicts, indicates that only partial (domainal) equilibrium was achieved during metamorphism. Small, inclusion-free, plagioclase collars, in association with pargasite, are commonly developed between garnet and clinopyroxene. These are interpreted to be the result of decompressional growth (Indares 1993). In most of the coronitic samples, pargasite, with intergrown biotite/phlogopite around ilmenite, is present. However, the exact timing of the formation of these coronas is not certain, and they may be due to the high-PT metamorphic breakdown of ilmenite or to retrogression in the presence of fluids.

2.3.2 Transitional metagabbros

Farther to the north-east (Figure 2.2), transitional metagabbros display similar original igneous features. The metamorphic minerals are the same as in the coronitic metagabbros, however plagioclase is strongly recrystallized, with cleavage-oriented spinel and occasional corundum inclusions. Locally plagioclase domains are pseudomorphed by garnet with little relict plagioclase remaining (Appendix A, Plate A1.8a). Olivine is completely replaced by orthopyroxene aggregates. These textures strongly suggest that metamorphic recrystallization was more pervasive in these samples. Large plagioclase xenocrysts, rich in spinel and corundum inclusions, also occur in these rocks and are surrounded by garnet coronas (Appendix A, Plate A1.8b). The pervasive metamorphic textures in these samples indicate a transition to

the northeast from coronites to granoblastic rocks. In addition, the transitional rocks display textures inferred to have developed during decompression. For instance, pargasite-bearing, plagioclase collars are common and clear plagioclase collars are found between garnet and remaining inclusion-rich plagioclase relicts. CL-images reveal twinning in plagioclase with spinel-rich areas and brighter luminescent areas of granular plagioclase which correspond to regenerated collars (Appendix A, Plate A2.1a). These are interpreted to form during decompression (e.g. Indares 1993). The abundance of this second type of plagioclase is indicative of major reequilibration of the assemblages during decompression. Pargasite coronas around ilmenite are present in these samples and, as in the coronites, their origin is also uncertain.

2.3.3. Eclogites

The assemblages of the Fe-Ti gabbros on the northeastern margin of the BNS (Figure 2.2) contrast strongly with the coronitic and transitional rocks in the south. Igneous phases have been almost completely replaced by metamorphic assemblages, and only sparse relicts of olivine and (inferred magmatic) clinopyroxene remain. Olivine is replaced by granular orthopyroxene, which in turn is largely replaced by granoblastic clinopyroxene. Igneous clinopyroxene relicts, which contain numerous rutile inclusions, are generally surrounded by garnet coronas. However, the main metamorphic texture of the rock is granoblastic and the assemblage is composed dominantly of pale green clinopyroxene and garnet. The garnet has clearly grown as pseudomorphs after plagioclase, preserving the original lath shape. Locally, "ribbons" of relict plagioclase, rich in spinel and corundum inclusions, are preserved inside garnet pseudomorphs (Appendix A, Plate A1.9a). These rocks represent the most pervasive stage of high-PT metamorphic recrystallization of the Fe-Ti gabbro protoliths in the BNS. As these rocks are dominated by granoblastic garnet and omphacitic clinopyroxene and contain less than 5% relict plagioclase, they can

be termed eclogite *sensu-stricto* (Carswell 1990). In common with the transitional Fe-Ti gabbros from the southern/central part of the BNS, these rocks also contain xenocrysts. In one sample xenocrysts of olivine and plagioclase occur adjacent to each other and they are separated by a triple corona of orthopyroxene, clinopyroxene and garnet (Appendix A, Plate A1.9b). In addition, the plagioclase xenocryst contains spinel, corundum and kyanite inclusions. Kyanite inclusions are extremely small, sparsely distributed and were only identified using the CL-microscope at high magnifications, where they show a bright red luminescence within the blue luminescent plagioclase (Appendix A, Plate A2.1b). The eclogites do not display secondary plagioclase collars, however, pargasite is found as coronas around ilmenite. This suggests that the pargasite coronas around ilmenite may be the result of high-PT growth in the presence of fluid rather than due to decompression, although this is speculative.

2.3.4. Migmatitic garnet amphibolites

The margins of the Fe-Ti gabbros throughout the BNS are deformed and amphibolitized, with primary textures completely overprinted by granoblastic, foliated assemblages. In the south-eastern BNS, the amphibolite margins contain leucosomes with large garnets often reaching several cm in diameter. The garnets are poikilitic displaying cores rich in inclusions of quartz, plagioclase, ilmenite and rutile with inclusion-free rims (Appendix A, Plate 1.11a-b). Inclusions form sigmoidal trails indicating that garnet poikiloblast cores grew during deformation (e.g. Passchier et al. 1992; Bell et al. 1992). Rutile increases in abundance outwards at the expense of ilmenite, and often forms aligned inclusion trails at the rims of the inclusion-rich cores indicating growth against the face of the original poikiloblast. Sparse clinopyroxene crystals also occur in the leucosomes, but are largely replaced by amphibole. Titanite is a relatively late phase, occurring around rutile and along cracks in the garnet near the inclusion-free rims (Appendix A, Plate 1.11c-d), and post-dates the growth of the rotational fabric recorded by the inclusion

trails. Accessory zircon and apatite are common in both the poikiloblasts and the matrix. The matrix assemblage is granoblastic-foliated and dominated by amphibole (pargasite), plagioclase, quartz, and lesser amounts of biotite, ilmenite and rutile. Both ilmenite and rutile are partially replaced by titanite. Titanite in the matrix is less abundant and smaller in grain-size than within the garnet, reflecting the involvement of rutile and garnet on the titanite-forming reaction. Based on the U-Pb ages of zircon (1046 \pm 3 Ma), titanite (1006 \pm 5 Ma, 997 \pm 3 Ma) and rutile (960 \pm 6 Ma, 946 \pm 2 Ma) from this sample the garnets and leucosomes are thought to represent partial melting of the amphibolitized Fe-Ti gabbro margins near the peak of metamorphism, and the growth of the garnet rims and matrix assemblages the result of retrogression during exhumation (Cox et al. 1998). Thus, in these rocks the conditions of the prograde, peak and retrograde PT-conditions may be recorded.

2.4. Mineral chemistry

All mineral analyses were carried out on a Cameca SX50 electron microprobe analyzer in ED mode at Memorial University with a 20 nA current and a 15 kV accelerating potential, except for plagioclase which was analyzed with a 10 nA current to reduce the effects of Na volatilization. Count times varied from 50 secs for garnet, 75 secs for plagioclase, spinel and ilmenite to 100 secs for pyroxene and amphibole. Representative analyses of minerals are presented in Table 2.1. All mineral abbreviations are from Kretz (1983) and Spear (1993). Zoning profiles across garnet were collected with spacing of 10 to 100 μ m, depending on grain size. Multiple analyses were also performed on plagioclase and pyroxene to check for chemical zoning. Structural formulae of minerals were calculated using the program THEBA v.6.0 (J. Martignole and others, personal communication 1995). The Fe³⁺-content of the ferromagnesian phases was calculated using the method of Droop (1987). However, the accurate determination of the Fe³⁺-

content of minerals remains problematic particularly in low-Fe minerals using the EDS analysis method. As a result the fluctuations in Fe³⁺-content recorded by clinopyroxene in this study may be an artifact of the analytical uncertainties. However, recent published analysis of metamorphic clinopyroxene in high-P mafic rocks (e.g. Zhang & Liou 1997; Camacho et al. 1997; Medaris et al. 1998) show similar fluctuations in the apparent Fe³⁺-content. Thus, for comparison we have reported the clinopyroxene compositions as calculated. The results however are discussed in terms of total Na, i.e. combined Jd+Ac-contents.

2.4.1. Garnet

In the eclogite (sample 21) the compositions of the garnet pseudomorphs have the highest Mg-content (Prp₃₈₋₄₀Alm₄₈₋₅₀Grs₀₈₋₁₀), compatible with the extensive development of high-P minerals in this rock. In contrast, in the coronitic metagabbro (sample 123) the garnet has much lower Mg and higher Fe-contents (Prp₂₆₋₂₈Alm₅₈₋₅₉Grs₁₂₋₁₄) than those in the eclogite (Figure 2.3) although both rocks have similar bulk chemical compositions (Cox et al. 1998). This is consistent with the partial replacement (corona formation) of the igneous phases by metamorphic assemblages. However, the compositions of the garnets from the transitional metagabbros (sample 85) are seemingly at odds with the textural evidence indicating more extensive replacement of the igneous assemblages, showing higher Fe and lower Mg-contents (Prp₂₁₋₂₂Alm₆₀₋₆₂Grs₁₃₋₁₄) than the coronitic samples (Figure 2.3). The transitional metagabbros have higher bulk Fe and Ca-contents than either the coronites or eclogites, reflecting variations in the plagioclase and ilmenite contents between the protoliths (Cox et al. 1998). Thus, the anomalous garnet compositions in this sample may be due to the differences in bulk chemical composition.

In all samples garnet coronas are variably zoned, whereas garnet pseudomorphs after plagioclase are homogeneous at the grain scale. The garnet coronas between xenocrysts in the eclogite (sample 21)

have the best preserved zoning with an increase in Ca towards the plagioclase (Grs_{12-40}), compensated by an increase in Mg and Fe ($\text{Prp}_{18-35}\text{Alm}_{40-49}$) towards the clinopyroxene corona (Figure 2.4a). The XFe content decreases towards the clinopyroxene. These patterns are typical of growth zoning in coronitic garnet (Indares and Rivers 1995; Indares and Dunning 1997). Growth zoning in coronitic garnet differs from the typical Rayleigh-type growth in granoblastic garnet by virtue of the fact that the corona grows from the inner to outer rim between reactant phases instead of concentrically outward. Thus, zoning is controlled by the chemical gradient between the minerals at the growth interfaces. In other words high Ca and high Mg and Fe are a direct result of growth in contact with plagioclase and clinopyroxene at the respective margins of the garnet corona. The garnet corona compositions at the clinopyroxene contacts are similar to those of the pseudomorphs (Figure 2.3).

Garnet coronas around plagioclase xenocrysts in the transitional metagabbros (sample 85) display the same type of zoning as in the eclogite but to a lesser degree. In addition, there is a steep drop in Ca at the rims towards the plagioclase and the XFe is almost flat across the corona (Figure 2.4b). This is most likely indicative of post-growth reequilibration during decompression (Indares and Rivers 1995). Garnet pseudomorphs in the sample have similar compositions as the parts of the corona with the maximum Mg-content ($\text{Grs}_{18}\text{Prp}_{40}\text{Alm}_{42}$). The garnet coronas from the coronitic metagabbros (sample 123) are the least strongly zoned with only a very slight variation from the plagioclase to the clinopyroxene contact ($\text{Grs}_{20-14}\text{Prp}_{12-14}\text{Alm}_{58-59}$). The lack of zoning (Figure 2.4c) and homogenous XFe may be related to diffusion resetting in the presence of fluid during the development of the pargasite-bearing plagioclase collars. The transition from corona textures to eclogite, together with the general increase from low to high Mg-content (Xprp) may indicate an increase in the metamorphic grade in the BNS from the south-west to the north-east.

Garnets from the migmatitic garnet-amphibolites (sample 313) have the lowest Mg and highest Fe (Figure 2.3) and display the highest Mn-concentrations (Sps₀₅₋₀₁). Zoning occurs in the largest (>1cm) garnet poikiloblasts (Figure 2.5a). The high XFe may correlate with higher Fe-content in the igneous precursor. The inclusion-rich core which occupies about 90% of the zoning profile (segment (i) on Figure 2.5a) shows a slight outward decrease in Mn, Fe (Sps₀₅₋₀₁Alm₆₀₋₅₈) and XFe along with an increase in Mg-content (XPrp₁₅₋₁₈). For the majority of the core region the Ca-content is homogenous. These trends may represent relict growth zoning that has been extensively modified at high temperatures, with the XFe decrease suggesting increasing temperature towards the rim. Growth zoning in granoblastic garnet is usually homogenized at T-conditions in excess of 600 °C. However, growth zoning has been shown to be preserved in garnets even at very high temperatures (Loomis 1983; Spear et al. 1990; Indares 1995; Neng-Song Chen et al. 1998). The inner (rutile-bearing) rim (segment (ii) on Figure 2.5a-b) displays a marked outward decrease in Fe (Alm₆₀₋₅₀) and XFe along with an increase in Mg-content (Prp₁₂₋₂₀) and homogenous Ca-content (Figure 2.5a). Zoning of the inclusion-free rims (segment (iii) on Figure 2.5a-b) is mainly represented by a drop in Ca (Grs₂₂₋₁₅) and continuous increase in Mg content. The Fe-content over the rim is homogeneous and lower than in the rest of the crystal, while XFe decreases (Figure 2.5b). The increase in Mg and decrease in Ca-content at the garnet rims may be the result of the formation of the overgrowth (inclusion-free rim) at lower pressures than the core along with exchange between the garnet rim and the matrix at high temperatures.

2.4.2. Clinopyroxene

As with the garnet, the clinopyroxene compositions depend upon both the textural setting and the rock type. In individual samples both coronas and granoblastic clinopyroxene have the same composition, and are homogeneous at the grain scale. The eclogites (sample 21) contain clinopyroxene which ranges

from high Na-augite to omphacite (Fig. 8) with the highest Na-content (Jd+Ac₂₇₋₄₀). The coronitic metagabbros (sample 123), however, contain only Na-augite with much lower total-Na (Jd+Ac₁₁₋₂₅) than the eclogites. The transitional metagabbros (sample 85) show lower Jd but a similar range in total Na-contents in the clinopyroxene (Jd+Ac₁₅₋₂₄) despite the more intense metamorphic recrystallization compared with the coronitic samples. Clinopyroxenes in the leucosomes of the migmatitic garnet-amphibolite (sample 313) have been partially replaced by hornblende. The remaining clinopyroxene crystals are homogeneous at the grain scale. The range of compositions may be compared with those of the clinopyroxene in the transitional rocks with lower Jd but similar total-Na (Jd+Ac₁₆₋₂₅) than those in the coronitic metagabbros (Figure 2.6).

2.4.3. Plagioclase and amphibole

In all rock types the plagioclase relicts and collars tend to be unzoned, although where relict igneous crystals occur adjacent to collars (e.g. sample 85, Figure 2.7) a slight increase in the Na-content outwards from relict core to collar can be detected. The highest Na-contents (Ab₂₈₋₄₆An₁₂₋₁₄) occur in the "ribbon" plagioclase relicts in the eclogite, with transitional (Ab₆₀₋₆₂An₄₀₋₃₈) and coronitic (Ab₇₀₋₇₅An₃₀₋₂₅) plagioclase relicts being much less sodic (Figure 2.7). The relict plagioclase lath compositions from the transitional metagabbros, along with the garnet and clinopyroxene compositions, are consistent with the fact that the bulk Na+Mg content was lower and the Fe+Ca content higher in the igneous precursor. Thus, although the textures suggest more pervasive metamorphic recrystallization than in the coronites, the metamorphic mineral compositions are lower in Na and Mg than may have been expected. The compositions of the plagioclase xenocrysts from the eclogite and transitional metagabbros are in the same range (Ab₆₄₋₅₇An₃₆₋₄₃) and are zoned with increasing Ca-content towards the contact with the garnet corona. The decompressional plagioclase collars in the coronitic and transitional metagabbros are higher

in Na than the relict laths in the same samples ($Ab_{77-82}An_{33-28}$). This suggests that Na-augite has been involved in the generation of the collars during decompression. This observation is supported by the presence of pargasite in many of the plagioclase collars, further suggesting that the retrograde formation of the collars was aided by fluid.

The compositions of the plagioclase inclusions in the migmatitic garnet-amphibolite (sample 313) show an increase in Na ($Ab_{60-66}An_{40-34}$) from those in the core to those in the rim of the garnet poikiloblast (Figure 2.7). The Na-content of the matrix crystals ($Ab_{68}An_{32}$) is higher than inclusions in the garnet. Amphibole compositions from the matrix (Table 1) lie in the compositional range between pargasite and Fe-pargasite (Leake et al. 1997). Neither amphibole or plagioclase in the sample show significant zoning across individual grains.

2.5. Reaction history

2.5.1. Transition from Fe-Ti gabbro to eclogite

The reaction textures and mineral chemistry of the metagabbros in the BNS indicate the breakdown of igneous plagioclase and olivine to produce Na-rich metamorphic phases (albite and Na-augite/omphacite) and Mg-rich garnet. As described above, differences in bulk Ca, Na, Fe and Mg of the igneous precursors between the transitional metagabbros and the coronites and eclogites have caused a deviation from this trend. However, textures in the transitional metagabbros, such as the formation of garnet pseudomorphs after plagioclase, support the hypothesis that they result from more pervasive breakdown of the original assemblages than the coronitic equivalents. Given the preservation of igneous crystal shapes and lack of penetrative fabric in these samples it appears that the metamorphic overprint was a static process. The formation of coronas and the progressive overprinting of the relict igneous

phases together with the development of granoblastic assemblages can be illustrated by a schematic evolution in four stages (Figure 2.8) which represent variably developed mineral assemblages. The reactions for each stage (Figure 2.8) represent global reactions based on domainal reactions in the samples. The domainal reactions are themselves indicated by both local textural and compositional features in the individual samples described above.

2.5.1.1. Transformation from Stages I (igneous phases) to II (grt-opx corona)

The breakdown of the igneous phases olivine and plagioclase (Stage I, Figure 2.8) involves the diffusion of Fe and Mg towards the plagioclase domain and Ca and Al towards the olivine, resulting first in the formation of double coronas of garnet and orthopyroxene (Stage II, Figure 2.8). In domains where there is a higher local concentration of olivine to plagioclase, excess Fe and Mg at the site of the forming coronas likely diffuses into the plagioclase, forming spinel inclusions with the remaining Al, following Ca diffusion from the plagioclase. In domains where plagioclase concentrations are locally higher, excess Al results in the formation of corundum inclusions. These two cases can be summarized by the following reactions.

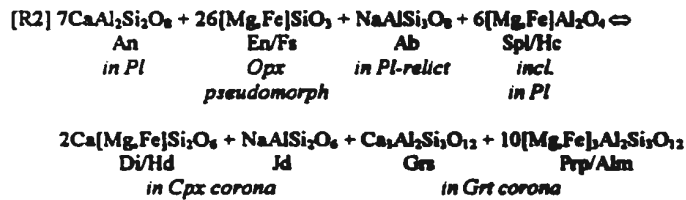


The result of the changing local concentrations of diffusing elements may account for the presence of both spinel and corundum inclusions in most of the samples. For example as the orthopyroxene and garnet coronas develop, less excess Mg (and Fe) reaches the plagioclase site. This would result in the

development of corundum instead of spinel inclusions in the plagioclase relicts, i.e. a progression from [R1a] to [R1b]. These reactions would also lead to an increase in the Na of the relict plagioclase and the formation of pseudomorphs of orthopyroxene after olivine.

2.5.1.2. Transformation from Stages II (opx-grt corona) to III (cpx-grt corona)

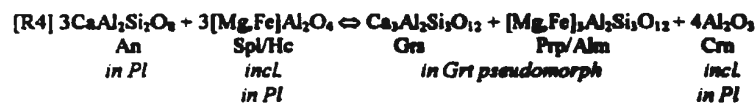
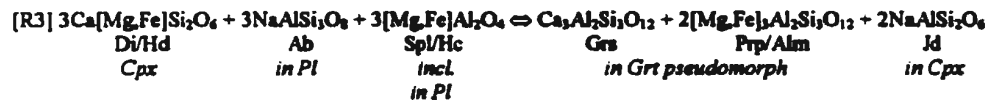
At more advanced stages of recrystallization, orthopyroxene (both relict igneous and pseudomorphs) will form clinopyroxene coronas, garnet will pseudomorph the plagioclase, consuming spinel, and both relict igneous clinopyroxene and clinopyroxene coronas will become more Na-rich as the Na-rich (Xab) component of the plagioclase becomes involved in the reaction (Stage III, Figure 2.8). The transition from Stage II to Stage III can be characterized by the following reaction.



The textures resulting from the above reaction occur in both the coronitic and transitional metagabbros suggesting both types have bypassed the Stage II transformation. However, the preservation of some olivine relicts along with the presence of clinopyroxene coronas in the coronitic metagabbros suggests that the reactions defining both Stage II and Stage III transformations are continuous. Furthermore, the lack of olivine in the transitional metagabbros and the presence of garnet pseudomorphs after plagioclase indicates that the Stage III transformation was more complete in these samples.

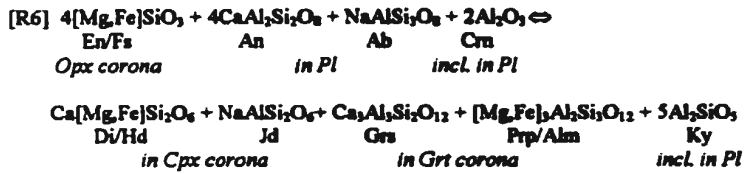
2.5.1.3. Transformation from Stages III (cpx-grt corona) to IV (eclogite)

The transformation of the Fe-Ti gabbros to eclogite involves the final breakdown of the remaining Na-rich plagioclase resulting in replacement of both the orthopyroxene pseudomorphs and clinopyroxene relicts and coronas by omphacite, whereas the plagioclase sites are completely replaced by garnet pseudomorphs (Stage IV, Figure 2.8). This would involve the following reactions.



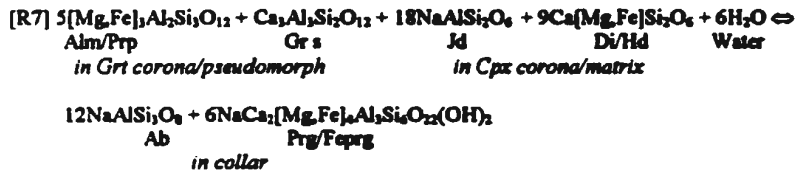
Some cores of garnet pseudomorphs in the eclogite contain Na-rich "ribbon" plagioclase, which has abundant spinel and corundum inclusions, and locally, orthopyroxene pseudomorphs are still present. Thus, the reactions have not gone to completion, even in the most eclogitized samples.

The coronas which form around, and between the plagioclase xenocrysts in the transitional metagabbros can also be described in terms of the above reactions. The plagioclase xenocryst in the eclogite, however, contains kyanite inclusions. This suggests an excess of Si as well as Al in the plagioclase during metamorphism. The reaction pathway may follow the reaction [R1b]. The excess of Si and Al which forms kyanite can be explained by [R2], rewritten as follows.



This would explain the formation of both the garnet and Na-augite/omphacite coronas at the expense of the orthopyroxene corona, and the presence of kyanite in the plagioclase.

Reactions that may be responsible for the formation of the pargasite-bearing plagioclase (Na-rich) collars are harder to quantify. The collars themselves do not contain spinel or corundum, and thus, retrograde back-reactions using those described above would not account for their formation. The presence of the pargasite also suggests the involvement of fluids. This may be explained by the following general reaction.

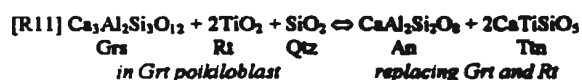


However, the localized development of the retrograde collars in the samples suggests that fluid influx was limited. The lack of a penetrative fabric in the samples probably inhibited the movement of fluids and thus, the development of retrograde assemblages.

2.5.2. Migmatite formation and amphibolite overprint

The deformed margins of the gabbros are characterized by high amounts of amphibole and by the presence of garnet-clinopyroxene bearing leucosomes. Fluid infiltration in these rocks is likely to have occurred early in their metamorphic evolution during dehydration of the surrounding country rocks. It is

Reaction [R10] above would account for the formation of the garnet overgrowths. Final evidence of retrogression is indicated by the replacement of rutile and garnet by titanite suggesting the following reaction.



Both these reactions are representative of later replacement of melt assemblages by amphibolite assemblages under lower-P conditions. Although the formation of garnet overgrowths and amphibolite matrix and the breakdown of the garnet and rutile to form titanite in the garnet rims can be represented as a two part process, given the lack of major resorption of the garnet poikiloblasts these two stages were most likely continuous. Late-stage Fe-Mg exchange between in garnet and pargasite likely occurred during the formation of titanite as indicated by the increase in Mg at the garnet rims (Figure 2.5b).

2.6. Thermobarometry

2.6.1. Point selection and general approach

For each sample, interpretation of textures and of mineral chemistry was followed by selection of appropriate microdomains for PT-determinations. In granoblastic areas, both the cores and contacts between the relevant mineral phases were used in order to calculate maximum and retrograde conditions. Although corona textures signify global disequilibrium, local equilibrium between garnet rims and adjacent phases is assumed and thermobarometry can be performed with suitable phases. At the rims of garnet coronas which display well preserved growth zoning, local equilibrium likely corresponds to peak-PT conditions, whereas homogenized garnet coronas may give minimum conditions for the peak of

metamorphism. Ideally both P- and T-estimates have to be obtained from a single microtextural domain. In the case of the coronitic samples T-estimates can only be obtained at the inner rims of the garnet coronas (in contact with clinopyroxene) whereas P-estimates come from the outer rims (in contact with plagioclase). However, with the exception of rims affected by retrograde resetting we assume that equilibrium in both domains was achieved during the thermal peak (e.g. Indares & Rivers 1995; Indares & Dunning 1997) and therefore the P- and T-estimates can be combined.

Metamorphic temperatures were calculated using Fe-Mg exchange reactions between adjacent rims of garnet-clinopyroxene in the coronas and cores and rims in the pseudomorphs/granoblastic areas. For the migmatitic garnet-amphibolites PT-estimates were calculated using inner-rim compositions along with the adjacent inclusions and clinopyroxene relicts, which are interpreted as representing the leucosome assemblage. Garnet rims and matrix pargasite contacts along with the titanite-bearing assemblages were used to determine the PT-conditions for the formation of the garnet overgrowths during amphibolite retrogression. The garnet-plagioclase-spinel-corundum reaction (Indares & Dunning 1997) was used for the eclogitic and coronitic samples except for the kyanite-bearing, xenocryst corona assemblage (sample 21) for which the garnet-plagioclase-kyanite-corundum reaction (Indares & Rivers 1995) was utilized. The garnet-clinopyroxene-plagioclase-quartz barometer (Newton & Perkins 1982) was used for the pressure estimate in the leucosome assemblage in migmatitic garnet-amphibolite (sample 313). Reaction [R11], which is a variation of the GRAIL barometer (e.g. Ghent & Stout 1984), was used for amphibolite P-estimates in this sample.

PT-conditions were calculated using the program TWEEQU v.2.02 (Berman 1991) utilizing the activity models of Fuhrman & Lindsley (1988) for plagioclase and Berman & Aranovich (1996) for pyroxene and garnet in an internally consistent database. Garnet-amphibole thermometry requires an older version of the program (v.1.01) using the activity models of Mäder & Berman (1992) for amphibole and Berman (1990) for garnet (R. Berman, personal communication 1998). For comparison, T-conditions

were also calculated with the Fe-Mg exchange thermometers of Ellis & Green (1979) and Krogh (1988) for garnet-clinopyroxene and Graham & Powell (1984) for garnet-amphibole in the migmatitic garnet-amphibolite as these calibrations are extensively used in many recent publications. Given the errors associated with the estimation of the Fe³⁺-content all temperatures were calculated assuming the Fe to be Fe²⁺. The calculated PT-conditions along with the calibrations used are shown in Table 2.2 and the results (using TWEEQU) are presented in Figure 2.10.

2.6.2. PT-determinations

The highest PT-conditions are recorded by the eclogite (sample 21). The corona assemblage between the olivine and plagioclase xenocrysts gives a range of PT-estimates (720-800 °C and 14-17 kbar), overlapping with PT-estimates using the garnet (pseudomorphs), omphacite and relict "ribbon" plagioclase assemblages (740-825 °C and 13-17 kbar). The grain boundaries of the granoblastic areas and garnet pseudomorphs give a lower range of PT-conditions (675-760 °C and 13-16 kbar) and have been likely affected by thermal reequilibration during cooling. However these estimates do overlap the estimates from both the cores and coronas (Figure 2.10a). The transitional metagabbros also give a broadly similar range of PT-conditions for the xenocryst corona assemblages (745-805 °C and 11-13 kbar) and granoblastic areas using pseudomorph core compositions (750-810 °C and 11-14 kbar). The rims record a lower PT-range (710-760 °C and 10-14 kbar) but again there is considerable overlap with the estimates from the cores and coronas (Figure 2.10a). The coronitic metagabbros give P-conditions which are slightly lower, but have similar T-ranges, to those of the transitional rocks and eclogites (770-810 °C and 12-14 kbar). PT-conditions were also calculated using several domains with extensive pargasite-bearing plagioclase collars. PT-conditions recorded in these areas (710-780 °C and 11-13 kbar) are lower on average than in "collar-free" coronas (Figure 2.10b).

The PT-estimates from migmatitic garnet-amphibolites (sample 313) have been calculated from two zones of the garnet. Mg-rich inner garnet-rims and inclusions (segment (ii) on Figure 2.5a-b) and matrix clinopyroxene give PT-conditions of 795-825 °C and 11-12 kbar. PT-estimates calculated using the garnet-rutile-titanite-amphibole-quartz assemblage in the inclusion-free garnet rims are lower, giving a range of 740-805 °C and 8-10 kbar (Figure 2.10b).

In comparison, the T-ranges calculated using the calibrations of Ellis & Green (1979) and Krogh (1988) for garnet-clinopyroxene and Graham & Powell (1984) for garnet-hornblende (sample 313) are in excellent agreement with those calculated using TWEEQU (Table 2.2).

2.6.3. Interpretation of data

The highest P-conditions recorded by the eclogites, transitional and coronitic metagabbros in the BNS show a clear increase from the coronites in the south-west to the eclogites in the north-east (Figure 2.10a-b). This is entirely consistent with the textural evidence for increasing metamorphic transformation in the samples. However, the highest recorded temperatures in these samples overlap to a considerable extent, generally in the 750-800 °C range. PT-estimates from the eclogites and transitional metagabbros calculated with grain boundaries in granoblastic areas are lower than the coronas or cores in granoblastic areas (Figure 2.10a) or from coronas with extensive pargasite-bearing plagioclase. Interestingly, the isopleths (top and bottom of PT-boxes in Figure 2.10a-b) which define the P-estimates are identical in both grain boundaries and cores. P-estimates, as calculated by the garnet-plagioclase-spinel-corundum reaction (Indares & Dunning 1997) are largely controlled by the diffusion of Ca in the garnet. It is apparent that the temperatures, controlled by Fe-Mg exchange, are the most affected by later resetting. This is consistent with the published rates of diffusion for Ca, Fe and Mg in garnet (Elphick et al. 1981; Brady & McCallister 1983; Lasaga 1983; Ganguly & Tazzoli 1994; Schwandt et al. 1996). Thus, the

apparent PT-path produced by combining the peak conditions recorded by the granoblastic/pseudomorph cores along with the coronas, and retrograde conditions using grain boundary determinations, may be incorrect.

Preservation of the growth zoning in the garnet coronas in the eclogite strongly suggests that the maximum PT-conditions recorded by this rock reflect near-peak conditions. The transitional metagabbro (sample 85) records lower PT-conditions in the coronas that those in the cores of the relict plagioclase, garnet pseudomorph, Na-clinopyroxene assemblages. It is evident from the apparent relaxation of the zoning in the garnet corona, regeneration of plagioclase (collars) and by the lack of zoning in the garnet pseudomorphs, that both the coronas and the granoblastic assemblage have undergone partial resetting at high-T during the early stages of cooling. The general range of T-estimates from the grain boundaries are lower (Figure 2.10a) and the PT-conditions recorded by the granoblastic cores and coronas are also interpreted as near peak conditions. The coronitic metagabbros (sample 123) record P-conditions which are lower than those in the eclogites and transitional metagabbros. However, the same general T-range is recorded by the coronites as in the eclogites and transitional rocks (Figure 2.10b). The PT-conditions recorded by the best preserved coronas are higher than those recorded by coronas with pargasite-bearing plagioclase collars. Furthermore, the near-complete relaxation of zoning in the garnet coronas (Figure 2.4c) suggests that the PT-conditions probably record those experienced by the sample during the initial stages of exhumation.

The apparent peak PT-conditions recorded by the migmatitic garnet-amphibolite (795-825 °C at 11-12 kbar) are recorded by the Prp-rich inner-rim. On the other hand, based on experimental results (e.g. Sen and Dunn 1995; Wolf and Wyllie 1993; 1994) and measurements on natural samples (Williams et al. 1995; Hartel and Pattison 1996), it is clear that temperatures >850 °C at 10 kbar are required for garnet to grow in an amphibolite undergoing dehydration melting. Only the highest T-estimates from inner-rims

are close to this minimum. Mg, Fe and Mn diffusion rates in garnet at such high temperatures would be sufficiently fast as to homogenize growth-zoning unless the duration of the high-T metamorphic event was extremely short (e.g. Ayres & Vance 1994). However, even Mn-growth zoning is at least partially preserved in the garnet poikiloblasts (Figure 2.5a). In addition, the presence of melt-generated zircon in the leucosomes (Cox et al. 1998) is consistent with rapid melt segregation (Watt et al. 1996). The partial preservation of growth zoning in the garnet and evidence for rapid melt segregation suggests that the melting phase was short lived. The highest PT-conditions recorded by the both the migmatitic garnet-amphibolite and the coronitic metagabbros are very similar and in both samples the conditions are likely close to, but not at, the peak of metamorphism. Thus, PT-conditions from the garnet inner-rims, inclusions and clinopyroxene-bearing leucosome assemblages (as with the coronitic metagabbros) are interpreted as recording the conditions attained by the sample shortly after, but not during, the migmatite event. PT-conditions representative of overprinting of the leucosome assemblage by the amphibolite assemblage, probably during the growth of the inclusion-free garnet rims give similar T-ranges (740-805 °C) but record lower pressures (8-10 kbar). The Fe-Ti gabbros in the BNS have clearly all recorded pressures which are consistent with burial to different crustal levels and high T-ranges which are similar. As all the samples likely achieved these PT-conditions shortly after peak metamorphism, the metamorphic field gradient (composite PT-path) they define indicates an isothermal regime operating during initial decompression. The implications of this are discussed below.

2.7. Discussion and conclusions

The textures, mineral chemistry and garnet zoning in the coronite and eclogite samples from the BNS characterize the progressive breakdown of plagioclase, olivine and clinopyroxene from the igneous

assemblage in metagabbros under high PT-conditions. Several studies (e.g. Mørk 1985; Indares & Dunning 1997; Zhang & Liou 1997) have described similar transition textures. A recent study by Austrheim et al. (1998) suggested that deformation followed by fluid influx and subsequent dehydration reactions resulted in the transformation of mafic rocks to eclogite in the Western Gneiss region, Norway. However, the samples described in this study clearly show static growth of the eclogite mineral assemblages. Indeed, the presence of anatectic melts and subsequent amphibolite facies overprinting of the deformed margins suggests that deformed and hydrated rocks will be unlikely to preserve eclogitic assemblages at the PT-conditions recorded in these samples. In this study, the PT-conditions from the eclogites and transitional metagabbros, using coronas around xenocrysts and cores of the granoblastic assemblages are higher than the granoblastic grain boundaries. This is common in metamorphic mineral assemblages. In addition, the PT-estimates from the coronitic rocks are higher in "fresh" corona assemblages than those recorded in coronas with decompressional, pargasite bearing plagioclase collars. However, the overlap in highest T-conditions suggests pervasive reequilibration at high-T to give the conditions recorded by these samples. This points to the fact that the eclogites, transitional and coronitic rocks probably do not record peak PT-conditions. Furthermore they have been reequilibrated at similar T-conditions which produces an isothermal metamorphic field gradient across the BNS. This is confirmed by the migmatitic garnet-amphibolites which record conditions which are lower than experimentally derived PT-estimates for dehydration melting. However, it is clear from the pressure differences that the samples were exhumed from different crustal levels. The coincidence of the highest temperatures in many of the samples, along with the PT-estimates for the amphibolite overprint in the migmatitic garnet-amphibolites (710-805 °C and 8-10 kbar) may be used to invoke near-isothermal decompression. This isothermal decompression and isothermal field gradient suggests an extremely high heat input through a reasonably thick layer of lower crust at depths from ca. 65-35 km during exhumation. The highest absolute T-conditions preserved also suggest that the BNS was metamorphosed under a high thermal

regime. The highest PT-conditions (ca. 825 °C at 17 kbar) recorded by the eclogites in the BNS overlap with those recorded by the overlying Lac Espadon suite and the underlying Lelukuau terrane (ca. 800-920 °C at 17-19 kbar °C, Indares 1997; Cox & Indares 1999b). The Lac Espadon suite also has a steep to near-isothermal field gradient also suggesting high heat flow during decompression (Cox and Indares, in press). Indeed, isothermal decompression of high-PT terranes is typically interpreted as representing a tectonic exhumation process with a high heat flow (e.g. Rubie 1984; Davy & Gillet 1986). The presence of syn-metamorphic mafic dykes in the adjacent Lelukuau terrane and the Harte Jaune granite, both emplaced shortly after or during peak metamorphic conditions (Indares et al. 1998), may explain the persistence of high temperatures and the apparent reequilibration of the coronites and eclogites at high T-conditions during the early stages of exhumation. Although these bodies are relatively small they represent mantle derived melts and thus heat input from the mantle into the lower crust. This idea has been recently suggested and is supported by the large volumes of AMCG suites emplaced after the main phases of metamorphism in the Grenville (Corrigan & Hanmer 1997). The high T-conditions recorded in the BNS and also in the Lac Espadon suite and Lelukuau terrane, indicate that mantle heat input during metamorphism and exhumation was probably pervasive throughout the Manicouagan Imbricate Zone.

Figure 2.1. Map of the eastern Grenville Province showing the location of the Manicouagan Imbricate Zone and surrounding terranes.

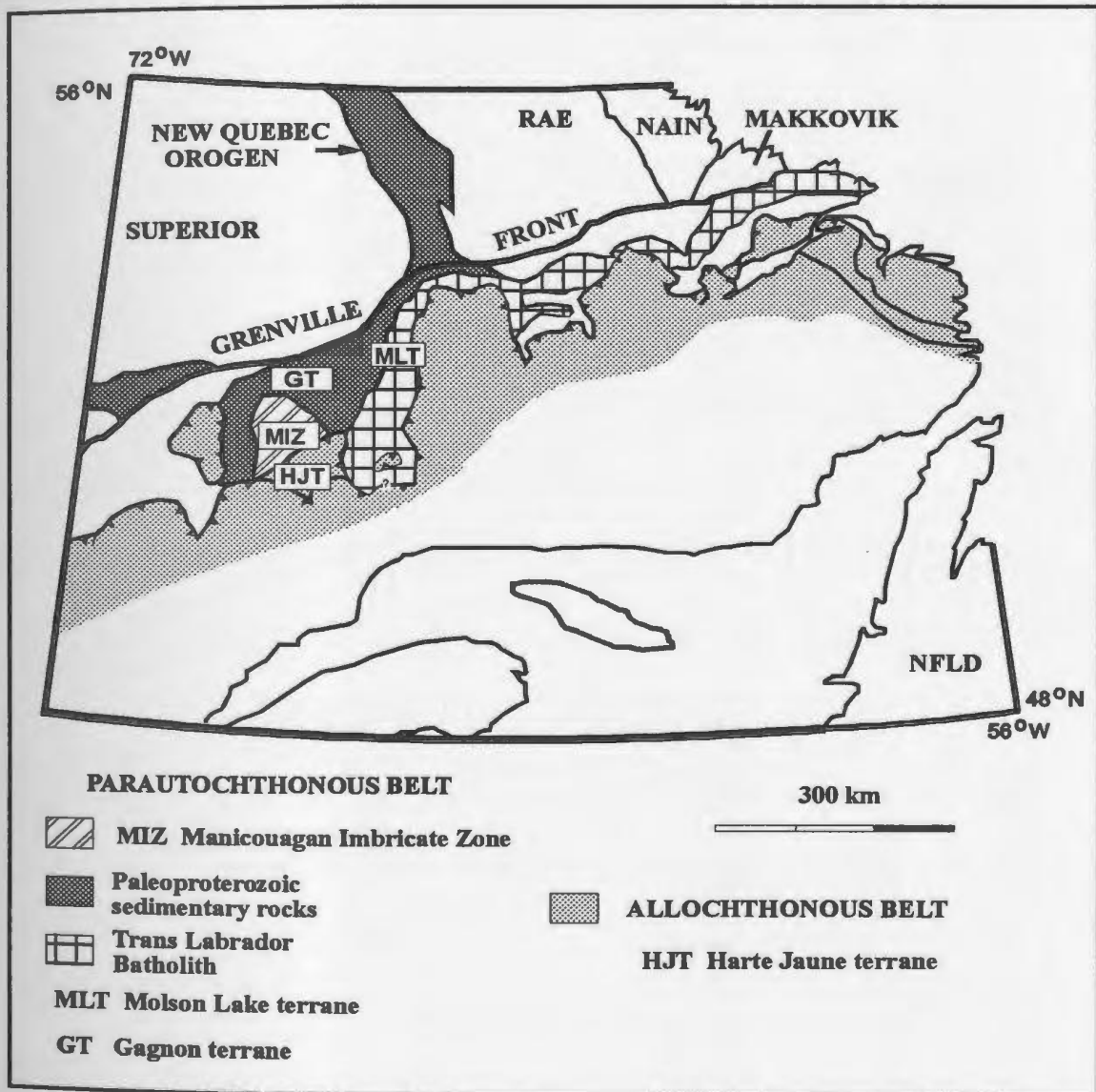
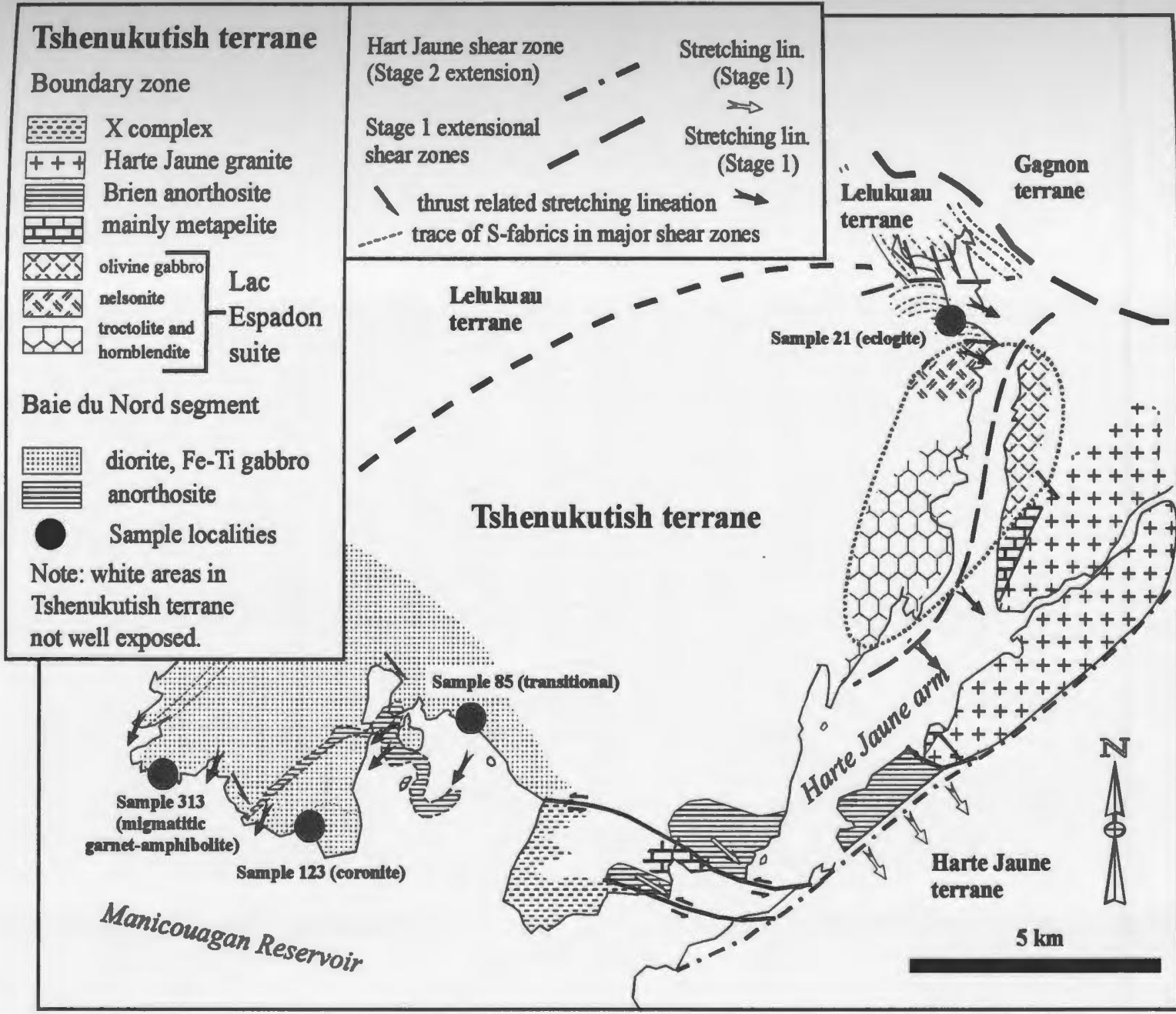







Figure 2.2. Simplified geological map of the Tshenukutish terrane and adjacent terranes with the locations sample localities in the Baie du Nord segment (coronites, amphibolites and eclogites) used for thermobarometry in this study.





Tshenukutish terrane

Boundary zone

-  X complex
 -  Harte Jaune granite
 -  Brien anorthosite mainly metapelite
 -  olivine gabbro nelsonite
 -  troctolite and hornblende
- Lac Espadon suite**

Baie du Nord segment

-  diorite, Fe-Ti gabbro anorthosite
-  Sample localities

Note: white areas in Tshenukutish terrane not well exposed.

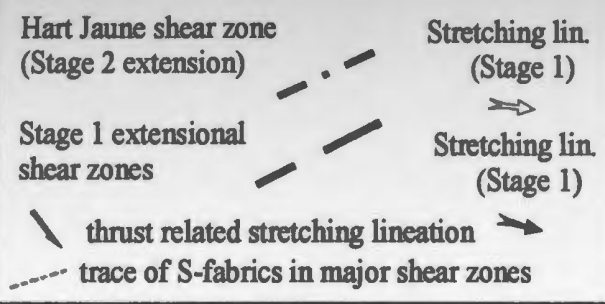


Figure 2.3. Garnet compositions plotted as Grs, Alm+Sps and Prp for the selected samples. Both coronas and pseudomorphs are shown where applicable, as described in the text.

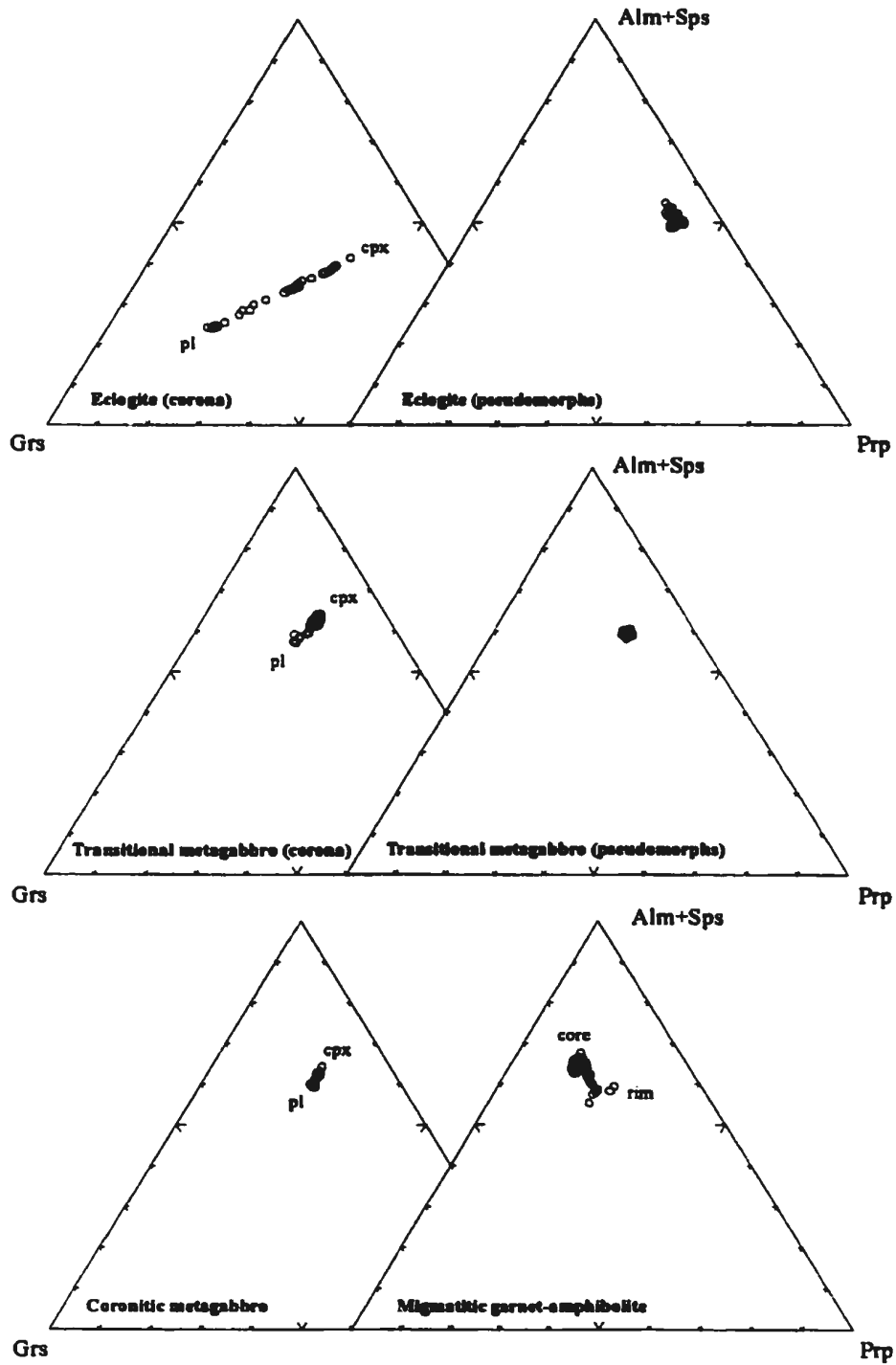


Figure 2.4 (a-c). Garnet zoning profiles for a) garnet corona between plagioclase and olivine (eclogite, sample 21), b) garnet coronas around plagioclase xenocryst in transitional metagabbro (sample 85) and c) garnet corona in a coronitic metagabbro (sample 123). Symbols all profiles are square=spessartine, cross=grossular, circle=pyrope, triangle=almandine and single line=XFe (i.e. Fe/Fe+Mg).

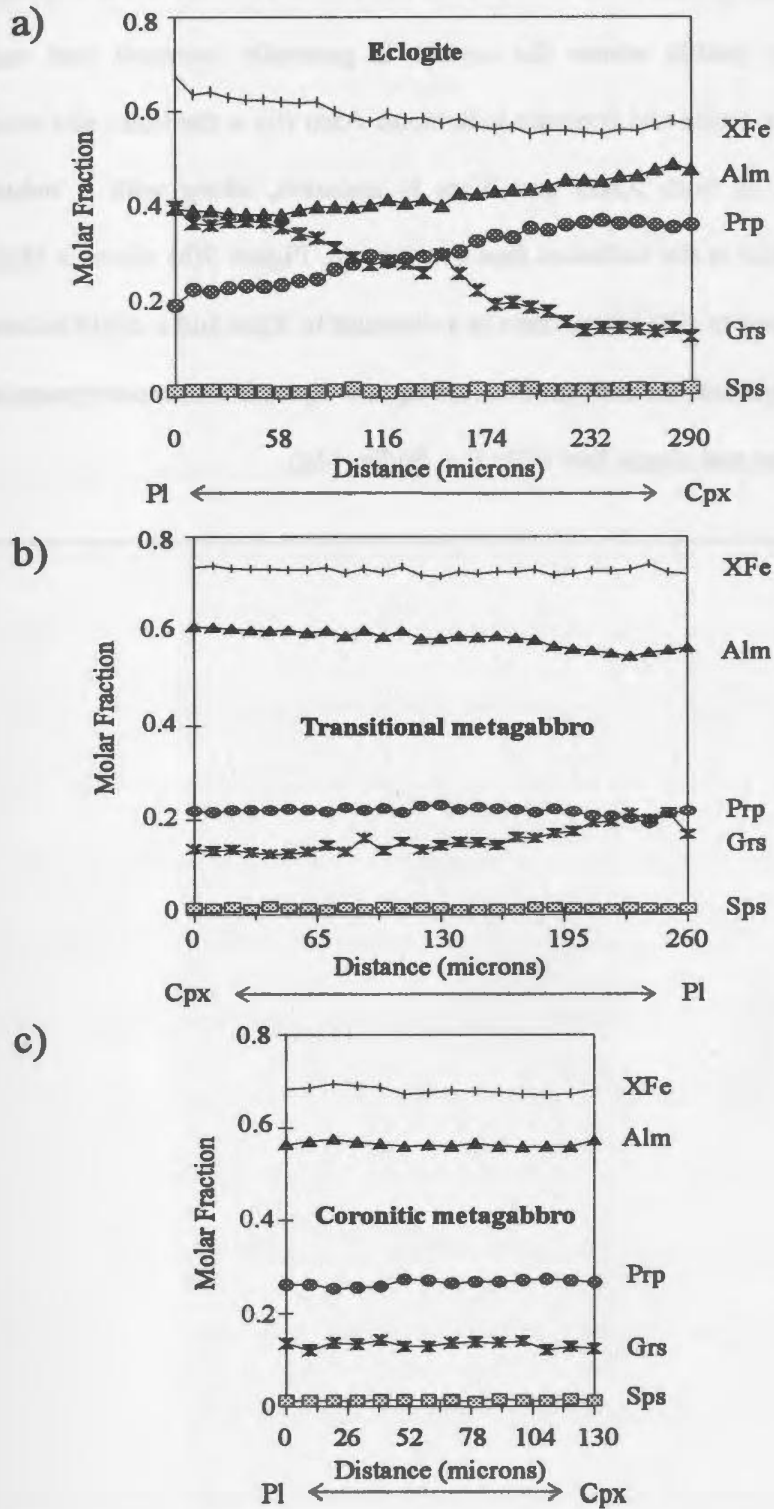


Figure 2.5 (a-b). Zoning profile for a large garnet poikiloblast in a migmatitic garnet-amphibolite (sample 313) with a) general profile from core to rim. Area (i) is the core of the crystal, occupying more than 90% of the profile where the crystal is generally unzoned and contains numerous plagioclase, quartz, rutile and ilmenite inclusions. Area (ii) is the inner rim where an increase in Prp and decrease in both Xalm and Xsps is apparent, along with a reduction in ilmenite inclusions. Area (iii) is the inclusion free overgrowth. Figure 9(b) shows a close up of the inner rim (ii) and overgrowth (iii) where there is a decrease in Xgrs and a slight increase in Xprp at the grain boundary. Symbols on both profiles are square=spessartine, cross=grossular, circle=pyrope, triangle=almandine and single line=XFe (i.e. Fe/Fe+Mg).

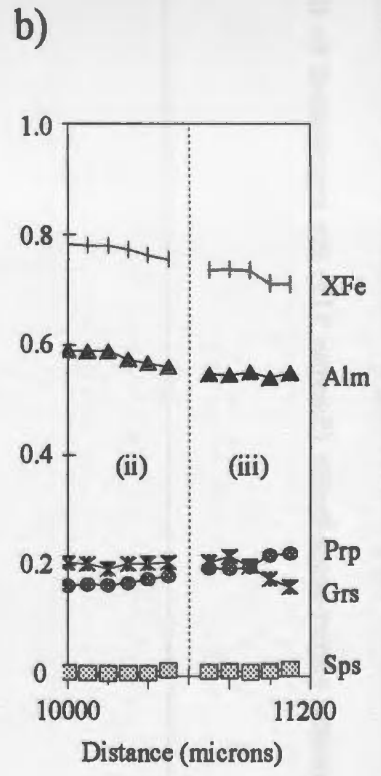
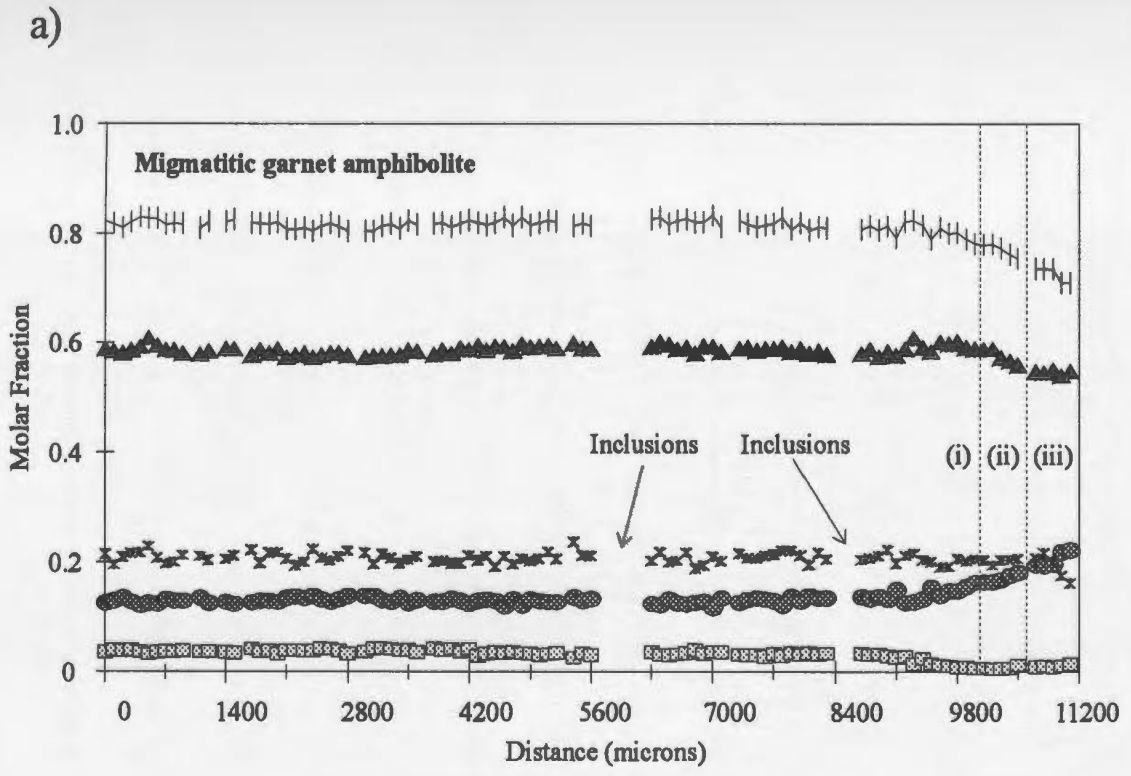


Figure 2.6. Clinopyroxene compositions plotted as Di+Hd, Ae and Jd measured in the selected samples as described in the text. The fields for Omp and Na-aug are indicated. Note: in the bottom left figure analyses for the migmatitic garnet-amphibolite (Sample 313) are represented by filled diamond symbol.

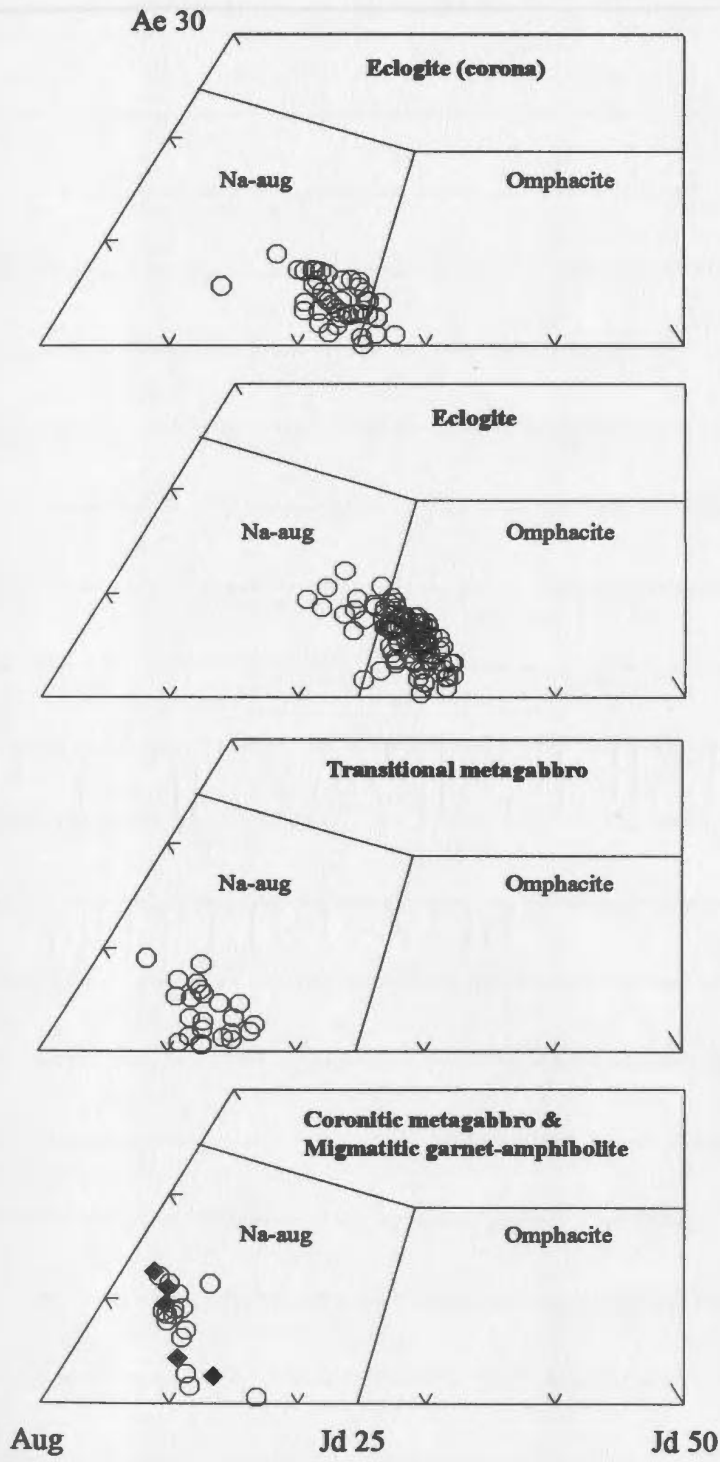


Figure 2.7. Plagioclase compositions (relicts and collars) measured in the selected samples.

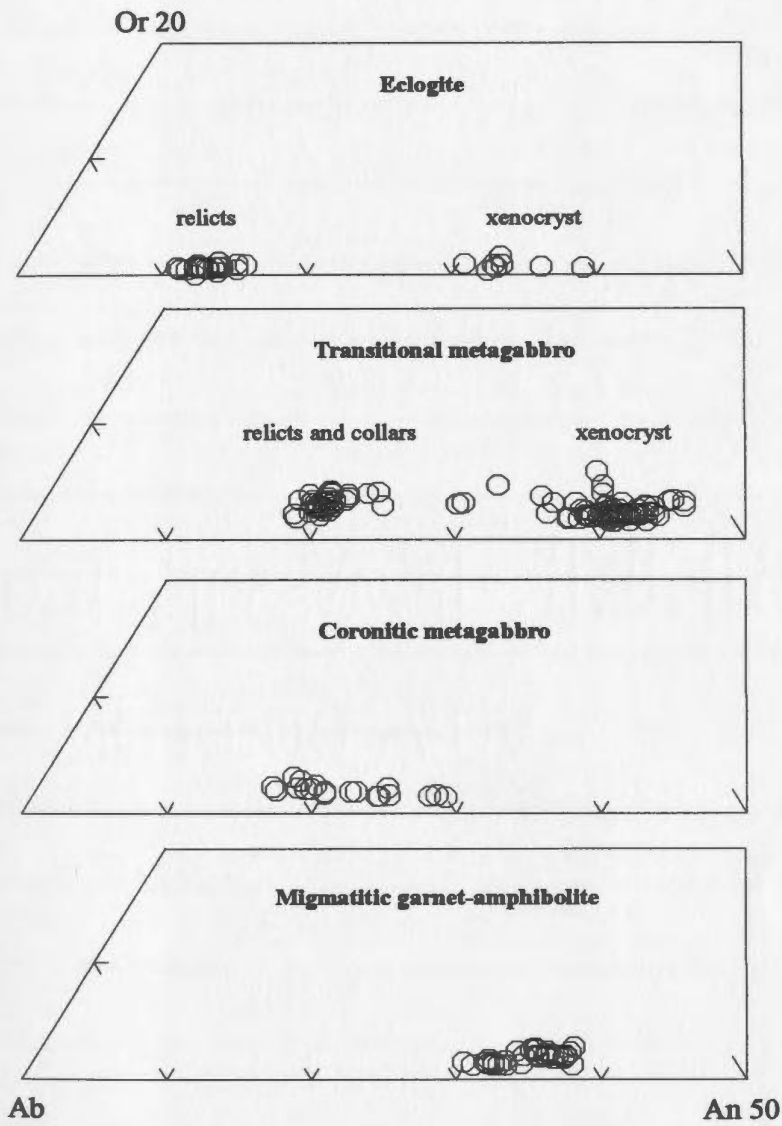


Figure 2.8. Summary of reaction stages and pathway for the formation of the main textures during the transition from Fe-Ti gabbro to eclogite in the samples described in the text.

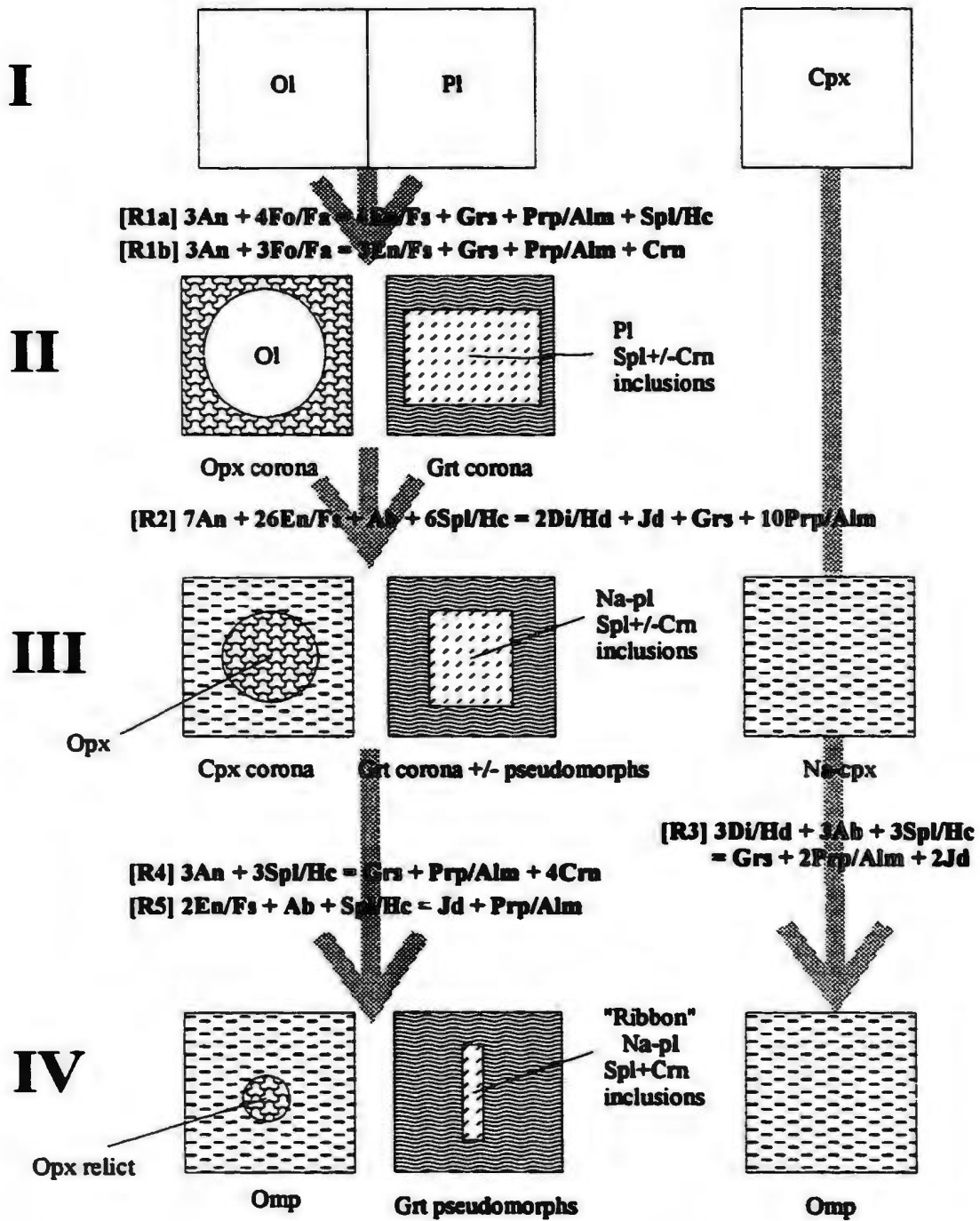


Figure 2.9. Summary of reaction stages and pathway for the formation of the main textures during the anatexis and amphibolite overprinting of the migmatitic garnet amphibolite (sample 313).

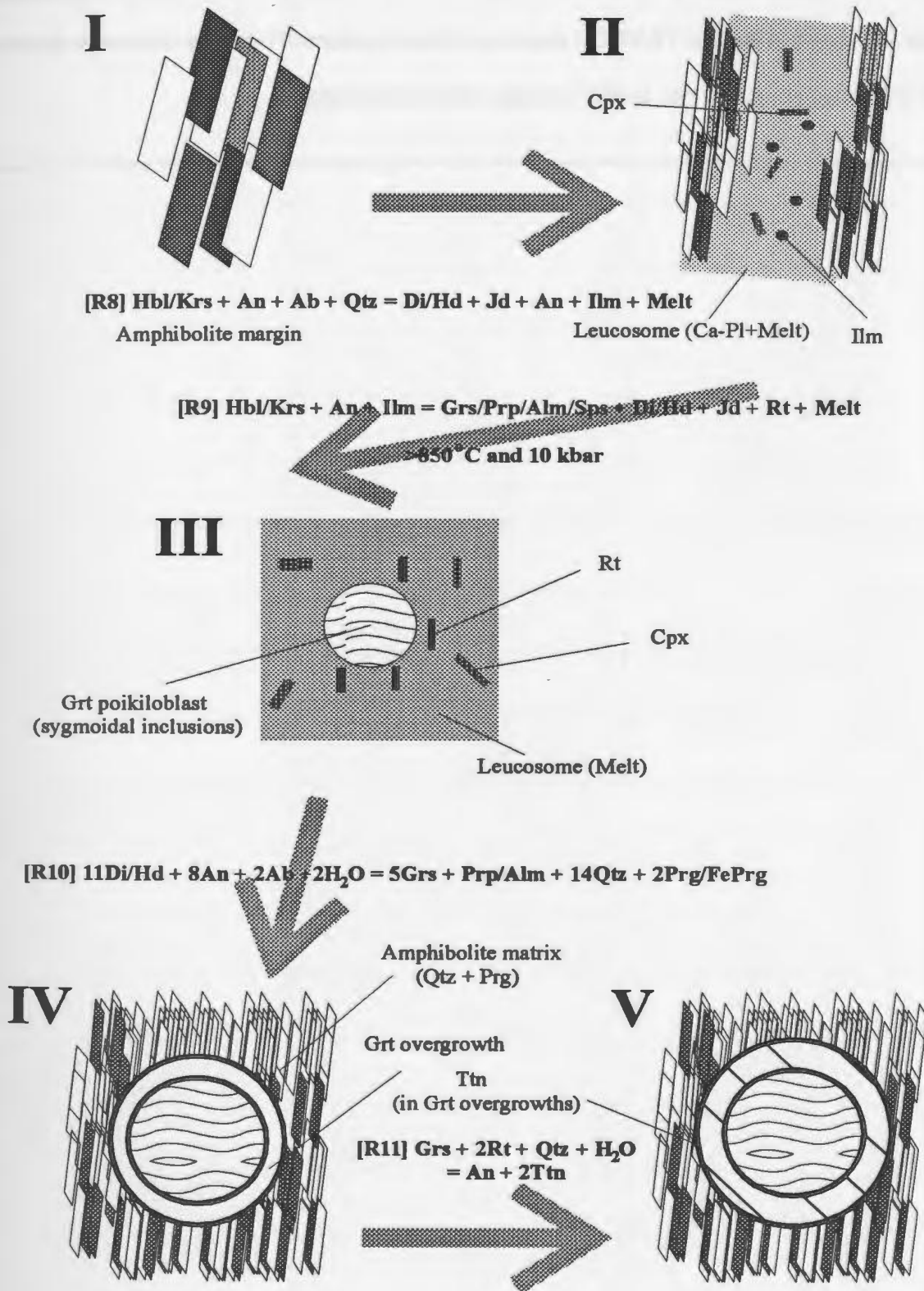


Figure 2.10. PT-conditions recorded by the samples from the BNS. PT-estimates shown in the diagram were calculated using the TWEEQU program. Boxes represent PT-ranges defined by between 4 and 20 independent analyses and PT-estimates for each sample.

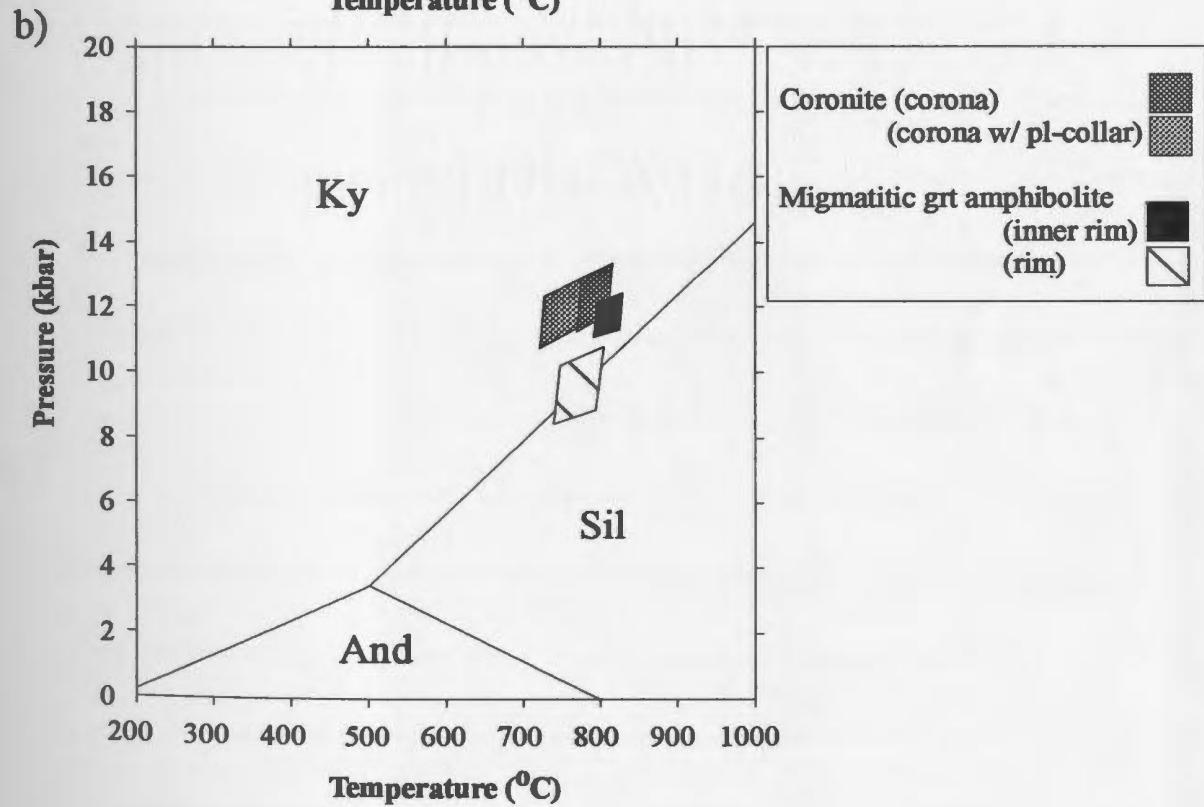
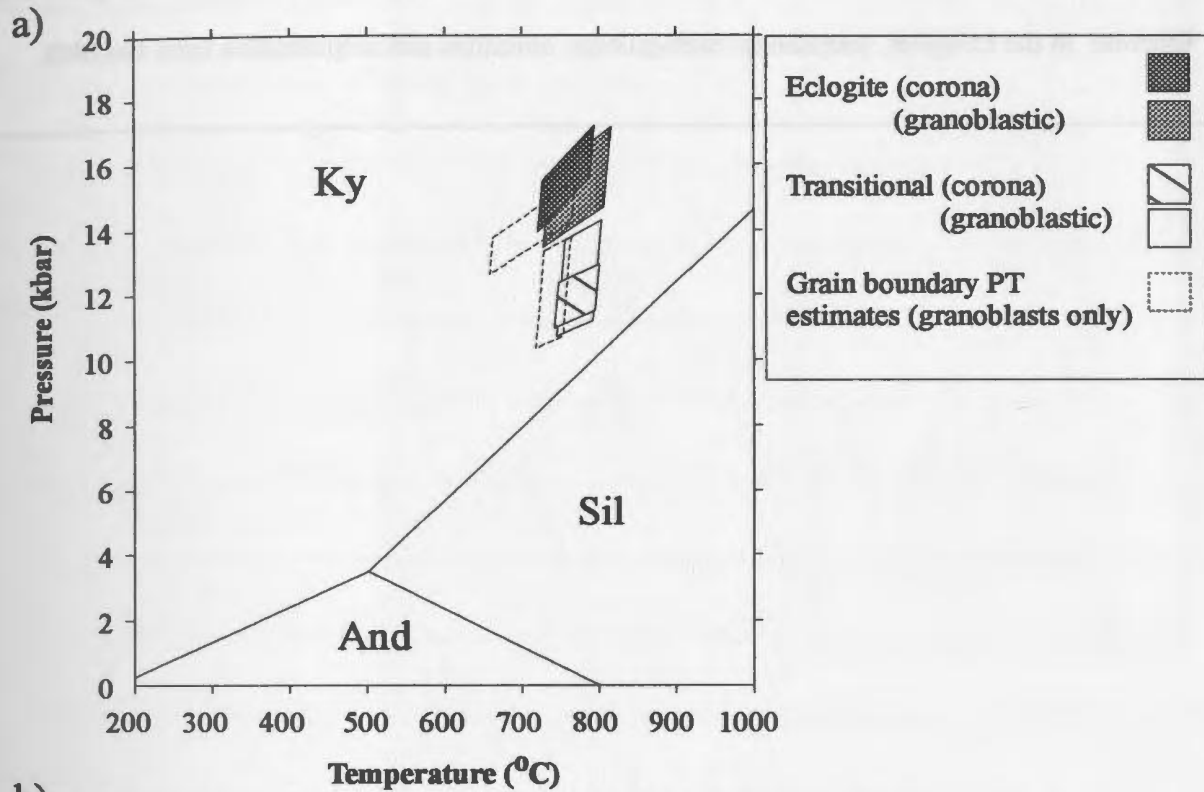


Table 2.1. Representative analyses of garnet, plagioclase, clinopyroxene, pargasite (amphibole), spinel and ilmenite, in the eclogites, transitional metagabbros, coronites and amphibolites from the BNS.

	Sample 21 (eclogite)				Sample 85 (transitional)				Sample 123 (coronite)		Sample 313 (migmatitic garnet-amphibolite)		
	Grt-pseudo (core)	Grt-pseudo (rim)	Grt-corona (Cpx-con)	Grt-corona (Pl-con)	Grt-pseudo (core)	Grt-pseudo (rim)	Grt-corona (Cpx-con)	Grt-corona (Pl-con)	Grt-corona (Cpx-con)	Grt-corona (Pl-con)	Grt (core)	Grt (inner rim)	Grt (rim)
SiO ₂	39.95	39.92	40.00	39.75	38.53	38.25	38.87	38.70	38.87	38.72	37.81	37.65	37.93
Al ₂ O ₃	22.25	22.57	22.24	21.90	22.77	21.43	21.52	21.33	21.79	21.80	21.04	21.18	21.43
TiO ₂	0.05	0.08	0.00	0.08	0.02	0.00	0.00	0.08	0.12	0.02	0.00	0.02	0.00
FeO (total)	24.13	24.05	23.66	18.55	27.94	29.72	29.10	27.29	26.45	27.00	28.35	29.34	28.56
MgO	10.35	10.94	9.42	5.49	5.67	5.41	5.72	5.11	7.56	7.03	3.28	3.39	4.34
MnO	0.44	0.37	0.63	0.39	0.39	0.62	0.66	0.63	0.61	0.50	1.64	1.30	0.27
CaO	4.01	3.82	5.48	15.00	6.72	5.92	5.76	8.75	5.82	5.62	9.01	8.87	8.70
Total	101.22	101.79	101.49	101.23	102.03	101.43	101.70	102.01	101.92	100.75	101.24	101.90	101.34
Si	3.00	2.98	3.01	3.01	2.95	2.98	3.00	2.98	2.99	2.99	2.98	2.95	2.96
Al	1.97	1.99	1.97	1.96	2.06	1.97	1.96	1.94	1.96	1.98	1.95	1.96	1.97
Ti	0.00	0.00	0.00	0.01	0.00	0.00	0.00	0.00	0.00	0.00	0.00	0.00	0.00
Fe ³⁺	1.49	1.47	1.46	1.14	1.79	1.88	1.84	1.68	1.69	1.71	1.79	1.84	1.80
Fe ²⁺	0.02	0.03	0.03	0.04	0.00	0.07	0.04	0.07	0.05	0.03	0.07	0.09	0.06
Mg	1.16	1.22	1.06	0.62	0.65	0.63	0.66	0.59	0.82	0.81	0.38	0.40	0.50
Ca	0.32	0.31	0.44	1.22	0.55	0.49	0.48	0.72	0.48	0.46	0.76	0.75	0.73
Mn	0.03	0.02	0.04	0.02	0.03	0.04	0.04	0.04	0.03	0.03	0.11	0.09	0.02
Total	8.01	8.02	8.01	8.01	8.02	8.04	8.02	8.04	8.03	8.02	8.05	8.07	8.05
XAlm	0.497	0.488	0.487	0.385	0.594	0.600	0.609	0.556	0.557	0.555	0.589	0.599	0.590
XPrp	0.362	0.403	0.352	0.203	0.215	0.224	0.218	0.193	0.272	0.275	0.126	0.129	0.166
XGrs	0.094	0.085	0.133	0.392	0.182	0.136	0.138	0.200	0.136	0.138	0.214	0.200	0.206
XSpa	0.009	0.008	0.013	0.018	0.008	0.014	0.014	0.014	0.011	0.014	0.036	0.028	0.006

Table 2.1. (continued).

	Sample 21 (eclogite)		Sample 85 (transitional)		Sample 123 (coronite)	Sample 313 (migmatitic grt-amphiblite)	
	Pl-relict	Pl-xeno	Pl-relict	Pl-xeno	Pl-relict	Pl-incl	Pl-matrix
SiO ₂	64.78	60.75	63.23	57.41	62.68	59.36	59.89
Al ₂ O ₃	22.45	25.63	22.92	27.85	23.41	25.20	24.96
FeO (total)	0.29	0.27	0.60	0.19	0.27	0.34	0.16
CaO	2.53	6.84	3.78	7.68	4.84	7.32	6.39
Na ₂ O	10.10	7.56	8.49	7.01	8.41	7.47	7.83
K ₂ O	0.11	0.16	0.47	0.33	0.27	0.47	0.29
Total	100.26	100.94	99.50	100.47	99.88	100.18	100.05
Si	2.846	2.680	2.809	2.559	2.778	2.654	2.673
Al	1.163	1.319	1.200	1.463	1.223	1.328	1.313
Fe ²⁺	0.011	0.010	0.022	0.007	0.010	0.013	0.006
Ca	0.119	0.324	0.179	0.367	0.230	0.351	0.331
Na	0.860	0.647	0.732	0.606	0.723	0.648	0.678
K	0.006	0.009	0.027	0.018	0.015	0.027	0.016
Total	5.006	4.988	4.970	5.021	4.979	5.020	5.017
XAn	0.121	0.330	0.192	0.370	0.238	0.342	0.323
XAb	0.873	0.661	0.780	0.611	0.747	0.632	0.661
XOr	0.006	0.009	0.028	0.019	0.016	0.026	0.016

Table 2.1. (continued).

	Sample 21 (eclogite)				Sample 85 (transitional)			Sample 123 (coronite)		Sample 313 (migmatitic grt- amphibolite)	
	Cpx-corona (Grt-con)	Cpx-corona (Opx-con)	Cpx-matrix (core)	Cpx-matrix (rim)	Cpx-matrix (con Grt- corona)	Cpx-matrix (core)	Cpx-matrix (rim)	Cpx-corona (Grt-con)	Cpx-corona (Opx-con)	Cpx (leucosome)	Prg (amp-matrix)
SiO ₂	54.78	54.68	54.31	54.78	52.20	51.98	52.20	53.71	53.16	52.47	41.77
Al ₂ O ₃	9.91	10.28	7.80	6.29	3.82	4.40	3.89	4.42	3.93	3.12	12.39
TiO ₂	0.56	0.61	0.18	0.28	0.37	0.35	0.37	0.12	0.18	0.23	2.25
FeO (total)	6.72	5.58	5.57	6.97	10.99	10.78	10.82	7.92	8.23	10.81	16.13
MgO	9.80	9.41	10.98	11.54	11.43	11.28	11.11	12.22	12.49	11.53	10.20
MnO	0.03	0.00	0.12	0.04	0.15	0.09	0.08	0.06	0.13	0.06	0.04
Cr ₂ O ₃	0.16	0.11	0.03	0.07	0.00	0.00	0.00	0.00	0.04	0.15	0.13
NiO	0.00	0.00	0.00	0.00	0.00	0.03	0.00	0.00	0.04	0.00	0.00
CaO	14.52	14.49	17.74	16.89	20.18	20.08	20.39	20.18	20.64	20.27	11.52
Na ₂ O	5.15	6.08	3.61	3.90	1.83	1.31	1.67	1.81	1.24	1.35	1.66
K ₂ O	0.00	0.00	0.00	0.00	0.08	0.04	0.00	0.00	0.00	0.00	1.48
Total	100.89	101.54	100.35	100.91	101.32	100.26	100.67	100.45	100.08	100.05	97.57
Si	1.96	1.93	1.96	1.98	1.92	1.94	1.94	1.97	1.96	1.96	6.20
Al	0.38	0.43	0.33	0.27	0.17	0.19	0.17	0.19	0.17	0.14	2.20
Ti	0.02	0.02	0.00	0.01	0.01	0.01	0.01	0.00	0.00	0.01	0.26
Fe ²⁺	0.18	0.07	0.17	0.16	0.23	0.32	0.28	0.24	0.25	0.32	1.84
Fe ³⁺	0.02	0.09	0.00	0.05	0.10	0.01	0.06	0.00	0.00	0.02	0.19
Mg	0.52	0.50	0.59	0.62	0.63	0.62	0.61	0.67	0.69	0.64	2.29
Mn	0.00	0.00	0.00	0.00	0.00	0.00	0.00	0.00	0.00	0.00	0.06
Ca	0.56	0.55	0.69	0.65	0.80	0.80	0.81	0.79	0.82	0.81	1.86
Na	0.36	0.42	0.25	0.28	0.13	0.09	0.12	0.13	0.089	0.10	0.48
K	0.00	0.00	0.00	0.00	0.00	0.00	0.00	0.00	0.00	0.00	0.27
Total	4.01	4.03	4.00	4.02	4.04	4.00	4.02	4.00	3.99	4.01	15.77
XHd	0.256	0.125	0.222	0.209	0.272	0.340	0.286	0.267	0.270	0.330	-
XDi	0.744	0.875	0.778	0.791	0.728	0.660	0.714	0.733	0.730	0.670	-
XActm	0.021	0.094	0.000	0.046	0.104	0.013	0.057	0.000	0.000	0.022	-
XJd	0.336	0.322	0.254	0.226	0.027	0.081	0.063	0.129	0.090	0.076	-

Table 2.1. (continued).

	Sample 21	Sample 85		Sample 123	Sample 313
	(eclogite)	(transitional)		(coronate)	(mig. grt-amph)
	Spl-incl	Spl-incl	Spl-incl	Spl-incl	Ilm-incl
	(Pl-relict)	(Pl-xeno)	(Pl-relict)	(Pl-relict)	(Grt)
SiO₂	0.81	0.18	0.53	0.37	0.07
TiO₂	0.07	0.02	0.07	0.06	46.15
Al₂O₃	61.57	61.23	60.79	60.88	0.02
Cr₂O₃	0.07	0.03	0.01	0.00	0.00
FeO (total)	22.88	30.86	30.43	26.96	52.27
MnO	0.09	0.07	0.01	0.02	0.36
MgO	12.71	7.91	7.13	9.56	0.95
ZnO	1.74	1.53	1.47	1.60	0.18
NiO	0.27	0.00	0.12	0.22	0.00
Total	100.21	101.83	100.56	99.67	99.97
Si	0.022	0.005	0.014	0.010	0.002
Al	1.912	1.938	1.946	1.938	0.001
Fe³⁺	0.509	0.700	0.698	0.615	0.872
Fe²⁺	0.000	0.000	0.000	0.000	0.267
Mn	0.002	0.001	0.000	0.000	0.006
Mg	0.504	0.320	0.292	0.389	0.037
Ti	0.001	0.000	0.001	0.001	0.905
Cr	0.002	0.001	0.000	0.000	0.000
Zn	0.034	0.031	0.030	0.032	0.003
Ni	0.006	0.000	0.000	0.005	0.000
Total	2.992	2.996	2.982	2.990	2.093

Table 2.2. PT-conditions recorded by the eclogites, transitional metagabbros, coronites and amphibolites from the BNS. Abbreviations for the thermometers are: E&G79=Ellis & Green (1979), K88=Krogh (1988) for garnet-clinopyroxene, G&P84=Graham & Powell (1984) for garnet-amphibole. Abbreviations for the barometers are In&D97=Indares & Dunning (1997) for the garnet-plagioclase-spinel-corundum reaction, In95=Indares & Rivers (1995) for the garnet-plagioclase-kyanite-corundum reaction, N&P82=Newton & Perkins (1982) for the garnet-clinopyroxene-plagioclase-quartz reaction and G&S84=Ghent & Stout (1984) for the garnet-plagioclase-rutile-quartz-titanite reaction (GRAIL variant).

	Sample 21 (eclogite)			Sample 85b (Transitional)			Sample 123 (Coronite)		Sample 313 (Migmatitic grt-amphibolite)		
	Corona assemblage Grt-Cpx-Pl-Spl-Crn (contacts)	Granoblastic assemblages Grt-Cpx-Pl-Spl-Crn (cores) Grt-Cpx-Pl-Ky-Crn (rims)		Corona assemblage Grt-Cpx-Pl-Spl-Crn (contacts)	Granoblastic assemblages Grt-Cpx-Pl-Spl-Crn (cores) Grt-Cpx-Pl-Spl-Crn (rims)		Corona assemblage Grt-Cpx-Pl-Spl-Crn (contacts)		Leucosomes & core Grt-Cpx-Pl-Qtz (grt-cores)	Leucosomes & inner rim Grt-Cpx-Pl-Qtz (grt-inner rims)	Rims & matrix Grt-Amp-Pl-Qtz-Ttn-Rt (amphibolite)
Thermometers (T-range from 0 to 20 kbars)											
TWEEQU	655-785	680-825	615-780	715-825	705-820	690-800	765-815	695-790	630-760	755-855	710-850
E&G79	680-800	685-840	635-805	740-850	720-840	680-805	760-825	705-795	670-795	780-885	
K88	620-775	670-820	595-790	700-805	690-795	685-790	730-785	675-770	605-745	745-850	
G&P84											705-755
Barometers (all TWEEQU) (P-range for the temperatures above)											
In&D97 (Grt-Pl-Sp-Crn)		14-17	13-16	11-13	11-14	10-14	11-14	11-13			
In95 (Grt-Pl-Ky-Crn)	14-17										
N&P82 (Grt-Cpx-Pl-Qt)									9-11	11-13	
G&S84 (GRAIL)											8-10

High pressure and temperature metamorphism of the mafic and ultramafic Lac Espadon suite, Manicouagan Imbricate Zone, eastern Grenville Province.

Abstract

The Lac Espadon suite (LES) of the Manicouagan Imbricate Zone (eastern Grenville Province, Quebec) is composed of layered mafic and ultramafic rocks, which are Labradorian in age (ca. 1650-1630 Ma) and were variably deformed and metamorphosed under high pressure and high temperature (high-PT) conditions during the Grenvillian Orogeny between ca. 1050-1000 Ma. Maximum PT-conditions of 780-930 °C at 16-19 kbar (high-T eclogite facies) are recorded in massive coronitic troctolite and hornblendite from the western part of the LES. In these rocks, coronas of orthopyroxene, clinopyroxene and garnet have grown at the expense of olivine and plagioclase. Relict plagioclase contains inclusions of kyanite and corundum, and garnet coronas locally preserve growth zoning. Deformed margins of the mafic rocks have granoblastic hydrous assemblages that are interpreted to have equilibrated during exhumation at ca. 700 °C at 10-12 kbar and then down to ca. 600 °C at 5 kbar (amphibolite facies conditions) suggesting a steep retrograde PT-path. Olivine gabbro from the eastern part of the LES records peak conditions of 775-870 °C at 14-16 kbar. Granoblastic areas in the rock are partially hydrated and give conditions of 760-820 °C at 12-14 kbar suggesting a near isothermal PT-trajectory. The suggested PT-paths are compatible with structural evidence suggesting tectonic exhumation of these rocks by northwest-directed thrusting with coeval extension on top of the pile. The high-PT conditions and steep

decompression paths recorded by the LES are similar to several adjacent and nearby terranes, suggesting widespread exhumation of the lower crust in this area of the Grenville Province.

Keywords: Grenville Province, mafic rocks, coronas, eclogite facies, amphibolite facies.

3.1. Introduction

High-grade metamorphic terranes constitute petrological windows through which processes in the deep crust in orogenic belts can be studied. In such terranes, rocks in which metamorphic reactions have not gone to completion may allow segments of their pressure and temperature (PT) history to be recovered. Rocks with corona textures are especially suitable for studies of this type, and may be regarded as displaying local or domainal equilibrium (Rubie 1990). The best examples of such textures are commonly found in coarse-grained, dry and relatively undeformed, mafic (meta-igneous) rocks (e.g. Mørk 1985, 1986; Pognate 1985; Koons et al. 1987; Rivers and Mengel 1988; Indares 1993; Indares and Rivers 1995). In contrast, their deformed equivalents commonly display granoblastic textures due to enhanced chemical diffusion and fluid infiltration from country rocks (e.g. Heinrich 1982; Rubie 1986; Koons et al. 1987). The result is that coronitic rocks at the cores of igneous bodies commonly preserve near-peak metamorphic conditions better than their recrystallized margins, as the latter are also more readily retrogressed again due to the presence of fluid that allows the development of hydrous phases at amphibolite facies conditions. Application of thermobarometry to coronitic rocks is particularly difficult because the presence of coronas suggests global disequilibrium. However, detailed petrographic study may allow identification of domains in which local (domainal) equilibrium can be assumed, and which can be used for PT-determinations.

Coronitic gabbros in the southern part of the parautochthonous belt of the eastern Grenville Province have been shown to record PT-conditions up to eclogite facies (e.g. Indares 1993; Indares and Rivers 1995). It seems likely, therefore, that coronitic textures have resulted from incomplete transformation at high-pressure and high-temperature (high-PT) conditions. Evidence for high-PT conditions is only preserved where fluid infiltration is limited or absent during retrogression and exhumation. The Manicouagan Imbricate Zone, eastern Grenville Province, contains a variety of mafic units with coronitic textures (e.g. Indares et al. 1994). Among them the ca. 1650-1630 Ma (Labradorian) Lac Espadon suite (LES) in the Boundary zone consists of lenses of coronitic mafic and ultramafic rocks along with amphibolites that were metamorphosed under high-PT conditions during the Grenvillian Orogeny (ca. 1050-1000 Ma, Cox et al. 1998). The aim of this study is to describe the textures of the mafic and ultramafic rocks of the LES and to determine the PT-conditions and PT-paths under which they developed.

3.2. Geological Setting

The Manicouagan Imbricate Zone is a 2000 km² stack of high-P crustal rocks exposed along the shores of the Manicouagan Reservoir in eastern Quebec. It occurs at the same structural level as the Molson Lake terrane (Figure 3.1a), which has previously been reported to contain eclogitized metagabbro (Rivers et al. 1989; Indares and Rivers 1995). To the north, both the Manicouagan Imbricate Zone and the Molson Lake terrane tectonically overlie a Grenvillian fold-thrust and nappe belt (the Gagnon terrane) along a thrust contact. To the south, the Manicouagan Imbricate Zone is overlain by the Harte Jaune terrane along an extensional shear zone (Figure 3.1a). The Harte Jaune terrane experienced medium-P metamorphism during the Grenvillian orogeny.

The Manicouagan Imbricate Zone consists of two fault-bounded lithotectonic packages. The lower package, known as the Lelukuau terrane (Figure 3.1b), is a stack of thrust slices largely composed of Labradorian (ca. 1650 Ma) rocks that are thought to represent an igneous AMCG suite. The terrane has experienced high-PT metamorphism (16-18 kbar and 850-900 °C, Indares 1997) which was coeval with the emplacement of mafic dykes between 1050 and 1000 Ma (Gale et al. 1994; Indares et al., 1998). The tectonically overlying Tshenukutish Terrane (Figure 3.1b) comprises two lithotectonic segments, the structurally lower Baie du Nord segment and the overlying Boundary zone. Both units are transected and bounded by extensional shear zones (Figure 3.1b) with evidence for top-to-the-southeast or -southwest transport (stage 1 extension, Indares et al. 1998).

The Baie du Nord segment is mainly composed of ca. 1450 Ma megacrystic diorite intruded by ca. 1170 Ma Fe-Ti gabbros. The Fe-Ti gabbros show a transition from coronite (770-810 °C and 11.5-13.5 kbar) in the southwest to eclogite (720-825 °C and 13.5-17.25 kbar) in the northeast (Cox and Indares, in press). The Boundary zone (Figure 3.2) consists of the Harte Jaune granite (1017+/-2 Ma), the Brien anorthosite (1169+/-3 Ma, Scott and Hynes 1994) and subordinate metasedimentary rocks. In addition, the Boundary zone contains Labradorian mafic and ultramafic rocks, referred to as the Lac Espadon suite (LES). To the south, the Boundary zone is bounded by the Harte Jaune shear zone that separates it from the Harte Jaune terrane and truncates all structural features in the Tshenukutish terrane. The Harte Jaune shear zone displays evidence for top-to-the-southeast transport (stage 2 extension, Indares et al., 1998).

The LES can be divided into two parts, exposed along the western and eastern shores of the Harte Jaune Arm (Figure 3.2). The western part comprises ultramafic rocks (troctolite, dunite and hornblendite) and amphibolite that occur locally as tectonic enclaves in a sheared orthogneiss, and an apatite-rich, Fe-Ti mafic intrusion (nelsonite) to the north (Figure 3.2). The eastern part of the LES comprises a massive body of mesocratic olivine gabbro. U-Pb geochronology and geochemical data suggest that the ultramafic rocks

and the olivine gabbro represent parts of ca. 1650-1630 Ma (Labradorian) mafic to ultramafic complex similar to the Labradorian rocks of the Lelukuau terrane. The nelsonite from the northern part of the LES contains metamorphic zircons which give an upper intercept also suggesting a Labradorian age of emplacement. U-Pb ages of metamorphic zircon and titanite (ca. 1040-1000 Ma) suggest that metamorphism in the LES was contemporaneous with the rest of the Manicouagan Imbricate Zone (Cox et al. 1998).

3.3. Petrography

3.3.1. Sample selection and petrographic study

The samples chosen for detailed petrographic study were collected from the massive parts of the igneous bodies and lenses and from their deformed margins. The massive parts preserve relics of igneous phases overprinted by high-P metamorphic minerals which display textures ranging from coronas to pervasive granoblastic assemblages. The margins comprise foliated granoblastic, amphibole-rich assemblages (amphibolite), indicating extensive infiltration of fluid at some stage of their metamorphic evolution. In order to assess possible differences in metamorphic conditions recorded by the dry interiors and hydrous margins, both were sampled from single outcrops where possible. For simplicity the igneous names have been used where the protolith rock type is easily recognized. From the western LES, a troctolite (sample 5a) and its amphibolite margin (sample 6am, olivine garnet amphibolite), a hornblendite (sample 3b) and a garnet amphibolite (sample 2b) were selected along with a sample of nelsonite (sample 9c). From the eastern LES, an olivine gabbro (sample 35b) with granoblastic and coronitic varieties was studied. Sample localities are shown in Figure 3.2.

Detailed petrographic study was complemented by cathodoluminescence (CL-) microscopy. Sections were examined using a Nuclide Luminoscope CL-unit with doubly magnified objectives giving magnification from 20x to 640x. Operating conditions varied, but in general an accelerating voltage of 10-15 kV and a beam current of 0.1-2 mA were used. CL-images were used to document fine-grained inclusions in relict igneous plagioclase and growth textures of secondary plagioclase in both corona and amphibolite assemblages.

3.3.2. Textures

Troctolite (sample 5a): Troctolite and associated rocks from the western LES preserve relict igneous assemblages represented by olivine, plagioclase, and minor ilmenite (Appendix A, Plate A1.1a). Olivine and plagioclase are separated by triple coronas of orthopyroxene, clinopyroxene and garnet (Appendix A, Plate A1.1b). Plagioclase has numerous oriented inclusions of kyanite, which shows a bright red CL-emission (Appendix A, Plate A2.2a), and non-luminescent corundum which forms small rounded grains. In addition amphibole and biotite coronas surround ilmenite. Amphibole also occurs locally in the triple coronas growing at the expense of clinopyroxene and garnet. Where amphibole is more extensively developed, clinopyroxene is also partially replaced by orthopyroxene (Appendix A, Plate A1.1c). Troctolite grades into coarse-grained dunite with minor magnetite and chromite and metamorphic serpentine (antigorite) and orthoamphibole (Appendix A, Plate A1.1d).

Hornblendite (sample 3b): Small pods of coarse-grained, poikilitic hornblendite are found in close association with dunite and troctolite. In these rocks, amphibole forms oikocrysts up to 10 cm in diameter. The oikocrysts in association with phlogopite and clinopyroxene megacrysts, enclose chadacrysts of olivine, plagioclase and minor proportions of opaque minerals and apatite and represent the relict igneous assemblage. Plagioclase and amphibole are separated by garnet coronas whereas olivine and

amphibole are separated by orthopyroxene coronas (Appendix A, Plate A1.2a-b). In contrast to the troctolite, both the garnet and plagioclase in the hornblendite contain numerous inclusions of kyanite, which are readily distinguished in CL (Appendix A, Plate A2.2b), and corundum, both of which are oriented parallel to cleavage in the plagioclase.

Olivine garnet amphibolite (sample 6am): Deformed margins of troctolite are transformed to granoblastic olivine garnet amphibolite that consists of abundant relict olivine, amphibole and orthopyroxene and is largely plagioclase-free. The igneous protoliths of these rocks probably contained more olivine and less plagioclase than in the original troctolite. Locally, the olivine amphibolite are foliated and granoblastic in texture and display large garnet porphyroblasts with inclusions of amphibole and small quantities of plagioclase (Appendix A, Plate A1.3a-d). The deformed margins of hornblendite in contrast do not develop obvious retrograde assemblages. This may be in part due to the hydrous (amphibole-rich) nature of the protolith.

Garnet amphibolite (sample 2b): Granoblastic garnet amphibolite outcrops adjacent to the hornblendite (Figure 3.2). It is composed of subhedral (Appendix A, Plate A1.4a) to anhedral (Appendix A, Plate A1.4b) garnet porphyroblasts with equigranular plagioclase, quartz, amphibole and lesser amounts of biotite, rutile, titanite, and ilmenite. CL-images reveal two generations of plagioclase growth. Plagioclase with bright blue CL-emission appears as inclusions in subhedral garnet porphyroblasts in association with dull, red-luminescent quartz and is also uniformly distributed in the matrix (Appendix A, Plate A2.2c). The blue CL-emission of the plagioclase is identical to that in the undeformed troctolite and hornblendite (and olivine gabbros, see below). However, anhedral garnet porphyroblasts are rimmed by plagioclase with a yellow CL-emission (Appendix A, Plate A2.2d). The luminescence colours in plagioclase may be caused by small amounts of REE, Mn, Fe³⁺ and Ti. In general REE (Eu in particular) combined with Ti, Mn and Fe³⁺ give blue to violet CL-colors whereas REE-poor feldspars with traces of

Mn and Fe²⁺ give yellow, give green or red CL-colors (Marshall 1988; Götze et al. 1999). The intensity of the colours is strongly dependent on the concentration of each activating trace element. Mn-diffusion is faster than REE in garnet (Coglan 1990) and it may be the breakdown of the Mn-bearing garnet that is responsible for the development of the yellow versus blue luminescent plagioclase around the subhedral crystals. Titanite is also found in these textural settings growing at the expense of rutile.

Nelsonite (sample 9c): The nelsonite is dominated by large, 1-5 cm apatite and ilmenite crystals. Original plagioclase has been recrystallized and contains minute spinel inclusions with rare, fine-grained corundum inclusions. Garnet forms an irregular corona between areas rich in mafic phases (ilmenite, amphibole, biotite) and plagioclase (Appendix A, Plate A1.5a). Biotite also occurs as coronas around ilmenite commonly in association with garnet, and also as inclusions in the latter (Appendix A, Plate A1.5b). Secondary plagioclase commonly forms between garnet and amphibole showing up as well-defined blue collars under the CL-microscope adjacent to bright yellow apatite. These phases contrast with the non-luminescent garnet, biotite, amphibole and ilmenite (Appendix A, Plate A2.2e). Plagioclase collars are interpreted to have grown during decompression (Indares 1993).

Olivine gabbro (sample 35b): In the olivine gabbro from the eastern LES the original igneous assemblage consists of plagioclase, olivine and clinopyroxene, the latter being rich in rutile inclusions. Large apatite crystals are common, and minor ilmenite is also present. The olivine gabbro shows more pervasive development of metamorphic textures, ranging from coronitic to granoblastic (Appendix A, Plate A1.6a-b). Plagioclase domains preserve an original igneous shape but are extensively recrystallized. Olivine has been replaced by aggregates of orthopyroxene rimmed by a corona of clinopyroxene. Garnet occurs as discontinuous coronas between clinopyroxene and plagioclase and locally as granoblastic porphyroblasts. Amphibole is present throughout the olivine gabbros, around original euhedral biotite and ilmenite, and also around clinopyroxene where it is commonly associated with granoblastic garnet and

inclusion-poor plagioclase (Appendix A, Plate A1.6b). In these areas, relict crystals of clinopyroxene also show a reduction in abundance of rutile inclusions adjacent to the garnet-amphibole-plagioclase contacts. Commonly both garnet and recrystallized plagioclase cores contain kyanite inclusions which are evident in CL-images (Appendix A, Plate A2.2f).

3.4. Mineral Chemistry

3.4.1. Mineral analysis

Garnet, olivine, orthopyroxene, clinopyroxene, amphibole and plagioclase and spinel were analysed with a CAMECA SX-50 electron microprobe, using a LINK EDS X-ray analyzer. Back-scattered electron (BSE) images were used to examine fine-scale features prior to analysis. The EDS analyzer was calibrated using a Co-gain procedure. Several mineral standards were analysed before and after each run. Conditions for analysis were set at 15 kV accelerating voltage, a beam current of 20 nA and a beam diameter of 1µm, except for plagioclase which was analysed using a 10 nA current and a beam diameter of 3µm to avoid Na-loss during analysis. Count times varied from 50 seconds for garnet to 100 seconds for pyroxene and amphibole. Results were corrected using the ZAF software. Typically 50-100 analyses of each mineral in each section were performed along with zoning profiles where appropriate. Representative results of electron-microprobe analyses of mineral compositions are shown in Table 3.1. The structural formulae for garnet, orthopyroxene, clinopyroxene, amphibole and plagioclase were calculated using THEBA v.6.0 (J. Martignole and others, personal communication 1995). The Fe³⁺-content of ferromagnesian minerals was estimated using the method of Droop (1987). All mineral abbreviations are from Kretz (1983) and Spear (1993).

3.4.2. Garnet

Representative garnet compositions are shown in **Figure 3.3**. Garnet compositions from the most Mg-rich rocks, i.e. troctolite (in contact with clinopyroxene), hornblendite, olivine gabbro and also the olivine garnet amphibolite all have high Mg-contents ($>Prp_{50}$). In contrast, the nelsonite and garnet amphibolite are more Fe-rich and their garnets have correspondingly lower Mg-contents (ca. Prp_{20-30}). Thus, there is a correlation between the Mg-content in garnet and bulk rock composition. On the other hand, the troctolite, hornblendite and olivine gabbro contain mineral assemblages indicative of high-P metamorphism, whereas the garnet amphibolite has amphibolite facies assemblages. The olivine garnet amphibolite contains evidence for both high-P metamorphism, e.g. coexisting garnet and olivine (Harley and Carswell 1990) and reequilibration e.g. orthopyroxene and amphibole. Thus, there may also be a correlation between the type of mineral assemblage (high-P versus retrograde) as well as whole-rock chemical composition.

Garnet zoning profiles are shown in **Figure 3.4**. The garnet coronas in the troctolite (sample 5a) are strongly zoned. In amphibole-free coronas, Ca increases towards plagioclase with a maximum Grs_{48} adjacent to the contact. This is compensated by decreasing Fe and Mg from clinopyroxene ($Pyp_{39}Alm_{42}$) to plagioclase ($Pyp_{19}Alm_{32}$) contacts (**Figure 3.4a**). The XFe (i.e. $Fe/Fe+Mg$) in these garnet coronas increases in conjunction with Ca-content. The above patterns are typical of growth zoning in coronitic garnet (Indares and Rivers 1995; Indares and Dunning 1997). Since coronitic garnet grows from the inner to outer rim between reactant phases instead of concentrically outward, zoning is controlled by the chemical gradient between the minerals at the growth interfaces. In other words, the garnet corona has higher Ca toward the plagioclase and higher Fe and Mg towards the clinopyroxene. In the coronas where orthopyroxene and amphibole replace clinopyroxene, garnet zoning displays a similar trend but in addition there is a reversal at the garnet rims. In such cases the Ca-content drops from a maximum of

Grs₄₀ to Grs₃₅ at the garnet-plagioclase contact. Mg decreases to Prp₃₇ and Fe increases to Alm₄₅ (Figure 3.4b) at the clinopyroxene/orthopyroxene/pargasite (triple-junction) contact. The reversal in zoning is interpreted to be the result of retrograde resetting. The amphibole-bearing garnet coronas also show less strong XFe zonation, probably due to the effects of chemical reequilibration.

Garnet coronas in the hornblendite (sample 3b) are weakly zoned (Figure 3.4c) with compositions ranging from Alm₃₉Prp₄₅Grs₁₃ (amphibole contact) to Alm₃₅Prp₄₉Grs₁₃ (plagioclase contact) probably due to homogenization at elevated temperatures. XFe also increases with Fe-content. Large garnet porphyroblasts from the garnet-olivine amphibolite (sample 6am) show a weak increase in Fe-content and decrease in Mg-content (Figure 3.4d) from the core (Alm₄₅Prp₅₀) to the rim (Alm₅₀Prp₄₇) along with an increase in XFe. These porphyroblasts are unzoned with respect to Ca and indeed Grs-contents are low (Grs₀₅). The lack of zoning displayed in the core of the garnet porphyroblasts suggests high-T homogenization. The increase in XFe toward the rim indicates that Fe-Mg exchange continued at the garnet rims during cooling.

Both subhedral and resorbed garnet porphyroblasts in the garnet amphibolite (sample 2b) are homogeneous. The subhedral grains (Figure 3.4e) locally display a slight decrease in Mg (Prp₄₅₋₄₀) and increase in Fe and Mn towards the rims (Alm₄₅₋₅₀Sps₀₂₋₀₅) along with an increase in XFe. The increase in XFe towards the garnet rim suggests retrograde resetting. Garnet coronas from the nelsonite (sample 9c) are also weakly zoned (Figure 3.4f) with Ca increasing slightly and Fe decreasing towards the plagioclase (Alm₇₀Grs₁₀ to Alm₆₅Grs₁₅). XFe increases towards biotite inclusions in the corona. In addition, the garnet compositions are higher in Mn-content (Sps₀₃) than in the other samples. Thus, the garnet zoning profiles in the nelsonite show clear evidence of homogenization and retrograde Fe-Mg exchange with biotite inclusions.

The olivine gabbro from the eastern LES (sample 35b) displays areas with both coronitic and porphyroblastic garnets. In coronitic examples garnet compositions generally increase in Ca (Grs_{27-10}) and decrease in Mg (Prp_{48-52}) towards the plagioclase contacts (Figure 3.4g). XFe also increases along with Ca. Garnet porphyroblasts (Figure 3.4h) are also zoned with (kyanite-bearing) cores richer in Ca ($\text{Alm}_{28}\text{Prp}_{42}\text{Grs}_{27}$) and rims richer in Fe and Mg ($\text{Alm}_{32}\text{Prp}_{50}\text{Grs}_{15}$). This indicates that despite their granoblastic texture, these garnets may have replaced original plagioclase domains and zoning is a relict growth feature. However, the XFe content of the garnet porphyroblasts is homogeneous. This indicates that the garnet porphyroblasts were partially homogenized during cooling.

3.4.3. Clinopyroxene, plagioclase and amphibole

In contrast to the garnet, clinopyroxene, plagioclase and amphibole display more restricted compositional ranges. The clinopyroxene compositions from the both the troctolite and olivine gabbro (Figure 3.5) are all Na-augite ($\text{Di}+\text{Hd}_{80-95}\text{Jd}+\text{Ae}_{5-20}$).

Plagioclase compositions for the troctolite and hornblendite lie in the range $\text{An}_{40-30}\text{Ab}_{60-70}$ (Figure 3.6). Plagioclase from the garnet amphibolite (sample 2b) and plagioclase inclusions in garnet poikiloblasts in the from the olivine garnet amphibolite (sample 6am) are slightly more sodic ($\text{An}_{32-22}\text{Ab}_{68-78}$). Plagioclase compositions in the olivine gabbro lie in the range $\text{An}_{32-30}\text{Ab}_{68-60}$. In the nelsonite plagioclase with spinel inclusions ranges in composition from $\text{An}_{38}\text{Ab}_{62}$ to $\text{An}_{30}\text{Ab}_{70}$, whereas secondary collars are more sodic ($\text{An}_{25-18}\text{Ab}_{75-82}$).

In all samples, the amphiboles lie in the compositional range pargasite-ferropargasite-edenite-ferroedenite (Figure 3.7). Samples with the best preserved textural evidence for high-P metamorphism (troctolite, hornblendite and olivine gabbro) also contain the most magnesian-pargasite amphibole compositions. This is consistent with the interpretation that the pargasitic amphibole grew as a

replacement of high-P (Mg-rich) garnet and clinopyroxene in the presence of fluid shortly after peak conditions. The amphibole-rich rocks, olivine garnet amphibolite, garnet amphibolite and nelsonite contain the most Fe-rich pargasitic amphiboles. Amphibole compositions in the olivine garnet amphibolite are the most Na-rich, lying close to pargasite-edenite compositional boundary (Figure 3.7). The more Fe-rich compositions in these samples may be the result of reequilibration with garnet or other Fe-rich phases during retrogression.

3.5. Interpretation of textures and thermobarometry

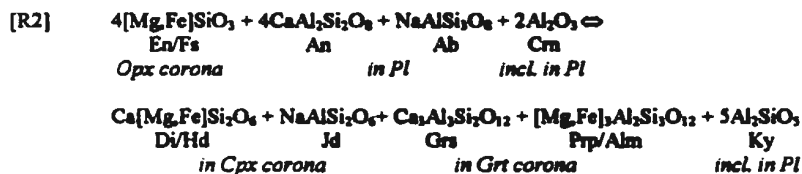
3.5.1. General approach

For each sample, interpretation of textures and of mineral chemistry was followed by selection of appropriate microdomains for PT-determinations. These are local domains in each sample for which local equilibrium may be inferred, and pressure and temperature dependent reactions can be written. Temperatures were calculated using garnet-clinopyroxene, garnet-orthopyroxene, garnet-olivine and garnet-amphibole Fe-Mg exchange reactions. Pressures were calculated using the garnet-plagioclase-kyanite-corundum reaction (Indares and Rivers 1995) for the troctolite, hornblendite and olivine gabbro. The assemblage garnet-plagioclase-quartz-rutile-titanite, a variation of the GRAIL barometer (e.g. Ghent and Stout 1984), was used in the garnet amphibolite. The garnet-plagioclase-spinel-corundum reaction, after Indares and Dunning (1997), was used for P-estimates in the nelsonite. Due to the lack of contacts between granoblastic domains and plagioclase inclusions in the olivine garnet amphibolite independent pressures could not be calculated for this sample. Given the errors associated with the estimation of the Fe³⁺-content all temperatures were calculated assuming the Fe to be Fe²⁺.

Temperatures and pressures were calculated using appropriate reactions with the program TWEEQU v.2.02 (Berman 1991) that uses an internally consistent database. Activity models used are those of Fuhrman and Lindsley (1988) for plagioclase, and Berman et al. (1995) and Berman and Aranovich (1996) for olivine, pyroxene and garnet. For garnet-amphibole thermometry, v.1.01 of the program was used (Berman pers. comm.) with the activity model of Mäder and Berman (1992) for amphibole and Berman (1990) for garnet. The results were compared with the Fe-Mg exchange thermometers of Ellis and Green (1979) and Krogh (1988) for garnet-clinopyroxene, Carswell and Harley (1990) for garnet-orthopyroxene, O'Neil and Wood (1980) for garnet-olivine and Graham and Powell (1984) for garnet-amphibole because these have been extensively used in the literature. The PT-conditions calculated using TWEEQU are shown in Table 3.2 and in Figure 3.8.

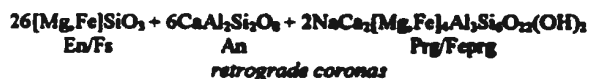
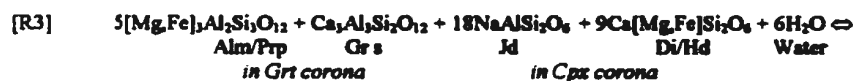
3.5.2. Troctolite (sample 5a)

In the troctolite, the development of the orthopyroxene, clinopyroxene and garnet triple corona between olivine and plagioclase involves Fe and Mg diffusion from the olivine and Ca and Al diffusion from the plagioclase. In addition, the corona sequence orthopyroxene-clinopyroxene-garnet is consistent with higher Al-concentration in the plagioclase domains and higher Fe and Mg in the olivine domains. Thus, high Ca and high Mg and Fe are a direct result of growth in contact with plagioclase and clinopyroxene at the respective margins of the garnet corona. The presence of corundum and kyanite inclusions in the plagioclase on the other hand is caused by the garnet acting as an Al-buffer (e.g. Yund 1986) causing an excess of Al in the plagioclase site. Thus, the development of the triple corona assemblage in a quartz-absent system along with the presence of corundum and kyanite in the plagioclase, can be represented by the general reactions;



In this textural setting the garnet-plagioclase-kyanite-corundum barometer (Indares and Rivers 1995) can be applied to garnet-plagioclase contacts. The distribution of Fe and Mg between the garnet and clinopyroxene rims can be used to constrain the metamorphic temperatures. The absence of retrograde resetting at both rims of the garnet corona suggests that the equilibrium compositions of the adjacent phases were achieved during peak T-conditions and are likely preserved (Indares and Rivers 1995). Therefore, calculating P-conditions with garnet compositions the plagioclase rims and T-conditions at the garnet-clinopyroxene contact should give conditions of peak metamorphism.

The breakdown of the corona assemblage locally to give amphibole and orthopyroxene can be represented by the general reactions;



Reactions [R3] and [R4] require plagioclase in both the reactants and products. Plagioclase is not adjacent to both the garnet and clinopyroxene in the corona assemblage. This suggests that some open system behavior involving fluid is likely responsible for retrogression in the amphibole-bearing corona assemblages. In these coronas the partial resetting of Ca, Fe and Mg is shown in the zoning profiles of the garnet (Figure 3.4b) which is indicative of retrogression. Therefore, the re-equilibration of Fe and Mg between the garnet-orthopyroxene, garnet-clinopyroxene and garnet-amphibole may be used to constrain the closure T-conditions during retrogression. During retrogression the exchange of Fe and Mg may continue at lower T-conditions than reactions involving Ca because of the decoupling of mass transfer and exchange reactions. However, if the recorded temperatures are high (>700 °C) then partial resetting of the Ca-zoning at the garnet-plagioclase rims will probably have occurred at the same time as the Fe-Mg exchange (e.g. Cygan and Lasaga 1985; Loomis et al. 1985; Chakraborty and Ganguly 1992; Schwandt et al. 1996). In this case P-conditions calculated using the garnet-plagioclase-kyanite-corundum reaction at the adjacent rims may be combined with the calculated temperatures to give a point on the retrograde PT-path. However, the results should be viewed with caution. In addition, comparative T-estimates were made using clinopyroxene inclusions in the garnet in the amphibole-bearing corona assemblages.

Peak PT-conditions obtained in amphibole-free coronas with garnet-clinopyroxene corona contacts are in the range 780-870 °C at 16-19 kbar (Figure 3.8a). In amphibole-bearing coronas the T-conditions calculated using garnet-clinopyroxene inclusions give overlapping PT-ranges of 780-880 °C at 14-17 kbar. However, the retrogressed parts of the amphibole-bearing coronas give a lower PT-range of 710-800 °C at 14-16 kbar. This is consistent with the development of amphibole or equilibration of this assemblage during cooling. The isopleths defining the reaction are almost identical for both assemblages (Figure 3.8a) despite the Ca-resetting shown by the garnet in the amphibole-bearing corona. This similarity indicates that the retrograde PT-path was either parallel to the isopleths of reaction during

retrogression or that decoupling of mass transfer (P-sensitive) and Fe-Mg exchange (T-sensitive) reactions has occurred.

The T-ranges calculated using TWEEQU were similar to those calculated using conventional exchange thermometers (Table 3.2). The garnet-clinopyroxene thermometers of Ellis and Green (1979) and Krogh (1988) gave overlapping T-ranges to TWEEQU although the Krogh (1988) calibration gave slightly lower T-estimates. The temperatures calculated using orthopyroxene-garnet (Carswell and Harley 1990) and garnet-amphibole (Graham and Powell 1984) were also in general agreement with TWEEQU.

3.5.3. Hornblendite (sample 3b)

Sample 3b displays well preserved igneous textures such as amphibole oikocrysts and olivine and plagioclase chadacrysts, with garnet coronas around the plagioclase and orthopyroxene coronas around olivine. Unfortunately, it is not possible to describe the formation of each type of corona by balanced reactions. The abundance of hydrous phases together with the lack of zoning in the garnet coronas (Figure 3.4c) suggests diffusion with some open system behavior. However, the presence of the garnet-plagioclase-kyanite-corundum assemblage in the plagioclase domains allows pressures to be calculated. Given the evidence of large-scale diffusion in the sample, it is reasonable to combine these P-estimates with the temperatures calculated at the adjacent garnet-amphibole contacts and assume that both domains achieved equilibrium during the same T-conditions, i.e. close to the metamorphic peak or at some early stage of cooling. The PT-conditions recorded by the hornblendite are 800-930 °C at 15-19 kbar (Figure 3.8a). The garnet-amphibole thermometer of Graham and Powell (1984) also gives overlapping T-ranges to TWEEQU.

3.5.4. Olivine garnet amphibolite (sample 6am)

Sample 6am is granoblastic and given the extent of metamorphic overprinting it is not possible to suggest reactions for the development of the main assemblage. The widespread presence of amphibole with orthopyroxene in the matrix does however suggest pervasive metamorphism, whereas olivine is clearly a relict igneous phase. On the other hand the presence of abundant amphibole inclusions in the garnet poikiloblasts suggests that fluid infiltration must have occurred prior to, or during garnet growth. In this rock, garnet cores and olivine compositions were chosen to estimate minimum peak T-conditions. In addition, areas with coarse-grained assemblages and straight contacts between the rims of garnet, olivine and orthopyroxene were chosen to determine the temperatures of retrogression/reequilibration. However, the absence of plagioclase in textural equilibrium with the garnet and matrix minerals prevents an independent P-estimate to be calculated for the sample.

T-conditions recorded by garnet cores using garnet-olivine thermometry show a wide range between 690-800 °C (assuming 10 kbar) to 740-860 °C (assuming 18 kbar). T-ranges recorded by the garnet rims and adjacent matrix phases are much narrower ranging from 590-670 °C for garnet-olivine, 605-700 °C for garnet-orthopyroxene and 610-720 °C for garnet-amphibole exchange also at 10 and 18 kbar (Table 3.2). The garnet-orthopyroxene thermometer of Carswell and Harley (1990) and garnet-amphibole thermometer of Graham and Powell (1984) give almost identical T-range to TWEEQU. However, the T-estimates using the garnet-olivine exchange thermometer of O'Neil and Wood (1980) are about 60 °C higher. Overall, the temperatures from the cores are similar to those for the retrograde (amphibole-bearing) coronas in the troctolite, whereas the temperatures recorded by the rims and matrix phases are lower.

3.5.5. Garnet amphibolite (sample 2b)

Like the olivine garnet amphibolite (sample 6am), sample 2b displays a granoblastic texture and it is not possible to suggest reactions for the development of the main metamorphic assemblage. The texture revealed by CL-images (Appendix A, Plate A2.2c-d) suggests the breakdown of the garnet and quartz along with rutile (i.e. high-P assemblage) to form titanite and secondary plagioclase (i.e. low-P assemblage). Garnet zoning is also indicative of retrogression (Figure 3.4e). Given these observations, reactions involving the garnet-amphibole-plagioclase-rutile-titanite-quartz assemblage can be used for calculation of retrograde PT-conditions using garnet rims and adjacent matrix minerals. Fe-Mg exchange reaction between garnet-pargasite and a variation of the GRAIL barometer (e.g. Ghent and Stout 1984) were used to estimate the retrograde PT-conditions. The PT-conditions using TWEEQU are estimated at 620-795 °C at 10-12 kbar. The T-range given by the Graham and Powell (1984) garnet-amphibole thermometer is almost identical (630-705 °C).

3.5.6. Nelsonite (sample 9c)

The nelsonite is markedly higher in Fe and lower in Si (Cox et al. 1998) than the other samples and displays distinctive textures. Despite the presence of coronitic textures, high-P minerals other than garnet are absent from the sample. In addition, plagioclase displays spinel inclusions instead of kyanite, probably due to extensive diffusion of Fe into the plagioclase site. Garnet compositions are extensively modified by homogenization and retrograde partial resetting. Diffusion rates in plagioclase have been shown to be greatly increased in the presence of F (Snow and Kidman 1991). Thus, the high amounts of apatite (up to 10%) and presumably high F-contents in the nelsonite may also have contributed to enhanced reequilibration during cooling. PT-conditions were calculated using the garnet-plagioclase-spinel-corundum barometer which has been recently applied in coronitic rocks (Indares and Dunning

1997) and combined with garnet-amphibole exchange thermometry gives PT-conditions of 550-690 °C and 4-6 kbar (Figure 3.8a). The Graham and Powell (1984) calibration gives lower T-conditions (485-560 °C). These PT-estimates are interpreted as representing reequilibration of the textures at some stage on the retrograde path.

3.5.7. Olivine gabbro (sample 35b)

The olivine gabbro displays both coronitic and granoblastic areas, both of which are locally amphibole-bearing. The presence of granoblastic garnet with preserved growth zoning in contact with plagioclase, both of which contain kyanite and corundum inclusions (Appendix A, Plate A2.2f), suggests that in places the granoblastic domains escaped retrogression. In these areas, and also in the coronitic domains, reactions [R1] and [R2] can be inferred. In such domains both granoblastic cores and coronas are likely to preserve high-P conditions. However, only in the coronas where both pressures and temperatures can be measured can thermobarometry be applied to calculate peak PT-conditions. In the granoblastic areas the garnet rims will tend to reequilibrate. Retrograde modifications indicated by the presence of amphibole replacing clinopyroxene may be represented by the same general reactions [R3] and [R4]. Indeed, the presence of both clear plagioclase and pargasite in the granoblastic rims suggests that these assemblages represent the reactions better than in the troctolite. Thus, the retrograde PT-conditions in this sample can be estimated assuming that equilibrium was achieved at some point during retrogression. The compositions of plagioclase, garnet and clinopyroxene were measured where all were in contact. However, kyanite and corundum in the plagioclase and garnet contacts are sparse and the effects of secondary reactions involving pargasite and clinopyroxene on the PT-estimates for retrogression in this sample are not known. Thus, the PT-estimates for the conditions of retrogression must be treated with caution. PT-estimates are 775-870 at 14-16 kbar for the corona assemblages and 750-850 °C at 12-14

kbar for retrogressed granoblastic assemblages (Figure 3.8b). T-ranges calculated using TWEEQU and Ellis and Green (1979) closely overlap and are only marginally higher than the Krogh (1988) estimates and the Graham and Powell (1984) estimates for garnet-amphibole are identical (765-880 °C, Table 3.2).

3.6. Discussion and conclusions

The highest PT-conditions are recorded by the amphibole-free coronas in the troctolite (780-870 °C at 16-19 kbar) and the kyanite-bearing garnet coronas in the adjacent hornblendite (800-930 °C at 15-19 kbar) in the western LES (Figure 3.8a). PT-conditions defined by the clinopyroxene inclusions (temperatures) and plagioclase-garnet contacts (pressures) in the amphibole-bearing coronas overlap those in the amphibole-free coronas and the hornblendite (780-870 °C at 15-18 kbar). The preservation of garnet growth zoning in the amphibole-free coronas of the troctolite suggests that the PT-conditions listed above are those close to the metamorphic peak. PT-conditions recorded by the garnet amphibolite (620-795 °C at 10-12 kbar) and the nelsonite (550-690 °C at 4-6 kbar) along with the type of textures and garnet zoning suggest that only retrograde conditions are recorded by these samples. The T-range suggested by the garnet contacts (with amphibole, orthopyroxene and clinopyroxene) in the amphibole-bearing coronas in the troctolite (710-800 °C) are very similar to those of the garnet amphibolite, whereas the apparent pressures are clearly higher. This pattern suggests that the net-transfer (P-sensitive) reactions involving Ca at the garnet-plagioclase contact closed at higher temperatures than the Fe-Mg exchange at the garnet-clinopyroxene-orthopyroxene-clinopyroxene contacts. Thus, the resultant retrograde PT-point may be erroneous and cannot be used to constrain the PT-path. The T-ranges recorded by the olivine garnet amphibolite are more difficult to assess as no independent pressure could be calculated. However, the highest temperatures, recorded by the garnet cores (740-860 °C assuming 18 kbar) may represent peak

conditions or cooling during the early stages of exhumation. The garnet rim-matrix T-range (590-720 °C) is clearly lower and probably indicates reequilibration at amphibolite facies conditions similar to the garnet amphibolite or nelsonite samples.

In the eastern LES, textures together with local preservation of growth zoning in garnet suggests that part of the assemblage should record conditions close to the metamorphic peak. The peak PT-conditions obtained (750-870 °C at 14-16 kbar) overlap those in the western LES. The retrograde conditions calculated (750-850 °C at 12-14 kbar) overlap those recorded by the amphibole-rich rocks in the western LES, albeit that the P-range is slightly higher. Given the evidence from the troctolite that the Ca and Fe-Mg exchange appear to have closed at different times, the same may be true for the olivine gabbro. However, the retrograde conditions from this sample are recorded by granoblastic rather than coronitic domains. In addition, the sample is not as extensively retrogressed as the amphibole-rich samples (garnet amphibolite and nelsonite) from the western LES. Therefore, it is likely that the retrogressed domains in the olivine gabbro simply preserve information from a different stage of the PT-path.

The PT-paths are difficult to compare as there are insufficient data from the eastern LES to fully constrain the PT-conditions during exhumation. However, the available data suggest that both PT-paths are steep, compatible with evidence for tectonic exhumation throughout the area (Indares et al. 1998). The highest recorded conditions in the LES overlap the metamorphic conditions recorded by the highest structural levels in the underlying Lelukuau terrane (e.g. Indares 1997). U-Pb geochronology constraining the ages of both protoliths and metamorphism show that both units are Labradorian in age and that peak Grenvillian metamorphism occurred in both between ca. 1050-1040 Ma (Gale et al. 1994; Cox et al. 1998; Indares et al. 1998). The above data support the hypothesis that the LES is related to the AMCG suite of rocks which make-up the bulk of the Lelukuau terrane. Similar peak PT-conditions (720-825 °C at 14-17 kbar) are also recorded by eclogite in the adjacent Baie du Nord segment (Cox and Indares 1999a). PT-

conditions in the same range and steep PT-paths also characterize eclogite, coronites and amphibolites in the nearby Molson Lake and Gagnon terranes (Rivers and Mengel 1988; Indares 1993; Connelly et al. 1995; Indares and Rivers 1995). These studies, along with the data from the LES, indicate a widespread exposure of deep crust in this area of the eastern Grenville Province.

An interesting feature of these rocks is that although they record PT-conditions in the eclogite facies field they have not been transformed into "true" eclogites (Carswell 1990). One reason for this is that in massive and dry igneous rocks with large grain sizes, such as the interiors of the LES mafic and ultramafic bodies, reaction rates are slow resulting in the formation of metamorphic coronas and the preservation of igneous relicts (Rubie 1990). Deformed and hydrated rocks however, allow metamorphic reactions to go to completion during the metamorphic peak (Austrheim and Griffin 1985; Rubie 1986; Koons et al. 1987; Austrheim et al. 1997) but are also more prone to retrogression (Heinrich 1982). However, high pressure coronites metamorphosed at eclogite facies commonly display omphacitic clinopyroxene (e.g. Mørk 1985, 1986; Indares 1993; Zhang and Liou 1997; Cox and Indares, in press) suggesting "partial" eclogitization. In contrast, the high-P samples in the LES contain clinopyroxene coronas which, although Na-bearing, are not omphacitic. The most likely reason for this is the nature of the protoliths, which are parts of a mafic and ultramafic suite and thus, have low bulk Na-contents.

Figure 3.1 (a-b). Maps showing a) location of the Manicouagan Imbricate Zone in the eastern Grenville Province, and b) simplified lithotectonic framework of the Manicouagan Imbricate Zone. Note: the tectonic divisions are from Indares et al. (1998).

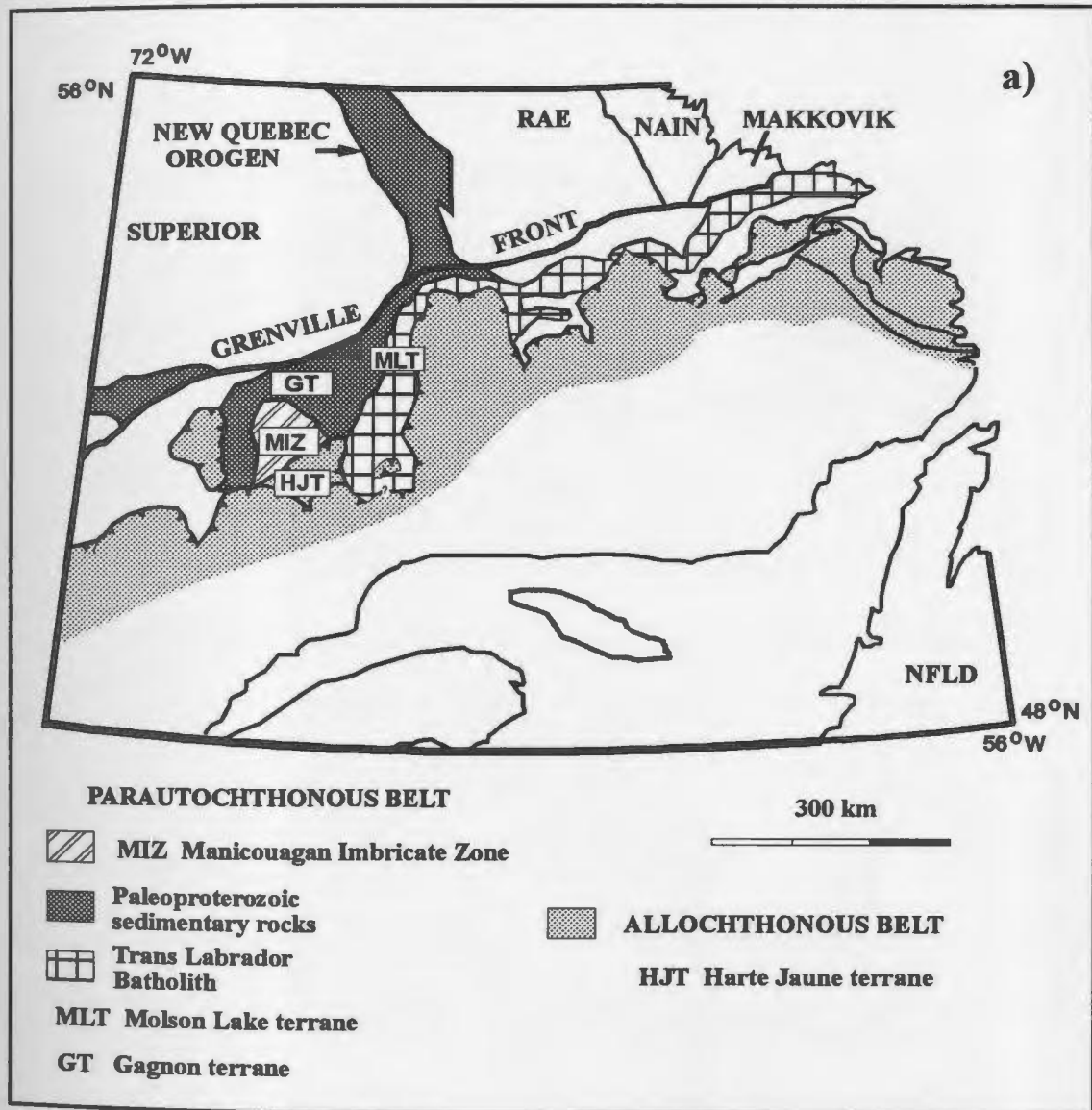
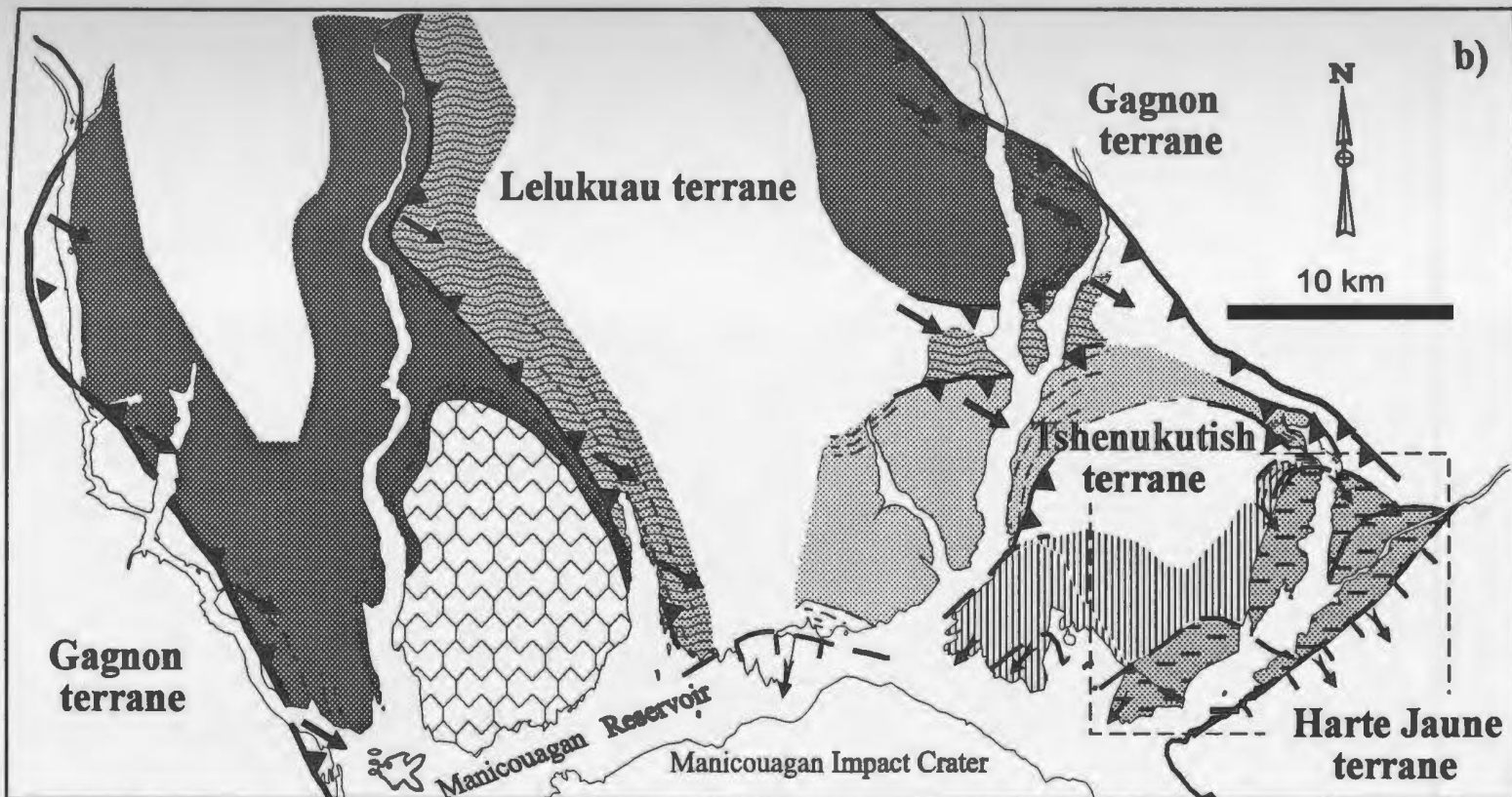









Figure 3.1 (continued).



Lelukuau terrane

-  Lower slice LT-1
-  Seignelay anorthosite
-  Middle slice LT-2
-  Upper slice LT-3

Tshenukutish terrane

-  Baie du Nord segment
-  Boundary zone
-  Area of Figure 3.2

-  Thrust boundaries
-  Extensional boundaries

Thrust boundaries

Extensional boundaries

-  Stretching lineation
-  Stretching lineation

Stretching lineation

Stretching lineation

Figure 3.2. Map showing the main lithologies structures and sample localities of the Lac Espadon complex in the Boundary zone.

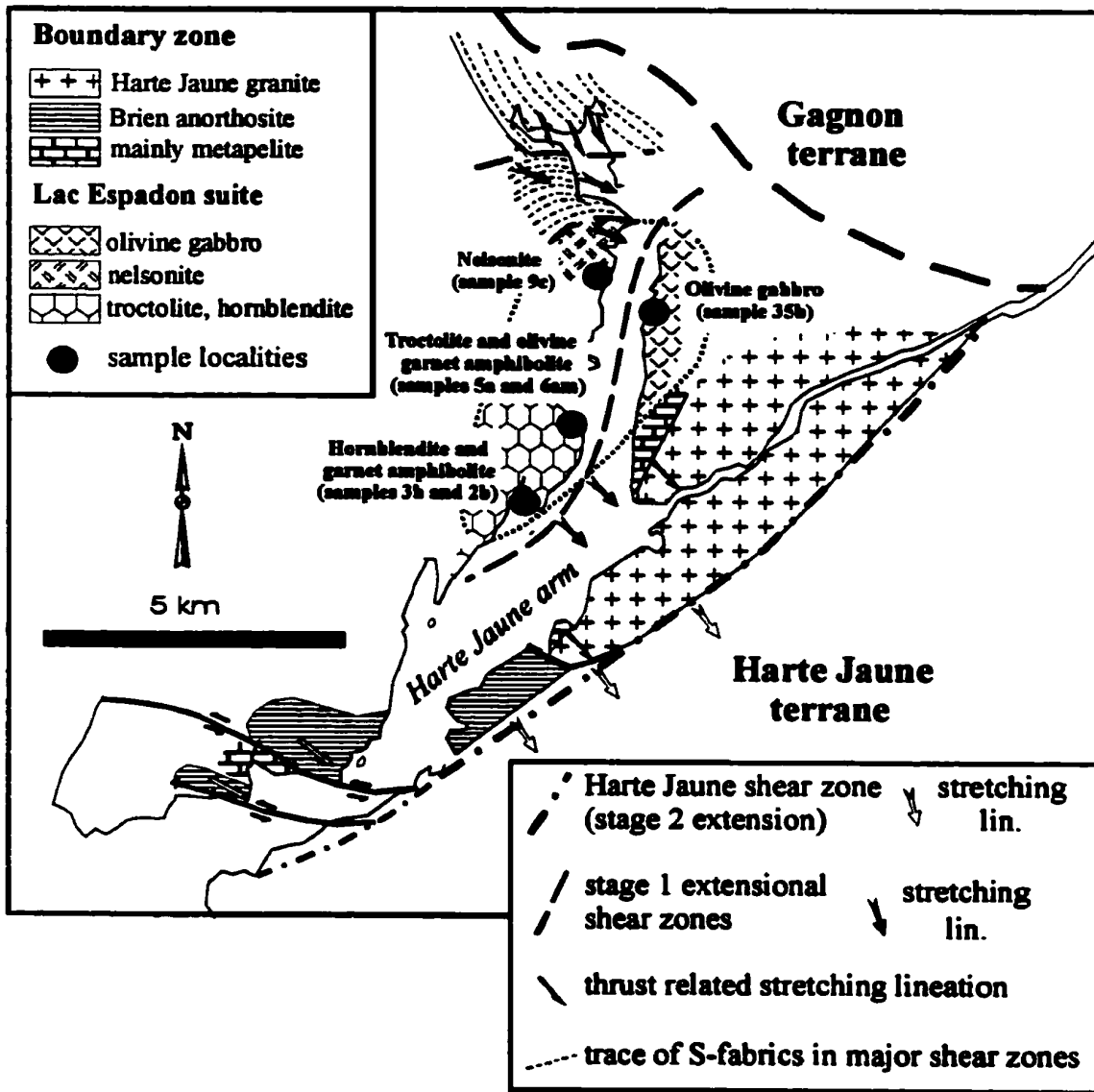


Figure 3.3. Garnet compositions plotted as Grs, Alm+Sps and Prp for the selected samples from the LES.

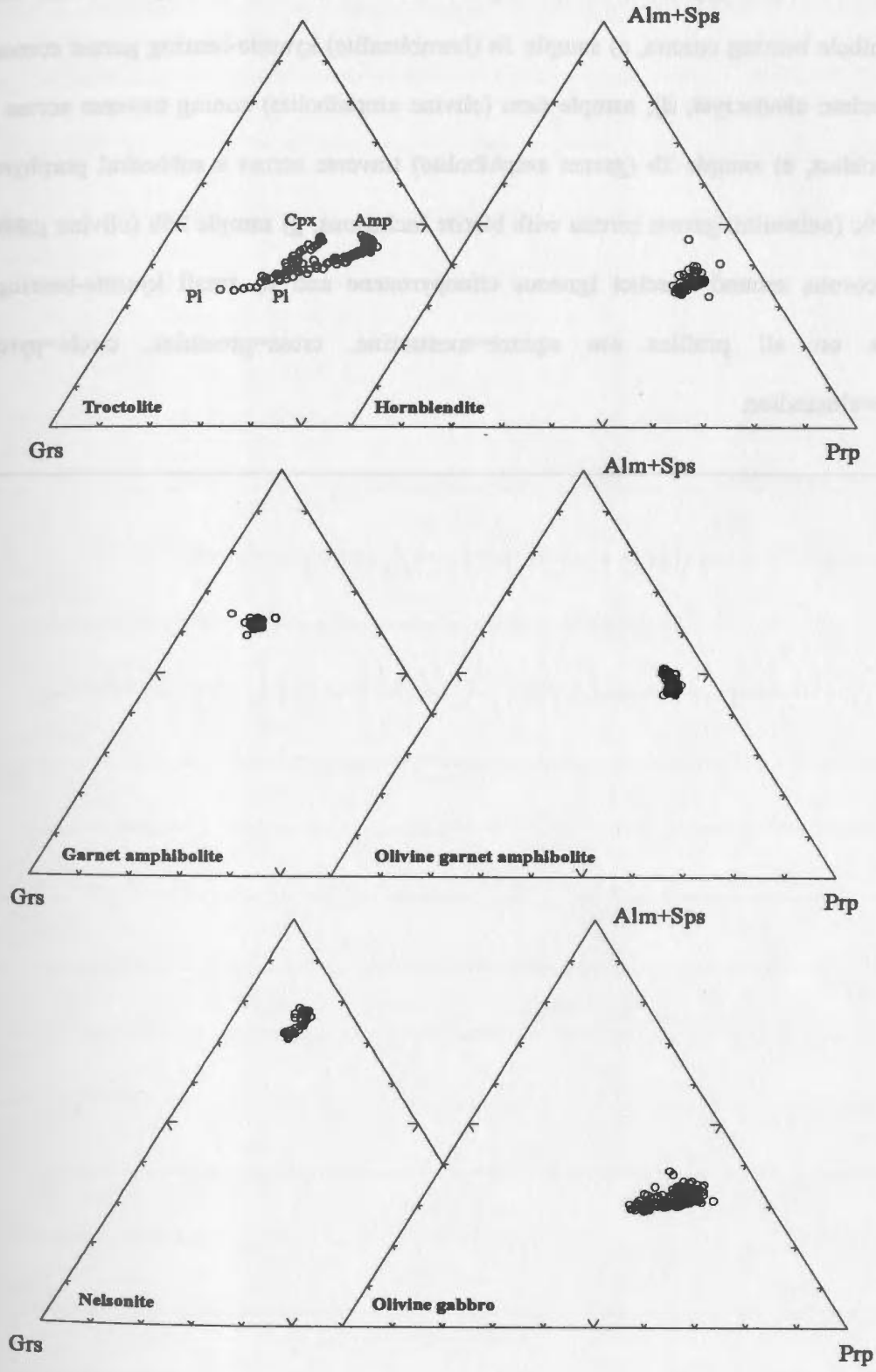


Figure 3.4 (a-h). Garnet zoning profiles for a) sample 5a (coronitic troctolite) amphibole-free corona and b) amphibole bearing corona, c) sample 3b (hornblendite) kyanite-bearing garnet corona around a plagioclase chadacryst, d), sample 6am (olivine amphibolite) zoning traverse across a garnet porphyroblast, e) sample 2b (garnet amphibolite) traverse across a subhedral porphyroblast, f) sample 9c (nelsonite) garnet corona with biotite inclusions, g) sample 35b (olivine gabbro) large garnet corona around a relict igneous clinopyroxene and h) small kyanite-bearing garnet. Symbols on all profiles are square=spessartine, cross=grossular, circle=pyrope and triangle=almandine.

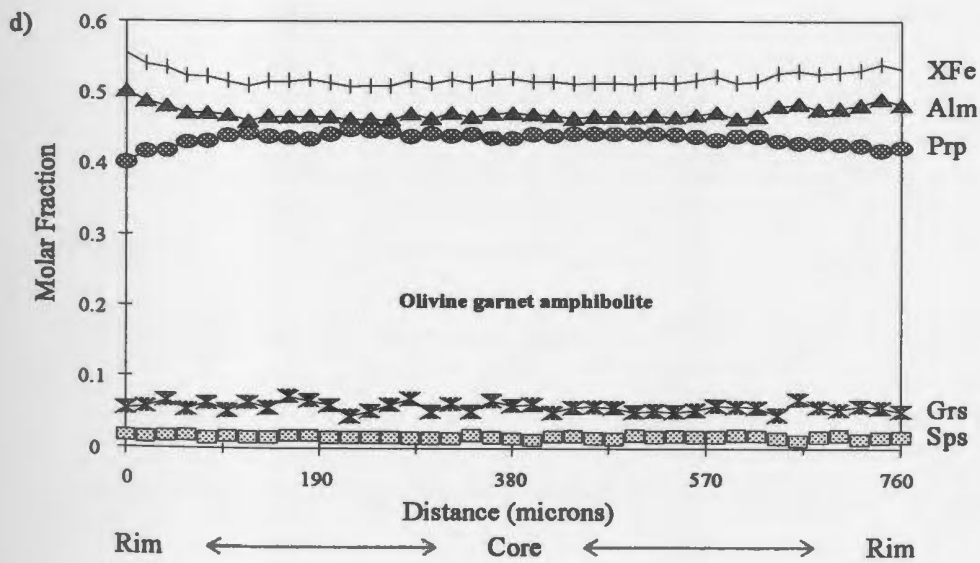
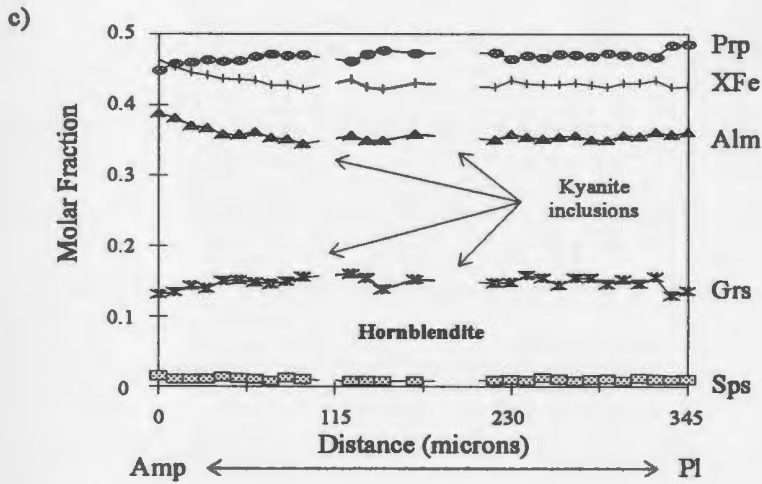
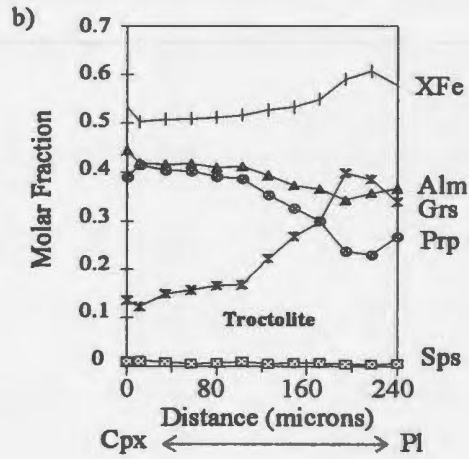
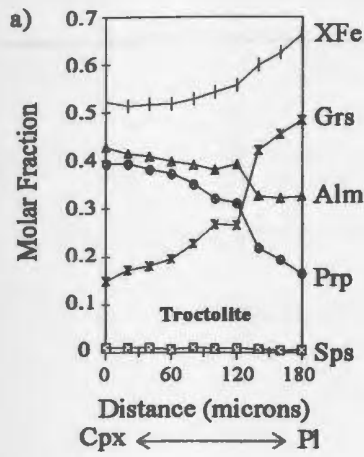


Figure 3.4. (continued).

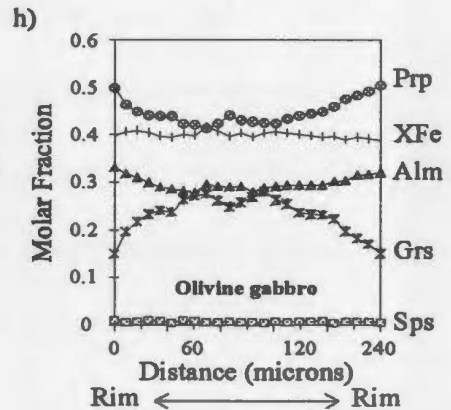
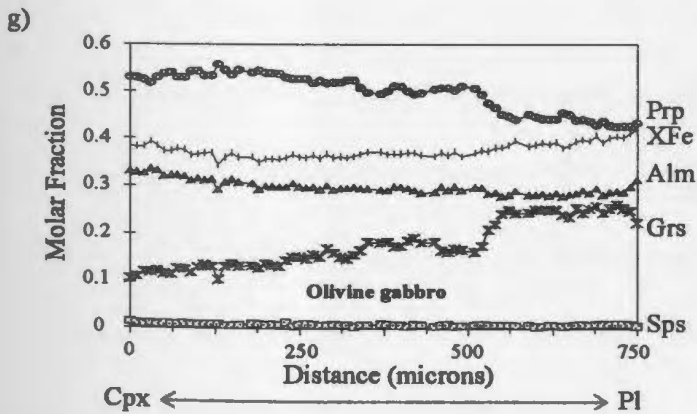
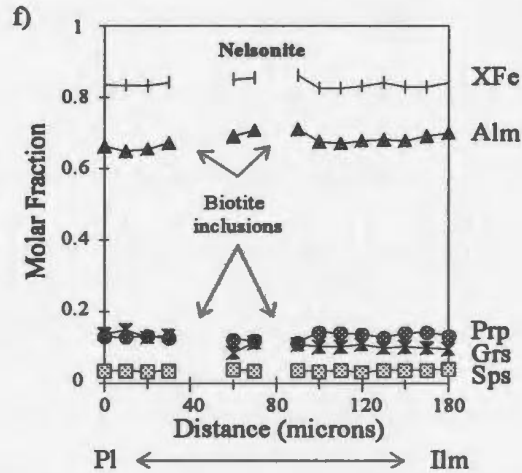
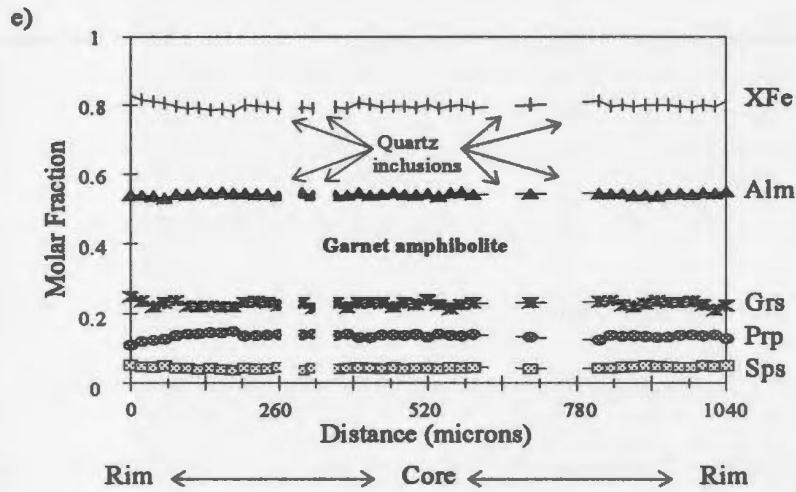


Figure 3.5. Compositional diagrams for clinopyroxene for the troctolite and olivine gabbro in the LES.

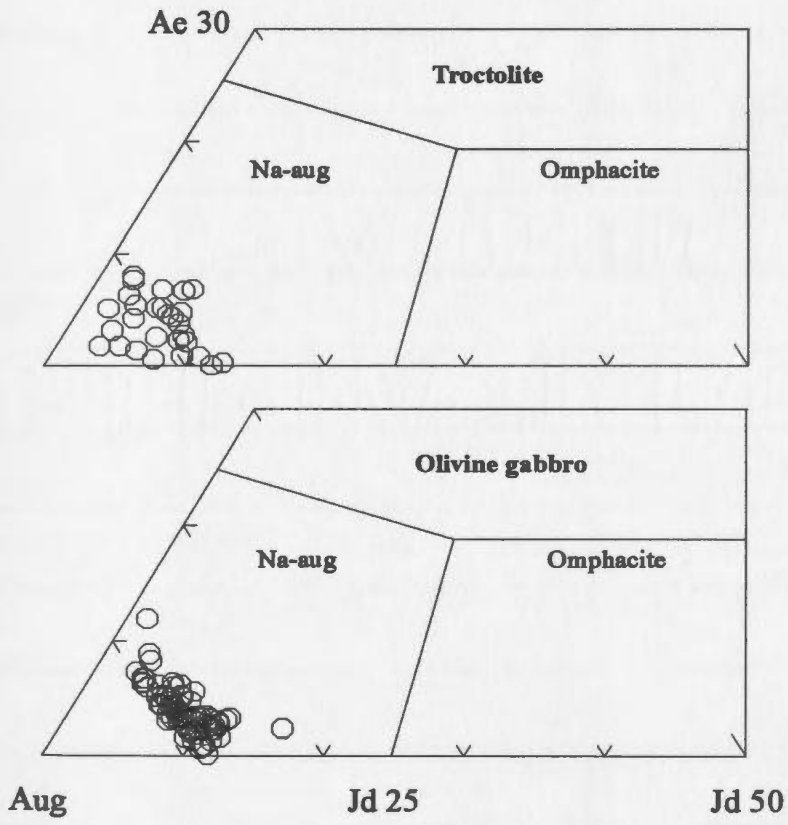


Figure 3.6. Plagioclase compositions for samples in the LES.

Or 20

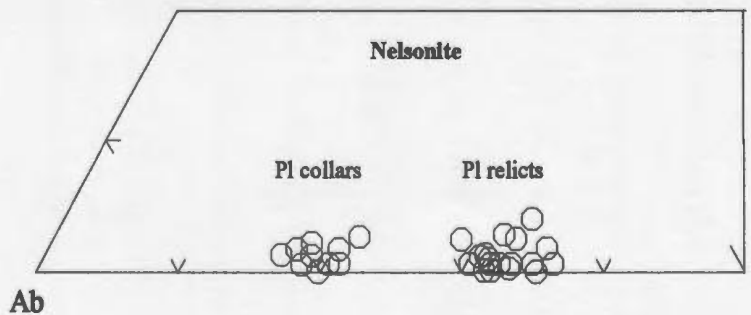
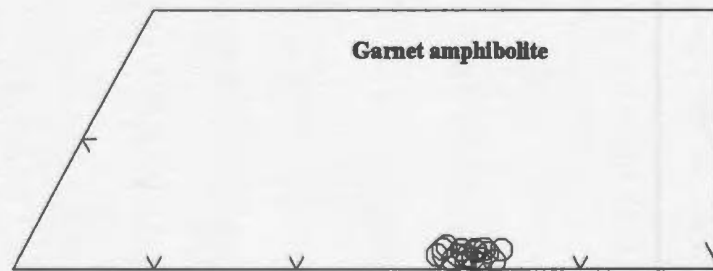
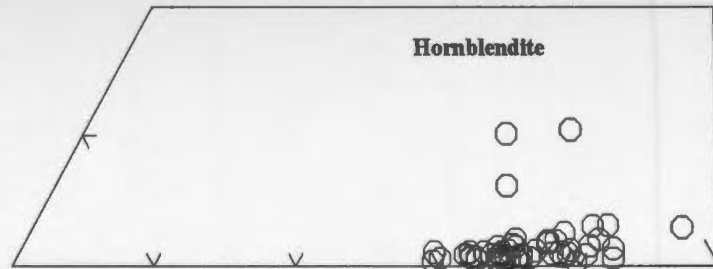
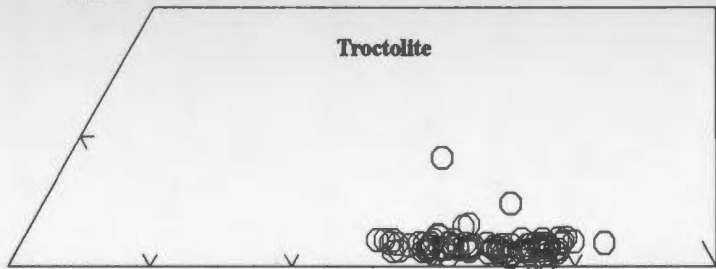


Figure 3.7. Ca-amphibole compositions for samples from the LES diagram parameters are $Ca_B \geq 1.50$;
 $(K+Na)_A \geq 0.50$ and $Ti \leq 0.50$ (after Leake et al 1997).

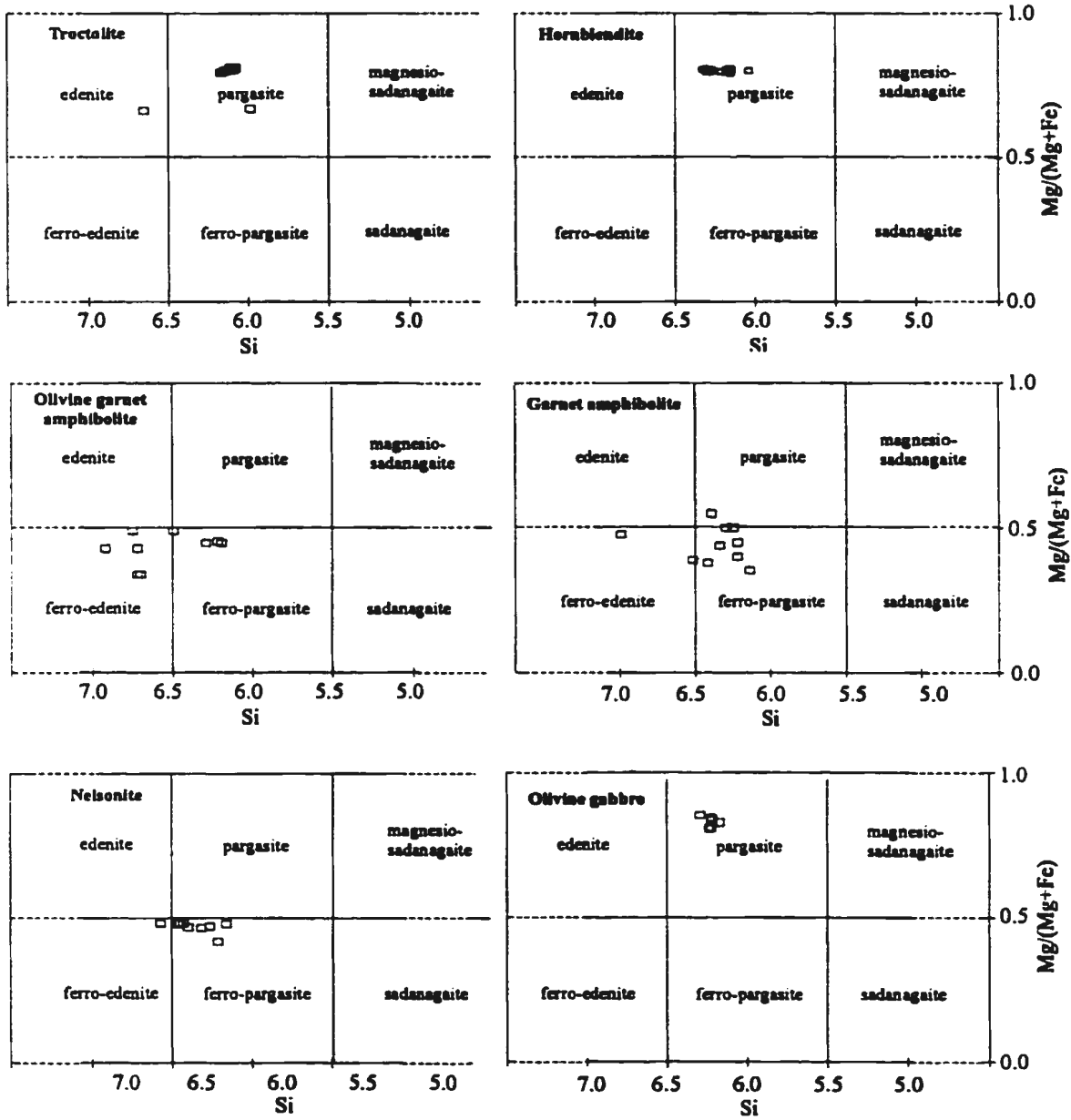


Figure 3.8 (a-b). PT-diagrams showing the maximum and minimum metamorphic conditions calculated partly using the analyses in Table 3.1. The range shown is the based on typically 5-20 analyses. All calculations were carried out as independent reactions using the program TWEEQU v.2.02 (Berman 1991) except for garnet-amphibole which uses v.1.01. PT-estimates quoted are to the nearest 5 °C and 1 kbars. The results of all PT-calculations are also shown in Table 3.2.

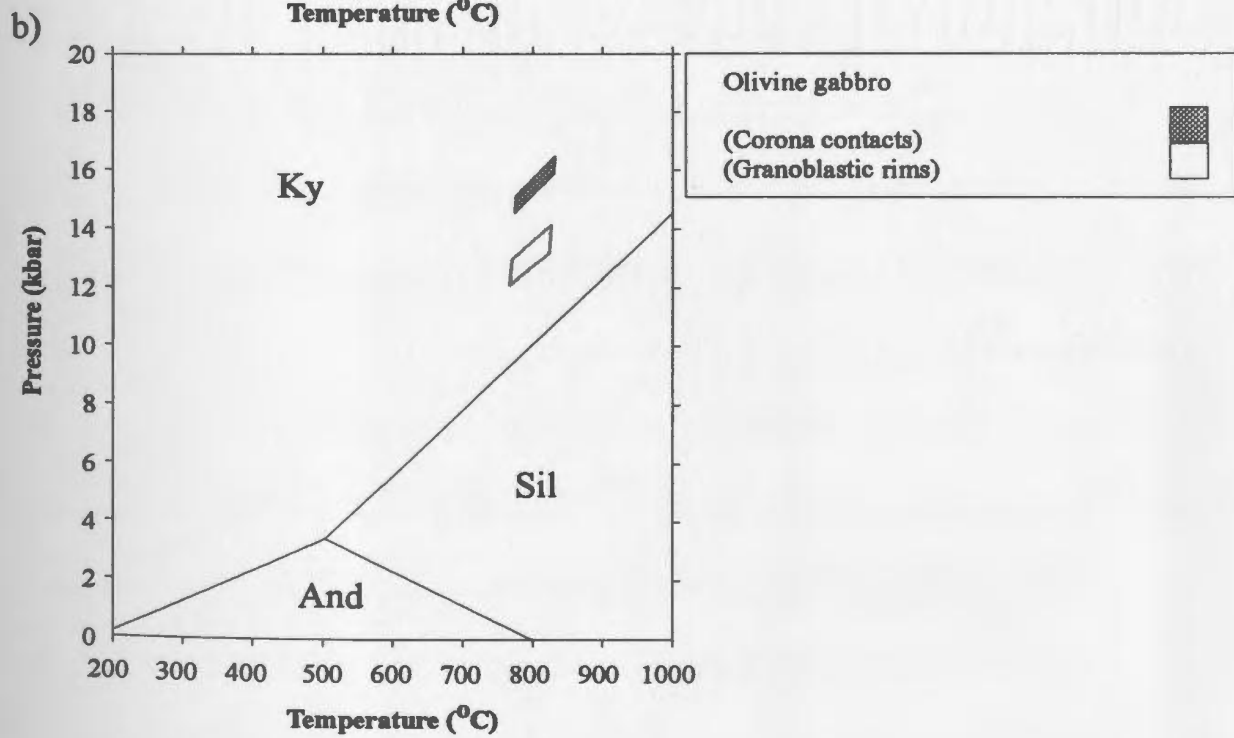
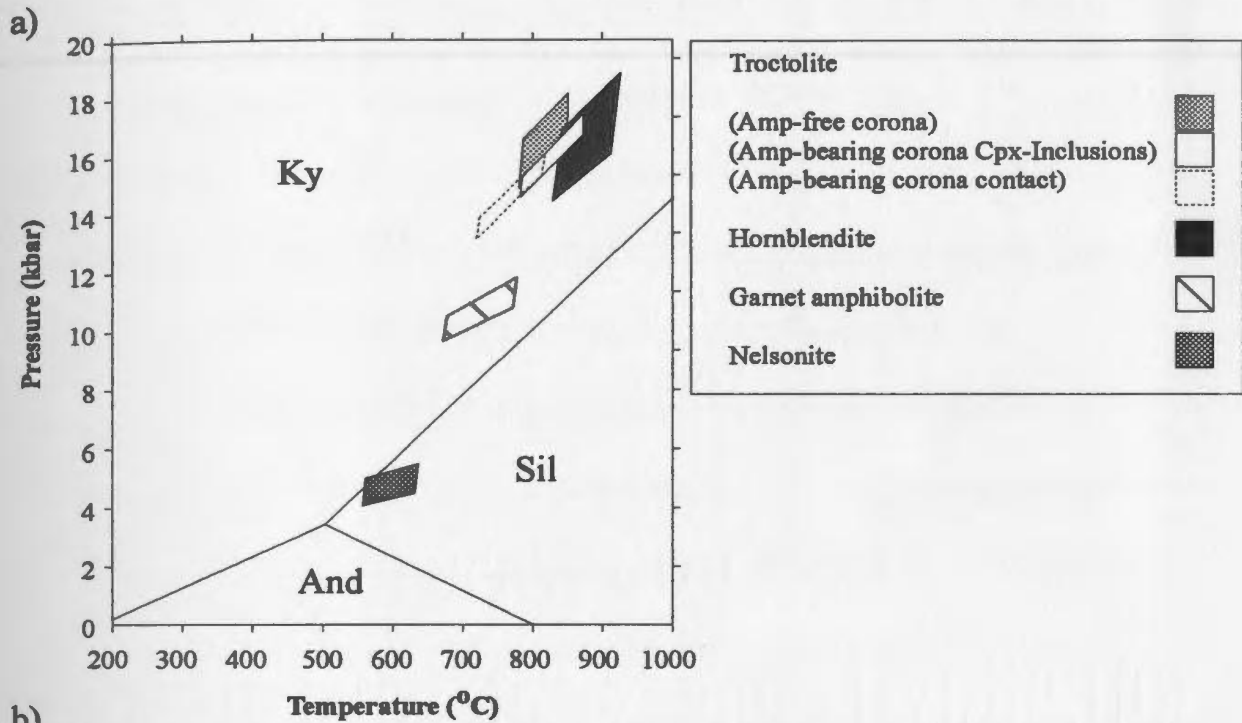


Table 3.1. Representative analyses of garnet, plagioclase, clinopyroxene, amphibole, orthopyroxene and olivine and spinel, in the mafic samples from the LES.

	Sample 5a (troctolite)						Sample 6am (ol grt amph)		Sample 3b (hornblende)	
	Grt-corona (Cpx-con)	Grt-corona (Pl-con)	Grt-retro (Amp-con)	Grt-retro (Cpx-con)	Grt-retro (Opx-con)	Grt-retro (Pl-con)	Grt (rim)	Grt (core)	Grt-corona (Pl-con)	Grt-corona (Amp-con)
SiO2	40.02	39.65	40.22	39.25	40.24	39.71	39.69	40.75	41.16	40.75
Al2O3	22.76	22.07	22.74	22.57	22.67	22.51	21.85	22.43	23.38	22.79
THO2	0.00	0.04	0.09	0.00	0.03	0.00	0.00	0.02	0.10	0.00
FeO(Total)	20.90	20.90	19.78	22.13	20.98	21.38	24.57	23.12	18.63	19.57
MgO	11.01	7.61	10.38	10.74	11.02	8.17	10.77	11.94	13.31	12.38
MnO	0.50	0.50	0.39	0.53	0.44	0.37	0.90	0.52	0.43	0.74
CaO	5.87	10.25	7.92	5.82	6.43	9.57	3.09	3.34	5.78	5.63
Total	101.09	101.06	101.56	101.11	101.87	101.76	100.95	102.12	102.82	101.92
Si	2.98	3.00	2.99	2.95	2.98	2.98	3.00	3.01	2.98	3.00
Al	2.00	1.97	1.96	2.00	1.98	1.99	1.95	1.95	2.00	1.97
Ti	0.00	0.01	0.04	0.00	0.00	0.00	0.00	0.00	0.05	0.00
Fe2+	1.29	1.29	1.16	1.34	1.27	1.32	1.50	1.38	1.11	1.17
Fe3+	0.01	0.03	0.05	0.05	0.03	0.03	0.05	0.04	0.02	0.03
Mg	1.22	0.86	1.09	1.20	1.22	0.91	1.21	1.32	1.44	1.36
Ca	0.47	0.83	0.75	0.47	0.51	0.77	0.25	0.26	0.50	0.44
Mn	0.03	0.03	0.03	0.03	0.03	0.02	0.06	0.03	0.03	0.05
Total	8.01	8.01	8.03	8.05	8.02	8.02	8.02	7.99	8.02	8.02
XAlm	0.428	0.429	0.401	0.440	0.419	0.435	0.497	0.462	0.367	0.388
XPrp	0.406	0.285	0.381	0.395	0.403	0.302	0.402	0.439	0.476	0.449
XGrn	0.149	0.260	0.197	0.130	0.151	0.241	0.057	0.065	0.136	0.132
XSpn	0.010	0.011	0.008	0.011	0.009	0.008	0.019	0.011	0.009	0.015

Table 3.1. (continued).

	Sample 35b (olivine gabbro)				Sample 2b (grt amph)	Sample 9c (nelsonite)	
	Grt-corona (Pl-con)	Grt-corona (Cpx-con)	Grt-rims	Grt-cores	Grt-rim	Grt-corona (Amp-con)	Grt-corona (Pl-con)
SiO ₂	40.96	41.33	41.03	41.39	38.08	37.71	37.75
Al ₂ O ₃	23.41	22.99	22.94	23.05	20.62	21.17	21.11
TiO ₂	0.00	0.00	0.00	0.02	0.00	0.05	0.09
FeO(Total)	15.94	16.34	16.24	14.96	26.57	33.90	33.85
MgO	12.06	13.42	14.33	12.01	2.89	3.52	3.56
MnO	0.37	0.40	0.43	0.26	2.42	1.79	1.89
CaO	9.12	7.25	5.79	10.56	10.79	4.08	4.23
Total	101.88	101.78	100.79	102.30	101.54	102.32	102.60
Si	2.98	3.00	3.00	2.99	2.99	2.97	2.97
Al	2.01	1.97	1.98	1.96	1.91	1.96	1.96
Ti	0.00	0.00	0.00	0.00	0.00	0.00	0.00
Fe ²⁺	0.97	0.95	0.97	0.85	1.65	2.17	2.17
Fe ³⁺	0.01	0.03	0.02	0.04	0.10	0.06	0.06
Mg	1.31	1.53	1.56	1.28	0.34	0.41	0.42
Ca	0.71	0.50	0.45	0.86	0.91	0.34	0.35
Mn	0.02	0.02	0.03	0.03	0.16	0.12	0.11
Total	8.01	8.01	8.01	8.02	8.05	8.05	8.04
XAlm	0.321	0.320	0.322	0.292	0.530	0.712	0.705
XPrp	0.435	0.484	0.519	0.431	0.128	0.136	0.137
XGrx	0.234	0.173	0.139	0.257	0.230	0.081	0.078
XSpa	0.008	0.008	0.009	0.005	0.051	0.039	0.041

Table 3.1. (continued).

	Sample 5a (troctolite)		Sample 6am (ol grt amph.)	Sample 3b (hornblende)	Sample 35b (ol gabbro)		Sample 2b (grt amph.)	Sample 9c (nelsonite)
	Pl-relict	Pl-relict (retro)	Pl-incl	Pl-relict	Pl-relict	Pl-relict (retro)	Pl-matrix	Pl-relict
SiO2	58.29	60.05	64.39	60.21	59.87	59.98	60.27	64.2
Al2O3	26.65	24.63	23.18	25.89	25.13	25.49	24.93	23.24
FeO(total)	0.24	0.69	0.31	0.17	0.12	0.12	0.43	0.19
CaO	7.72	6.16	4.13	6.62	6.83	7.15	6.68	4.24
Na2O	7.35	7.60	8.88	7.03	7.76	7.58	7.75	8.72
K2O	0.26	0.20	0.12	0.03	0.24	0.19	0.26	0.12
Total	100.51	99.33	101.01	99.95	99.95	100.5	100.32	100.71
Si	2.69	2.66	2.81	2.66	2.67	2.66	2.68	2.81
Al	1.30	1.33	1.19	1.37	1.32	1.33	1.31	1.20
Fe²⁺	0.03	0.01	0.01	0.01	0.00	0.00	0.02	0.01
Ca	0.30	0.33	0.19	0.32	0.33	0.34	0.32	0.20
Na	0.66	0.67	0.75	0.61	0.67	0.65	0.67	0.74
K	0.01	0.02	0.01	0.00	0.01	0.01	0.01	0.01
Total	4.99	5.02	4.97	4.96	5.01	5.00	5.01	4.96
XAn	0.362	0.306	0.210	0.342	0.323	0.339	0.318	0.210
XAb	0.624	0.683	0.790	0.656	0.664	0.650	0.668	0.783
XOr	0.015	0.012	0.000	0.002	0.014	0.011	0.015	0.007

Table 3.1. (continued).

	Sample 5a (troctolite)			Sample 35b (ol gabbro)	
	Cpx-corona (Grt-con)	Cpx-incl (retro)	Cpx-corona (retro)	Cpx-corona (Grt-con)	Cpx (grano)
SiO2	54.06	53.75	54.23	53.22	53.39
Al2O3	3.92	4.76	3.00	5.06	5.18
TiO2	0.18	0.27	0.09	0.27	0.18
FeO(total)	5.13	5.22	4.66	3.31	3.64
MgO	14.21	13.69	15.21	14.78	14.59
MnO	0.07	0.02	0.12	0.09	0.00
Cr2O3	0.17	0.00	0.27	0.16	0.34
NiO	0.12	0.04	0.00	0.00	0.13
CaO	21.31	21.45	22.60	23.23	22.85
Na2O	1.53	1.59	0.97	1.06	1.32
Total	100.72	100.80	101.20	101.23	101.74
Si	1.96	1.95	1.96	1.91	1.91
Al	0.17	0.20	0.13	0.21	0.22
Ti	0.01	0.01	0.00	0.01	0.01
Fe2+	0.15	0.16	0.13	0.08	0.07
Fe3+	0.01	0.00	0.01	0.02	0.04
Mg	0.77	0.74	0.82	0.79	0.78
Mn	0.00	0.00	0.00	0.00	0.00
Cr	0.01	0.00	0.02	0.01	0.01
Ni	0.02	0.01	0.00	0.00	0.01
Ca	0.83	0.83	0.87	0.89	0.88
Na	0.11	0.11	0.07	0.07	0.09
Total	4.00	4.00	4.00	4.01	4.01
X_{Hd}	0.161	0.175	0.135	0.095	0.087
X_{Dh}	0.839	0.825	0.865	0.905	0.913
X_{An}	0.008	0.001	0.013	0.017	0.035
X_{Jd}	0.100	0.111	0.055	0.057	0.057

Table 3.1. (continued).

	Sample 5a (troctolite) Amp retro corona	Sample 6am (ol grt amph) Amp matrix	Sample 3b (hbl-dite) Amp oikocryst	Sample 35b (ol gabbro) Amp retro corona	Sample 2b (grt amph) Amp matrix	Sample 9c (nelsonite) Amp corona
SiO₂	42.49	40.31	44.15	43.49	43.08	42.31
Al₂O₃	15.57	12.33	15.46	15.78	12.79	12.94
TiO₂	0.93	1.76	0.11	0.63	0.50	0.60
FeO (total)	6.70	18.45	15.95	5.53	18.46	19.03
MnO	0.07	0.16	0.00	0.03	0.21	0.08
MgO	15.34	8.64	11.65	15.90	9.72	9.52
NiO	0.09	0.08	0.47	0.15	0.00	0.00
CaO	11.91	11.63	3.36	12.34	10.84	10.48
Na₂O	2.88	1.89	6.01	2.30	1.75	1.83
K₂O	1.10	1.81	0.01	1.12	0.53	0.67
Total	97.19	97.10	97.29	97.52	97.89	97.53
Si	6.15	6.22	6.28	6.22	6.46	6.40
Al	2.66	2.24	2.59	2.66	2.63	2.31
Ti	0.10	0.20	0.01	0.07	0.06	0.07
Fe²⁺	0.69	2.24	0.60	0.56	1.72	1.72
Fe³⁺	0.12	0.14	0.25	0.10	0.60	0.69
Mn	0.01	0.02	0.00	0.00	0.03	0.01
Mg	3.31	1.99	3.38	3.39	2.17	2.15
Ni	0.01	0.01	0.05	0.02	0.00	0.00
Ca	1.85	1.92	1.78	1.89	1.74	1.70
Na	0.81	0.56	0.93	0.64	0.51	0.54
K	0.20	0.36	0.00	0.20	0.10	0.13
Total	15.92	15.92	15.96	15.79	16.02	15.71

Table 3.1. (continued).

	Sample 5a	Sample 6am	
	(troctolite)	(ol grt amphibolite)	
	Opx-corona	Opx	Ol
	(Grt-con)	(matrix)	(matrix)
SiO ₂	54.53	53.29	37.22
Al ₂ O ₃	1.77	2.59	0.00
TiO ₂	0.03	0.09	0.00
FeO(total)	15.81	18.14	30.12
MgO	27.52	25.53	32.51
MnO	0.11	0.20	0.33
CaO	0.23	0.07	0.07
Total	100.00	99.91	100.25
Si	1.96	1.94	1.00
Al	0.08	0.11	0.00
Ti	0.00	0.01	0.00
Fe ²⁺	0.47	0.55	0.68
Fe ³⁺	0.00	0.01	0.00
Mg	1.47	1.38	1.307
Mn	0.00	0.01	0.02
Ca	0.02	0.00	0.00
Total	4.00	4.00	3.00
		X _{Fe}	0.658
		X _{Mn}	0.341

Table 3.1. (continued).

	Sample 9c (nclsenic)
	Spl (incl)
SiO2	0.77
ThO2	0.00
Al2O3	60.48
Cr2O3	0.00
FeO (total)	27.10
MnO	0.08
MgO	9.21
ZnO	1.37
NiO	0.14
Total	99.15
Si	0.021
Al	1.933
Fe3*	0.621
Fe2*	0.000
Mn	0.002
Mg	0.376
Ti	0.000
Cr	0.000
Zn	0.028
Ni	0.003
Total	2.983

Table 3.2. PT-conditions recorded by the mafic sample of the LES. Abbreviations for the conventional thermometers are: E&G79=Ellis and Green (1979), K88=Krogh (1988) for garnet-clinopyroxene, C&H90=Carswell and Harley (1990) for garnet-orthopyroxene, O&W80=O'Neil and Wood (1980) for garnet-olivine and G&P84=Graham and Powell (1984) for garnet-amphibole. Barometric reactions are In95=Indares and Rivers (1995) for garnet-plagioclase-kyanite-corundum, G&S=Ghent and Stout (1984) for garnet-plagioclase-rutile-quartz-titanite (GRAIL+Ttn variant) and In&D97=Indares and Dunning (1997) for garnet-plagioclase-spinel-corundum.

	Sample 5a (coronitic troctolite)					Sample 6am (olivine garnet amphibolite)				Sample 3b (hbl-dite)	Sample 2b (grt amph)	Sample 9c (nelsonite)	Sample 35b (olivine gabbro)	
	Amp-free corona Grt-Cpx- Pl-Kyn- Cm	Amp-bearing corona				Grt porphyroblast core and rim				Coronas	Grt rims and matrix	Coronas	Grano	Coronas
	Grt-Cpx- Pl-Kyn- Cm	Grt-Cpx- Pl-Kyn- Cm	Grt-Cpx (incl)	Grt-Opx (contact)	Grt-Amp (contact)	Grt-Ol (grt- cores)	Grt-Ol (con)	Grt-Opx (con)	Grt- Amp (con)	Grt-Amp- Pl-Kyn- Cm	Grt-Amp- Pl-Qtz- Ttn-Rt	Grt-Amp- Pl-Spl-Cm	Grt-Cpx- Pl-Kyn- Cm	Grt-Cpx- Pl-Kyn- Cm
Thermometers (T-range from 0 to 20 kbars)														
TWEEQU	780-870	700-775	790-890	685-790	745-810	650-860	590-670	605-700	610-720	800-925	620-795	550-690	750-860	775-870
E&G79	720-810	650-715	730-830										760-880	790-885
K88	670-765	600-660	695-790										715-825	745-840
C&H90				750-865				665-815						
O&W80						710-915	685-730							
G&P84					760-825				640-750	825-950	630-705	485-560	765-880	
Barometers (all TWEEQU) (P-range for the temperatures above)														
In95 (Grt-Pl- Ky-Cm)	16-19	14-16	14-17							15-19			12-14	14-16
G&S84 (GRAIL)											10-12			
In&D97 (Grt-Pl- Spl-Cm)												4-6		

Temperature-time paths and exhumation rates in the high-P Manicouagan Imbricate Zone, eastern Grenville Province.

Abstract

The Manicouagan Imbricate Zone (MIZ) of the north-eastern Grenville Province comprises a series of lithotectonic units which were deformed and metamorphosed at conditions up to eclogite facies at 1050-1000 Ma during the Grenvillian orogeny. The maximum P-conditions (ca. 14-20 kbar) recorded by metamorphic assemblages are consistent with variations in burial depth that suggest the MIZ is an assembly of rocks units from different crustal levels. However, the maximum T-conditions recorded by metamorphic assemblages from apparently different structural levels are rather similar (ca. 800-900 °C). In addition, PT-conditions and retrograde textures show abundant evidence for reequilibration at high T-conditions (700-800 °C) suggesting very steep to near-isothermal decompression. However, U-Pb ages from across the MIZ infer two separate metamorphic events separated by about 30 Ma. The first event is not only characterized by high-PT conditions but also by the presence of syn-metamorphic mafic dykes. The high temperatures recorded during this event throughout the whole crustal section represented by the MIZ suggests heat input from the mantle. The second event is recorded by retrograde assemblages overprinting some of the high-PT rocks and by metamorphism and syn-metamorphic garnite emplacement in the upper most tectonic slice (Boundary zone) in the southeast MIZ. Published diffusion rates for Pb in monazite, titanite and rutile suggest that their ages record part of the cooling history of the terranes within the MIZ. The initial rates of cooling and exhumation were relatively fast (>5 °C/Ma and >1 mm/yr), consistent with tectonic exhumation by extrusion of the lower and middle levels of the MIZ. The rates of cooling and exhumation subsequently slowed during thrust emplacement of the higher structural levels (Boundary zone). The high-P metamorphism and the early high-T stages of exhumation of the MIZ occurred during the Ottawa Pulse (1050-

1020 Ma) of the Grenvillian orogeny. The emplacement of the Boundary Zone may correspond to a second pulse of metamorphism between 1020-1000 Ma. This is indicated by some zircon ages, overgrowths of some garnets, textural reequilibration of high-P assemblages and may correspond to a late metamorphic event known as the Rigolet Pulse. Because monazite was not affected by the second event, despite the relatively high-T conditions (>700 °C), it is likely that this was a rather short lived metamorphic pulse. Different crustal depths across the MIZ record variations in cooling (rutile ages) over the range 946-920 Ma which suggests that later cooling and exhumation was rather slow, consistent with geologically young high-P terranes. Evidence for different pulses of metamorphism corresponding to separate Grenvillian metamorphic events in both the eastern (Ottawan and Rigolet) and western (Shawinigan and Ottawan) Grenville Province may account for the apparently slow rates of cooling recorded by terranes in these areas.

Keywords: high-PT metamorphism, PT-paths, metamorphic gradients, U-Pb ages, closure temperatures, Tt-paths, exhumation.

4.1. Introduction

Temperature-time paths (Tt-paths) are constructed using precise age determinations on single minerals with different closure temperatures (Dodson 1973). In certain circumstances, the combination of PT-determinations and age data can be used to calculate both cooling and exhumation rates. This method works best in high-PT terranes (e.g. Duchêne et al. 1997; Jamieson et al. 1998). Most studies of high-T terranes use U-Pb ages of accessory phases such as zircon, monazite, titanite and rutile to construct Tt-paths (e.g. Mezger et al. 1991; Mezger et al. 1993; van der Pluijm 1994; Spear and Parrish 1996) which in turn are used to help understand the tectonic processes operating during the exhumation and cooling. For example a tight clustering of ages determined on minerals with different closure temperatures (T_c) indicates rapid cooling. This Tt-path might be used to suggest

tectonic exhumation rather than erosional denudation of a terrane. Exhumation rates are difficult to measure directly because the mineral ages are difficult to correlate with independent decompression reactions. Therefore, exhumation rates have to be derived using a combination of PT-paths and cooling ages. PT-paths are best constrained in areas where both peak and retrograde assemblages are available. In such circumstances, ages determined on a number of rock types and minerals will give the best estimates of exhumation rates as well as cooling rates.

In calculating Tt-paths, complications may arise because the growth of “datable” minerals can occur both above or below their T_c . For example, titanite is commonly found as a retrograde replacement product after rutile. However, in high-PT terranes, the temperatures attained are often above the T_c for titanite and the most commonly dated mineral phases. Thus, in many instances, retrograde reactions will form “datable” minerals such as titanite during exhumation, but well above their T_c . Alternatively, phases such as monazite and titanite may form or even recrystallize well below their T_c (e.g. Lanzirotti and Hanson 1996; Corfu and Stone 1998) resulting in anomalous Tt-data. Despite this, the apparent rates of cooling and exhumation may be compared with adjacent areas to suggest whether the tectono-thermal processes operating were similar or different. In the case of older orogens with complex tectonic histories the Tt-paths and exhumation rates may be compared with younger metamorphic belts where the tectonic evolution is better established. Comparisons can also be made using the measured Tt-paths and calculated exhumation rates, with theoretical PTt-paths (e.g. England and Thompson 1984; Davy and Gillet 1986; Shi and Wang 1987; Ruppel and Hodges 1994) resulting from different tectono-metamorphic processes.

The Manicouagan Imbricate zone (MIZ) in the eastern Grenville Province (**Figure 4.1**) has been the focus of research including U-Pb geochronology on a variety of accessory minerals, and determination of the range in PT-conditions recorded by the main rocks types. The MIZ represents an assembly of crustal slices that experienced high-PT conditions during the Grenvillian orogeny (1050-1000 Ma), that were subsequently exhumed from deep crustal levels. The range of PT-estimates from across the area suggests very high-T conditions during both peak metamorphism and during the early stages of exhumation (e.g. Cox and Indares 1999a and 1999b). In

contribution we use the available metamorphic PT-data and U-Pb ages to construct Tt-paths and calculate the exhumation rates. The tectonic processes which controlled the cooling and exhumation of the MIZ are discussed by comparing the results with younger metamorphic belts and published tectonic models. The Tt-information from the MIZ is also compared with available Tt-data from other areas in the Grenville Province.

4.2. Geological Setting

4.2.1. Regional context

The MIZ is located at the southern boundary of the parautochthonous (high-P) belt in the north-east Grenville Province (Rivers et al. 1989; Indares et al., in press). To the north the MIZ overlies the Gagnon terrane and to the south it is overlain by the Harte Jaune terrane (Figure 4.1). The Gagnon terrane consists of Paleoproterozoic continental margin sequences and Archean basement (Rivers et al. 1993). The terrane is a fold-thrust nappe belt with metamorphic grade increasing from greenschist facies near the Grenville Front to high-P amphibolite and eclogite facies to the south (Rivers et al. 1993; Indares 1995). The Harte Jaune terrane includes Pinwarian (ca. 1450 Ma) mafic granulites and coronitic Fe-Ti gabbro that contain Grenvillian metamorphic assemblages up to amphibolite facies in its northern section (Scott and Hynes 1994). Thus, the regional metamorphic field gradient (southwards from the Grenville front) ranges from, low-PT (greenschist) to high-PT (eclogite) in the Gagnon terrane section and is at high-PT (eclogite) across virtually the entire MIZ section. The gradient is then reversed with PT-conditions ranging from high-PT (upper amphibolite) to much lower grades across the Harte Jaune terrane. The area has been imaged by seismic profile (Lithoprobe transect N° 51) which suggests that the MIZ is a shallow-dipping thrust-bounded wedge. The MIZ represents a high-PT segment, and appears to have been exhumed (extruded) from deep crustal levels between the Gagnon and Harte Jaune terranes.

4.2.2. Lithotectonic framework of the MIZ

The MIZ has a SE-plunging synformal shape and consists of two lithotectonic packages, the structurally lower Lelukuau terrane and the overlying Tshenukutish terrane (Figure 4.2). The Lelukuau terrane (LT) consists mainly of an imbricated anorthosite-mangerite-charnockite-granite (AMCG) suite (Indares et al. 1998; Indares et al. 1999). The LT is divided into three slices (LT-I, LT-II and LT-III, Figure 4.2) and display evidence of north-west directed thrusting (Indares et al. 1998). Most information about the Lelukuau terrane comes from the structurally highest slice (LT-III). Slice LT-III contains anorthosite and olivine gabbro intruded by mangerite, ranging in age from ca. 1650-1630 Ma (Indares et al. 1998). These rocks are intruded by 1300 Ma leucogranite that is in turn cross-cut by syn-metamorphic mafic dykes and sills, known locally as the Thimes dyke swarm, dated by U-Pb zircon ages at 1039 \pm 2 Ma (Indares et al. 1998).

The Tshenukutish terrane (TT) can be divided into two main lithotectonic packages, the Baie du Nord segment (BNS) and the Boundary zone (BZ). The BNS overlies slice LT-III to the east. The BNS mainly comprises ca. 1450 Ma megacrystic diorite that grades into an orthogneiss, locally injected by granitic material (Indares et al. 1998). These rocks also contain rafts of metapelite, calc-silicate and quartzite and are intruded by Fe-Ti gabbro sills, dated at 1170 \pm 5 Ma (Cox et al. 1998). Other rock types include a tectonic sliver of anorthosite in the Baie du Nord area (Figure 4.2). The BNS has the overall configuration of a north-west verging synform and tectonic fabrics within the BNS are consistent with an early phase of folding and thrusting towards the north-west, and a later phase of extension towards the south-east (Indares et al., in press).

The Boundary zone (BZ) which outcrops to the south-east, is a disparate assembly of lithotectonic units and defines the highest structural level of the MIZ (Figure 4.2). The Boundary zone (BZ) contains a variety of lithotectonic units (Figure 4.2). To the north the Lac Espadon suite (LES) includes Labradorian (ca. 1650) mafic and ultramafic rocks which locally occur as small-scale tectonic lenses within a sheared orthogneiss. These, together with nelsonite, are exposed along the western shore of the Harte Jaune arm. On the eastern shore of the Harte Jaune arm the LES is represented by olivine gabbro (Figure 4.2). The LES is interpreted to represent a

Labradorian layered mafic-ultramafic suite and may correlate with the AMCG rocks in the LT (Cox et al. 1998). The southern BZ consists of the Harte Jaune granite (1017 \pm 2 Ma) which contains rafts of metasediment, tectonic slices of the Brien anorthosite (1169 \pm 2 Ma) and the X-suite which consists of gabbro-anorthosite in tectonic layers alternating with (1007 \pm 2 Ma) granite sills (Scott and Hynes 1994; Indares et al 1998). The LES is interpreted to have been emplaced over the BNS by a north-west directed, out of sequence thrust (Indares et al. 1999). However, shear zones both within the BZ and at the northern boundary display abundant evidence of south-east directed (normal) transport, consistent with extension. To the south the BZ is truncated by the Harte Jaune shear zone (Figure 4.2) that separates it from the Harte Jaune terrane. The Harte Jaune shear zone also displays evidence of south-east directed transport (extension).

4.3. High-PT metamorphism in the MIZ

Evidence of high-PT metamorphism is widespread throughout the MIZ. The localities of samples from which the estimates of metamorphic conditions and U-Pb ages across the MIZ are shown in Figure 4.3. The PT-data and U-Pb ages are presented in Table 4.1 and Table 4.2. The samples are arranged in a cross-section from the north-east to the south-west MIZ which represents the broad tectono-stratigraphy and the major structural boundaries from the lowest (LT-I) to the highest (south-west BZ) structural slices. However, it should be noted that the section does not represent a continuous suite of samples, and that many do not have both PT-data and U-Pb data available. However, to allow comparison of the MIZ using the complete data set, all samples (with either PT-determination and/or U-Pb ages) are included in Figure 4.4 and Figure 4.5.

4.3.1. Lelukauu terrane (LT)

PT-conditions in the Lelukauu terrane (LT) have been documented from only one sample (melanogabbro) in the north-west of slice LT-I and more completely in the highest tectonic slice LT-III. Metamorphic

conditions recorded by the melano-gabbro in slice LT-I are 700-750 °C at 12-14 kbar (Indares et al. 1994). Evidence for high-P metamorphism of the rocks in LT-III includes garnet-kyanite-K-feldspar restites as rafts within granitic rocks and variable transformation of mafic rocks to plagioclase-free, kyanite-garnet clinopyroxenite (Indares 1997). Olivine gabbros transformed to garnet-kyanite clinopyroxenites record conditions of 800-900 °C at 16-18 kbar in the west section of LT-III and 850-920 °C at 18-20 kbars in the east section (Table 4.1 and Figure 4.4). The high-PT assemblages in rocks throughout the LT are only locally retrogressed and no PT-estimates of retrograde conditions have been determined.

4.3.2. Baie du Nord segment (BNS)

In the Baie du Nord segment (BNS), high-P metamorphic assemblages are best preserved in the 1170 Ma Fe-Ti gabbros and in the metapelitic rafts (Cox and Indares 1999a; Indares and Dunning, in press). The gabbros display textural evidence for increasing degree of transformation from coronitic metagabbro (770-810 °C at 12-14 kbar), to transitional metagabbro (750-820 °C at 11-14 kbar) and to eclogite (740-825 °C at 14-18 kbar). The deformed and hydrated margins of the coronitic rocks have undergone anatexis with recorded conditions of 795-825 °C at 11-12 kbar. Experimental results suggest that the minimum conditions required for the melting of amphibolite are between 800-850 °C at 10-15 kbar (e.g. Sen and Dun 1994; Wolf and Wyllie 1994; Williams et al. 1995; Hartel and Pattison 1996). PT-estimates from partly retrogressed microtextural domains give PT-estimates (coronites, 710-780 °C at 11-13 kbar; migmatitic garnet amphibolite, 795-825 °C at 8-10 kbar) which overlap those representative of peak-T (Table 4.1 and Figure 4.4). Thus, the apparent peak PT-conditions in these rocks have probably been partially reset during the early stages of exhumation and cooling. Metapelites from across the BNS display garnet-kyanite-K-feldspar restites and display evidence of dehydration melting of both muscovite and biotite at PT-conditions of >14 kbar and >850 °C (Indares and Dunning, in press). This further supports the suggestion that the highest T-conditions recorded by the metagabbros in the BNS may be representative of post-peak, reequilibration. The difference in recorded P-conditions (12-18 kbars) suggests that the BNS was an

approximately 26 km thick segment of crust (assuming a crustal density of 2.8 gm/cm³), which experienced similar high-T conditions (>800 °C) during exhumation.

4.3.3. Boundary Zone (BZ)

The Lac Espadon Suite (LES) comprises two units which are separated by a shear zone (Figure 4.3). Mafic and ultramafic rocks from the western LES record peak PT-conditions of 780-930 °C and 16-19 kbar and retrograde conditions from ca. 700 °C at 10-12 kbar down to ca. 600 °C at 5-6 kbar. In the eastern LES, metamorphosed olivine gabbro records peak PT-conditions of 775-850 °C at 14-16 kbar and retrograde conditions at 750-850 °C at 12-14 kbar which overlap with those in the western LES (Table 4.1 and Figure 4.4). In the northern BZ metapelites display similar assemblages (garnet-kyanite-K-feldspar restites) to those in the BNS and also suggest dehydration melting at PT-conditions of >14 kbar and >850 °C (Indares and Dunning, in press). In the southern BZ metapelitic rafts within the Harte Jaune granite contain kyanite-bearing leucosomes and are interpreted to have experienced dehydration melting of muscovite but not biotite. Estimated peak conditions are 750-850 °C at 10-13 kbar (Indares and Dunning, in press). Thus, the LES has experienced rather different (higher-P) metamorphic conditions to the rest of the BZ. Apart from the LES, the BZ has in general experienced lower peak P-conditions than the rest of the MIZ. However, it is noteworthy that the peak-PT conditions recorded by rocks in the BZ are rather similar to those representative of retrogression in the BNS and LES (Figure 4.4).

The tectonic evolution of the MIZ can be summarized as follows; a) High-PT metamorphism and intrusion of syn-metamorphic mafic intrusions in the LT, BZ and LES, b) initial exhumation of the MIZ by north-west directed extrusion with extension in the higher levels of the tectonic pile and c) metamorphism of the BZ and possibly overprinting in the rest of the MIZ. a final phase of extension to the south-east along the Harte Jaune shear zone. Tt-paths may provide key information to constrain the timing and characteristics of exhumation in the MIZ.

4. 4. The behaviour of accessory phases during high-PT metamorphism

4.4.1. Summary of U-Pb data in the MIZ

The behaviour of zircon during high-PT metamorphic events is discussed in detail below. However, it is likely that the maximum metamorphic temperatures in the MIZ are below the absolute T_c for zircon (probably >1000 °C). High-T Pb-loss ages in these rocks are constrained by lower intercepts fitted through discordant populations which in fact still lie close to their original protolith age (Cox et al. 1998; Indares et al. 1998). On the other hand, most of the metamorphic zircon ages from across the MIZ lie between 1060-1030 Ma, with the majority of (including the most precise) overlapping in the range 1050-1040 Ma (Figure 4.5). It is interesting to note that in areas which contain rocks which have experienced the highest-PT metamorphism also record zircon age ranges with the largest spread. In some areas, e.g. the south-west BNS (Figure 4.5), there are different generations of metamorphic zircons ranging in age from 1046 \pm 3 Ma, to 1030 \pm 10/-7 Ma and 1012 \pm 12 Ma. It may be possible that the large spread in metamorphic ages, particularly in the LES and LT-III, may be due to mixed populations of multiple generations of zircon which grew during high-T metamorphism between 1060-1030 Ma. However, more detailed work on the zircons from these samples is required to address this. As with the PT-data, the zircon age data from the BZ (excluding the LES) contrasts with the rest of the MIZ. The zircons from the Harte Jaune granite and later granite intrusions range in age from 1019-1005 Ma (Figure 4.5). These are younger than the majority of metamorphic zircons in the remainder of the MIZ.

The ages of the monazites across the MIZ (Figure 4.5) show a similar pattern to the zircon in that the areas which experienced the highest-PT conditions (LT-III and BNS) have the oldest ages (ca. 1040-1034 Ma) whereas, ages from the BZ are younger (ca. 1020-1015 Ma). In addition, the ages of the zircons in the Harte Jaune granite and monazites from metapelites which have undergone anatexis are identical. This strongly suggests that the BZ (excluding the LES) experienced a different (younger) pulse of metamorphism to the rest of the MIZ and at lower PT-conditions.

Titanite ages across the MIZ are much more consistent than either zircon or monazite, and can be broadly divided into two groups ranging from ca. 1010-995 Ma and from 995-985 Ma (Figure 4.5). The older group of ages is commonly represented by samples larger grain sizes. However, it is also apparent that the titanite ages record different processes from one sample to another. For example, titanite in the BNS and LES occurs in rocks which have experienced extensive amphibolite facies retrogression and all give ages in the older 1010-995 Ma range. These are also broadly contemporaneous with the emplacement of late granite stocks, dated by both zircon and large grain sizes of titanite at 1007 \pm 2 Ma, in the southern BZ (Figure 4.5). It is likely then that these ages represent the end of retrogression following metamorphism recorded by the monazites in the BZ at ca. 1020 Ma. Smaller grain sizes of titanite in the country rock (Harte Jaune gneiss) and late granites in the BZ, and in one sample (leuco-granite) in slice LT-III give ages in the 995-985 Ma range. These may represent cooling or a later, more localized crystallization events that affected these samples. This is discussed in detail below, however, it is clear that the titanite (and rutile) ages in the MIZ date the constrain the maximum age for high grade metamorphism in the MIZ.

4.4.2. Zircon

Zircon has been shown in several studies to survive high-T processes with U-Pb isotopic signatures preserved and is commonly found as inherited crystals (xenocrysts) in intermediate and felsic igneous rocks. Metamorphism of zircon can produce discordant age patterns in pre-existing (igneous) populations and new grown crystals but the effective closure temperature (T_c , Dodson 1973) for Pb-diffusion is higher than temperatures recorded by most crustal processes (Mezger and Krogstad 1997). Thus, the complete resetting of the U-Pb system in zircon by Pb-diffusion is unlikely during metamorphism. However, zircons can show both high and low-T Pb-loss. The percentage discordance of zircon is often directly related to the absolute concentration of radiogenic elements (U, Th, etc) which in turn suggests that Pb-loss in zircon is controlled by radiation damage in the crystal lattice. Studies into the effects of crystal lattice orientation and radiation damage on diffusion rates (e.g. Lee 1995;

Dahl 1997; Meldrum et al. 1998) confirm this observation. Fission-track damage in zircon anneals in the T-range ca. 210-320 °C (Yamada et al. 1995) whereas the crystal lattice completely anneals, preventing rapid Pb-loss, at temperatures around 600 °C (Kröggstad and Mezger 1996). It is apparent from these and other studies that Pb-loss in zircons occurs independently of fission-track and crystal-lattice annealing. Therefore, metamorphic ages defined by lower intercepts fitted through discordant zircon populations, must be constrained by other means as discussed below.

The effects of high-T recrystallization of zircon has been the focus of a number of recent studies. Under certain conditions, zircon can be recrystallized and/or overgrown leading to young zones on older cores, even in relatively undeformed rocks (e.g. Pidgeon et al. 1998). Metamorphic conditions causing the resorption and regeneration of zircon may range from solid-state, fluid assisted reactions, to new crystals formed in leucosomes created by partial melting (e.g. Jeackel et al. 1997; Schalteger et al. 1999; Vavra et al. 1999). New crystals of zircon can grow under high-T metamorphic conditions occasionally by the replacement of accessory minerals such as baddeleyite (Davison and van Breemen 1988; Heaman and LeCheminant 1993; Dudás et al. 1994). Metamorphic zircon may grow after peak metamorphism, with growth controlled by the breakdown of zirconium-bearing phases such as garnet and hornblende (Fraser et al. 1997). Only a few reactions for the growth of zircon in metamorphic rocks have been suggested (e.g. Pan 1997) and none to date have been quantified by thermodynamic models. On the other hand, reaction textures can occasionally be directly related to sample petrography (e.g. Davidson 1988; Pehrsson et al. 1996; Creaser 1997; Jeackel et al. 1997; Cox et al. 1998) indicating high-PT growth of zircon. Thus, the interpretation of U-Pb zircon ages from rocks which have been subjected to high-T metamorphism can be constrained by metamorphic textures, PT-data on the main phase assemblages, by detailed studies of zoning, crystal morphology and the measured U-Pb isotopic data.

In the MIZ, metamorphic zircon ages are defined by a) discordant populations which have lower intercepts caused by low-T Pb-loss, found in crystals with high U-contents, b) discordant populations which have lower intercepts defining high-T Pb-loss even after annealing of the crystal lattice, c) metamorphic resorption and

overgrowth of existing zircon producing discordant to concordant populations which have lower intercepts constraining the age of the high-T event, d) new growth of metamorphic crystals producing concordant populations (both in solid-state and during partial melting) and e) breakdown of baddeleyite to produce metamorphic zircon. There are mixtures of these types of ages and more than one process may account for a zircon age pattern, e.g. high-T Pb-loss and reactions to form new zircon. Both high and low-T Pb-loss can affect newly grown, metamorphic crystals and even existing discordant populations can undergo later Pb-loss to produce additional discordance. As zircon completely anneals at ca. 600 °C (Mezger and Krogstad 1997) most Pb-loss ages are unreliable unless other age constraints supporting their validity are available. Zircon ages from the MIZ (Table 4.2 and Figure 4.5) are interpreted in terms of their relationships to the main-phase textures and PT-data available in each sample. In general, this means that the ages represent the formation of metamorphic zircon and/or high-T (diffusional) Pb-loss close to the maximum T-conditions recorded in the MIZ (800-900 °C). However, this can only be justified where the zircon ages themselves are sufficiently precise to constrain the timing of peak metamorphism.

4.4.3. Monazite

Monazite behaviour in metamorphic rocks has been almost as widely applied to metamorphic rocks as zircon. U-Pb monazite ages are usually regarded as robust to resetting at high-T. For example monazite is typically only partially reset by granulite facies metamorphism and can be found as inherited crystals in granitoids (Parrish 1990; Kingsbury et al. 1993). Although monazite contains high concentrations of both U and Th (up to 10% Th) discordant populations are rare, which suggests that monazite anneals at rather low temperatures and is less susceptible to Pb-loss than zircon. This is supported by studies on the effects of radiation damage on the monazite lattice (e.g. Meldrum et al. 1998). Reverse discordance is relatively common, especially in younger rocks, and this has been attributed to excess ^{206}Pb produced by incorporation of ^{230}Th during crystal growth. However, in older rocks (>100 Ma), any excess ^{206}Pb will have an almost negligible effect on the age. All the monazite ages from the MIZ are within 0.2% of concordia (Indares and Dunning, in press) and thus, any excess ^{206}Pb has caused at most

a 2 million year discrepancy between the U/Pb and Pb/Pb ages and is considered to be insignificant in terms of the duration of tectonic processes operating in the study area.

Metamorphic monazite has been shown to form during granulite facies metamorphism from the breakdown of other light-REE bearing accessory phases such as allanite and apatite (Pan and Fleet 1995) although much lower T-growth of monazite has also been noted (e.g. Teufel and Heinrich 1993). Monazite dating by various microbeam techniques, high precision dating of single grains, and even small fragments of grains have led to the realisation that multiple generations of monazite are present in polyphase terranes (e.g. Childe et al. 1993; DeWolf et al. 1993; Lenzarotti and Hanson 1996; Zhu et al. 1997; Cocherie et al. 1998; Vavra and Schaltegger 1999). This in turn has led to the conclusion that the closure temperature for monazite is higher than the 700-750 °C first suggested by Copeland et al. (1988) and Parrish (1990).

Studies modelling the rates of Pb-diffusion in monazite (Suzuki et al. 1994; Smith and Giletti 1997) allow for a precise calculation of the T_c . When compared with measured U-Pb ages and PT-conditions it has been argued that these two studies give low T_c estimates for monazite (e.g. Spear and Parrish 1996). However, when examined in detail the latter conclusion may be misleading. For example rocks from the Valhalla Complex, British Columbia showed ca. 1400 Ma monazite (100-150 μ ms diameter) to be 79-95% discordant (Parrish 1990). The rocks were metamorphosed under PT-conditions of 790-850 °C at 7-9 kbar (Spear and Parrish 1996). Using the diffusion data in Smith and Giletti (1996), the 79-95% Pb-loss observed, requires that the duration of high-T metamorphism (i.e. >800 °C) lasted between 1-10 million years. Petrologic cooling rates in the Valhalla Complex, constrained by Fe-Mg exchange between garnet and biotite) are between 3-80 °C/Ma (Spear and Parrish 1996) using the diffusion coefficients of Chakraborty and Ganguly (1992). If the Valhalla Complex cooled at the rates suggested by the authors during the initial stages of exhumation, then the terrane would have cooled to 700-750 °C in just a few million years. Thus, the monazite age pattern (79-95% discordant) would in fact be consistent with the experimental diffusion data of Smith and Giletti (1996).

A second detailed examination of multiple generations of monazite focused on Paleoproterozoic migmatites from the eastern Grand Canyon in Arizona (Hawkins and Bowring 1999). In this study, the rocks were metamorphosed up to 700-720 °C at 6 kbar. Monazite crystals and small fragments ranging in diameter from 40-60 µm were dated along with slices from larger (50-100 µm) crystals. Idioblastic crystals contained no older (igneous) age component but did record broadly concordant or slightly discordant ages (ca. 10%) in the range 1708-1702 Ma. Xenoblastic grains, interpreted as having grown during the melting event, gave ages from 1702-1696 Ma. In other words the entire melting event in this study lasted about 6-12 Ma. According to the diffusion data of Smith and Giletti (1996) monazites with diameters of around 50 µm would be reset in around 10 Ma. This would explain why there are no older age components in these grains. Continuous monazite crystallization in the cooling rocks along with small amounts of Pb-diffusion for 5 million years following melting would explain the observed age spread. In summary, data on the rates of diffusion of Pb in monazite (Suzuki and Adachi 1994; Smith and Giletti 1996) are in fact consistent with published U-Pb and PT-data sets from high-grade terranes and may be applied to help establish part of the Tt-history of the MIZ.

4.4.4. Titanite and Rutile

Of the accessory minerals commonly dated by the U-Pb method, titanite and rutile are by far the best understood in terms of mineral reactions. Therefore, these two accessory phases are relatively easy to interpret in terms of the textures represented by the main-phase assemblages. Indeed several reactions involving rutile and titanite, along with the other most common Ti-rich phase ilmenite, have been thermodynamically constrained (e.g. Bohlen et al. 1983; Ghent and Stout 1984; Essene and Bohlen 1985). Titanite and ilmenite are common retrograde or lower-P phases replacing rutile during metamorphism. Recent studies have shown that titanite U-Pb ages show a similar behaviour to that of monazite. For example most titanite populations are concordant or show minor Pb-loss suggesting low annealing temperatures and a high T_c . The presence of multiple titanite age populations in high-T terranes (e.g. Verts et al. 1996) and even from within the same rock sample (Ketchum et al. 1998) along with

evidence for inherited crystals in plutonic rocks (Corfu 1996; Pidgeon et al. 1996) further suggest that titanite may have a high T_c . Alternatively, a range of ages from different titanite populations in a single sample may be related to complex, fluid-assisted reactions and recrystallization events (Corfu and Stone 1998). In samples where metamorphic PT-data and titanite U-Pb data have been combined, the ages are understood to represent either growth ages (e.g. Scott and St. Onge 1995; Resor et al. 1996) or cooling ages after high-T growth (e.g. Mezger et al. 1991; Mezger et al. 1993) with the latter being the more commonly accepted interpretation. Hawkins and Bowring (1999) showed a clear relationship between the diameter of titanite and its age (larger diameter giving older ages). This strongly supports the view that following most high-T (>700 °C) metamorphic events titanite will likely record cooling ages. Titanite can be stable during metamorphism from ca. 500-900 °C (Spear 1993) and thus, may grow below its T_c . Consequently, the interpretation of titanite U-Pb ages has to be considered in light of both PT-determinations, comparative ages and the calculated T_c . Rutile occurs as a high-P phase in many assemblages and U-Pb rutile ages are usually defined by concordant or near concordant fractions. However, the ages are commonly much younger than other accessory phases such as monazite and titanite suggesting a much lower T_c . This is indeed the case with all rutile fractions dated in the MIZ (Table 4.2 and Figure 4.4). The most commonly quoted T_c for rutile is based on the empirical calibration of Mezger et al. (1989) suggesting a range of ca. 370-430 °C for typical (0.01-0.2 mm) grain sizes. Even though larger grain sized populations have been shown to give slightly older ages (van der Pluijm et al. 1994; Cox et al. 1998) the maximum T_c for rutile is thought to be ca. 500 °C. Therefore, rutile ages in most, if not all high-PT terranes are significant in terms of cooling history only.

4.5. Tt-paths and exhumation rates

4.5.1. Calculating closure temperatures

Closure temperatures (T_c) for monazite, titanite and rutile were calculated using the classical Dodson (1979) method where the T_c is expressed as:

$$T_c = \frac{E/R}{\ln \left[\frac{AR(T_c)^2 D_0 / a^2}{ECr} \right]}$$

E = activation energy

R = gas constant

A = geometry factor (55 for a sphere, 27 for a cylinder and 8.7 for a plane sheet)

D_0 = is the pre-exponential term (usually derived by experimental methods)

a = the diffusion radius and C_r = cooling rate.

The diffusion data from Smith and Gilletti (1997) for monazite and Cherniak (1993) for allow the application of Dodson's equation for these minerals. The ranges of T_c for rutile were partially derived from the measured diffusion rates of Ti and Fe in rutile (Freer 1980). Preliminary studies on the rates of Pb-diffusion in rutile (Smith and Gilletti 1995) show that it is ca. 30 times faster than in monazite (i.e. $D_0 \cong 30x$ that of monazite). This diffusion data used for T_c calculation is presented in **Table 4.3**. Grain sizes for each mineral population were measured using a Maurzhauser motorised stage attached to a petrographic microscope, which has a reproducibility of $<0.1 \mu\text{m}$ over 20 cm of total movement. Twenty grains of each mineral were measured and the averages and final T_c for 10C/My and 1000C/My are presented in **Table 4.4** and **Figure 4.6a-c**. One point to note is that rutile populations in the MIZ, when examined in polished section, are euhedral and show a 4:1 Z/X-axis ratio. Thus, although the geometry of rutile can be regarded as a cylinder ($A = 27$) the diffusional radius was assumed to be 0.25 times the measured grain size in these samples. The results of estimating the T_c of rutile with the above diffusion parameters must be regarded with caution. However, the calculated ranges in T_c for different grain sizes of rutile and at various cooling rates (**Figure 4.6c**) are very similar to those calculated by Mezger et al. (1989). The similarity of the two estimated ranges supports the use of this data.

4.5.2. Cooling rates in Lelukau terrane (LT-III)

The Tt-path recorded by the rocks in LT-III shows a pattern of fast initial cooling and the apparently slower rates both during and after titanite growth (Figure 4.7). High-PT metamorphism is constrained by the emplacement of syn-metamorphic dykes (1039 \pm 2 Ma, Table 4.2) and a range of less precise metamorphic zircon ages. Starting from an assumed peak age of around 1050 Ma, initial cooling and exhumation in LT-III lies in the range 80-6 °C/My (Figure 4.7). The wide range in initial cooling rate are caused by imprecise estimate of peak metamorphic ages and the very small difference between these and the monazite ages. The fact that the ages of the syn-metamorphic dykes and monazite ages overlap do suggest relatively fast cooling and/or a short duration for the high-T event recorded. However, the lower parts of the Tt-path give cooling rates from monazite to titanite ages at around 5-10 °C/My. The lowest part of the Tt-paths, from titanite to rutile ages gives rates of 1-5 °C/My.

4.5.3. Cooling rates in the Baie du Nord segment (BNS)

Samples in the south-west BNS have the best constrained "peak" metamorphic zircon age in the TT. Leucosomes in migmatitic garnet amphibolites contain populations of zircon with morphologies suggesting both solid-state and melt-generated growth. The rapid segregation of melt during anatexis has been documented in other high-T terranes (Watt et al. 1996) therefore, it is likely that the ages of the melt generated zircons represent the age of peak conditions attained (850 °C and >12 kbar). In fact, both populations give the same well constrained age of 1046 \pm 3 Ma (Table 4.2) suggesting that indeed high-PT metamorphism and melting occurred at the same time. The oldest monazite age in the MIZ also occurs in the south-west BNS (1040 \pm 2) from metapelitic rocks adjacent to the migmatitic garnet amphibolite. If the age reflects cooling through the T_c for the grain size of 227 μ m then clearly cooling was rapid (>50 °C/My) and the duration of high-T metamorphism was short. The next part of the Tt-path is constrained by the differences in age between monazite and large grain sizes of titanite. Titanite displays textural evidence of growth during amphibolite-granulite facies retrogression in the migmatitic garnet amphibolite (Cox and Indares 1999a, in press) although well above it's T_c (Figure 4.6b). The cooling rates indicated is about

5 °C/My (Figure 4.8) and, similar to slice LT-III, are apparently slower than for the initial stages. The rates defined using the ages of small grain sizes of titanite in the same sample are anywhere between 5 and 30 °C/My and may actually suggest faster cooling. However, this could be due to the small age difference between the titanite populations (1-10 Ma, Table 4.2). The age differences between titanite and rutile populations define the lowest-T part of the Tt-path with cooling rates of between 1 and 10 °C/My. In summary, the south-west BNS shows a progressive slowing in cooling from ca. >50 °C/My to 10-5 °C/My with the most abrupt change occurring between first stages of exhumation and high-T and cooling following retrogression.

The timing of high-T metamorphism is also constrained by monazite (1033±1 Ma) and saccharoidal zircon (1030±7/-12 Ma) in coronitic metagabbro which lie across the North Bay shear zone. Unfortunately, cooling rate is not easy to constrain using these ages. The latter age is hard to quantify in terms of growth temperature but complete replacement of baddeleyite by zircon requires metamorphic conditions above amphibolite facies and is greatly assisted by the presence of fluid (van Breeman and Davidson 1988; Heaman and LeCheminant 1993). Thus, saccharoidal zircon may be considered as recording the maximum (growth) age for reequilibration during early stage cooling in this area. This in turn supports the interpretation that the monazite data represents cooling and that the duration of high-T metamorphism was probably fairly short, on the order of a few to ten million years.

In the central BNS, the initial cooling and exhumation rates are not well quantified because of the lack of precise zircon data constraining peak metamorphism. The difference in age between monazite and titanite in the central BNS give rates of between 5 and 10 °C/My for cooling after the thermal peak (Figure 4.8), rather similar to the rates in the south-west BNS and LT-III. The Tt-path from titanite to rutile gives a rate of between 1-5 °C/My. Again, this apparent slowing of cooling is similar to the south-west BNS and LT-III. However, metamorphic zircons which give ages younger than those of monazite in the central BNS (zircon, 1012±/-12 Ma; monazite, 1033±/-2 Ma, Table 4.2) warrant further discussion. Textures and PT-conditions recorded in the transitional metagabbros (Table 4.1) suggest pervasive reequilibration. A recent study (Fraser et al. 1997) suggests that the distribution of zirconium in high-grade rocks may be controlled by garnet breakdown. If this were the case in the

transitional metagabbros these zircons may have grown during reequilibration. The age of these zircons also corresponds with a stage of slower cooling and exhumation in the BNS. The reequilibration of these samples, slow cooling and exhumation and new zircon growth may have tectonic significance. In addition, metamorphic ages recorded by zircon from the North Bay anorthosite have an extremely large spread (>100 My). This may be regarded as rather unusual for zircon that was only ca. 130 My old (Indares et al. 1998) when metamorphosed. On the other hand, the sheared nature of the North Bay anorthosite may have promoted regrowth and/or recrystallization of the zircons present. However, the fact that this appears to have occurred over much of the duration of metamorphism in the area may also be significant.

4.5.4. Cooling rates in the Boundary zone (BZ)

The timing of peak conditions in the southern BZ are constrained by the emplacement age of the Harte Jaune granite (1017 \pm 2 Ma, Table 4.2) interpreted to represent the timing of peak metamorphism in the southern BZ. The first stage of cooling and exhumation is constrained by the difference in ages between the emplacement of the granite (zircon) and cooling down to the T_c of monazite (Figure 4.9). This suggests a very fast rate of 50-100 $^{\circ}$ C/My. Subsequent rates are given by the difference from monazite to large grain sizes of titanite (5-10 $^{\circ}$ C/My). The rates recorded in the lower part of the Tt-path down to the T_c for small grain sizes of titanite and rutile (1-5 $^{\circ}$ C/My) and are similar to those in the BNS and LT-III. In the northern BZ the age of metamorphism is constrained by monazite in metapelite/anatexite at 1019 \pm 1 Ma. However, there is no independent estimate of the cooling rate following peak metamorphism except that the average rate from monazite to rutile in this sample is about 5 $^{\circ}$ C/My, similar to the MIZ as a whole.

Precise metamorphic zircon and monazite ages which constrain the timing of early stage, high-T cooling are not available for the LES. However, saccharoidal zircon ages (1030 \pm 12 Ma) do give a lower limit for high-T metamorphism. The rate of cooling from saccharoidal zircon to titanite ages (cooling after amphibolite facies overprinting) is about 10 $^{\circ}$ C/My. Subsequent cooling down to rutile ages are apparently slower 1-5 $^{\circ}$ C/My. This

pattern of slower rates during the latter stages of the PT-evolution is the same in the LES as throughout the MIZ. Interestingly, igneous zircons with metamorphic overgrowths in the nelsonite sample from the northern part of the LES, give a large spread in ages (50 My). This rock has been extensively retrogressed and indeed gives the lowest PT-estimates in the entire MIZ (695-550 °C at 6-4 kbar, **Figure 4.4**). In addition, the LES is essentially a series of variably deformed tectonic lenses (Cox et al. 1998). Therefore, it is possible that more than one episode of metamorphic zircon growth occurred in this sample giving the spread in ages across the high-T part of the metamorphic history of the area.

4.6. Discussion

4.6.1. Models for the tectonic evolution of the MIZ

Peak metamorphism (ca. 800-920 °C and up to 20 kbar) affected the majority of the units in the MIZ between 1050-1040 Ma (**Figure 4.5**). Despite the large possible range in cooling rates during the early stages of the Tt-paths, minimum rates of >50 °C/My are consistent with a high closure temperature for monazite. The small age differences between zircon (peak) and monazite (high-T cooling) ages support this interpretation that initial cooling was relatively fast across the MIZ. This in turn suggests a process of tectonic exhumation as indicated by similar rates in modern high-P terranes (Duchêne et al. 1997). Initial exhumation of the MIZ was likely driven by north-west directed extrusion (**Figure 4.10**). The high overall T-range recorded during decompressive reequilibration of the assemblages further suggests that high heat flow was prevalent during exhumation (**Figure 4.10**). The hypothesis that mantle heat input due to asthenospheric upwelling occurred in the MIZ (Indares et al., in press) is supported by the presence of the syn-metamorphic gabbro swarm in slice LT-II. If tectonic exhumation rapidly removed the MIZ from this heat source the cooling would explain the apparently rapid cooling rates following peak metamorphism.

Following the early stages of exhumation, cooling rates clearly slowed down (between ca. 1030-1000 Ma) as indicated by the relatively large age differences between monazite and titanite. The general rates of cooling during this time period are virtually identical across the MIZ (ca. 5-10 °C/My). Although these are slower than the initial rates these values are still indicative of tectonic exhumation (e.g. Duschêne et al. 1997; Jamieson et al. 1998). The rates recorded by the southern BZ however are considerably faster and indeed are similar to the rates recorded during early-stage exhumation in the rest of the MIZ with an average of 50-100 °C/My. This strongly suggests that the southern BZ was tectonically emplaced (thrust) over the rest of the MIZ at this time (Figure 4.10). The underlying LES was also probably emplaced over the BNS during this thrusting event as indicated by structural constraints (Indares et al., in press). Unfortunately, the rates of cooling and exhumation are not as well constrained in the LES due to the lack of monazite data. Thus, this interpretation is somewhat speculative. Evidence for textural reequilibration and the age of metamorphic zircons (1012±12 Ma) in the transitional metagabbros from the central BNS lend support for this interpretation. The high-T conditions and in some cases strong deformation experienced (e.g. North Bay anorthosite) during this thrusting event may also have led to the complex discordant zircon populations with large errors on lower intercept ages. This in turn may indicate multiple zircon growth and/or high-T Pb-loss events in the MIZ. In addition, migmatitic garnet amphibolites show evidence for two phases of garnet growth. Garnet porphyroblasts display inclusion rich cores of a migmatitic origin and inclusions-free overgrowths (Cox et al. 1998; Cox and Indares 1999a, in press). The overgrowths may have been produced when the BZ was emplaced over the rest of the MIZ. The duration of this event must have been extremely short lived as suggested by the rapid cooling rates in the southern BZ and the lack of any effect on the monazites in the underlying LT-III and BNS. These samples may be further investigated to test this hypothesis.

In comparison, the cooling and rates for the later stages of the metamorphic evolution are much slower (ca. 1-5 °C/Ma) and occurred until ca. 935-920 Ma. These rates are similar to those recorded in terranes where exhumation was controlled by tectonically assisted erosion and/or gravitational collapse (e.g. Jamieson 1991; Duschêne et al. 1997; Jamieson et al. 1998, Figure 4.10). Small variations such as the slightly younger rutile

(cooling) ages in LT-III (ca. 920 Ma) and older ages in the south-west BNS (ca. 946 Ma) are probably due to the different crustal levels of these units. As all the units are now at the same structural level, exhumation must have been differential and continued until after the cooling ages indicated by rutile. The later stages of exhumation may be investigated by examining ages of minerals generated in the shear zones themselves, precise dating of late, cross-cutting pegmatite and by dating phases which record lower-T cooling ages e.g. Ar-Ar geochronology of hornblende, mica and K-feldspar.

An estimate of the exhumation rate is possible only in the south-west BNS where peak-P conditions recorded by migmatitic garnet amphibolite and metapelite are in the range 14-18 kbars and retrograde overprinting recorded pressures of 8-10 kbar. Assuming an average crustal density of 2.8 gm/cm³ this represent a change in depth of between 40-50 km and 22-28 km. This occurred between peak metamorphism at 1046 \pm 3 Ma and the emplacement of the BZ after 1020 Ma. This gives an exhumation rate of between 0.41 and 1.22 mm/yr which are indicative of tectonic exhumation (Dushêne et al. 1997).

4.6.2. Comparisons with other Grenvillian terranes

Although there are a large number of published ages in the Grenville Province (see Easton 1986 and Rivers 1997), Tt-paths have only been established in the Adirondacks (New York) and along north-west transects in Ontario and western Quebec. In the Adirondacks, two major units have been identified, the lowlands which lie to the north-west and the highlands which occupy most of the Adirondack region (McLelland and Isachsen 1986). Geochronology and Tt-paths show that the lowlands achieved peak metamorphism (ca. 600-700 °C and 7 kbar) at ca. 1150 Ma and cooled down to 300 °C by 950 Ma (Bohlen et al. 1985; Mezger et al. 1989). The highlands were metamorphosed at >800 °C and up to 11 kbar at ca. 1050 and cooled down to 300 °C between 850-800 Ma (Anovitz and Essene 1990; van der Pluijm et al. 1994). A similar pattern of ages is observed in the Grenville in Ontario (e.g. van Breemen et al. 1986; Culshaw et al. 1991; Mezger et al. 1993; Wodika et al. 1996; Ketchum et al. 1998; Cosca et al. 1991 and 1992). Several terranes which can be regarded as part of the allochthonous belt

record older peak metamorphic ages, whereas ages in the parautochthonous belt are more typical of those in the MIZ. Moreover, high-P rocks recently discovered in the south-west Grenville give peak ages (metamorphic zircon) of ca. 1090-1050 Ma (Indares and Dunning 1997; Ketchum and Krogh 1998). Modelled Tt-paths for the south-west Grenville show rather slow average cooling rates (e.g. van der Pluijm et al 1994) however, it is apparent that this interpretation is complicated by the presence of both old and young metamorphic ages. In the Grenville of western Quebec an age transect also records the same pattern where the southern (allochthonous) terranes record peak metamorphism at ca. 1150 and older cooling ages (ca. 1050-950 Ma). The northern (parautochthonous) terranes give metamorphic ages 1050-950 and cooling ages down to 800 Ma (Friedman and Martignole 1995; Martignole and Reynolds 1997). These older metamorphic ages are thought to represent a phase of metamorphism which in general reached mid-amphibolite to granulite facies (Davidson et al. 1982; Bohlen et al. 1985; Rivers et al. 1989). The term Shawinigan Pulse has been proposed for this event (Rivers 1997). Peak metamorphic ages between 1100-1000 Ma (termed Ottawa Pulse) are found throughout the Grenville and represent the main orogenic event which includes high-P metamorphism. Despite the complication of separate pulses of metamorphism in New York, Ontario and western Quebec, the pattern of cooling ages younging to the south-west is consistent with data throughout the Grenville (Easton 1986; Rivers 1997). This in turn supports current models of initial exhumation with thrusting to the north-west and extension on top of the pile to the south-east.

Evidence of more than one pulse of metamorphism is also present in the eastern Grenville. Most peak metamorphic ages are between 1100-1030 Ma (e.g. Phillippe et al 1993; Tucker and Gower 1994; Wasteneys et al. 1996). These ages are associated with the pervasive high-grade metamorphism. However, zircon and monazite ages from 1020-950 Ma are also present along with pegmatites which have been deformed by late shear zone movement (Schärer et al. 1986; Bussy et al. 1995). This indicates a later phase of metamorphism which has been termed the Rigolet Pulse (Rivers 1997). The timing of the Rigolet Pulse is broadly coeval with both the tectonic emplacement of the BZ in the MIZ and the high-T/low-P metamorphism of the Harte Jaune terrane immediately

to the south of the MIZ (Hynes et al. 1997). Thus, the Rigolet Pulse may be responsible for the emplacement of the BZ in the MIZ which corresponds to the apparent slowing of the cooling and exhumation rates.

4.7. Conclusions

In the north-east Grenville Province, the MIZ records evidence of high-PT metamorphism and initial near ITD-paths with steep metamorphic gradients. The initial rates of cooling and exhumation are consistent with tectonic uplift, probably via thrusting to the north-west and extension on the top of the pile to the south-east. However, a second pulse of thrusting in the highest structural levels (BZ) appears to correspond to a phase of slow cooling and exhumation in the MIZ. The timing of this phase overlaps with the Rigolet Pulse recorded in the eastern Grenville. Subsequent cooling and exhumation as indicated by the ages of rutile in the MIZ was relatively slow and clearly continued for some time until at least 925 Ma (i.e. the youngest rutile ages). Thus, two stages of burial and exhumation are recorded by the MIZ namely the high-P Ottawa Pulse and a less pervasive event which is likely related to the Rigolet Pulse. The exhumation history of the MIZ is therefore controlled by two stages of thrusting and extension. The average cooling and exhumation rates are apparently rather slow compared with modern high-P belts and a similar pattern is documented across the Grenville. As both the western Grenville (Shawinigan and Ottawa) and eastern Grenville (Ottawa and Rigolet) apparently record two pulses of crustal shortening and metamorphism, these slow rates of cooling are the net result of a complex tectonic evolution. The rates of cooling and exhumation will therefore be best constrained in terranes where the individual pulses can be distinguished.

Figure 4.1. Map of the eastern Grenville Province showing the location of the Manicouagan Imbricate Zone and surrounding terranes.

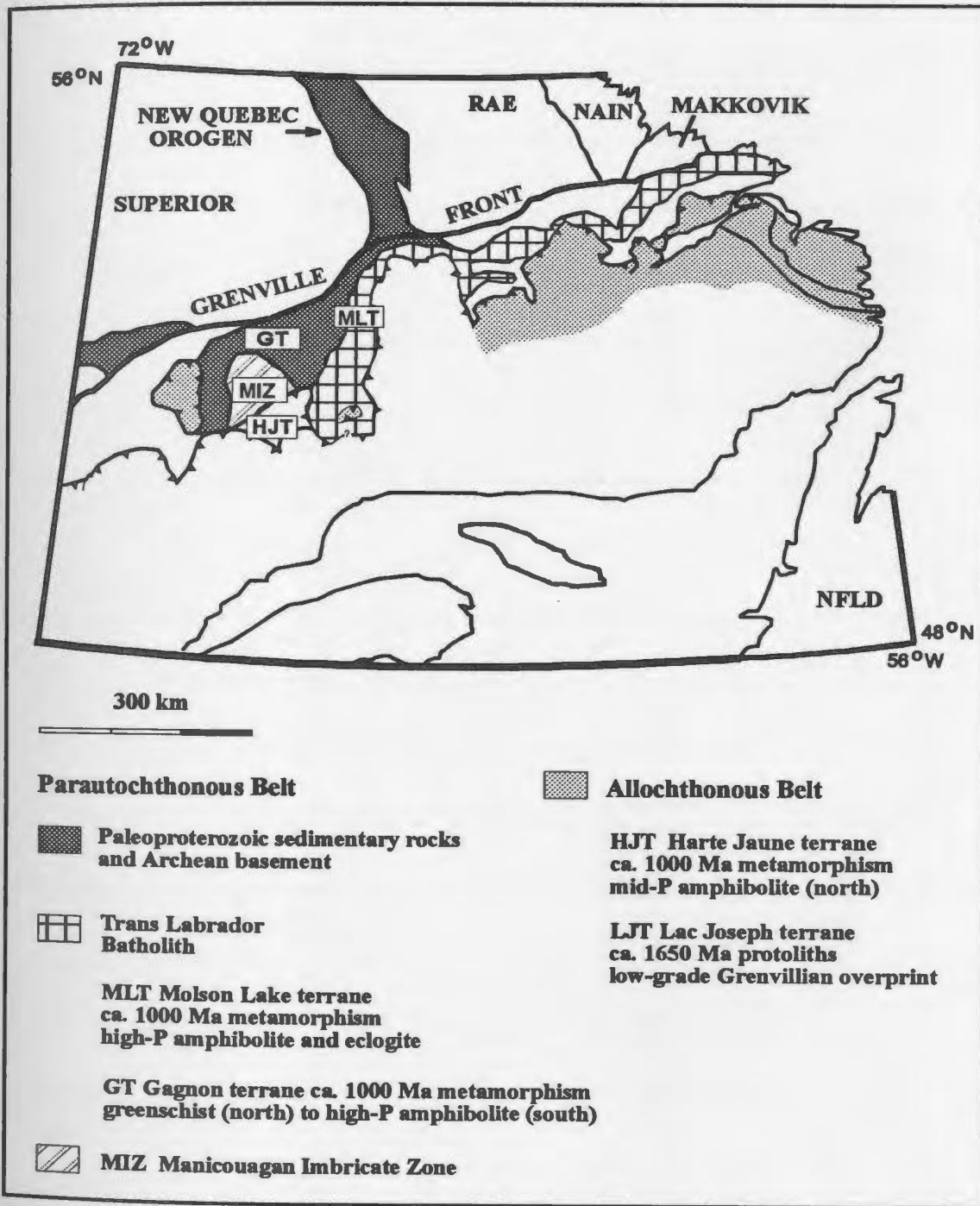


Figure 4.2. Simplified geological map of the MIZ with the locations of Figures 4.3a-b shown.

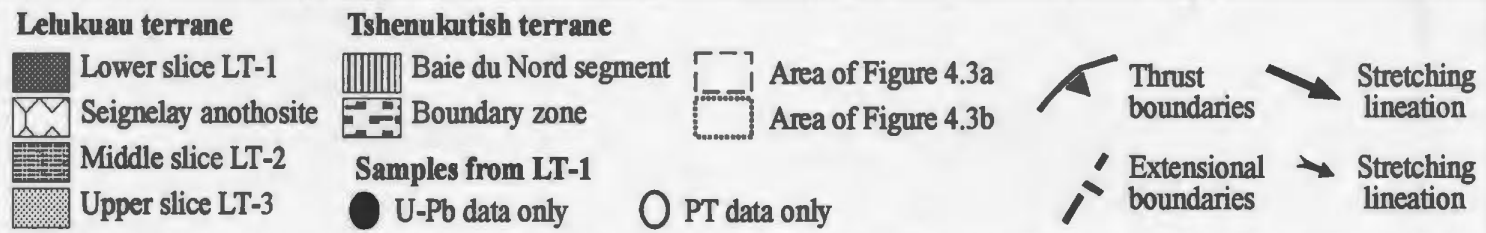
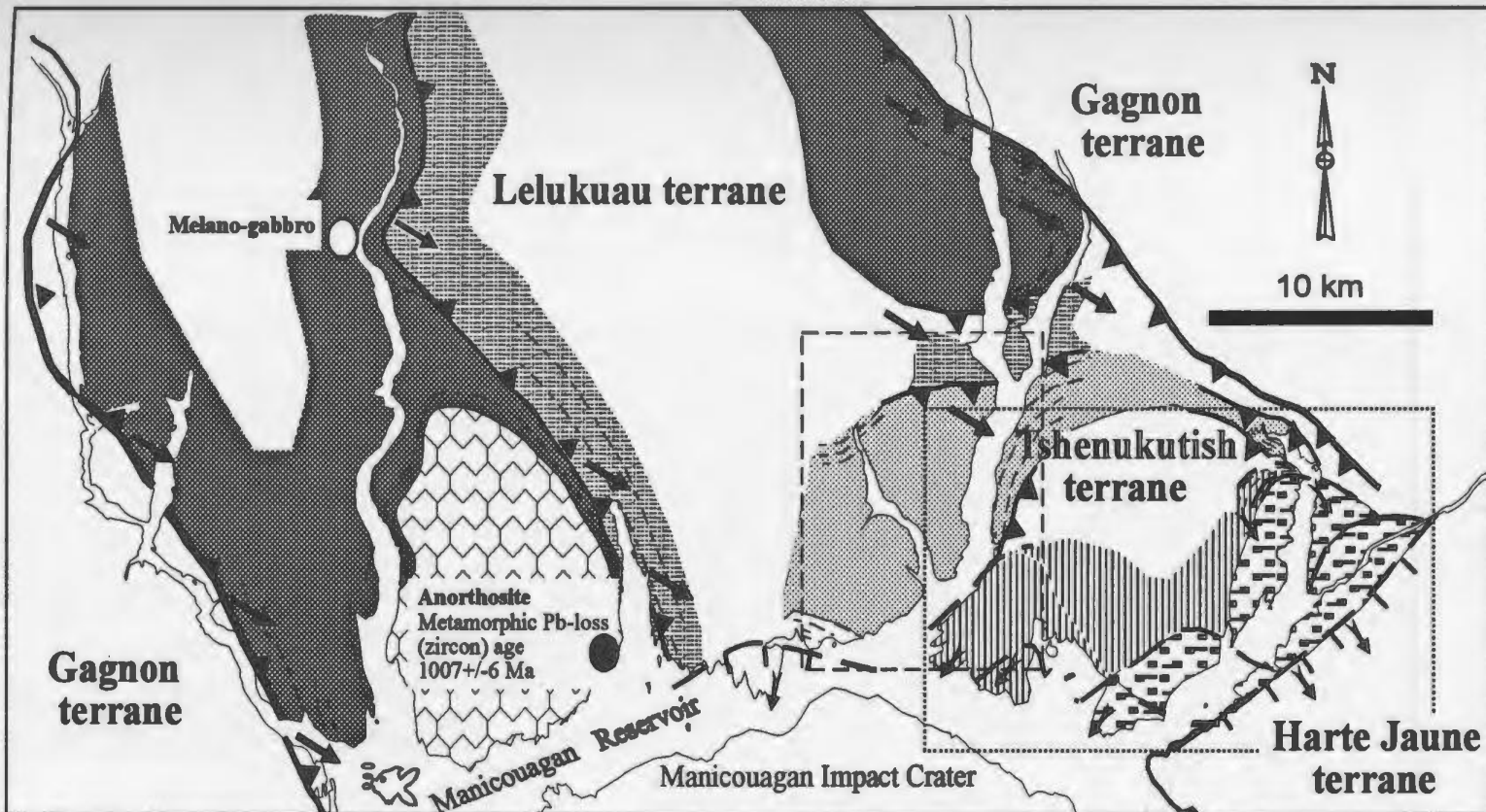


Figure 4.3. Map of slice LT-III (south east LT) and TT with localities of samples used for PT-determinations (data in Table 4.1) and U-Pb ages (Table 4.2).

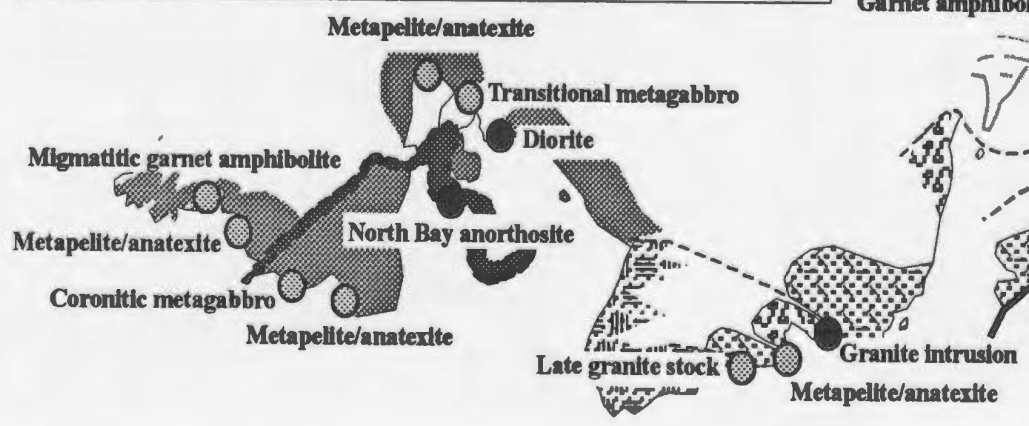
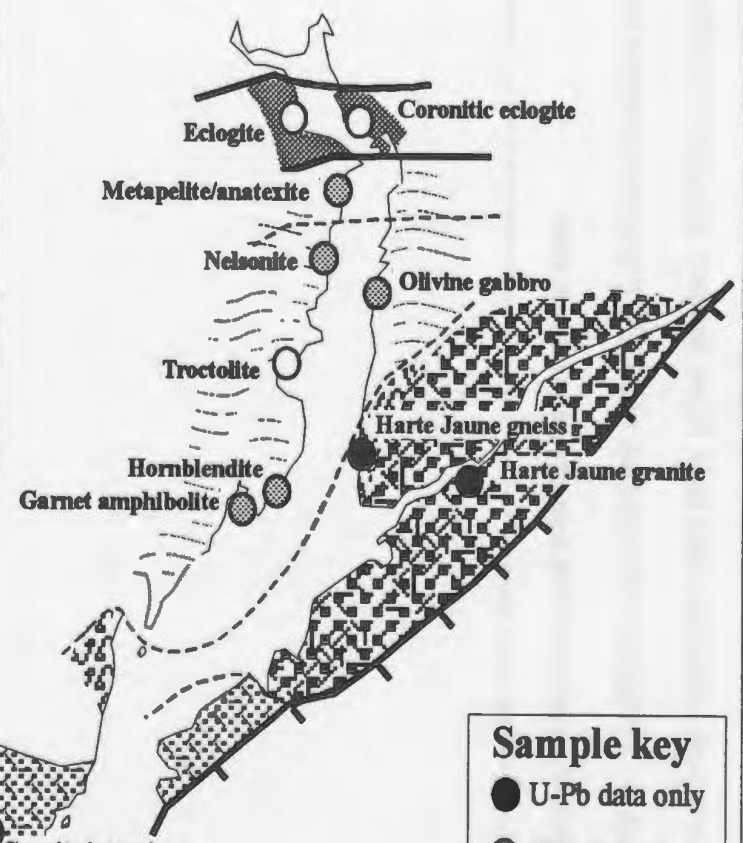
Lelukuau terrane (LT-III)

a)



Tshenukutish terrane

b)



Sample key

- U-Pb data only
- PT-data only
- ◐ Both U-Pb and PT-data

Figure 4.4. Diagram showing a) temperatures and b) pressures recorded by rocks across the MIZ. Dark boxes indicate peak conditions and light boxes indicate retrograde conditions. Note that some rocks contain no PT-data but are included where U-Pb data was collected from the sample. This allows a direct comparison of the data coverage in each area

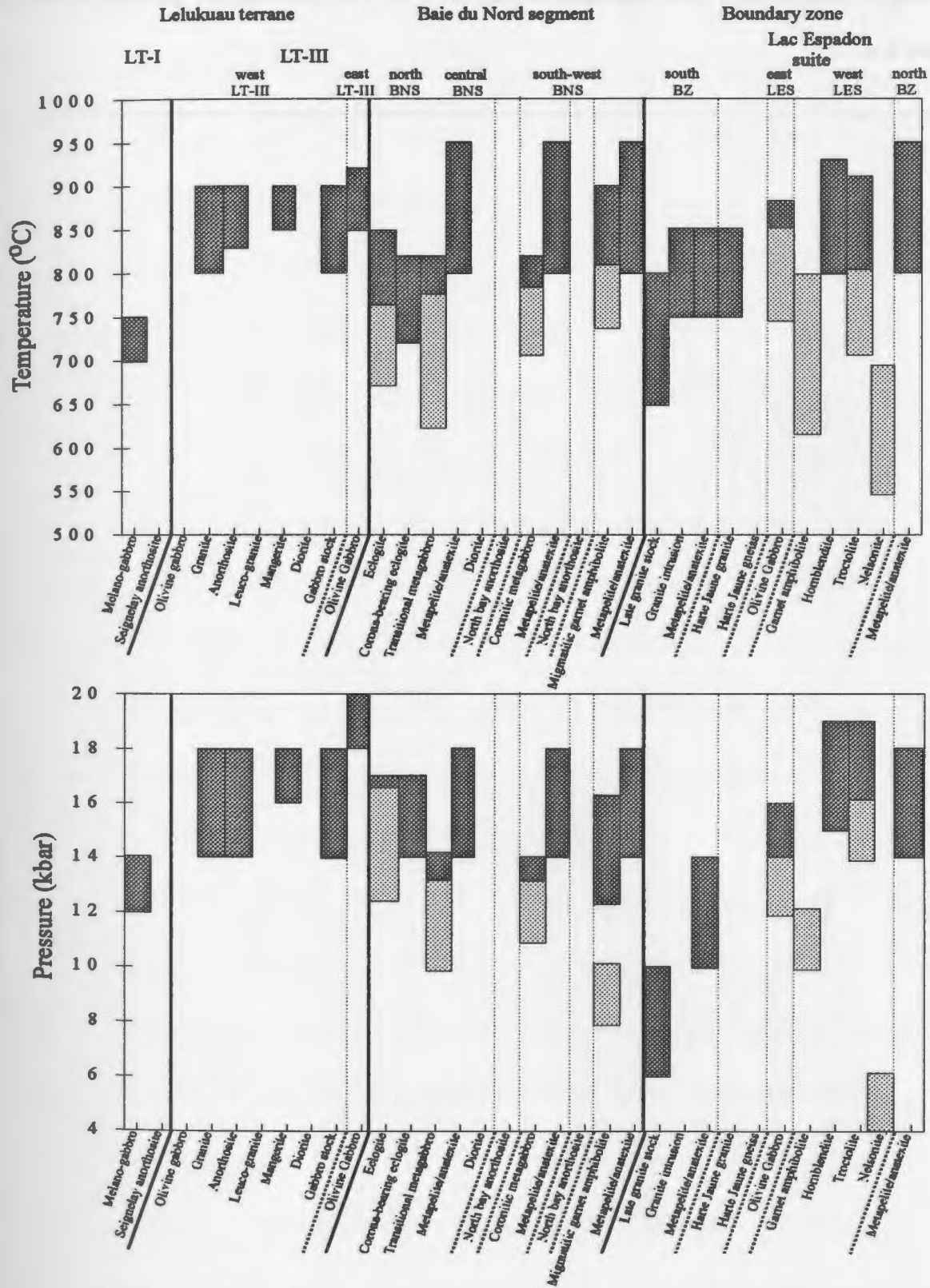


Figure 4.5. Diagram showing the U-Pb ages from across the MIZ. The locations are identical to those in Figure 4.4.

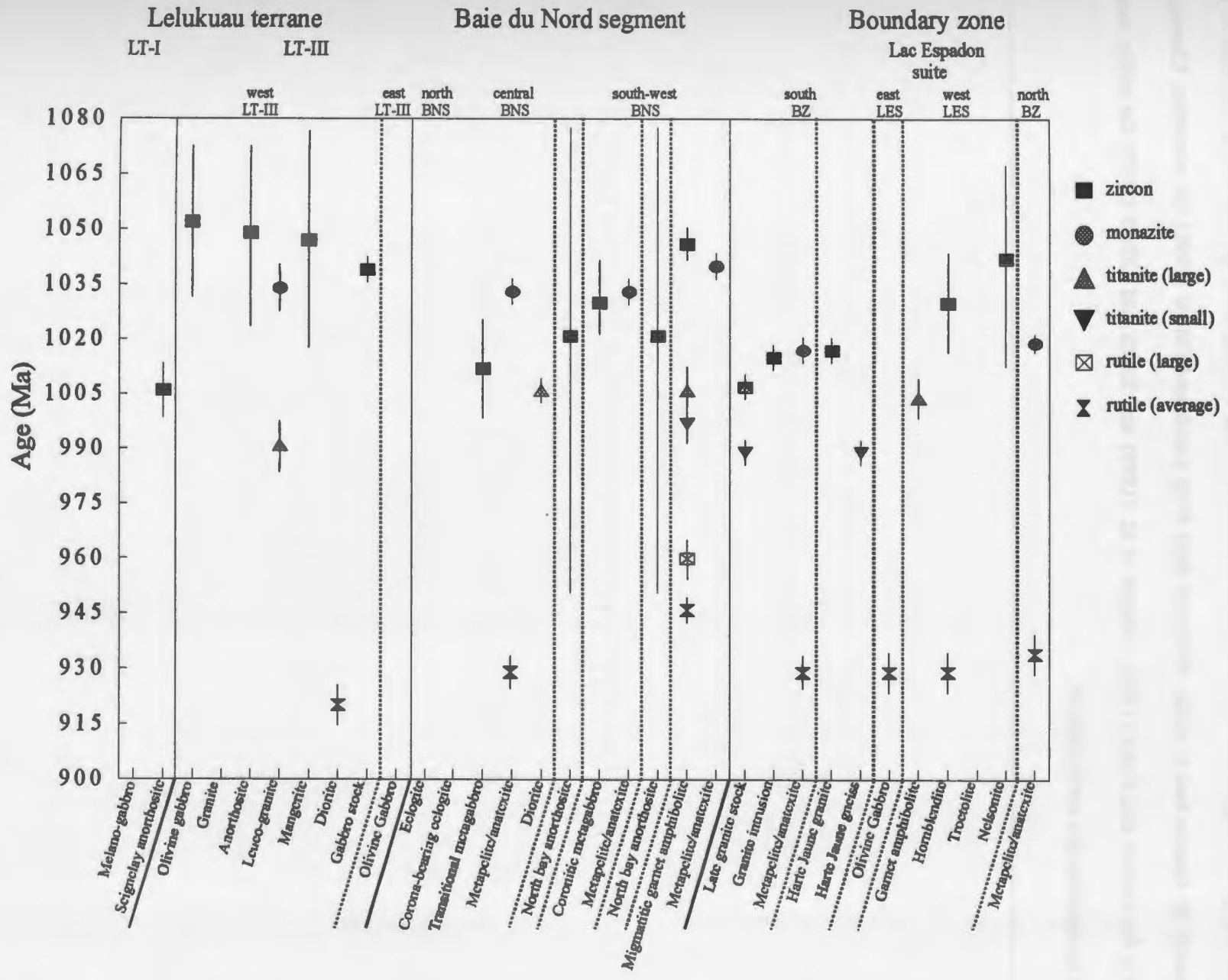


Figure 4.6 (a-c). Graphs showing closure temperature versus cooling rates for different grain sizes of a) monazite, b) titanite and c) rutile. Diffusion data from Smith and Giletti (1996) for monazite, Cherniak (1993) for titanite and Freer (1980), Mezger et al. (1989) and Smith and Giletti (1995) for rutile, were used to calculate the curves shown.

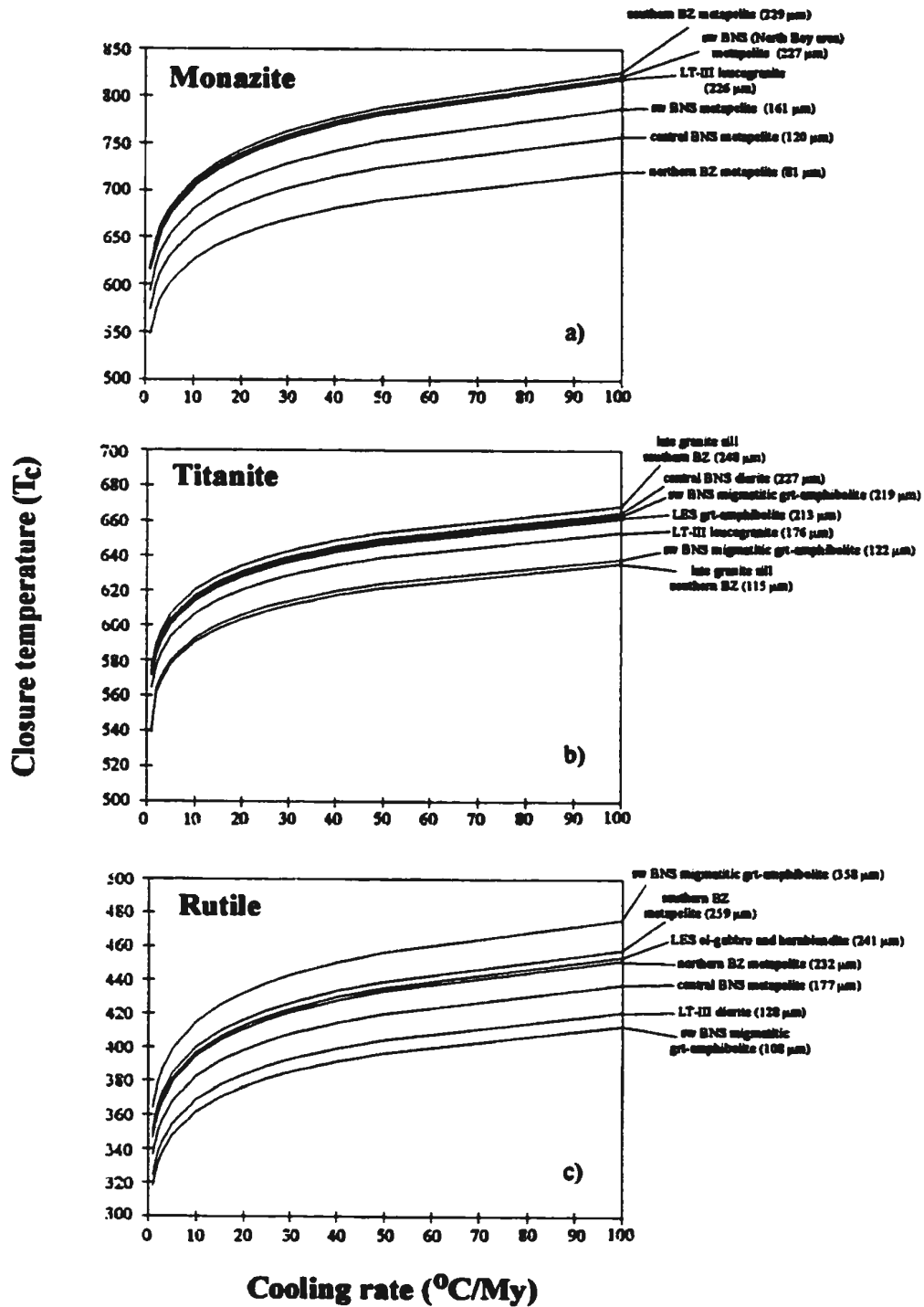


Figure 4.7. Tt-path for slice LT-III. The top of each box represents the maximum and minimum growth temperature for zircon and the calculated T_c at 1 °C/My and 100 °C/My for monazite, titanite and rutile. The broken lines around the zircon data represent fractions which have poorly constrained lower intercepts, the significance of which is discussed in the text.

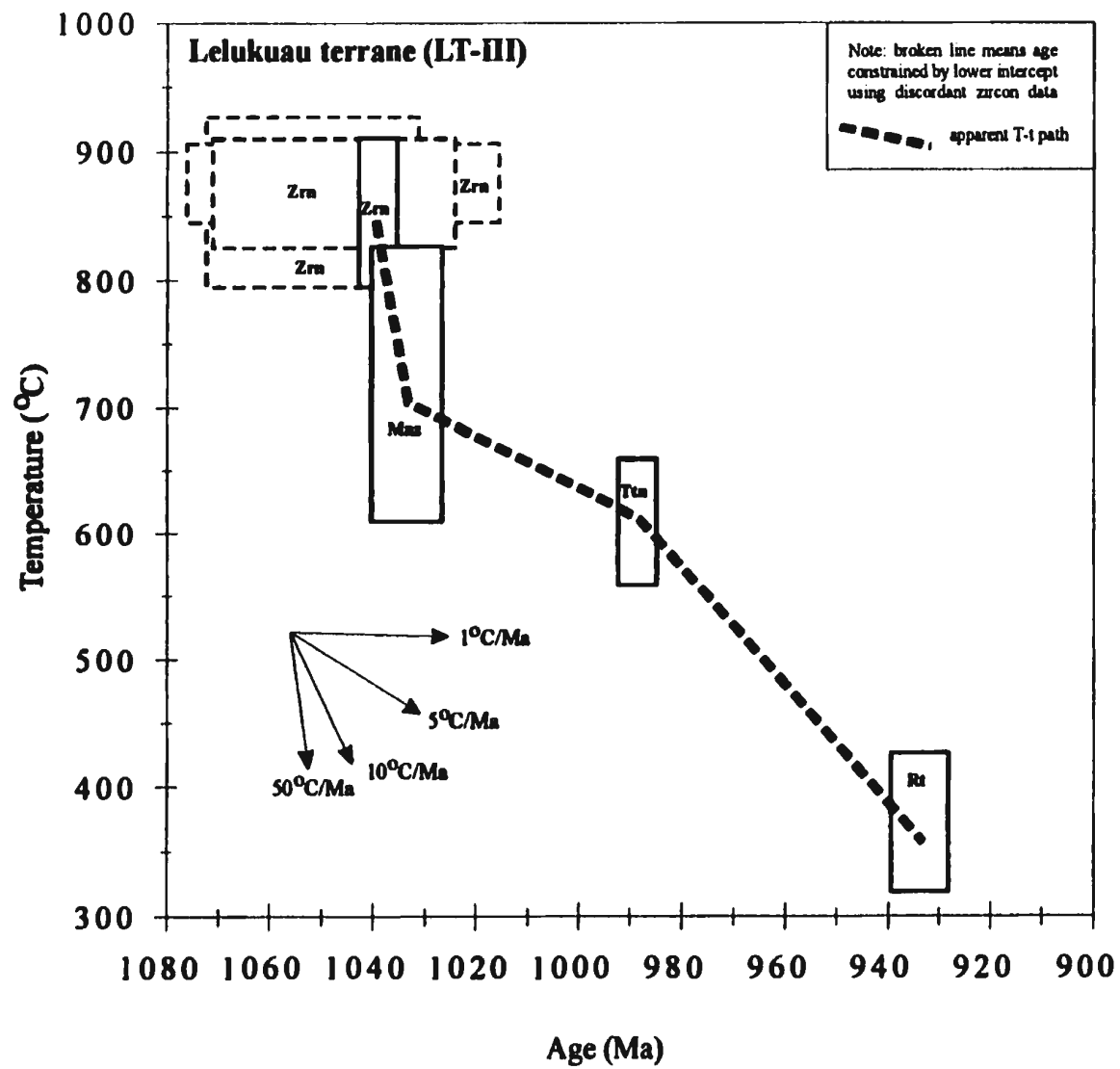


Figure 4.8. Tt-path for the central and south-west BNS. The top of each box represents the maximum and minimum growth temperature for zircon and the calculated T_c at 1 °C/My and 100 °C/My for monazite, titanite and rutile. The broken lines around the zircon data represent fractions which have poorly constrained lower intercepts, the significance of which is discussed in the text.

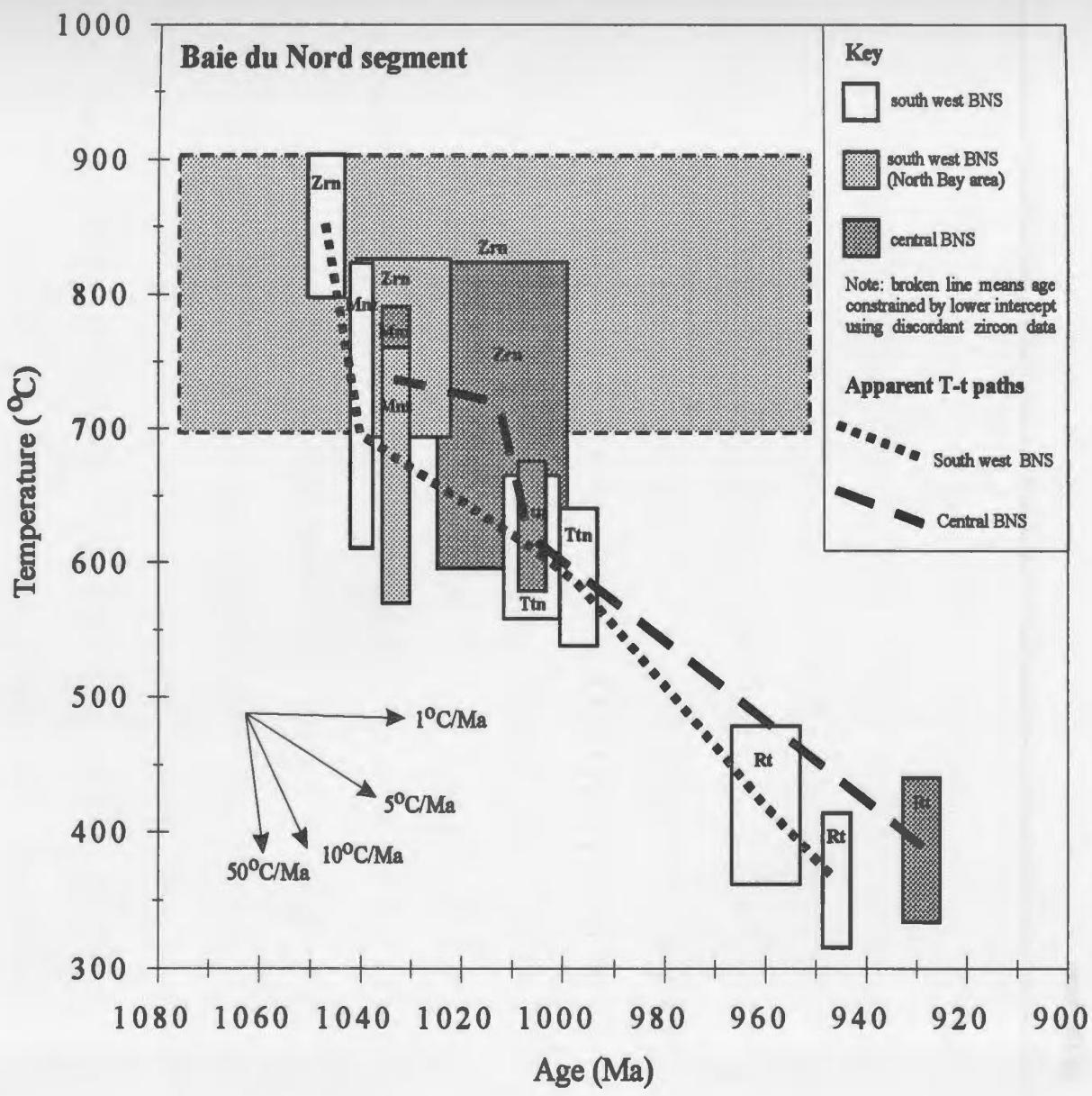


Figure 4.9. Tt-path for the northern and southern BZ and the LES. The top of each box represents the maximum and minimum growth temperature for zircon and the calculated T_c at 1 °C/My and 100 °C/My for monazite, titanite and rutile. The broken lines around the zircon data represent fractions which have poorly constrained lower intercepts, the significance of which is discussed in the text.

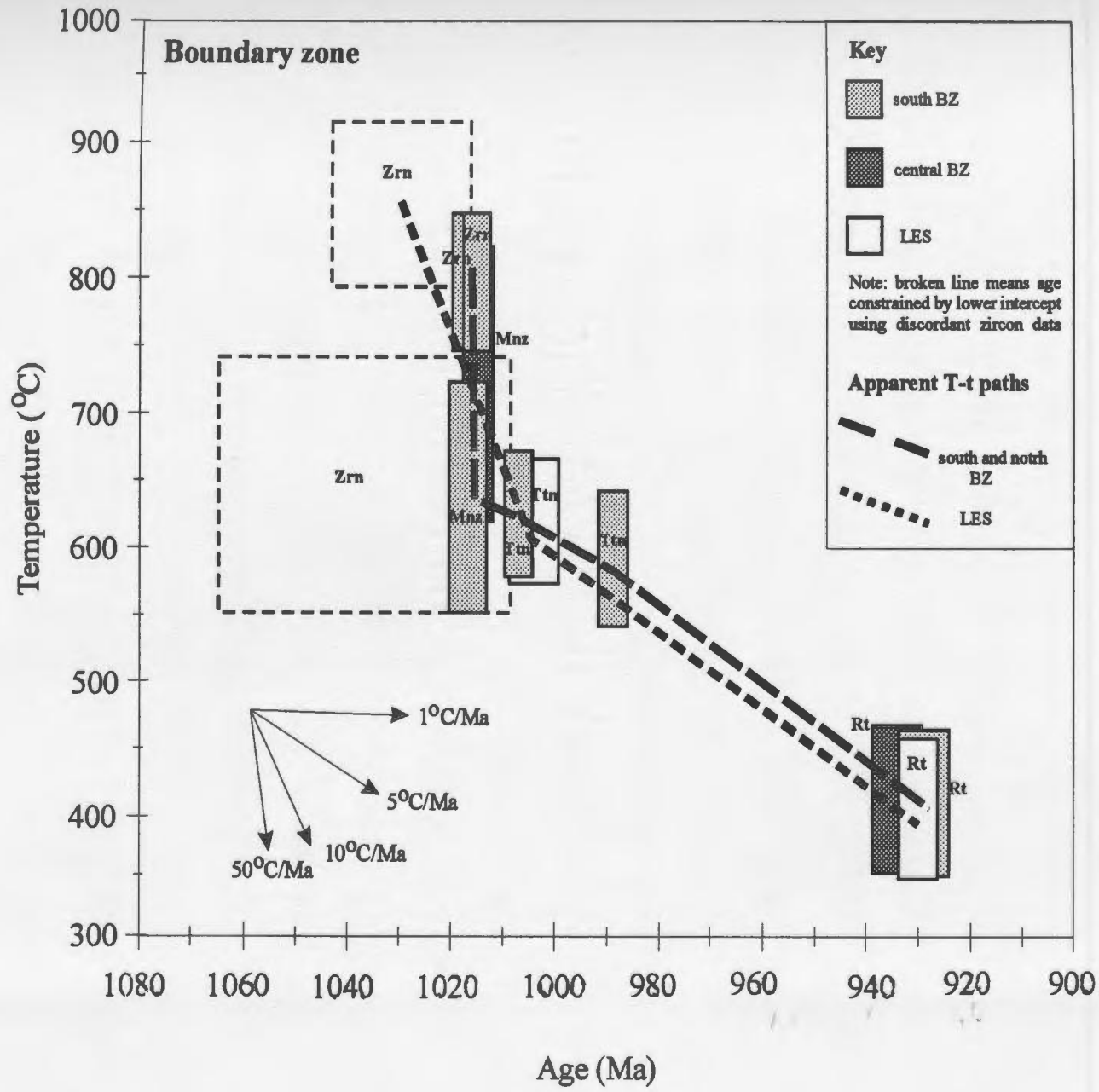


Figure 4.10. Summary of the metamorphism and tectonic exhumation of the MIZ. Dark colored boxes represent high-T conditions constrained by zircon and monazite ages. Light grey and white boxes represent titanite and rutile cooling ages respectively.

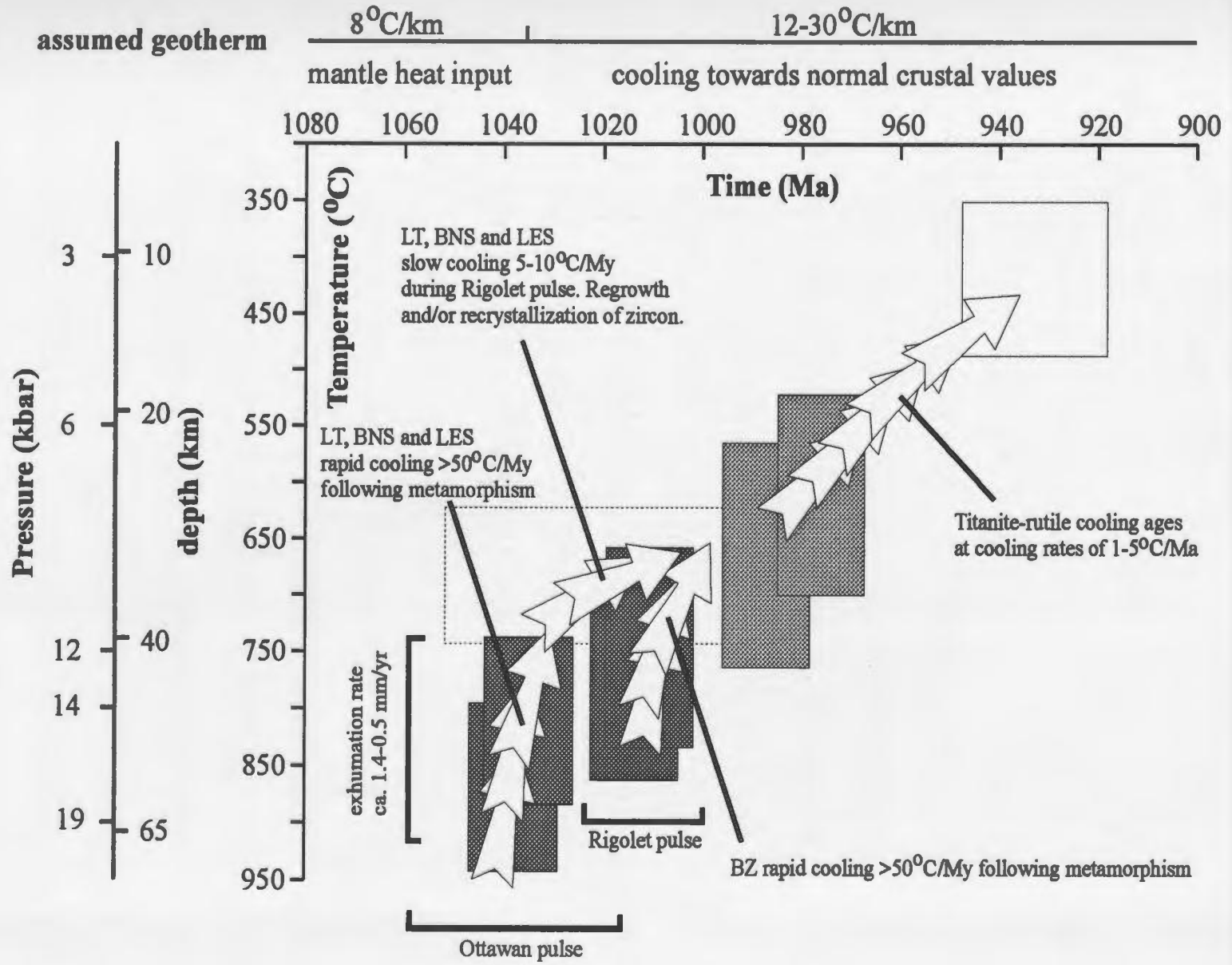


Table 4.1. Summary of PT-data from the MIZ. References are given in the text.

Sample and location	PT-conditions	Interpretation and comments
Lelukusa terrane		
LT-I		
Melano-gabbro	700-750 °C at 12-14 kbar	Recorded conditions of metamorphism in mafic samples and lack of granitoid melting
East LT-III		
Grt-Ky clinopyroxenite	850-920 °C at 18-20 kbar	Near-peak conditions recorded by assemblages
West LT-III		
Grt-Ky clinopyroxenite	850-900 °C at 16-18 kbar	Near-peak conditions recorded by assemblages
Grt-Ky clinopyroxenite	850-920 °C at 18-20 kbar	Near-peak conditions recorded by assemblages
Granitic gneiss	>800 °C and >14 kbar	Partial melting of granitoid
Gabbro stocks	>800 °C and >14 kbar	Syn-metamorphic emplacement of plagioclase-free assemblages
Tshenukutish terrane		
Northern BNS		
Granoblastic eclogite	740-825 °C at 13-17 kbar	Near-peak assemblage
	675-760 °C at 13-16 kbar	Reequilibration of granoblastic eclogite assemblages (rims)
Coronitic eclogite	720-800 °C at 14-17 kbar	Near-peak coronitic assemblage
Central BNS		
Transitional metagabbro	750-820 °C at 11-14 kbar	Peak conditions recorded by granoblastic assemblages (cores)
	655-800 °C at 10-13 kbar	Reequilibration of granoblastic assemblages (rims)
	740-820 °C at 11-13 kbar	Maximum conditions recorded by high-P coronas
Metapelite	800-950 °C at >14 kbar	Minimum conditions for melting of muscovite and maximum stability for biotite during melting of metapelite (muscovite absent)
South-west BNS (North Bay area)		
Metapelite	800-950 °C and >14 kbars	Minimum conditions for melting of muscovite and maximum stability for biotite during melting of metapelite (muscovite absent)
Coronitic metagabbro	770-810 °C at 12-14 kbar	Maximum conditions recorded by high-P coronas
	710-780 °C at 11-13 kbar	Reequilibration of coronas (pargasite-plagioclase collars)
South-west BNS		
Migmatitic garnet amphibolite	>850 °C and >10 kbar	Conditions for amphibolite partial melting and garnet growth in leucosome
	795-825 °C at 11-12 kbar	Conditions recorded by garnet-leucosome assemblage
	740-805 °C at 8-10 kbar	Post-migmatite garnet rims overgrowth and amphibolite matrix
Metapelite	800-950 °C and >14 kbar	Minimum conditions for melting of muscovite and maximum stability for biotite during melting of metapelite (muscovite absent)

Table 4.1 (continued).

Sample and location	PT-conditions	Interpretation and comments
Southern BZ		
Harte Jaune Granite	750-850 °C	Crystallization of intrusion (post -peak emplacement)
Granite sheet	750-850 °C	Crystallization of intrusion (post -peak emplacement)
Late granite sheet	>650 °C and >6 kbar	Syn-amphibolite facies emplacement
Metapelite	>750 °C and 10 kbar	Minimum conditions for melting of muscovite (muscovite present)
West LES		
Troctolite	780-870 °C at 16-19 kbar	Near-peak (amphibole-free) coronitic assemblages
	780-880 °C at 14-17 kbar	Conditions recorded by cpx-inclusions and garnet in pargasite-bearing corona assemblage
	710-800 °C at 14-16 kbar	Retrograde conditions recorded by pargasite-bearing coronas (rims)
Hornblende	800-930 °C at 15-19 kbar	Near-peak coronitic assemblages
Garnet amphibolite	620-795 °C at 10-12 kbar	Amphibolite retrogression
Nelsonite	550-690 °C at 4-6 kbar	Reequilibration of coronitic assemblages during amphibolite retrogression
East LES		
Olivine gabbro	775-870 °C at 14-16 kbar	Conditions recorded by high-P coronas
	750-850 °C at 12-14 kbar	Reequilibration of granuloblastic assemblages
Northern BZ		
Metapelite	>800-950 °C and >14 kbar	Minimum conditions for melting of muscovite and maximum stability for biotite during melting of metapelite (muscovite absent)

Table 4.2. Summary of U-Pb age determinations from the MIZ. References are ¹Cox et al. (1998), ²Indares et al. (1998), ³Indares and Dunning (in press) and ⁴Gale et al. (1994).

Sample and location ^(reference)	Zircon ages (Ma)	Monazite ages (Ma)	Titanite ages (Ma)	Rutile ages (Ma)
Lefkousa terrane				
LT-I				
Seignelay anorthosite ²	1007±1.6			
West LT-III				
Mangerite ²	1047±1.28			
Anorthosite ²	1049±1.22			
Olivine Gabbro ²	1052±1.19			
Leucogranite ²		1034±1.5	991±1.5	
Diorite gneiss ⁴				920±1.4
Gabbro stock ²	1039±1.2			
Tshenukutish terrane				
Central BNS				
Transitional metagabbro ¹	1012±1.12			
Metapelite ³		1033±1.2		929±1.3
North Bay anorthosite ²	1021±54/-69			
Diorite (country rock) ²			1006±1.2	
South-west BNS				
Migmatitic garnet-amphibolite ¹	1046±1.3		(Large) 1006±1.5 (Small) 997±1.4	(Large) 960±1.6 (Small) 946±1.2
Metapelite ³		1040±1.2		
South-west BNS (North Bay area)				
Coronitic metagabbro ¹	1030±10/-7			
Metapelite ³		1033±1.2		
Southern BZ				
Harte Jaune Granite ²	1017±1.2			
Granite sheet ²	1015±1.2			
Late granite sheet ²	1007±1.2		(Large) 1007±1.2 (Small) 989±1.2	
Metapelite ³		1015±1.2		934±1.4
Harte Jaune gneiss (country rock) ³			989±1.2	
West LES				
Hornblende ¹	1030±1.12			929±1.4
Garnet amphibolite ¹			1004±1.4	
Nelsonite ¹	1042±22/-28			
East LES				
Olivine gabbro ¹				929±1.4
Northern BZ				
Metapelite ³		1019±1.1		929±1.3

Table 4.3. Diffusion data used to calculate the respective closure temperatures in Table 4.4. Data taken from ¹ Smith and Giletti (1996), ²Cherniak (1993) and ³Freer (1980), Mezger et al. (1989) and Smith and Giletti (1994).

Mineral	Activation energy (E) kcal/mol	Pre-exponential coefficient (D ₀) cm ² /sec	Geometry factor
Monazite ¹	43021	1.1	55
Titanite ²	79496	2 x 10 ¹¹	55
Rutile ³	34898	6.6 x 10 ¹¹	27

Table 4.4. Interpretation of zircon ages along with grain sizes and closure temperatures (T_c) at cooling rates of 1 °C/My and 100 °C/My for monazite, titanite and rutile using the method described in the text.

Sample and location	Zircon interpretation	Monazite maximum diffusion diameter and Tc (1°C/Ma and 100°C/Ma)	Titanite maximum diffusion diameter and Tc (1°C/Ma and 100°C/Ma)	Rutile maximum diffusion diameter and Tc (1°C/Ma and 100°C/Ma)
Lelukuu terrane				
West LT-III				
Mangerite	High-T Pb-loss from igneous crystals (800-920 °C)			
Anorthosite	High-T Pb-loss from igneous crystals (800-920 °C)			
Olivine Gabbro	High-T Pb-loss from igneous crystals (800-920 °C)			
Leucogranite		226 μm (617 - 824)	176 μm (564 - 654)	
Diorite gneiss				128 μm (324 - 421)
Gabbro stock	Syn-metamorphic emplacement (>850 °C)			
Tshewakutish terrane				
Central BNS				
Transitional metagabbro	Post-peak (reequilibrium) metamorphic growth (600-800 °C)			
Metapelite		120 μm (573 - 758)		177 μm (336 - 437)
North Bay anorthosite	High-T Pb-loss from igneous crystals (800-900 °C)			
Diorite gneiss (country rock)			227 μm (574 - 665)	
South-west BNS				
Migmatitic garnet-amphibolite	Near-peak, melt-generated and solid-state metamorphic crystals (800-900 °C)		Large 219 μm (572 - 663) Small 122 μm (541 - 638)	Large 358 μm (363 - 476) Small 108 μm (318 - 412)
Metapelite		227 μm (616-823)		
South-west BNS (North Bay area)				
Coronitic metagabbro	Post-peak zircon pseudomorphs after baddeleyite (710-780 °C)			
Metapelite		161 μm (593-788)		

Table 4.4 (continued).

Sample and location	Zircon interpretation	Monazite maximum diffusion diameter and Tc (1°C/Ma and 100°C/Ma)	Titanite maximum diffusion diameter and Tc (1°C/Ma and 100°C/Ma)	Rutile maximum diffusion diameter and Tc (1°C/Ma and 100°C/Ma)
Southern BZ				
Harte Jaune Granite	Syn-metamorphic Harte Jaune granite emplacement (850-750 °C)			
Granite sheet				
Late granite sheet			115 µm (539 - 634)	
Metapelite	Late granite dyke (750-650 °C)	229 µm (619 - 828)		259 µm (351 - 457)
Harte Jaune gneiss			Assumed to record identical conditions to small titanites from late granite sheet	
West LES				
Hornblende	Post-peak zircon pseudomorphs after baddeleyite (780-920 °C)			241 µm (348 - 458)
Nelsonite	Near-peak metamorphic overgrowths on igneous cores (780-920 °C)			
Garnet amphibolite			213 µm (571 - 662)	
East LES				
Olivine gabbro				241 µm (348 - 458)
Northern BNS				
Metapelite		81 µm (548-721)		232 µm (346 - 451)

The Manicouagan Imbricate Zone within the context of the Grenville Province and orogenic belts.

C.1. Terrane correlation

The metamorphic and U-Pb geochronological studies of the mafic and ultramafic rocks in the Manicouagan Imbricate Zone (MIZ) examined in this thesis can be combined with available data from other rocks in the same area (e.g. Gale et al. 1994; Indares 1996; Indares et al. 1998; Indares and Dunning, in press). The lithological units in the MIZ are separated by shear zones into a number of terranes and segments (Indares et al. 1999) all of which have experienced high-PT metamorphism during the Grenvillian orogeny. The combination of both protolith ages and metamorphic characterisation of these areas allows correlations to be made both within the MIZ and with other areas in the Grenville Province.

C.1.1. Protolith ages

The Lelukauu terrane (LT), which is structurally the lowest, is characterized by large tectonic slices containing mafic and granitoid rocks which comprise a Labradorian anorthosite-mangerite-charnockite-granite (AMCG) suite (Indares et al. 1998). The slice LT-III also contains ca. 1300 Ma granite and a swarm of syn-tectonic mafic dykes (1039 \pm 2 Ma). The Tshenukutish terrane (TT) overlies the LT and is structurally more complex. The lowest tectonic unit within the TT, the Baie du Nord segment (BNS), comprises Pinwarian (1458 \pm 5 Ma) granitic-dioritic country rocks with metapelitic rafts (Indares et al. 1998). These are intruded by Fe-Ti gabbros and associated anorthosites, which are mid-Proterozoic (ca. 1220-1170 Ma) in age. The highest unit within the TT, the Boundary Zone (BZ), contains ultramafic cumulate rocks, gabbro and nelsonite, known as the Lac Espadon suite (LES), formed during Labradorian magmatic activity (Cox et al. 1998). The southern BZ is the highest tectonic unit and also contains the

youngest rocks. The southern BZ comprises the Brien anorthosite (1169 \pm 3 Ma, Scott and Hynes 1994), the syn-tectonic Harte Jaune granite (1017 \pm 2 Ma, Indares et al. 1998) metapelitic rafts and late granite sheets.

C.1.2. Labradorian units: the Lelukuau terrane (LT) and Lac Espadon suite (LES)

The terranes and litho-tectonic units within the MIZ can be correlated in a number of ways. The LT and the LES are lithologically similar (both comprise AMCG type rocks) and have contemporaneous (Labradorian) protolith ages (Cox et al. 1998; Indares et al. 1998). Thus, it is possible these units were in close association during emplacement. Geochemical analysis of olivine gabbro and REE-fractionation models suggest that the LES represents within-plate tholeiitic melts emplaced at a high crustal level (see Paper 1). Outside the MIZ, rocks of a similar age are found predominantly in the eastern Grenville and are located mainly in the parautochthonous (high-P) belt, although terranes in the allochthonous (low-P) belt and even north of the Grenville front contain rocks of a similar age (e.g. Schärer et al. 1986; Corrigan et al. 1994; Culshaw et al. 1994). These intrusions represent a major magmatic event following the Labradorian orogeny (Rivers 1997).

C.1.3. Pinwarian and other Mid-proterozoic rocks

The LT contains 1300 Ma granite intrusions and sparsely distributed calc-alkaline, alkaline and tholeiitic (AMCG) rocks in the range 1350-1250 Ma occur throughout the Grenville (Rivers 1997). The largest group of igneous rocks in this age range is the Nain Plutonic AMCG suite which is located to the north of the Grenville in central Labrador. The lithologies and interpreted tectonic setting of rocks of this age are diverse and the nature of the 1300 Ma granite within the Lelukuau terrane remains uncertain.

The BNS segment is dominated by the Pinwarian country rocks (1458 \pm 5 Ma) intruded by 1220-1170 Ma gabbro and anorthosite (Indares et al. 1998). The Harte Jaune terrane which overlies the MIZ to

the south contains granulites with protolith ages similar to the BNS (Scott and Hynes 1998). Interestingly, the Pinwarian rocks in the BNS show evidence for metamorphism prior to the emplacement of the mid-Proterozoic gabbro and anorthosite. Although the exact timing and nature of this event is as yet undefined in the BNS, it may be postulated that these two areas may have been in close association prior to the Grenvillian orogeny. Rocks of this age are also found in the western Grenville (e.g. van Breemen et al. 1986; Ketchum et al. 1994) and in the eastern Grenville including the Pinware terrane, the type locality (e.g. Krogh et al. 1996; Wasteneys et al. 1997). Pinwarian rocks in the western Grenville are thought to represent a back-arc setting whereas those in the eastern Grenville were emplaced during and shortly after the Pinwarian orogeny and may also be related to back-arc spreading (Rivers 1997).

The Fe-Ti gabbros and anorthosites in the BNS represent within-plate tholeiites which were emplaced at a high crustal level (Cox et al. 1998). The age of these rocks is identical to the Brien anorthosite in the Boundary zone. Similar lithologies in this age range are found across the Grenville and are chiefly located in the southern allochthonous terranes (e.g. Martignole et al. 1994; Wodicka et al. 1996) and are thought to represent emplacement following peak metamorphism. In this case most of these intrusions were intruded shortly after the 1250-1190 Ma Elzevirian orogeny (Moore and Thompson 1980) probably during a phase of crustal thinning.

C.1.4. Syn-metamorphic intrusions

The occurrence of syn-metamorphic mafic dykes (1039 \pm 2 Ma, Indares et al. 1998) is significant in terms of the style of metamorphism experienced by the MIZ. These rocks have within-plate tholeiite geochemical signatures and are thought to represent magmas formed during asthenospheric upwelling (Indares et al. 1998). These magmas were intruded into the MIZ shortly after peak metamorphism. AMCG suites of this age are numerous throughout the Grenville with the timing of emplacement commonly shortly after the highest grades of metamorphism (e.g. Gower et al. 1991; Tucker and Gower 1994; Corrigan and van Breeman 1997). The Harte Jaune granite and related intrusions in the southern BZ are similar in age to

AMCG suite granites in the allochthonous units of the Grenville (e.g. Owens et al. 1994). Thus, the southern BZ can be correlated with the allochthonous (low-P) belt. The presence of the LES in the western BZ suggests that the MIZ is highly composite in nature.

C.2. Grenvillian metamorphism

C.2.1. Timing of high-PT metamorphism

The rocks of the MIZ show abundant evidence for high-PT metamorphism at ca. 1050-1020 Ma as indicated by zircon and monazite ages. Peak metamorphic conditions are consistent with burial to depths of 50-65 km under a high thermal regime. The temperatures recorded during peak metamorphism (800-900 °C) and initial exhumation (700-800 °C) suggest high heat flow through the base of the crust. This is supported by the presence of syn-metamorphic dykes emplaced into the Lelukuau terrane (the base of the MIZ) shortly after peak metamorphism. High temperatures have also promoted reequilibration of the high-PT assemblages during exhumation. This in turn led to textures such as garnet overgrowths on large poikiloblasts, pargasite-bearing plagioclase collars and locally new zircon growth and zircon replacing baddeleyite (1030+10/-7 Ma, 1030+/-12 Ma and 1012+/-2 Ma). Several metamorphic zircon morphologies give lower intercept ages which overlap this range and may indicate several stages of resorption and regrowth during this period and this requires further investigation. Ages of high-PT metamorphism in the Boundary zone however, are substantially younger, constrained by the age of the Harte Jaune granite and monazite within anatectic pelites (1019-1013 Ma). Evidence for earlier metamorphic events is restricted to the BNS segment where partial melting and/or granite injection of the dioritic country rocks predated the emplacement of the 1250-1170 Ma anorthosite and gabbro bodies.

C.2.2. Conditions of metamorphism

PT-conditions in the LT (Indares 1997) and the LES (Cox and Indares 1999b, see Paper 3) are similar. The highest PT-conditions are recorded by the garnet-kyanite clinopyroxenites (850-920 °C at 18-20 kbar) in the LT and in high-P coronas in troctolite (780-870 °C at 16-19 kbar) and hornblendite (800-930 °C at 15-19 kbar) in the LES. These PT-conditions and the timing of metamorphism suggest that the AMCG rocks in the LT and LES were likely in close association until after the main Grenvillian event. Amphibolite facies overprinting down to ca. 550 °C and 5 kbar in the LES defines a very steep to near-isothermal decompression path.

In the BNS the Fe-Ti gabbros document the textural transformation of these rocks to coronite, transitional metagabbro and eclogite. Anatectic melts in adjacent amphibolite and metapelite indicate a minimum peak of >850 °C and >12 kbar. The highest T-conditions recorded (ca. 750-825 °C) suggest that reequilibration took place shortly after peak metamorphism and confirms the interpretation that high heat flow was pervasive during initial exhumation. Subsequent amphibolite facies overprinting (710-805 °C and 8-10 kbar) further points to near-isothermal decompression. The southern BZ has only limited constraints for metamorphic conditions. However, the metapelitic rocks display evidence for melting reactions which give a range of PT-conditions of 10-13 kbar and >750 °C (Indares and Dunning, in press).

In general, the MIZ records steep metamorphic gradients and Tt-paths which indicate that tectonic exhumation was the dominant process during the early stages of uplift. Structures within the MIZ indicate that the initial exhumation occurred by thrusting to the northwest with southwest directed extension on the top of the pile. This pattern is apparently similar across much of the Grenville. The tectonic emplacement of the BZ corresponds to a phase of slow cooling and exhumation in the rest of the MIZ. The timing of this phase is similar to the Rigolet Pulse recorded in the eastern Grenville (Rivers 1997). Subsequent cooling and exhumation, as indicated by the ages of rutile in the MIZ, was relatively slow and clearly continued until after ca. 920 Ma (i.e. the youngest rutile ages).

C.3. Conclusions

The pattern of protolith ages suggests that most of the lithological units of the MIZ formed during the main stages of accretion at the Laurentian margin. This occurred before the onset of the Grenvillian orogeny during the Labradorian, Pinwarian and Elzeverian events. Indeed, the pattern of protolith ages across the Grenville Province as a whole suggests that the orogen was accumulated largely as a result of igneous activity which closely followed major metamorphic events (Rivers 1997).

The PT-conditions recorded by the rocks in the TT and in the LT indicate metamorphism under a high thermal regime. This along with very steep to near-isothermal metamorphic gradients suggests high heat flow through the lower crust both during the high-PT Grenvillian (Ottawan) event and through the initial stages of exhumation. High heat flow during exhumation was also contemporaneous with the emplacement of both mafic dykes and granites and thus, a pattern of post-peak igneous activity is documented by the MIZ. Current models for the evolution of collisional orogens (e.g. Jamieson 1991; Hodges 1998; Jamieson et al. 1998) indicate the importance of mantle derived heat input following extensional collapse of thickened crust. In the Grenville, Corrigan and Hanmer (1996) suggest that high-PT metamorphism, high heat flow and associated emplacement of mantle derived melts is a result of asthenospheric upwelling during extension. Other orogens, such as the Caledonian and Variscan, also display evidence for the emplacement of mafic and granitoid intrusions shortly after peak metamorphism (e.g. Rogers and Dunning 1991; von Quadt and Gebauer 1993; Rogers et al. 1994; Wendt et al. 1994; Sergeev et al. 1995). Thus, the involvement of asthenospheric mantle in producing high thermal regimes following extensional collapse appears to be a relatively common feature of many orogens. Metamorphism recorded by the rocks within the MIZ documents this process in the lower crust. The data from the MIZ adds to the growing body of evidence which links high-PT metamorphism to heat input from the asthenosphere during extension in the lower parts of orogenic belts.

References

- Andrehs, D., Heinrich, W. (1998): Experimental determinations of REE distributions between monazite and xenotime: potential for temperature-calibrated geochronology.
- Andreissen, P.A.M., Zeck, H.P. (1996): Fission-track constraints on timing of Alpine nappe emplacement and rates of cooling and exhumation, Torrox area, Betic Cordilleras, S. Spain. *Chem. Geol.*, 131, 199-206.
- Anovitz, L.M., Essene, E.J. (1990): Thermobarometry and pressure-temperature paths in the Grenville Province of Ontario. *J. Petrol.*, 31, 197-241.
- Arth (1976): Behaviour of trace elements during magmatic processes: a summary of theoretical models and their applications. *J. Res. USGS.*, 4, 41-47.
- Austrheim, H, Erambert, M , Engvik, A.K (1998): Processing of crust in the root of the Caledonian continental collision zone: the role of eclogitization. *Tectonophysics*, 273, 129-153.
- Austrheim, H., Griffen, W.L. (1985): Shear deformation and eclogite formation within granulite-facies anorthosites of the Bergen Arcs, western Norway. *Chem. Geol.*, 50, 267-281.
- Ayres, M., Vance, D. (1994): Constraints on the thermal evolution of the Indian Himalaya from manganese and erbium distributions in metapelitic garnets. *Min. Mag.*, 58A, 34-35.
- Baer, A.J. (1981): Two orogenies in the Grenville Belt? *Nature*, 290, 129-131.
- Bell, T.H., Johnson, S.E., Davis, B., Forde, A. Hayward, N. , Wilkins, C. (1992): Porphyroblast inclusion-trail orientation data: eure non son girate. *J. Meta. Geol.*, 10, 295-307.
- Berman, R.G., Aranovich, L.Y., Pattison, D.R.M. (1995): Reassessment of the garnet-clinopyroxene Fe-Mg thermometer: II. Thermodynamic analysis. *Contrib. Mineral. Petrol.*, 119, 30-42.

References

- Berman, R.G., Aranovich, L.Y. (1996): Optimized standard state and solution properties of minerals of minerals, I. Model calibration for olivine, orthopyroxene, cordierite, garnet and ilmenite in the system FeO-MgO-CaO-Al₂O₃-TiO₂-SiO₂. *Contrib. Mineral. Petrol.*, 126, 1-24.
- Berman, R.G. (1990): Mixing properties of Ca-Mg-Fe-Mn garnets. *Am. Min.*, 75, 328-344
- Berman, R.G. (1991): Thermobarometry using multi-equilibrium calculations: a new technique, with petrological applications. *Can. Min.*, 29, 833-855.
- Blythe, A.E., Bird, J.M., Omar, G.I. (1996): Deformation history of the central Brooks Range, Alaska: Results from fission-track and ⁴⁰Ar/³⁹Ar analysis.
- Bohlen, S.R., Valley, J.W., Essene, E.J. (1985): Metamorphism in the Adirondacks. I. Petrology, pressure and temperature: *Jn. Petrol.*, 26, 971-922.
- Bohlen, S.R., Wall, V.J., Boettcher, A.L. (1983): Experimental and geological applications of equilibria in the system Fe-TiO₂-Al₂O₃-SiO₂-H₂O. *Am. Min.*, 68, 1049-1058.
- Bohlen, S.R. (1987): Pressure-temperature-time paths and a tectonic model for the evolution of granulites. *J. Geol.*, 95, 617-632.
- Brady, J.B., McCallister, R.H. (1983): Diffusion data for clinopyroxenes from homogenization and self-diffusion experiments. *American. Min.*, 68, 95-105.
- Busch, J.P., van der Pluijm, B.A., Hall, C.M., Essene, E.J. (1996): Listric normal faulting during post-orogenic extension revealed by ⁴⁰Ar/³⁹Ar thermochronology near Robertson Lake shear zone, Grenville orogen, Canada. *Tectonics*, 15, 387-402.
- Bussy, F., Krogh, T.E., Klemens, W.P., Schwerdtner, W.M. (1995): Tectonic and metamorphic events in the westernmost Grenville Province, central Ontario: new results from high-precision U-Pb zircon geochronology. *Can. J. Earth Sci.*, 32, 660-671.
- Camacho, A., Compston, W., McCulloch, M., McDougall, I. (1997): Timing and exhumation of eclogite facies shear zones, Musgrave Block, central Australia. *J. Meta. Geol.*, 15, 735-751.

-
- Carswell, D.A. (1990): Eclogites and the eclogite facies: definitions and classifications. In: *Eclogite Facies Rocks* (Carswell, D.A., ed). Blackie and Son Ltd., Glasgow and London. 1-13.
- Carswell, D.A. , Harley, S.L. (1990): Mineral barometry and thermometry. In: *Eclogite Facies Rocks* (Carswell, D.A., ed). Blackie and Son Ltd., Glasgow and London. 83-110.
- Chakraborty, S., Ganguly, J. (1992): Cation diffusion in aluminosilicate garnets: experimental determination in spessartine-almandine diffusion couples, evaluation of effective binary coefficients, and applications. *Contrib. Mineral. Petrol.* 111, 74-86.
- Cherniak, D.J. (1993): Lead diffusion in titanite and preliminary results on the effects of radiation damage. *Chem. Geology*, 110, 177-194.
- Childe, F, Doig, R., Gariépy, C. (1993): Monazite as a metamorphic chronometer, south of the Grenville Front, west Quebec. *Can. J. Earth Sci.*, 30, 1056-1065.
- Christensen, J.N., Selverstone, J., Rosenfeld J.L., DePaolo, D.J. (1994): Correlation by Rb-Sr geochronology of garnet growth histories from different structural levels within the Tareun Window, Eastern Alps. *Contrib. Mineral. Petrol.*, 118, 1-12.
- Cocherie, A., Legendre, O., Peucat, J.J., Kouamelan, A.N. (1998): Geochronology of polygenetic monazite constrained by in situ microprobe Th-U-total lead determination: Implications for lead behaviour in monazite. *Geochim. Cosmo. Acta*, 62, 2475-2497.
- Connelly, J.N., Heaman, L.M. (1993): U-Pb geochronological constraints on the tectonic evolution of the Grenville Province, western Labrador. *Precambrian Res.*, 63, 123-142.
- Connelly, J.N., Rivers, T., James, D.T. (1995): Thermotectonic evolution of the Grenville Province of western Labrador. *Tectonics*, 14, 202-217.
- Corfu, F., Stone, D. (1998): The significance of titanite and apatite U-Pb ages: constraints for the post magmatic thermal-hydrothermal evolution of a batholithic complex, Berens Rivers area, northwestern Superior Province, Canada. *Geochim. Cosmo. Acta*, 62, 2979-2995.

- Corfu, F. (1996): Multistage zircon and titanite growth and inheritance in an Archean gneiss complex, Winnipeg River Subprovince, Ontario. *Earth. Planet. Sci. Lett.*, 141, 175-186.
- Corrigan, D., Culshaw, N.G., Mortensen, J.K. (1994): Pre-Grenvillian evolution and Grenvillian overprinting of the Parautochthonous Belt in Key Harbour, Ontario: U-Pb and field constraints. *Can. J. Earth Sci.*, 31, 583-596.
- Corrigan, D., Hanmer, S. (1997): Anorthosites and related granitoids in the Grenville orogen: a product of convective thinning of lithosphere? *Geology*, 25, 61-64.
- Corrigan, D., van Breemen, O. (1997): U-Pb age constraints for the lithotectonic evolution of the Grenville Province along the Mauric transect, Quebec. *Can. J. Earth Sci.*, 34, 299-316.
- Cosca, M.A., Essene, E.J., Kunk, M.J., Sutter, J.F. (1992): Differential unroofing within the Central Metasedimentary Belt of the Grenville Orogen: Constraints from $^{40}\text{Ar}/^{39}\text{Ar}$ thermochronology. *Contrib. Mineral. Petrol.*, 110, 211-225.
- Cosca, M.A., Sutter, J.F., Essene, E.J. (1991): Cooling and inferred uplift/erosion history of the Grenville Orogen, Ontario: Constraints from $^{40}\text{Ar}/^{39}\text{Ar}$ thermochronology. *Tectonics*, 10, 959-977.
- Cox, R.A., Dunning, G.R., Indares, A. (1998): Petrology and U-Pb geochronology of mafic, high-pressure, metamorphic coronites from the Tshenukutish domain, eastern Grenville Province. *Precam. Res.*, 90, 59-83.
- Cox, R.A., Indares, A. (1999a): Transformation of Fe-Ti gabbro to coronite, eclogite and amphibolite in the Baie du Nord segment, Manicouagan Imbricate Zone, eastern Grenville Province. *J. Meta. Geol.*, 17, 537-555.
- Cox, R.A., Indares, A. (1999b): High-pressure and high-temperature metamorphism of the mafic and ultramafic Lac Espadon suite, Manicouagan Imbricate Zone, eastern Grenville Province, Quebec. *Can. Min.*, 37, 335-357.

- Creaser, R.A., Heaman, L.M., Erdmer, P. (1997): Timing of high-pressure metamorphism in the Yukon-Tanana terrane, Canadian Cordillera: constraints from U-Pb zircon dating of eclogite from the Teslin tectonic zone. *Can. J. Earth Sci.*, 34, 709-715.
- Culshaw, N.G., Ketchum, J.W.F., Wodika, N., Wallace, P. (1991): Ductile extension following thrusting in the deep crust: evidence from southern Britt Domain, southwest Grenville Province, Georgian Bay, Ontario. *Can. J. Earth Sci.*, 31, 160-175.
- Cygan, R.T., Lasaga, A.C. (1985): Self-diffusion of magnesium in garnet at 750 to 900 °C. *Am. J. Sci.* 285, 328-350.
- Dahl, P.S. (1997): A crystal-chemical basis for Pb-retention and fission-track annealing systematics in U-bearing minerals, with implications for geochronology. *Earth Planet. Sci. Lett.*, 150, 277-290.
- Davidson, A., van Breemen, O. (1988): Baddeleyite-zircon relationships in coronitic metagabbro, Grenville Province, Ontario: implications for geochronology. *Contrib. Mineral. Petrol.*, 100, 291-299.
- Davis, D.W. (1982): Optimum linear regression and error estimation applied to U-Pb data: *Can. J. Earth Sci.*, 19, 2141-2149.
- Davy, P., Gillet, P. (1986): The stacking of thrust slices in collision zones and its thermal consequences. *Tectonics*, 5, 913-929.
- Dempster, T.J., Hudson, N.F.C., Rogers, G. (1995): Metamorphism and cooling of the northeast Dalradian. *J. Geol. Soc. Lon.*, 152, 383-390.
- Dewey, J.F., Ryan, P.D., Anderson, T.B. (1993): Orogenic uplift and collapse, crustal thickness, fabrics and metamorphic phase changes: the role of eclogites. In: *Magmatic Processes and Plate Tectonics* (Prichard, H.M., Alabaster, T., Harris, N.B.W., Neary, C.R. eds). *Geol. Soc. Sec. Pub.*, 76, 325-343.

- DeWolf, C.P., Belshaw, N.S., O'Nions, R.K. (1993): A metamorphic history from micro-scale chronometry of monazite. *Earth. Planet. Sci. Lett.*, 120, 207-220.
- Dodson, M.H. (1979): Closure temperature in cooling geochronological and petrological systems. *Contrib. Mineral. Petrol.*, 40, 259-274.
- Dostal, J., Baragar, W.R.A., Dupuy, C. (1983): Geochemistry and petrogenesis of basaltic rocks from Coppermine River area, Northwest Territories. *Can. J. Earth Sci.*, 20, 684-698.
- Droop, G.T.R., Lomardo, B., Pognate, U. (1990): Formation and distribution of eclogite facies rocks in the Alps. In: *Eclogite Facies Rocks* (Carswell, D.A., ed). Blackie and Son Ltd., Glasgow and London. 225-259.
- Droop, G.T.R. (1987): A general equation for estimating Fe^{3+} concentrations in ferromagnesian silicates and oxides from microprobe analyses, using stoichiometric criteria. *Min. Mag.*, 51, 431-435.
- Dubé, B., Dunning, G.R., Lauzière, K., Roddick, J.C. (1996): New insights into the Appalachian Orogen from geology and geochronology along the Cape Ray fault zone, southwest Newfoundland. *Geol. Soc. America. Bul.*, 108, 101-116.
- Duchêne, S., Lardeaux, J-M., Albarède, F. (1997): Exhumation of eclogites: Insights from depth-time path analysis. *Tectonophysics*, 280, 125-140.
- Dudás, F.Ö., Davidson, A., Bethune, K.M. (1994): Age of the Sudbury diabase dykes and their metamorphism in the Grenville Province, Ontario. *Geol. Surv. Can., Current Res., Rep.* 8, 97-106.
- Easton, R.M. (1986): Geochronology of the Grenville Province. In: *The Grenville Province* (Moore, J.M., Davidson, A., Baer, A.J. eds). GAC Special Paper 31, 127-173.
- Eaton, D., Hynes, A., Indares, A., Rivers, T. (1995): Seismic images of eclogites, crustal-scale extension and Moho relief in the eastern Grenville Province, Quebec. *Geology* 23, 855-858.

- Ellis, D.J., Green, D.H. (1979): An experimental study of the effect of Ca upon garnet-clinopyroxene Fe-Mg exchange equilibria. *Contrib. Mineral. Petrol.*, 71, 13-22.
- Elphick, S.C., Ganguly, J., Loomis, T.P. (1981): Experimental study of Fe-Mg interdiffusion in aluminium silicate garnet. *EOS Trans. Am. Geophy. Union*, 62, 411.
- England, P.C., Thompson, A.B. (1984): Pressure-Temperature-time paths of regional metamorphism I: Heat transfer during the evolution of regions of thickened continental crust. *J. of Petrol.*, 25, 894-928.
- Essene, E.J., Bohlen, S.R. (1985): New garnet barometers in the system CaO-FeO-Al₂O₃-SiO₂-TiO₂ (CFAST). *EOS Trans. Am. Geophy. Union*, 66, 386.
- Floyd, P.A., Winchester, J.A. (1975): Magma-type and tectonic setting discrimination using immobile elements. *Earth Planet. Sci. Lett.*, 27, 211-218.
- Florence, F.P., Darling, R.S., Orrell, S.E. (1995): Moderate pressure metamorphism and anatexis due to anorthosite intrusion, western Adirondack Highlands, New York. *Contrib. Mineral. Petrol.*, 121, 424-436.
- Fraser, D., Ellis, D., Eggis, S. (1997): Zirconium abundance in granulite facies minerals with implications for zircon geochronology in high-grade rocks. *Geology*, 25, 607-610.
- Freer, R. (1980): Self-diffusion and impurity in oxides. *J. Material Sci.*, 15, 803-824.
- Friedman, R.M., Martignole, J. (1995): Mesoproterozoic sedimentation, magmatism and metamorphism in the southern part of the Grenville Province (western Quebec): U-Pb geochronological constraints. *Can. J. Earth Sci.*, 32, 2103-2114.
- Fujimaki, H., Tatsumoto, M., Aoki, K. (1984): Partition coefficients of Hf, Zr and REE between phenocrysts and groundmasses. *J. Geophy. Res. (B)*, 89, 662-672.
- Fujimaki, H. (1986): Partition coefficients of Hf, Zr and REE between zircon, apatite and liquid. *Contrib. Mineral. Petrol.*, 94, 42-45.
- Furtman, M.L., Lindsley, D.H. (1988): Ternary-feldspar modeling and thermometry. *Am. Min.*, 73, 201-215.

- Gaal, R.A.P. (1976): Cathodoluminescence of gem materials. *Gems and Gemology*, 15, 238-44.
- Gale, D., Dunning, G.R., Indares, A. (1994): U-Pb geochronology in the western Manicouagan Shear Belt, Parautochthonous Belt, eastern Grenville Province. *AG-lithoprobe rep.*, 41, 77-78.
- Ganguly, J., Tazzoli, V. (1994): Fe²⁺-Mg interdiffusion in orthopyroxene: retrieval from the data on intercrystalline exchange reaction. *Am. Min.*, 79, 930-937.
- Gebauer, D. (1990): Isotopic systems, geochronology of eclogites. In: *Eclogite Facies Rocks* (Carswell, D.A., ed). Blackie and Son Ltd., Glasgow and London. 141-159.
- Ghent, E.D., Stout, M.Z. (1984): TiO₂ activity in metamorphosed pelitic and basic rocks: principles and assemblages. *Contrib. Mineral. Petrol.*, 76, 92-97.
- Gotze, J., Habermann, D., Neuser, R.D., Richter, D. (1999): High-resolution spectrometric analysis of rare earth element-activated cathodoluminescence in feldspar minerals. *Chem. Geol.*, 153, 81-91.
- Gower, C.F., Heaman, L.M., Loveridge, W.D., Schärer, U., Tucker, R.D. (1991): Grenville magmatism in the eastern Grenville Province, Canada. *Precambrian Res.*, 51, 315-336.
- Gower, C.F., Rivers, T., Brewer, T.S. (1991): Middle-proterozoic mafic magmatism in Labrador, eastern Canada. *Geol. Assoc. of Canada, Spec. Paper*, No.38, 485-506.
- Gower, C.F. (1996): The evolution of the Grenville Province in eastern Labrador, Canada. In: T. S. Brewer (Editor). *Precambrian Crustal Evolution in the North Atlantic Region*. *Geol. Soc. Spe. Pub.*, 112, 197-218.
- Graham, C.M., Powell, R. (1984): A garnet-hornblende geothermometer: calibration testing and application to the Pelona Schist, Southern California. *J. Meta. Geol.*, 2, 13-21.
- Grant, S.M. (1988): Diffusion models for corona formation in metagabbros from the western Grenville Province, Canada. *Contrib. Mineral. Petrol.*, 98, 49-63.

- Haggart, M.J., Jamieson, R.A., Reynolds, P.H., Krogh, T.E., Beaumont, C., Culshaw, N.G. (1993): Last gasp of the Grenville orogeny: Thermochronology of the Grenville Front Tectonic Zone near Killarney, Ontario. *J. Geology*, 101, 575-589.
- Harley, S.L., Carswell, D.A. (1990): Experimental studies on the stability of eclogite facies mineral parageneses. In: *Eclogite Facies Rocks* (Carswell, D.A., ed). Blackie and Son Ltd., Glasgow and London. 53-82.
- Hartel, T.H.D., Pattison, D.R.M. (1996): Genesis of the Kapiskasing (Ontario) migmatitic mafic granulites by dehydration melting of amphibolite: the importance of quartz to reaction progress. *J. Meta. Geol.*, 14, 591-611.
- Hawkins, D.P., Bowring, S.A. (1999): U-Pb monazite, xenotime and titanite geochronological constraints on the prograde to post-peak metamorphic thermal history of Paleoproterozoic migmatites from the Grand Canyon, Arizona. 134, 150-169.
- Heaman, L.M., LeCheminant, A.N. (1993): Paragenesis and U-Pb systematics of baddeleyite (ZrO₂). *Chem. Geology*, 110, 95-126.
- Heinrich, C.A. (1982): Kyanite-eclogite to amphibolite facies evolution of hydrous mafic and pelitic rocks, Adula Nappe, central Alps. *Contrib. Mineral. Petrol.*, 81, 30-38.
- Hodges, K.V. (1991): Pressure-temperature-time paths. *Ann. Rev. Earth Planet. Sci. Lett.*, 19, 207-236.
- Hodges, K.V. (1998): Himalayan orogenesis. In: *What drives metamorphism and metamorphic reactions?* (Treloar, P.J., O'Brien, P.J. eds). *Geol. Soc. London Spec. Pub.*, 138, 7-22.
- Hynes, A., St. Jean, A. (1997): Metamorphic signatures of faulting in the Manicouagan Reservoir region, Grenville Province, eastern Quebec. *Can. Min.*, 35, 1173-1189.
- Indares, A., Dunning, G.R., Cox, R., Gale, D., Connelly, J.N. (1998): High-PT rocks from the base of thick continental crust: geology and age constraints from the Manicouagan Imbricate Zone, eastern Grenville Province. *Tectonics*, 17, 426-440.

-
- Indares, A., Dunning, G., Cox, R.A. (1995): **The Manicougan Shear Belt: an update. AG-lithoprobe rep., 49, 43-47.**
- Indares, A., Dunning, G.R. (1997): **Coronitic metagabbro and eclogite from the Grenville Province of western Quebec: interpretation of U-Pb geochronology and metamorphism. Can. J. of Earth Sci., 34, 891-901.**
- Indares, A., Dunning G.R. (in press): **Partial melting of high-PT metapelites from the Manicouagan Imbricate Zone (Grenville Province): evidence, interpretation and U-Pb geochronology. J. Of Petrol.**
- Indares, A., Rivers, T. (1995): **Textures, metamorphic reactions and thermobarometry of eclogitized metagabbros: a Proterozoic example. Euro. J. Min., 7, 43-56.**
- Indares, A. (1993): **Eclogitized gabbros from the eastern Grenville Province: textures, metamorphic content and implications. Can. J. Earth Sci., 30, 159-173.**
- Indares, A. (1994): **Lithotectonic characteristics of the eclogite-bearing Manicouagan Shear Belt, Parautochthonous Belt, eastern Grenville Province. AG-lithoprobe rep., 41, 83-86.**
- Indares, A. (1997): **Garnet-kyanite clinopyroxenites and garnet-kyanite restites from the Manicouagan Imbricate Zone: A case of high-P/high-T metamorphism in the Grenville Province. Can. Min., 35, 1161-1171.**
- Irvine, T. N., Baragar, W.R.A. (1971): **A guide to the chemical classification of the common volcanic rocks. Can. J. Earth Sci., 8, 523-548.**
- Jamieson, R.A., Culshaw, N.G., Corrigan, D. (1995): **Northwest propagation of the Grenville orogen: Grenvillian structure and metamorphism near Key Harbour, Georgian Bay, Ontario, Canada. J. Metamorphic. Geol., 13, 185-207.**
- Jamieson, R.A., Beaumont, C., Fullsack, P., Lee, B. (1998): **Barrovian regional metamorphism: where's the heat? In: What drives metamorphism and metamorphic reactions? (Treloar, P.J., O'Brien, P.J. eds). Geol. Soc. London Spec. Pub., 138, 23-52.**

- Jamieson, R.A. (1991): P-T-t paths of collisional orogens. *Geol. Rundschau*, 80, 321-332.
- Jeackel, P., Kröner, S.L., Kamo, G., Brandl, G., Wendt, J.I. (1997): Late Archean to early Proterozoic granitoid magmatism and high-grade metamorphism in the central Limpopo belt, South Africa. *J. Geol. Soc. London*, 154, 25-44.
- Jenner, G.A., Dunning, G.R., Malpas, J., Brown, M., Brace T. (1990): ICP-MS: A powerful tool for high-precision trace-element analysis in Earth sciences: Evidence from analysis of selected U.S.G.S. reference samples. *Chem. Geol.*, 83, 133-148.
- Johnson, C.D., Carlson, W.D. (1990): The origin of olivine-plagioclase coronas in metagabbros from the Adirondack Mountains, New York. *J. Meta. Geol.*, 8, 697-717.
- Kalt, A., Hanel, M., Schleicher, H., Kramm, U. (1994): Petrology and geochronology of eclogites from the Variscan Schwarzwald (F.R.G.). *Contrib. Mineral. Petrol.*, 115, 287-302.
- Ketchum, J.W.F., Jamieson, R.A., Heaman, L.M., Culshaw, N.G., Krogh, T.E. (1994): 1.45 Ga granulites in the southwestern Grenville Province. Geological setting, P-T conditions and U-Pb geochronology. *Geology*, 22, 215-218.
- Ketchum, J.W.F., Heaman, L.M., Krogh, T.E., Culshaw, N.G., Jamieson, R.A. (1998): Timing and thermal influence of late orogenic extension in the lower crust: a U-Pb geochronological study from the southwest Grenville orogen, Canada. *Precam. Res.*, 89, 25-45.
- Ketchum, J.W.F., Krogh, T.E. (1998): U-Pb constraints on high-pressure metamorphism in the southwestern Grenville orogen, Canada. *Min. Mag.*, 62A, 775-776.
- Kingsbury, J.A., Miller, C.F., Wooden, J.L., Harrison, T.M. (1993): Monazite paragenesis and U-Pb systematics in rocks of the eastern Mojave Desert, California, U.S.A.: implications for thermochronometry. *Chem. Geol.*, 110, 147-167.

References

- Koons, P.O., Rubie, D.C., Frueh-Green, G. (1987): The effects of disequilibrium and deformation on the mineralogical evolution of quartz-diorite during metamorphism in the eclogite facies. *J. Petrol.*, 29, 679-700.
- Kretz, R. (1983): Symbols for rock-forming minerals. *Am. Min.*, 68, 277-279.
- Krogh, E.J. (1988): The garnet-clinopyroxene Fe-Mg geothermometer: a reinterpretation of existing experimental data. *Contrib. Mineral. Petrol.*, 99, 44-48.
- Krogh, T.E., Gower, C.F., Wardle, R.J. (1996): Pre-Labradorian crust and later Labradorian, Pinwarian and Grenvillian metamorphism in the Mealy Mountain terrane, Grenville Province, eastern Labrador. In: Proterozoic evolution in the North Atlantic realm, (Gower, C.F. comp). COPENA-ECSOOT-IBTA Conference (program and abstracts), 106-107.
- Krogh, T.E. (1973): A low-contamination method for hydro-thermal decomposition of zircon and extraction of U and Pb for isotopic age determinations. *Geochim. Cosmo. Acta*, 37, 485-494.
- Krogh, T.E. (1982): Improved accuracy of U-Pb ages by the creation of more concordant systems using an air abrasion technique: *Geochim. Cosmo. Acta*, 46, 637-649.
- Krogstad, E.J., Walker, R.J. (1994): High closure temperatures of the U-Pb system in large apatites from the Tin Mountain pegmatite, Black Hills, South Dakota, U.S.A. *Geochim. Cosmo. Acta*, 58, 3845-3853.
- Kushiro, I. (1980): Viscosity, density and structure of silicate melts at high-pressures and their petrological applications. In: R. B. Hargraves (Editor), *Physics of magmatic processes*. Princeton Univ. Press, Princeton: 93-120.
- Lanyon, R., Black, L.P., Seitz, H-M. (1993): U-Pb zircon dating of mafic dykes and its application to the Proterozoic geological history of the Vestfold Hills, East Antarctica. *Contrib. Mineral. Petrol.*, 115, 184-203.

References

- Lanzirotti, A., Hanson G.N. (1996): Geochronology and geochemistry of multiple generations of monazite from the Wepawaug schist, Connecticut, U.S.A.: Implications for the stability in metamorphic rocks. *Contrib. Mineral. Petrol.*, 125, 332-340.
- Lasaga, A.C. (1983): Geospeedometry: An extension of geothermometry. In: *Advances in Physical Geochemistry*, 3, Kinetics and Equilibrium in Mineral Reactions, (Saxena, S.K. ed). Springer-Verlag, New York, Berlin, Heidelberg and Tokyo. 60-80.
- Leake, B.E., Wolley, A.R. Arps, C.E.S, Birch, W.D., Gilbert, M.C., Grice, J.D., Hawthorne, F.C., Kato, A., Kisch, H.J., Krivovichev, V.G., Linthout, K., Laird, J., Mandarino, J.A., Maresch, W.V., Nickel, E.H., Rock, N.M.S., Schumacher, J.C., Smith, D.C., Stephenson, N.C.N., Ungaretti, L., Whittaker, E.J.W. , Youzhi, G. (1997): Nomenclature of amphiboles: Report of the Subcommittee on Amphiboles of the International Mineralogical Association, Commission on New Minerals and Mineral Names. *Am. Min.*, 82, 1019-1037.
- Lee, J.K.W. (1995): Multipath diffusion in geochronology. *Contrib. Mineral. Petrol.*, 120, 60-82.
- Longerich, H.P. (1995): Analysis of pressed pellets of geological samples using wavelength-dispersive X-ray fluorescence spectrometry: *X-ray Spec.*, 24, 123-136.
- Loomis, T.P. (1983): Compositional zoning of crystals: A record of growth and reaction history. In: *Advances in Physical Geochemistry*, 3, Kinetics and Equilibrium in Mineral Reactions, (Saxena, S.K. ed). Springer-Verlag, New York, Berlin, Heidelberg and Tokyo. 1-60.
- Loomis, T.P., Ganguly, J., Elphick, S.C. (1985): Experimental determination of cation diffusivities in aluminosilicate garnets: II. Multi-component simulation and tracer diffusion coefficients. *Contrib. Mineral. Petrol.* 90, 45-51
- Maboko, M.A.H., Nakamura, E. (1995): Sm-Nd ages from the Uluguru granulite complex of Eastern Tanzania: further evidence for post-metamorphic slow cooling in the Mozambique belt. *Precam. Res.*, 74, 195-202.

- Mäder, U.K., Berman, R.G. (1992): Amphibole thermobarometry: a thermodynamic approach. Geological Survey of Canada, Current Research, Part E, 92-IE, 393-400.
- Mahood, G., Hildreth, W. (1983): Large partition coefficients for trace elements in high-silica rhyolites. *Geochem. Cosmo. Acta*, 47, 11-30.
- Manhès, G., Allègre, C.J., Dupré, B., Hamelin, B. (1978): Pb-Pb systematics, the age of the Earth and the chemical evolution of our planet in a new representation of space. *Earth Planet. Sci. Lett.*, 44, 91-104.
- Mariano, A.N. (1973): Notes at CL workshop, University of Tennessee, Knoxville. Reported in: *Cathodoluminescence of Geological Materials* (Marshall, D.J.). Unwin Hyman, London, Sydney, Wellington.
- Marshall, D.J. (1988): *Cathodoluminescence of Geological Materials* (Marshall, D.J.). Unwin Hyman, London, Sydney, Wellington. 37-56.
- Martignole, J., Machado, N., Indares, A. (1994): The Wakeham terrane: a Mesoproterozoic terrestrial rift in the eastern part of the Grenville Province. *Precambrian. Res.*, 68, 291-306.
- Martignole, J., Reynolds, P. (1997). $^{40}\text{Ar}/^{39}\text{Ar}$ thermochronology along a western Quebec transect of the Grenville Province, Canada. *J. Metamorphic. Geol.*, 15, 283-296.
- McEachern, S.J., van Breemen, O. (1993): Age of deformation within the Central Metasedimentary Belt boundary thrust zone, southwest Grenville orogen: Constraints on the collision of the Mid-Proterozoic Elzevir terrane. *Can. J. Earth Sci.*, 30, 1155-1165.
- McLelland, J.M., Isachsen, Y.W. (1986): Synthesis of geology of the Adirondack Mountains, New York, and their tectonic setting within the southwestern Grenville Province. In: *The Grenville Province* (Moore, J.M., Davidson, A., Baer, A.J. eds). GAC Special Paper 31, 75-94.
- Meldrum, A., Boatner, L.A., Weber, W.J., Ewing, R.C. (1998): Radiation damage in zircon and monazite. *Geochem. Cosmo. Acta*, 62, 2509-2520.

- Meschede, M. (1986): A method for discriminating between different types of mid-ocean ridge basalts and continental tholeiites with the Nb-Zr-Y diagram. *Chem. Geology*, 56, 207-218.
- Messiga, B., Scambelluri, M. (1991): Retrograde P-T-t path for the Voltri Massif eclogites (Ligurian Alps, Italy): some tectonic implications. *J. Meta. Geol.*, 9, 93-109.
- Messiga, B., Tribuzio, R., Bottazzi, P., Ottolini, L. (1995): An ion microprobe study on trace element composition of clinopyroxene from blueschist and eclogitized Fe-Ti gabbros, Ligurian Alps, northwestern Italy: Some petrological considerations. *Geochem. Cosmo. Acta*, 59, 59-75.
- Mezger, K., Hanson, G.N., Bohlen, S.R. (1989): High-precision U-Pb ages of metamorphic rutile: application to the cooling history of high-grade terranes. *Earth Planet. Sci. Lett.*, 96, 106-118.
- Mezger, K., Rawnsley, C.M., Bohlen, S.R., Hanson, G.N. (1991): U-Pb garnet, sphene, monazite and rutile ages: implications for the duration of high-grade metamorphism and cooling histories, Adirondack Mts., New York. *J. Geology*, 99, 415-428.
- Mezger, K., Essene, E.J., van der Pluijm, B.A., Halliday, A.N. (1993): U-Pb geochronology of the Grenville orogen of Ontario and New York: constraints on ancient crustal tectonics. *Contrib. Mineral. Petrol.*, 114, 13-26.
- Mezger, K., Krogstad, E.J. (1997): Interpretation of discordant U-Pb zircon ages: An evaluation. *J. Meta. Geol.*, 15, 127-140.
- Mitchell, R.E., Xiong, J., Mariano, A.N., Fleet, M.E. (1997): Rare earth element activated cathodoluminescence in apatite. *Can. Min.*, 35, 979-998.
- Mongkoltip, P., Ashworth, J.R. (1983): Quantitative estimation of an open-system symplectite-forming reaction: Restricted diffusion of Al and Si in coronas around olivine. *J. of Petrol.*, 24, 635-661.
- Moore, M.J. Jr, Thompson, P.H. (1980): The Flinton Group: A late Precambrian metasedimentary succession in the Grenville Province of eastern Ontario. *Can. J. Earth Sci.*, 17, 1685-1707.

References

- Mørk, M.B. (1985): Incomplete high P-T metamorphic transitions within the Kvamsøy pyroxenite complex, west Norway: a case study of disequilibrium. *J. Meta. Geol.*, 3, 245-264.
- Mørk, M.B. (1986): Coronite and eclogite formation in olivine gabbro (Western Norway): reaction paths and garnet zoning. *Min. Mag.*, 50, 417-426.
- Muir, R. J., Ireland, T. R., Bentley, M. R., Fitches, W. R., and Maltman, A. J. (1997). A Caledonian age for the Kiloran Bay appinite intrusion on Colonsay, Inner Hebrides. *Scot. J. Geol.*, 33, 75-82.
- Murray, J.R., Oreskes, N. (1997): Uses and limitations of cathodoluminescence in the study of apatite paragenesis. *Econ. Geol.*, 92, 368-376.
- Neng-Song Chen, Min Sun, Zhen-Dong You, Malpas, J. (1998): Well-preserved garnet zoning in granulite from the Dabie Mountains, central China. *J. Meta. Geol.*, 16, 213-222.
- Newton, R.C., Perkins, D.I. (1982): Thermodynamic calibration of geobarometers based on the assemblages garnet-plagioclase-orthopyroxene (clinopyroxene)-quartz. *Am. Min.*, 67, 203-222.
- O'Brien, P.J. (1999): Asymmetric zoning profiles in garnet from HP/HT granulite and implications for volume and grain boundary diffusion. *Min. Mag.*, 63, 227-238.
- O'Neill, H. St.C., Wood, B.J. (1980): An experimental study of Fe-Mg partitioning between garnet and olivine and its calibration as a geothermometer. *Contrib. Mineral. Petrol.* 70, 59-70.
- Ono, A. (1976): Chemistry and zoning of zircon from some Japanese granitic rocks. *J. Jap. Assoc. Min. Pet. Econ. Geol.*, 71, 6-17.
- Otten, M.T. Busek, P.R. (1987): TEM study of the transformation of augite to sodic pyroxene in eclogitized ferrogabbro. *Contrib. Mineral. Petrol.*, 96, 529-538.
- Owens, B.E., Dymek, R.F., Tucker, R.D., Brannon, J.C., Podosek, F.A. (1994): Age and radiogenic isotope composition of a late to post-tectonic anorthosite in the Grenville Province: the Labrieville massif. *Lithos*, 31, 189-206.

- Pan, Y., Fleet, M.E. (1995): Rare earth element mobility during prograde granulite facies metamorphism: significance of fluorine. *Contrib. Mineral. Petrol.*, 123, 251-262.
- Pan, Y. (1997): Zircon- and monazite-forming metamorphic reactions at Manitouwadge, Ontario. *Can. Min.*, 35, 105-118.
- Paquette, J-L., Ménot, R.P., Peucat, J.J. (1989): REE, Sm-Nd and U-Pb zircon study of eclogites from the Apline External Massifs (Western Alps): evidence for crustal contamination. *Earth Planet. Sci. Lett.*, 96, 181-198.
- Paquette, J-L., Monchoux, P., Couturier, M. (1995): Geochemical and isotopic study of a norite eclogite transition in the European Variscan belt: implications for U-Pb zircon systematics in metabasic rocks. *Geochim. Cosmo. Acta.*, 59, 1611-1622.
- Parrish, R.R. (1990): U-Pb dating of monazite and its application to geological problems. *Can. J. Earth. Sci.*, 27, 1431-1450.
- Parrish, R.R., Krogh, T.E. (1987): Synthesis and purification of ^{205}Pb for U-Pb geochronology. *Chem. Geol.*, 66, 103-110.
- Passchier, C.W., Trouw, R.A.J., Zwart, H.J., Vissers, R.L.M. (1992): Porphyroblast rotation: eure si muove? *J. Meta. Geol.*, 10, 283-294.
- Patterson, J.G., Heaman, L.M. (1991): New geochronological limits on the depositional age of the Hurwitz Group, Trans-Hudson hinterland, Canada. *Geology*, 19, 1137-1140.
- Pattison, D.R.M., Newton, R.C. (1989): Reversed experimental calibration of the garnet-clinopyroxene Fe-Mg exchange thermometer. *Contrib. Mineral. Petrol.*, 101, 87-103.
- Pearce, J.A., Cann, J.R. (1973): Tectonic setting of basic volcanic rocks determined using trace element analysis. *Earth Planet. Sci. Lett.*, 19, 290-300.
- Pearce, J.A. (1982): Trace element characteristics of lavas from destructive plate boundaries. In: *Andesites* (Thorpe, R.S. ed). Wiley, Chichester. 525-548.

References

- Pehrsson, S., Hanmer, S., van Breemen, O. (1996): U-Pb geochronology of the Raglan gabbro belt, Central Metasedimentary Belt, Ontario: implications for an ensialic marginal basin in the Grenville Orogen. *Can. J. Earth Sci.*, 33, 691-702.
- Peucat, J.J., Vidal, Ph., Godard, G., Postaire, B. (1982): Precambrian U-Pb zircon ages in eclogites and garnet pyroxenites from South Brittany (France): an old oceanic crust in the West European Hercynian Belt? *Earth Planet. Sci. Lett.*, 60, 70-78.
- Phillipe, S., Wardle, R.J. and Schärer, U. (1993): Labradorian and Grenvillian crustal evolution of the Goose Bay region, Labrador: new U-Pb geochronological constraints. *Can. J. Earth Sci.*, 30, 2315-2327.
- Pidgeon, R.T., Bosch, D., Bruguier, O. (1996): Inherited zircon and titanite U-Pb systems in an Archean syenite from southwestern Australia: implications for U-Pb stability of titanite. *Earth Planet. Sci. Lett.*, 141, 187-198.
- Pidgeon, R.T., Nemchin, A.A., Hitchen, G.J. (1998): Internal structures of zircons from Archean granites from the Darling Range batholith: implications for zircon stability and the interpretation of zircon U-Pb ages. *Contrib. Mineral. Petrol.*, 132, 288-299.
- Pognate, U. (1985): Coronitic reactions and ductile shear zones in eclogitized ophiolite metagabbro, western Alps, north Italy. *Chem. Geol.*, 50, 99-109.
- Rapp, R.P., Watson, E.B., Miller, C.F. (1991): Partial melting of amphibolite/eclogite and the origin of Archean trondhjemites and tonalites. *Precambrian Res.*, 51, 1-25.
- Rapp, R.P. (1995): Amphibole-out phase boundary in partially melted metabasalt, its control over liquid fraction and composition, and source permeability. *J. Geophys. Res.*, 100, 15601-1610.
- Resor, P.G., Chamberlain, K.R., Frost, C., Snoke, A.W., Frost, B.R. (1996): Direct dating of deformation: U-Pb age of syndeformational sphene growth in the Proterozoic Laramie Peak shear zone. *Geology*, 24, 623-626.

References

- Rivers, T., Chown, E.H. (1986): The Grenville orogen in eastern Quebec and western Labrador-definition, identification and tectonometamorphic relationships of autochthonous, parautochthonous and allochthonous terranes. In: *The Grenville Province* (Moore, J.M., Davidson, A., Baer, A.J. eds). GAC Special Paper 31, 127-173.
- Rivers, T., Martignole, J., Gower, C. F. and Davidson, A. (1989): New tectonic divisions of the Grenville Province, southeast Canadian Shield. *Tectonics*, 8, 63-84.
- Rivers, T., Mengel, F.C. (1988): Contrasting assemblages and petrogenetic evolution of corona and non-corona gabbros in the Grenville Province of western Labrador. *Can. J. Earth Sci.*, 25, 1629-1648.
- Rivers, T., van Gool, J.A.M., Connelly, J.N. (1993): Contrasting tectonic styles in the northern Grenville Province: implications for the dynamics of orogenic fronts. *Geology*, 21, 1127-1130.
- Rivers, T. (1997): Lithotectonic elements of the Grenville Province: review and tectonic implications. *Precam. Res.*, 86, 117-154.
- Rogers, G., Paterson, B.A., Dempster, T.J., Redwood, S.D. (1994): U-Pb geochronology of the 'newer' gabbros, Northeast Grampians. In: *Caledonian terrane relationships in Britain. Program with abstracts*, 8.
- Rogers, G., Dunning, G.R. (1997): Geochronology of appinitic and related granitic magmatism in the West Highlands of Scotland: constraints on the timing of transcurrent fault movement. *J. Geol. London*, 148, 17-27.
- Rubie, D.C. (1986): The catalysis of mineral by water and restrictions on the presence of aqueous fluid during metamorphism. *Min. Mag.*, 50, 399-415.
- Rubie, D.C. (1984): A thermal-tectonic model for high-pressure metamorphism and deformation in the Sesia Zone, western Alps. *J. Geology*, 92, 21-36.
- Rubie, D.C. (1990): Role of kinetics in the formation and preservation of eclogites. In: *Eclogite Facies Rocks* (Carswell, D.A. ed). Blackie and Son Ltd., Glasgow and London. 111-140.

- Ruppell, C., Hodges, K.V. (1994): Pressure-temperature-time paths from two-dimensional thermal models: Prograde, retrograde and inverted metamorphism. *Tectonics*, 13, 17-44.
- Rushmer, T. (1991): Partial melting of two amphibolites: Contrasting experimental results under fluid-absent conditions. *Contrib. Mineral. Petrol.*, 107, 41-59.
- Schock, H.H. (1979): Distribution of rare earth and other trace elements in migmatites. *Chem. Geol.*, 26, 119-133.
- Schaltegger, U., Fanning, C.M., Günther, D., Maurin, J.C., Schulmann, K., Gebauer, D. (1999): Growth, annealing and recrystallization of zircon and preservation of monazite in high-grade metamorphism: conventional and in-situ U-Pb isotope, cathodoluminescence and microchemical evidence. *Contrib. Mineral. Petrol.*, 134, 186-201.
- Schärer, U., Gower, C.F. (1988): Crustal evolution in eastern Labrador: constraints from precise U-Pb ages. *Precambrian Res.*, 38, 405-421.
- Schärer, U., Krogh, T.E., Gower, C.F. (1986): Age and evolution of the Grenville Province in eastern Labrador from U-Pb systematics in accessory minerals. *Contrib. Mineral. Petrol.* 94, 438-451.
- Schwandt, C.S., Cygan, R.T., Westrich, H.R. (1996): Ca self-diffusion in grossular garnet. *American Min.*, 81, 448-451.
- Scott, D.J., Hynes, A. (1994): U-Pb geochronology along the Manicouagan Corridor, preliminary results: Evidence for ca. 1.47 Ga metamorphism. *AG-lithoprobe rep.*, 41, 109-110.
- Scott, D.J., St. Onge, M.R. (1995): Constraints on Pb closure temperature in titanite based on rocks from Ungava orogen, Canada: Implications for U-Pb geochronology and P-T-t paths determinations. *Geology*, 23, 1123-1126.
- Sergeev, S.A., Meier, M., Steiger, R.H. (1995): Improving the resolution of single-grain U/Pb dating by use of zircon extracted from feldspar: Application to the Variscan magmatic cycle in the central Alps. *Earth Planet. Sci. Lett.*, 134, 37-51.

References

- Sen, C., Dunn, T. (1994): Dehydration melting of a basaltic composition amphibolite at 1.5 and 2.0 GPa: implications for the origin of adakites. *Contrib. Mineral. Petrol.*, 117, 394-409.
- Shi, Yaolin, Wang Chi-Yuean (1987): Two-dimensional modeling of the P-T-t paths of regional metamorphism in simple overthrust terrains. *Geology*, 15, 1048-1051.
- Sisson, T. W., Grove, T. L. and Coleman, D. S. (1997). Hornblende gabbro sill complex at Onion Valley, California, and a mixing origin for the Sierra Nevada batholith. *Contrib. Mineral. Petrol.*, 126, 81-108.
- Smith, H.A., Giletti, B.J. (1995): Measurement of Pb diffusion in rutile and monazite with applications to U-Pb geochronology. *EOS Trans. Am. Geophys. Union*, 76, 707.
- Smith, H.A., Giletti B.J. (1997): Lead diffusion in monazite. *Geochim. Cosmo. Acta*, 61, 1047-1055.
- Snow, E., Kidman, S. (1991): Effects of fluorine on solid-state alkali interdiffusion rates in feldspar. *Nature* 349, 231-233.
- Spear, F.S., Hickmott, D.D. , Selverstone, J. (1990): Metamorphic consequences of thrust emplacement, Fall Mountain, New Hampshire. *Geol. Soc. Am. Bull.*, 102, 1344-1360.
- Spear, F.S., Parrish, R.R. (1996): Petrology and cooling rates of the Valhalla Complex, British Columbia, Canada. *J. Petrol.*, 37, 733-765.
- Spear, F.S. (1993): Table of Mineral Abbreviations. In *Metamorphic Phase Equilibria and Pressure-Temperature-Time Paths. Monograph Series, Mineralogical Society of America, Washington D.C., U.S.A.*
- Stacey, J.S., Kramers, J.D., (1975): Approximation of terrestrial lead isotope evolution by a two stage model: *Earth Planet. Sci. Lett.*, 26, 207-221.
- Stowell, H.H., Goldberg, S.A. (1997): Sm-Nd garnet dating of polyphase metamorphism: northern Coast Mountains, south-eastern Alaska, U.S.A. *J. Meta. Geol.*, 15, 439-450.

- Suzuki, K., Adachi, M., Kajizuka, I. (1994): Electron microprobe observations of Pb diffusion in metamorphosed detrital monazites. *Earth Planet. Sci. Lett.*, 128, 391-405.
- Teufel, S., Heinrich, W. (1993): Experimentally induced Pb-loss in monazite through hydrothermal recrystallization: Towards modern U-Pb ages. *Terra Abs.*, 5, 396.
- Thompson, A.B., England, P.C. (1984): Pressure-Temperature-time paths of regional metamorphism II: Their inference and interpretation using mineral assemblages in metamorphic rocks. *J. of Petrol.*, 25, 929-955.
- Thompson, A.B., Ridley, J.R. (1987): Pressure-temperature-time (P-T-t) histories of orogenic belts. *Phil. Trans. Royal Soc. of London*, 321, 27-45.
- Tucker, R.D., Gower, C.F. (1994): U-Pb geochronological framework for the Pinware terrane, Grenville Province, southeast Labrador. *J. Geology*, 102, 67-78.
- Vance, D., O'Nions, R.K. (1990): Isotopic chronometry of zoned garnets: growth kinetics and metamorphic histories. *Earth Planet. Sci. Lett.*, 97, 227-240.
- van Breemen, O., Davidson, A., Loveridge, W.D., Sullivan, R.W. (1986): U-Pb zircon geochronology of Grenville tectonites, granulites and igneous precursors, Parry Sound, Ontario. In: *The Grenville Province*. (Moore, J.M., Davidson A., Baer, A.J. eds). *Geol. Assoc. Can. Spec. Pap.*, 31, 191-207.
- van der Pluijm, B., Mezger, K., Cosca, M.A., Essene, E.J. (1994): Determining the significance of high-grade shear zones by using temperature-time paths, with examples from the Grenville orogen. *Geology*, 22, 743-746.
- Vavra, G., Schmid, R., Gebauer, D. (1999): Internal morphology, habit and U-Th-Pb microanalysis of amphibolite to granulite facies zircons: geochronology of the Ivrea Zone (Southern Alps). *Contrib. Mineral. Petrol.*, 134, 380-404.

References

- Vavra, G., Schaltegger, U. (1999): Post-granulite facies monazite growth and rejuvenation during Permian to Lower Jurassic thermal and fluid events in the Ivrea Zone, Southern Alps. *Contrib. Mineral. Petrol.*, 134, 405-411.
- Verts, L., Chamberlain, K.R., Frost, C.D. (1996): U-Pb sphene dating of metamorphism: the importance of sphene growth in the contact aureole of the Red Mountain pluton, Laramie Mountains, Wyoming. *Contrib. Mineral. Petrol.*, 125, 186-199.
- von Quadt, A., Gebauer, D. (1993): Sm-Nd and U-Pb dating of eclogites and granulites from Oberpfalz, NE. Bavaria, Germany. *Chem. Geol.*, 109, 317-339.
- Wasteneys, H.A., Kamo, S.L., Moser, D., Krogh, T.E., Gower, C.F. and Owen, J. V., 1997. U-Pb geochronological constraints on the geological evolution of the Pinware terrane and adjacent areas, Grenville Province, southeast Labrador, Canada. *Precambrian Res.*, 81, 101-128.
- Watt, G.R., Burns, I.M., Graham, G.A. (1996): Chemical characteristics of migmatites: accessory phase distribution and evidence for fast melt segregation. *Contrib. Mineral. Petrol.*, 125, 100-111.
- Wayte, G.J., Worden, R.H., Rubie, D.C., Droop, G.T.R. (1989): A TEM study of plagioclase breakdown at high pressure: the role of infiltrating fluid. *Contrib. Mineral. Petrol.*, 101, 426-437.
- Wendt, J.I., Kroner, A., Fiala, J., Todt, W. (1994): U-Pb zircon and Sm-Nd dating of Moldanubian HP/HT granulites from South Bohemia, Czech Republic. *J. Geol. Soc. London*, 151, 83-90.
- Williams, M.L., Hanmer, S., Kopf, C., Darrach, M. (1995): Syntectonic generation and segregation of tonalitic melts from amphibolite dikes in the lower crust., Striding-Athabasca mylonite zone, northern Saskatchewan. *J. Geophys. Res. (B)*, 100, 15717-15734.
- Windley, B.F. (1986): Comparative tectonics of the western Grenville and western Himalaya. In: *The Grenville Province* (Moore, J.M., Davidson, A., Baer, A.J. eds). *Geol. Assoc. Can. Spec. Pap.*, 31, 341-348.

- Wodicka, N., Parrish, R.R., Jamieson, R.A. (1996): The Parry sound domain: A far-travelled allochthon? New evidence from U-Pb zircon geochronology: *Can. J. Earth Sci.*, 33, 1087-1104.
- Wolf, M.B., Wyllie, P.J. (1993): Garnet growth during amphibolite anatexis: Implications of a garnetiferous restite. *J. of Geol.*, 101, 357-373.
- Wolf, M.B., Wyllie, P.J. (1994): Dehydration-melting of amphibolite at 10 kbar: the effects of temperature and time. *Contrib. Mineral. Petrol.* 115, 369-383.
- Wolf, M.B. , Wyllie, P.J. (1995): Liquid segregation parameters from amphibolite dehydration melting experiments. *J. Geophys. Res.*, 100, 15717-15734.
- Yamada, R., Tagami, T., Nishimura, S., Ito, H. (1995): Annealing kinetics of fission tracks in zircon: an experimental study. *Chem. Geol.*, 122, 249-258.
- Yund, R.A. (1986): Interdiffusion of NaSi-CaAl in peristerite. *Phys. Chem. Minerals*, 7, 185-189.
- Zhang, R.Y., Liou, J.G. (1997): Partial transformation of gabbro to coesite-bearing eclogite from Yangkou, the Sulu terrane, eastern China. *J. Meta. Geol.*, 15, 183-202.
- Zhu, X.K., O'Nions, R.K., Belshaw, N.S., Gibb, A.J. (1997): Significance of in situ SIMS chronometry of zoned monazite from Lewisian granulites, northwest Scotland. *Chem. Geol.*, 135, 35-53.
- Zinkernazell, U. (1978): Cathodoluminescence of quartz and its application to sandstone petrology. In: *Contributions to sedimentology*, No. 8. Schweizerbart'sche Verlagsbuchhandlung, Stuttgart.

Appendix A: Polarizing microscopy, cathodoluminescence, scanning electron microscope techniques and photomicrographs.

A.1. Polarized transmitted and reflected light microscopy

A.1.1. Sample preparation

Samples were carefully selected for sectioning from previously sliced rock specimens. The area under investigation was trimmed to the required section size before mounting on section glass. Samples were then polished to 35 μm with progressively finer diamond paste (15-0.3 μm) to a fine polish. Some samples were repolished to 30 μm thick to assist in mineral identification using true pleochroism and birefringence.

A.1.2. Microscopy and photomicrography

Polished sections were examined using transmitted and reflected light on a Canon BHSP polarizing microscope. Textures were documented best with the 10 times ocular and 1.5-20 times objectives giving 15 to 200 times combined magnifications. Photomicrographs were taken using a Cannon AD35S camera and automatic exposure system with 35 mm 100 ASA colour film. Grain boundaries have been enhanced in some images. The dimensions of the photomicrographs are indicated in the figure captions (in brackets).

Plate A1.1 (a-d). Textures in mafic and ultramafic rocks (LES). *Troctolite and dunite (samples 5a and 6):*

a) troctolite with olivine and plagioclase igneous assemblage and metamorphic coronas of pyroxene, pargasitic amphibole and garnet. The plagioclase is rich in kyanite and corundum inclusions (5 x 3.4 mm), b) amphibole-free corona assemblage and c) amphibole-bearing corona assemblage (0.75 x 0.5 mm), d) dunite with orthoamphibole, and antigorite (5 x 3.4 mm).

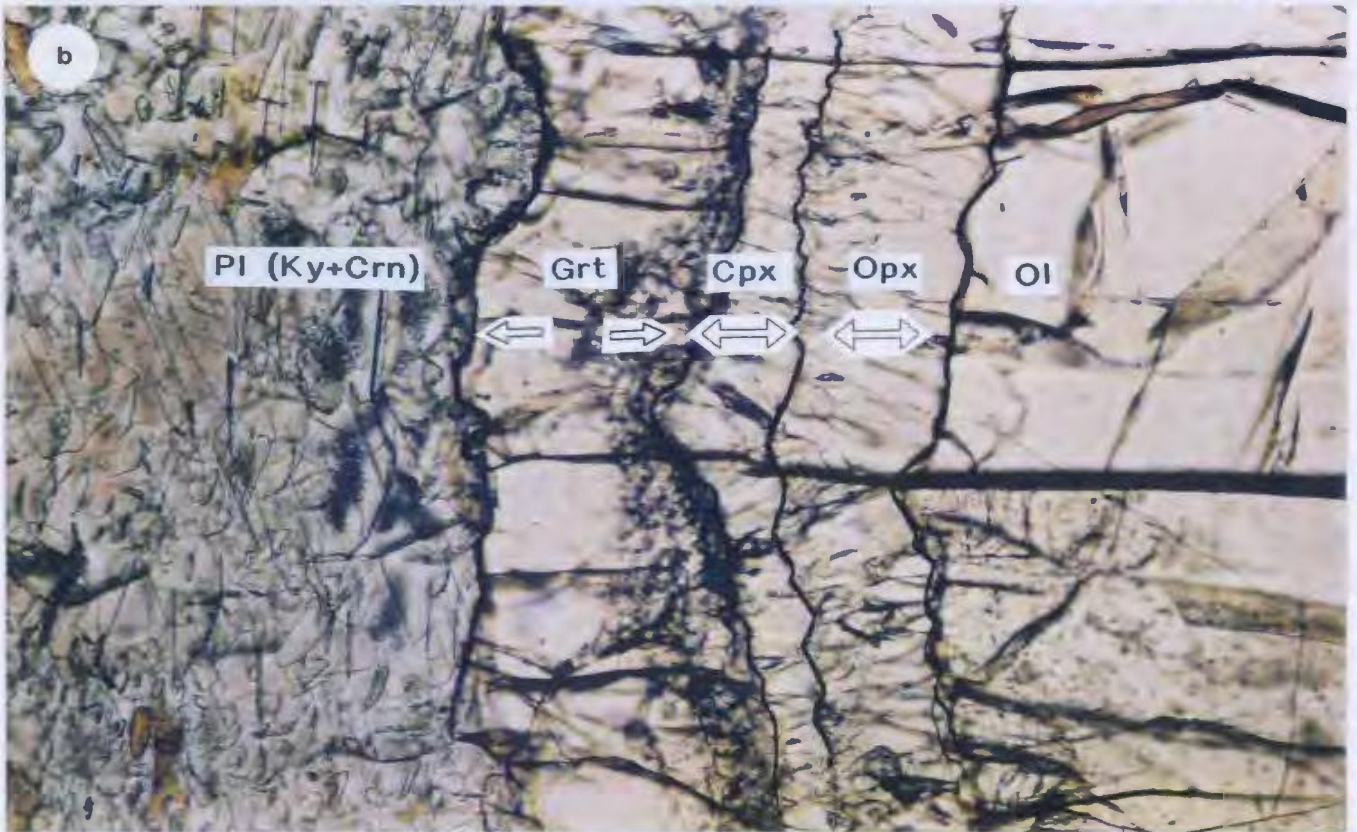


Plate A1.1 (cont.)

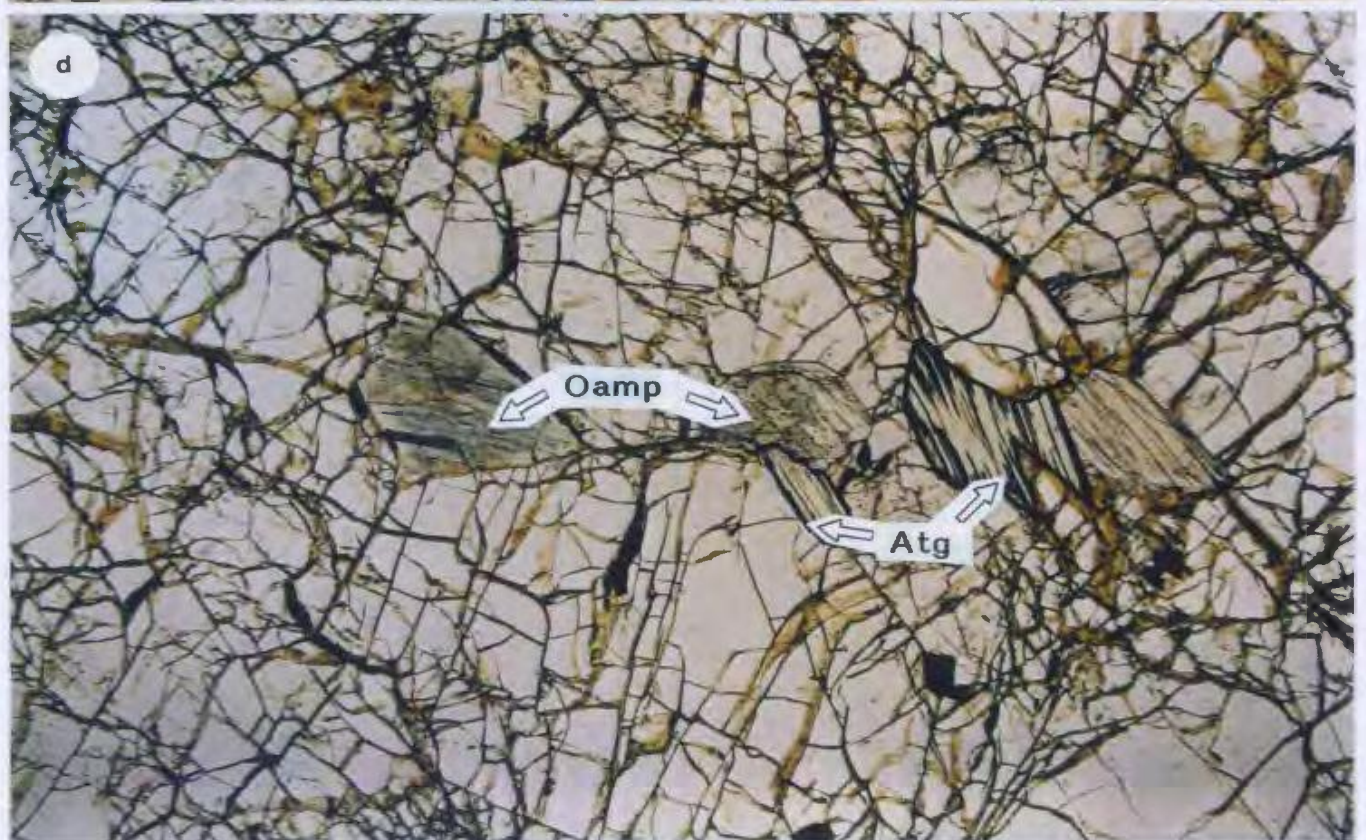
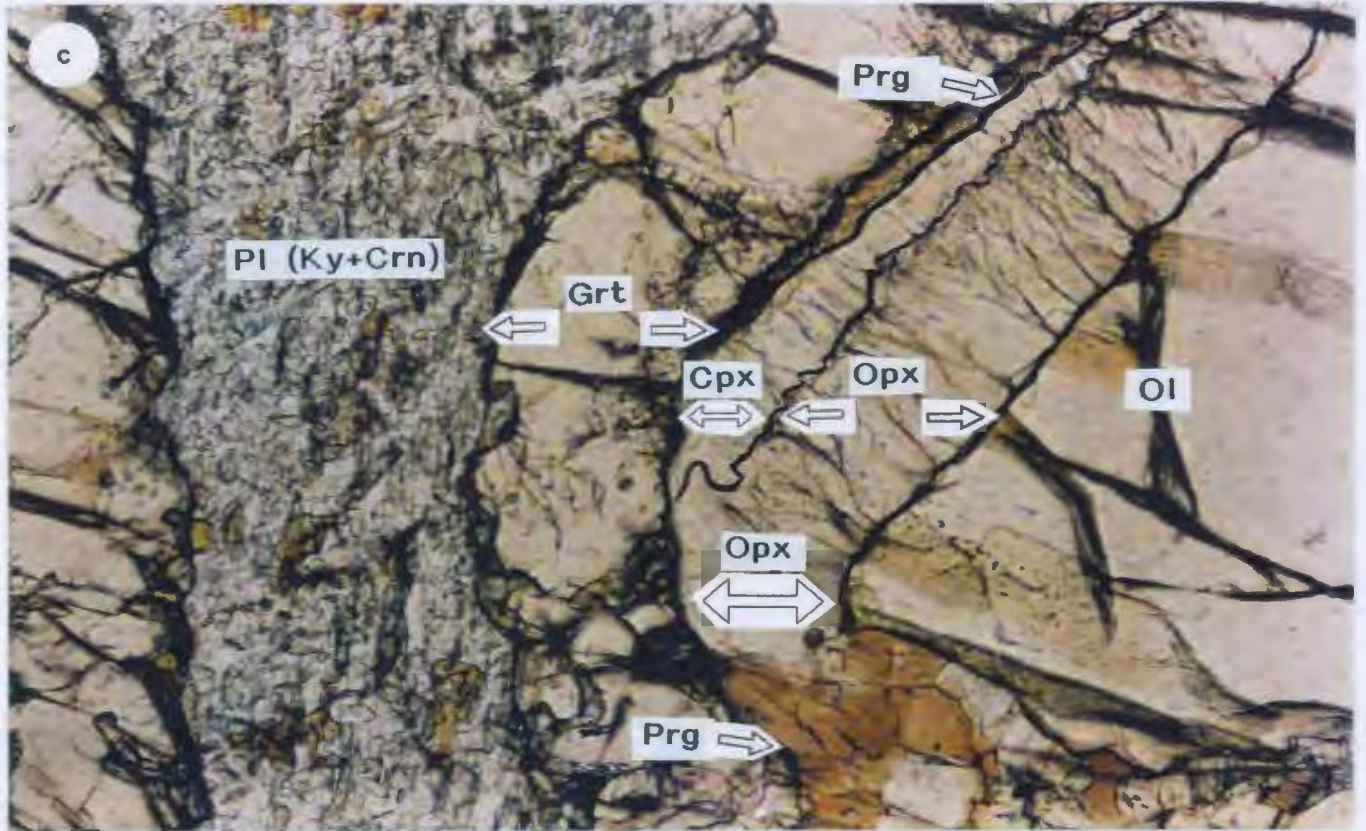


Plate A1.2 (a-b). *Hornblendite (sample 3b)*: a) general texture with a large oikocryst of amphibole and relict phlogopite. Chadacrysts of plagioclase (with corundum and kyanite inclusions) with coronas of garnet are also apparent, d) Olivine chadacrysts in a large amphibole oikocryst. Orthopyroxene corona around relict olivine chadacryst (5 x 3.4 mm).

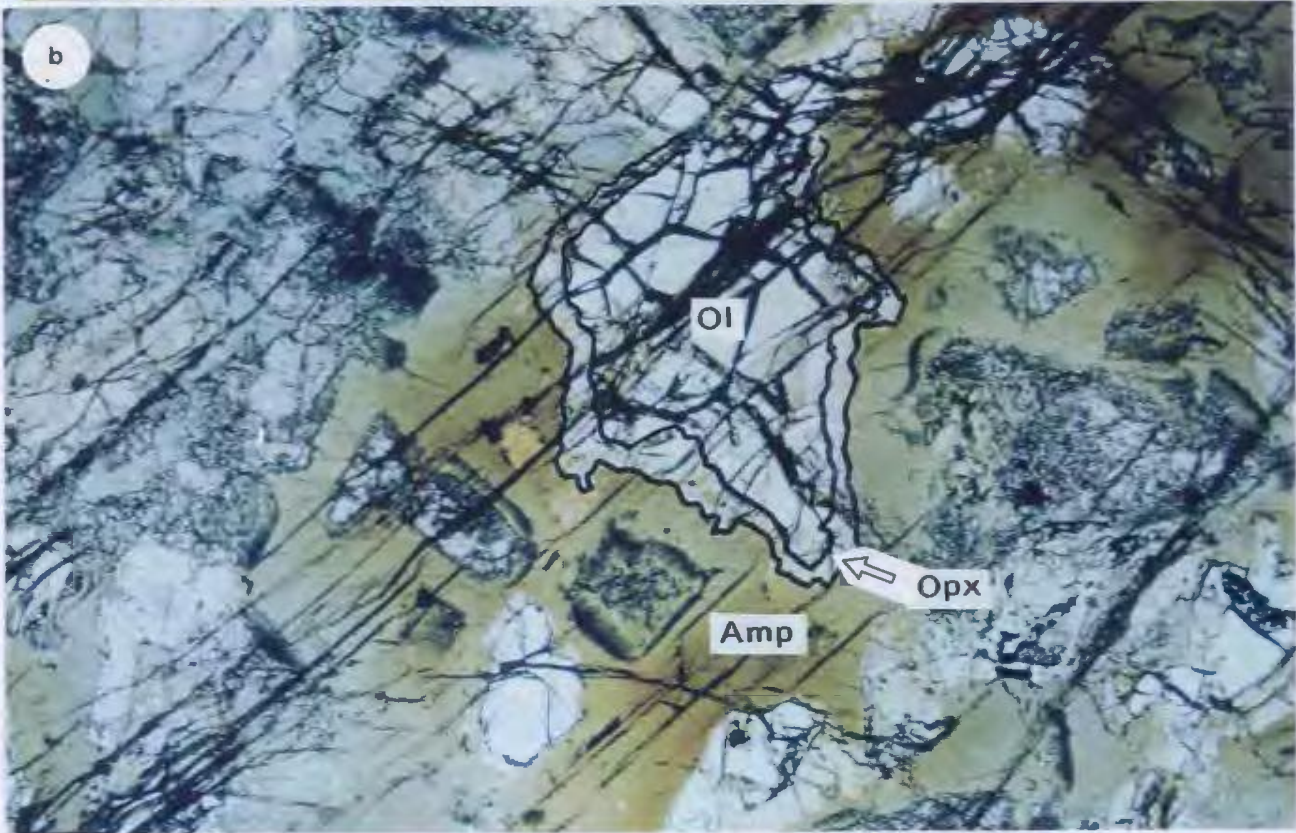
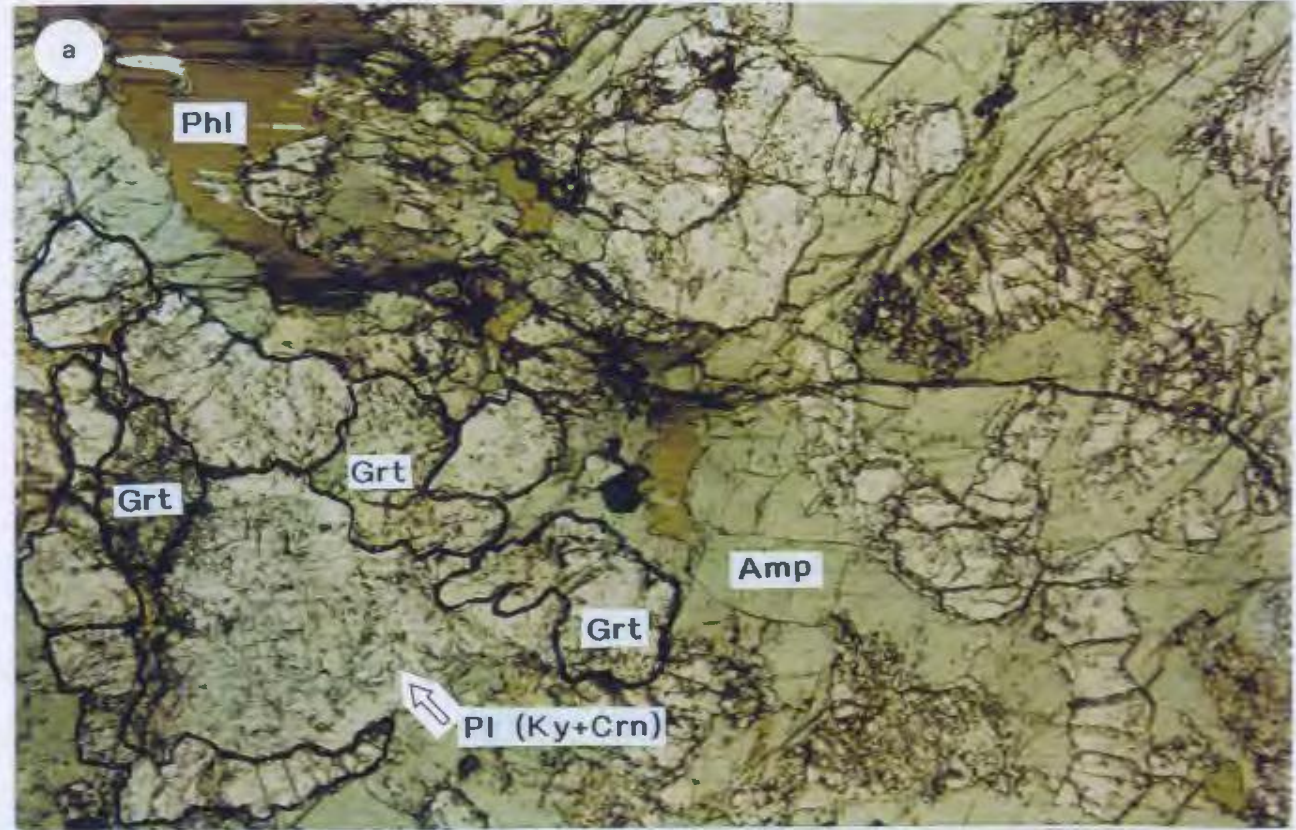


Plate A1.3 (a-d). *Olivine garnet amphibolite (sample 6am)*: a) garnet porphyroblast and slightly foliated, granoblastic matrix assemblage of amphibole, orthopyroxene and relict olivine. Note the amphibole and plagioclase inclusions in the garnet which are especially visible in b) same view in crossed-polars, c) granoblastic foliated texture in the olivine garnet amphibolite and d) crossed-polars where garnet (isotropic), olivine (3° birefringence) and orthopyroxene ($1-2^\circ$ birefringence) are clearly visible (1.5 x 1 mm).

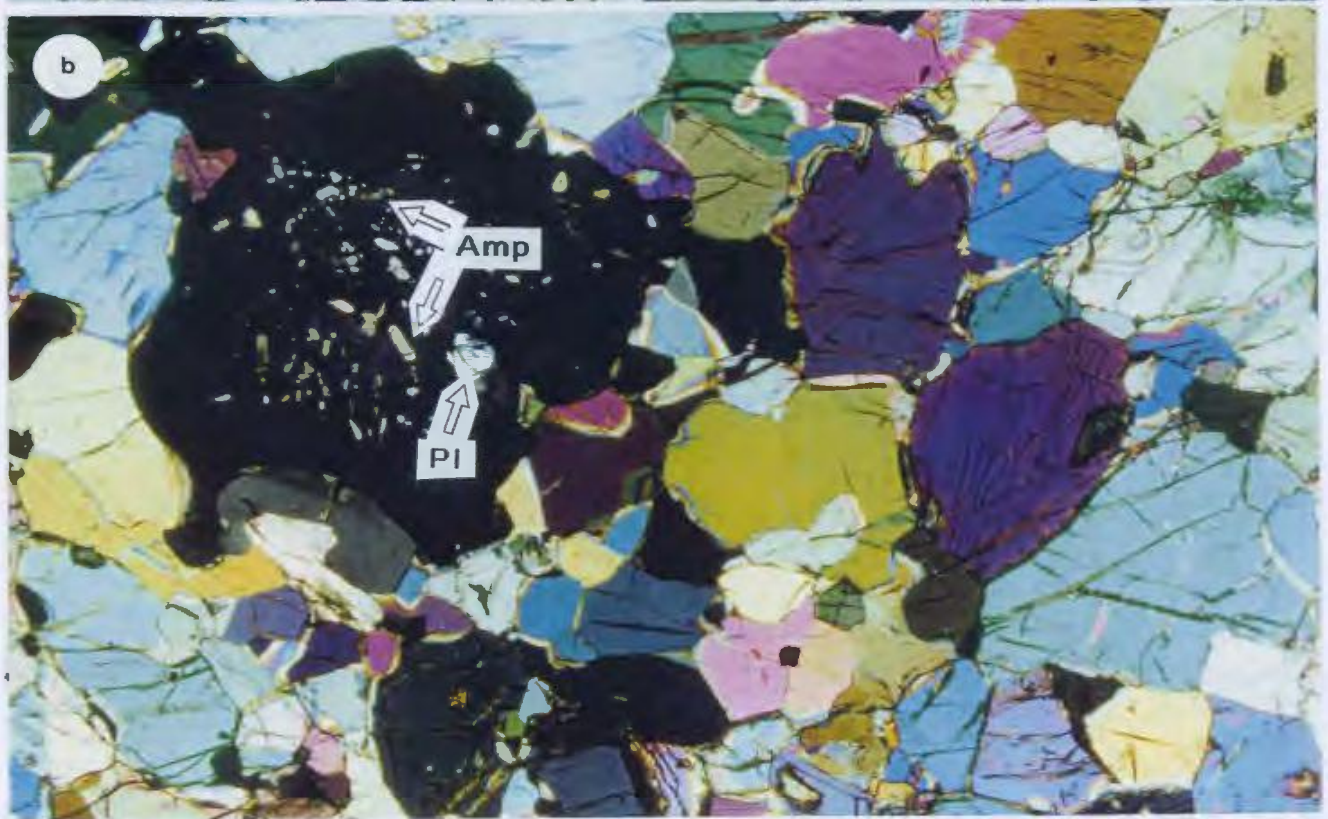
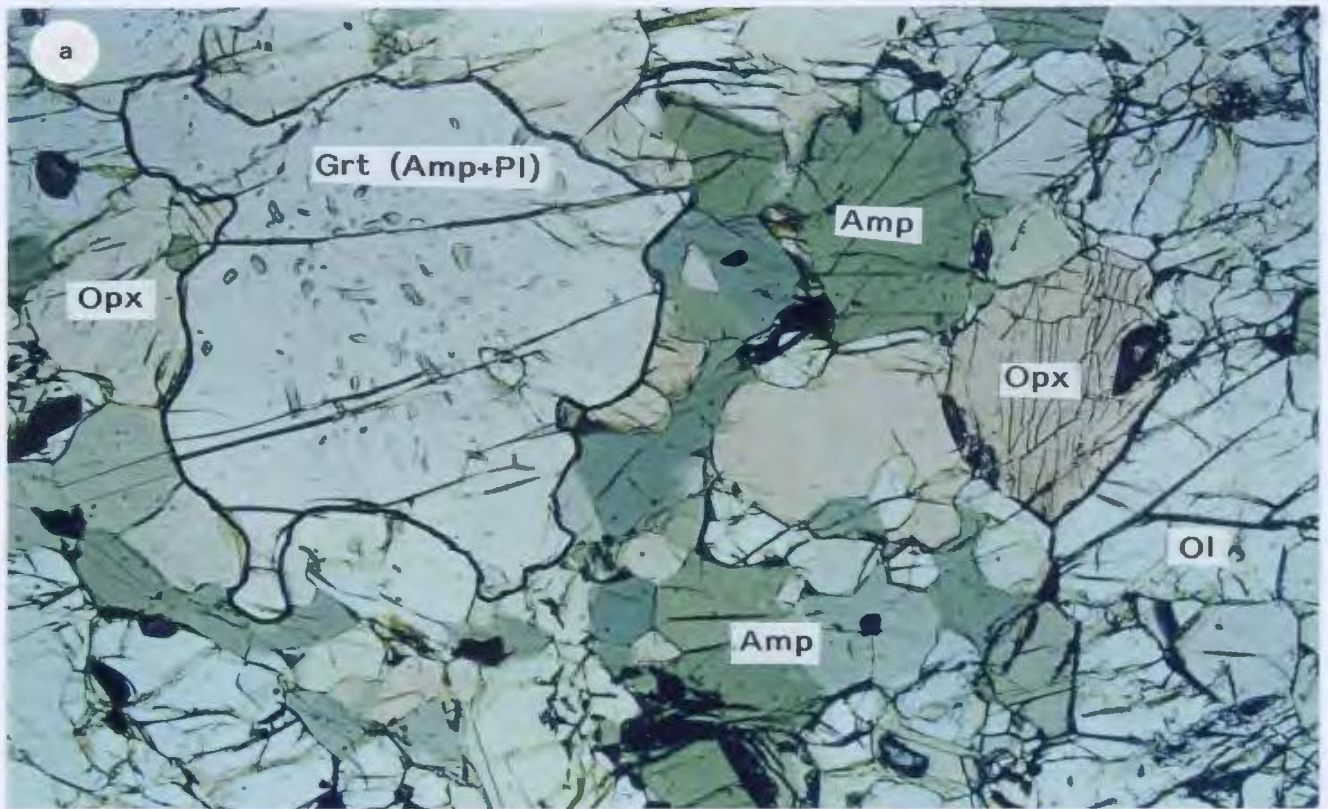


Plate A1.3 (cont.)

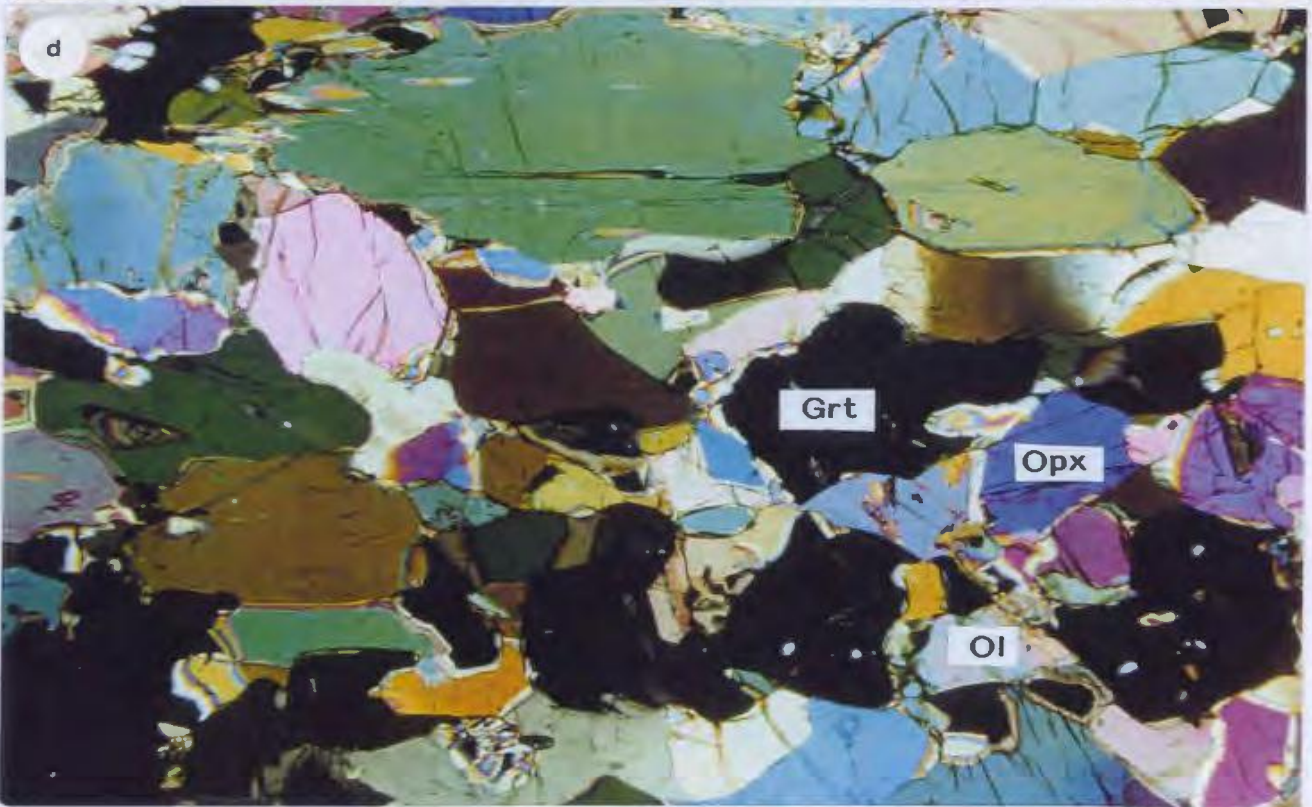
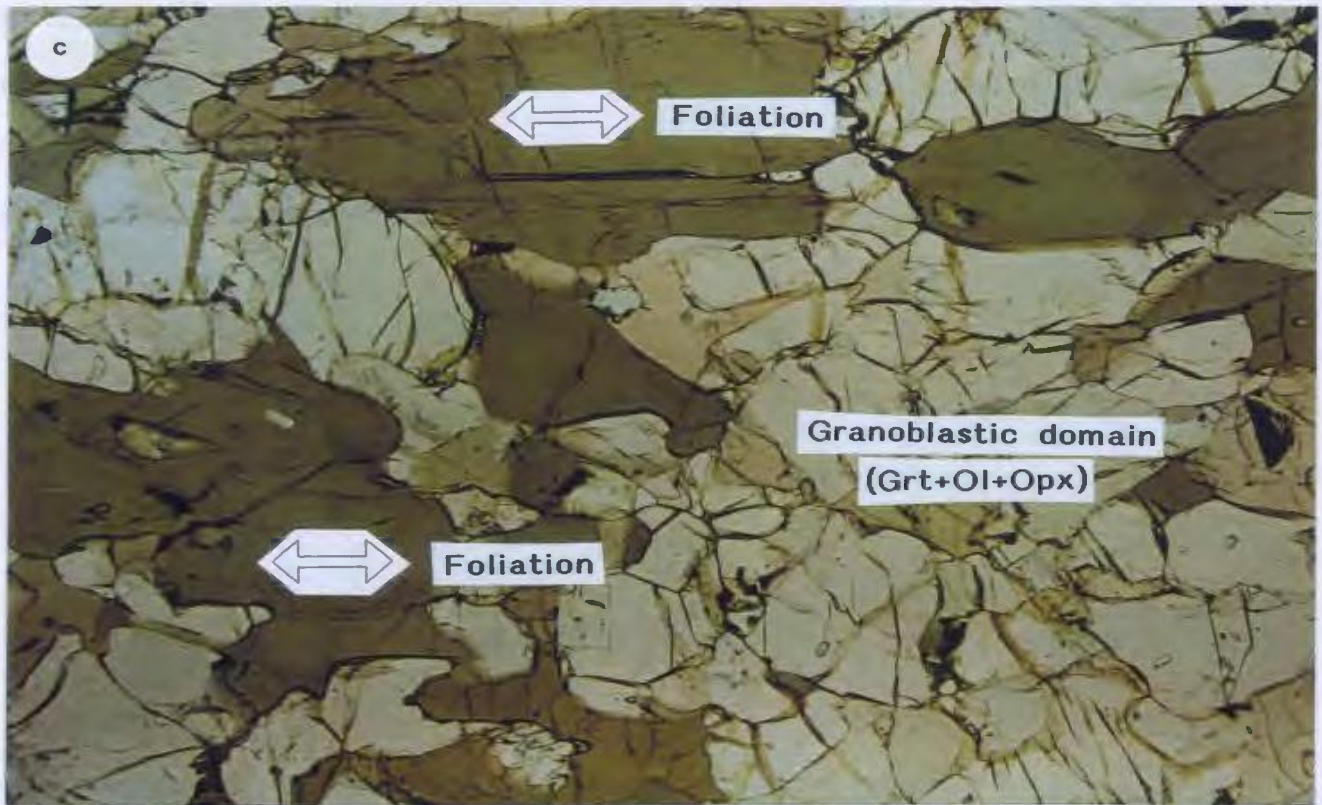


Plate A1.4 (a-b). *Garnet amphibolite (sample 2b)*: a) general texture with granoblastic foliated matrix of plagioclase, amphibole and quartz, with minor ilmenite and biotite, and a subhedral garnet porphyroblast, b) similar garnoblastic foliated matrix assemblage with an anhedral garnet porphyroblast, note the apparent rotation of the (colourless) plagioclase replacing the garnet (1.5 x 1 mm).

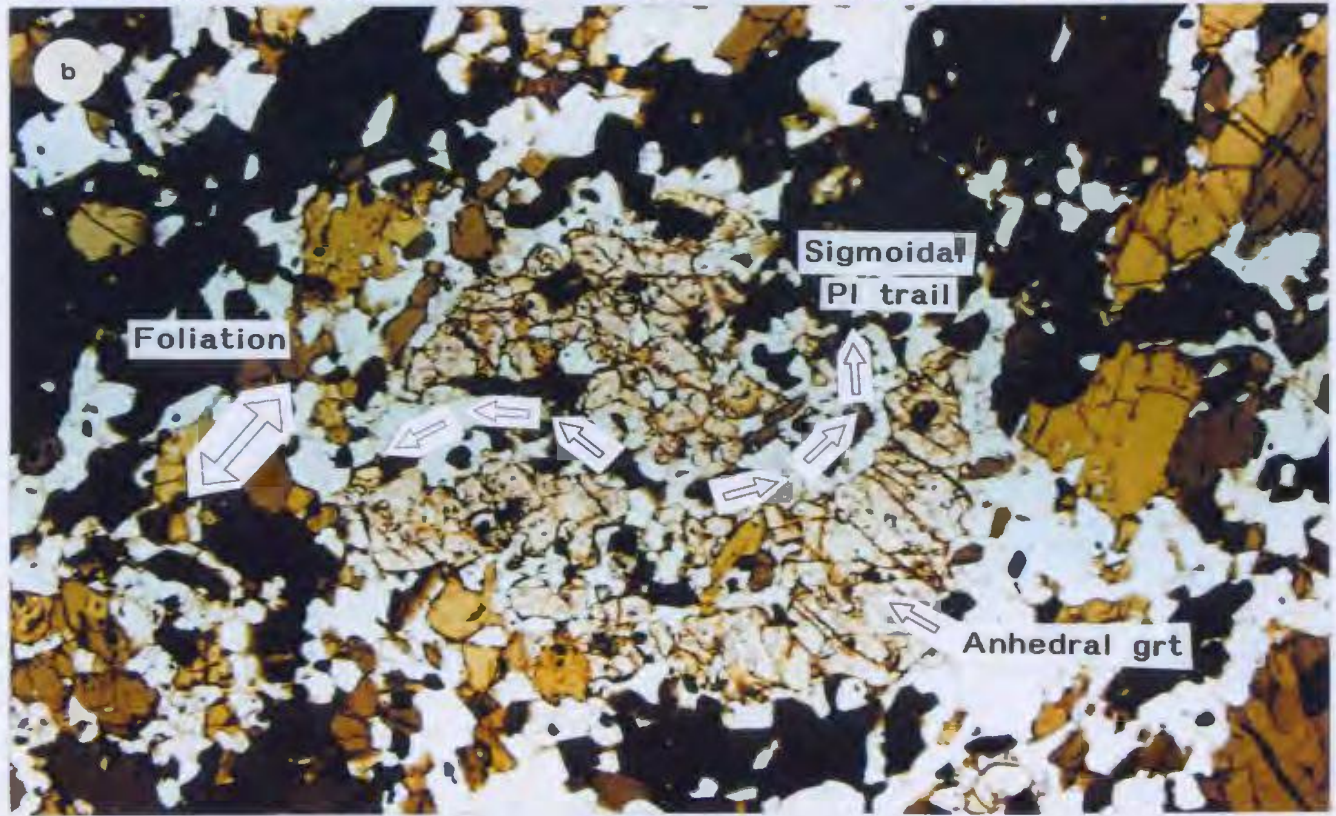
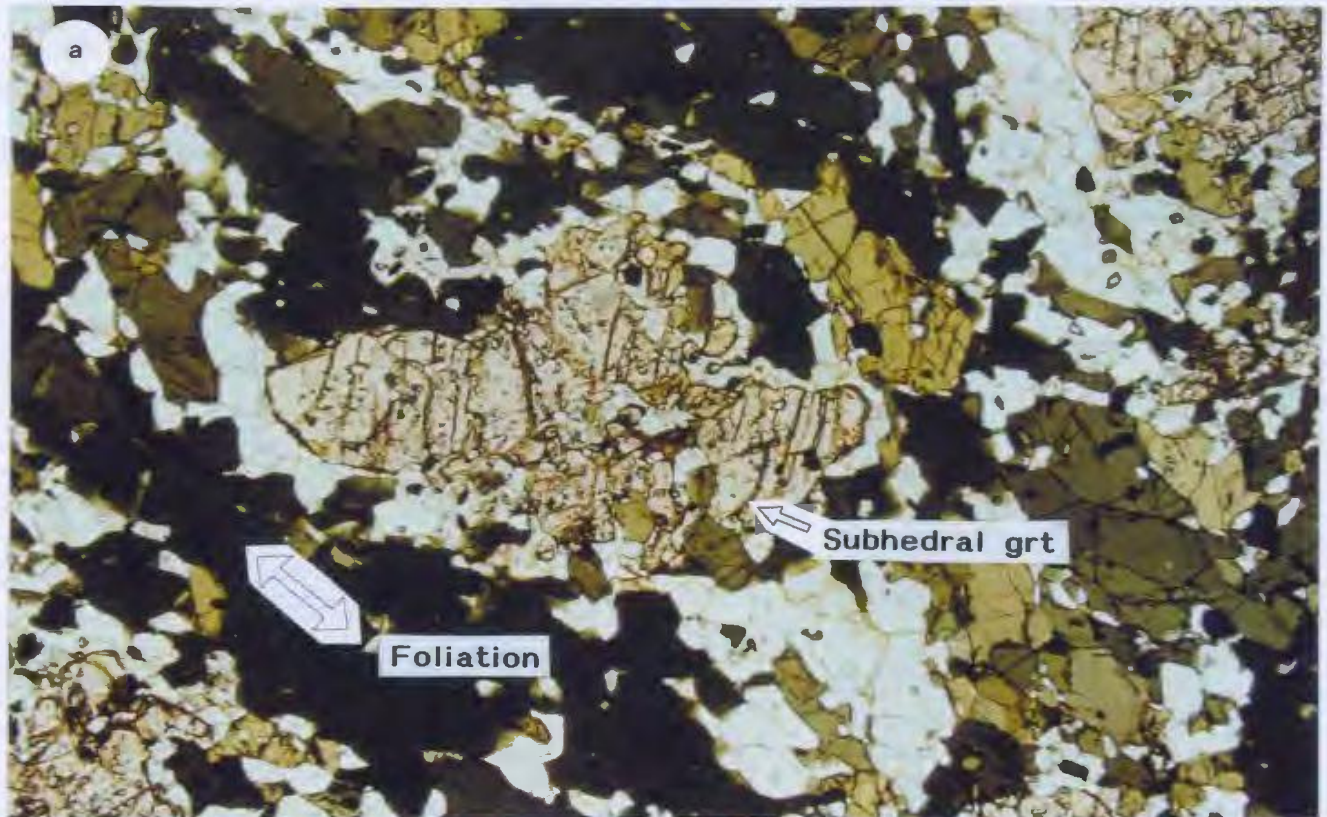


Plate A1.5 (a-b). *Nelsonite* (sample 9c): a) general texture showing partially preserved corona of garnet adjacent to amphibole, apatite, ilmenite and plagioclase which contains fine-grained spinel and corundum inclusions (1.5 mm x 1 mm), b) corona of garnet around ilmenite and apatite with abundant biotite inclusions and spinel in plagioclase (0.75 x 0.5 mm).

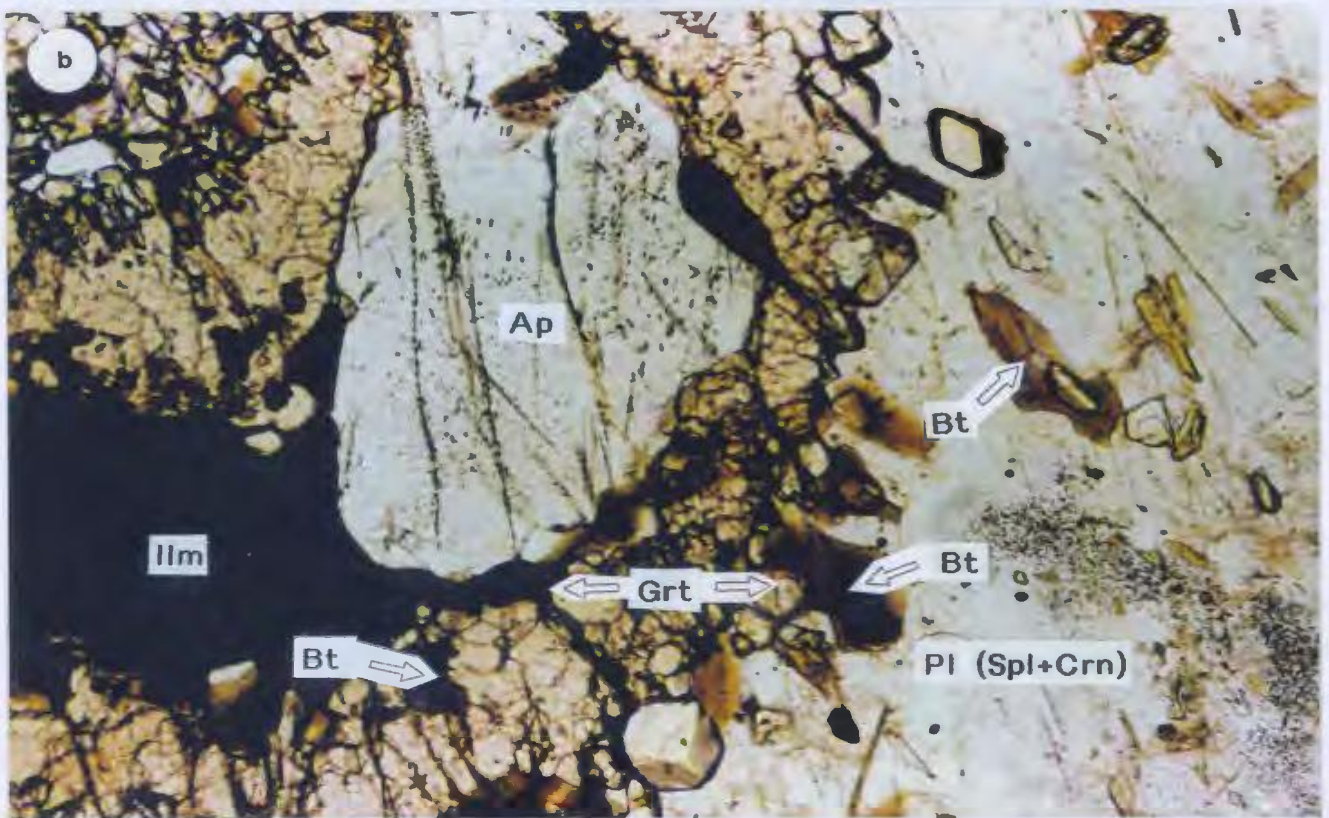
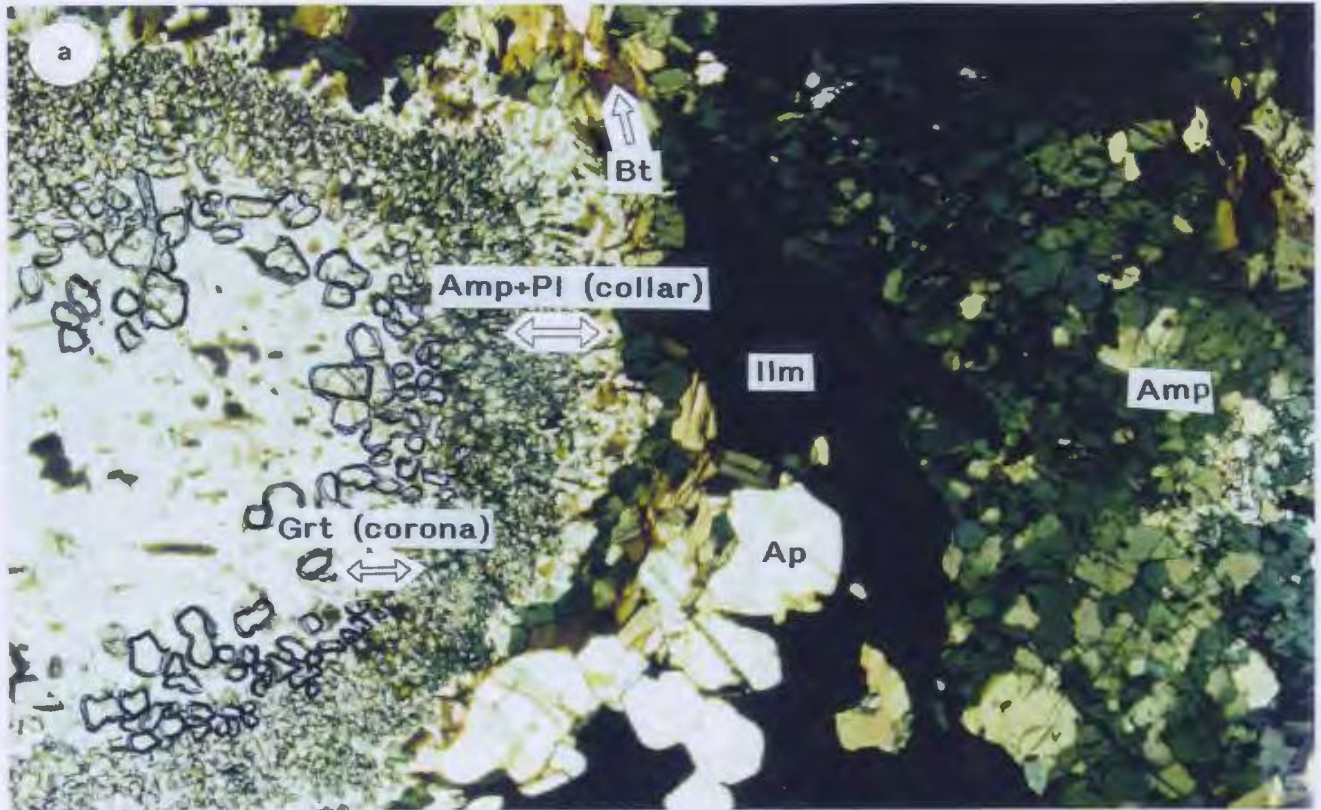


Plate A1.6 (a-b). *Olivine gabbro (sample 35b)*: a) garnet corona between ferromagnesian minerals and plagioclase which contains numerous kyanite and corundum inclusions, b) granoblastic area with garnet, amphibole, plagioclase (relict and recrystallized) and relict clinopyroxene which contains rutile inclusions (1.5 x 1 mm).

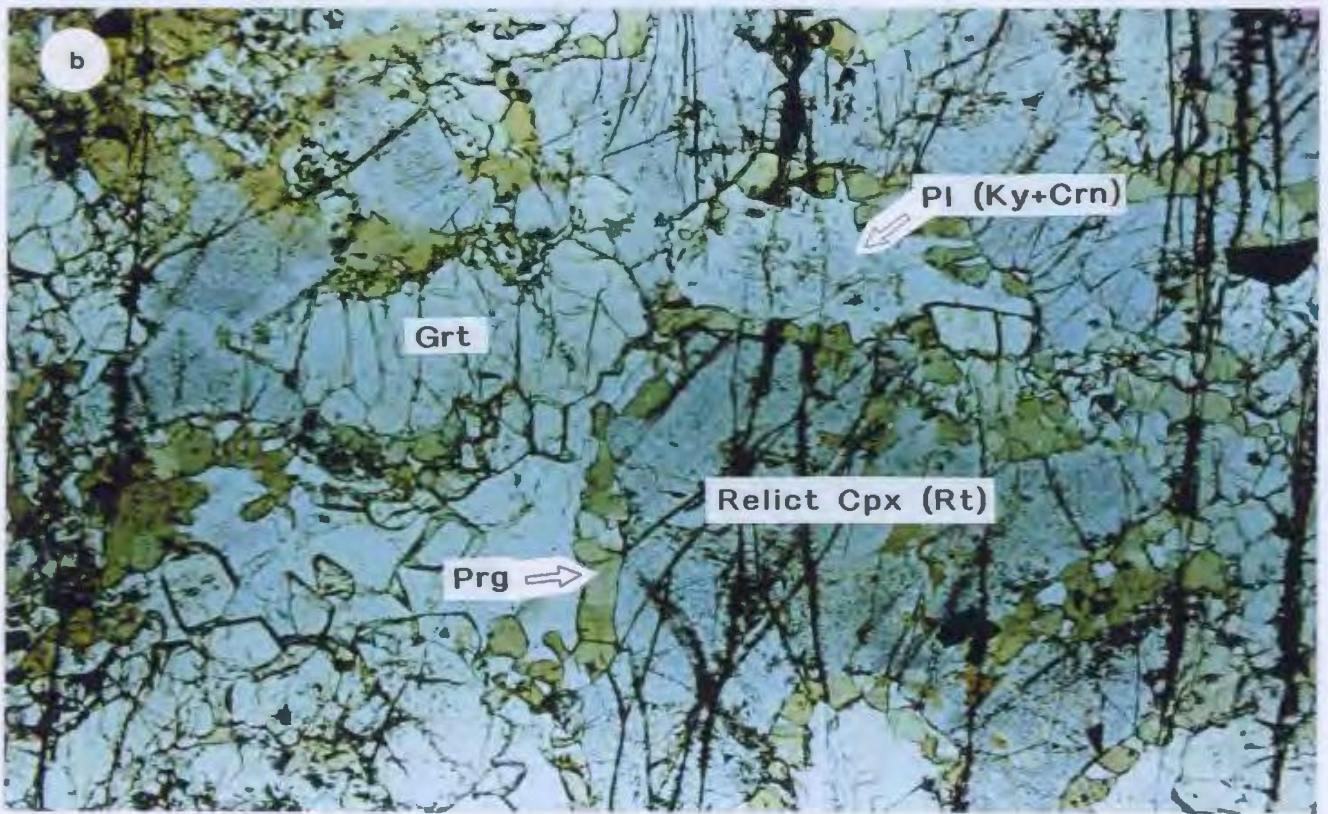
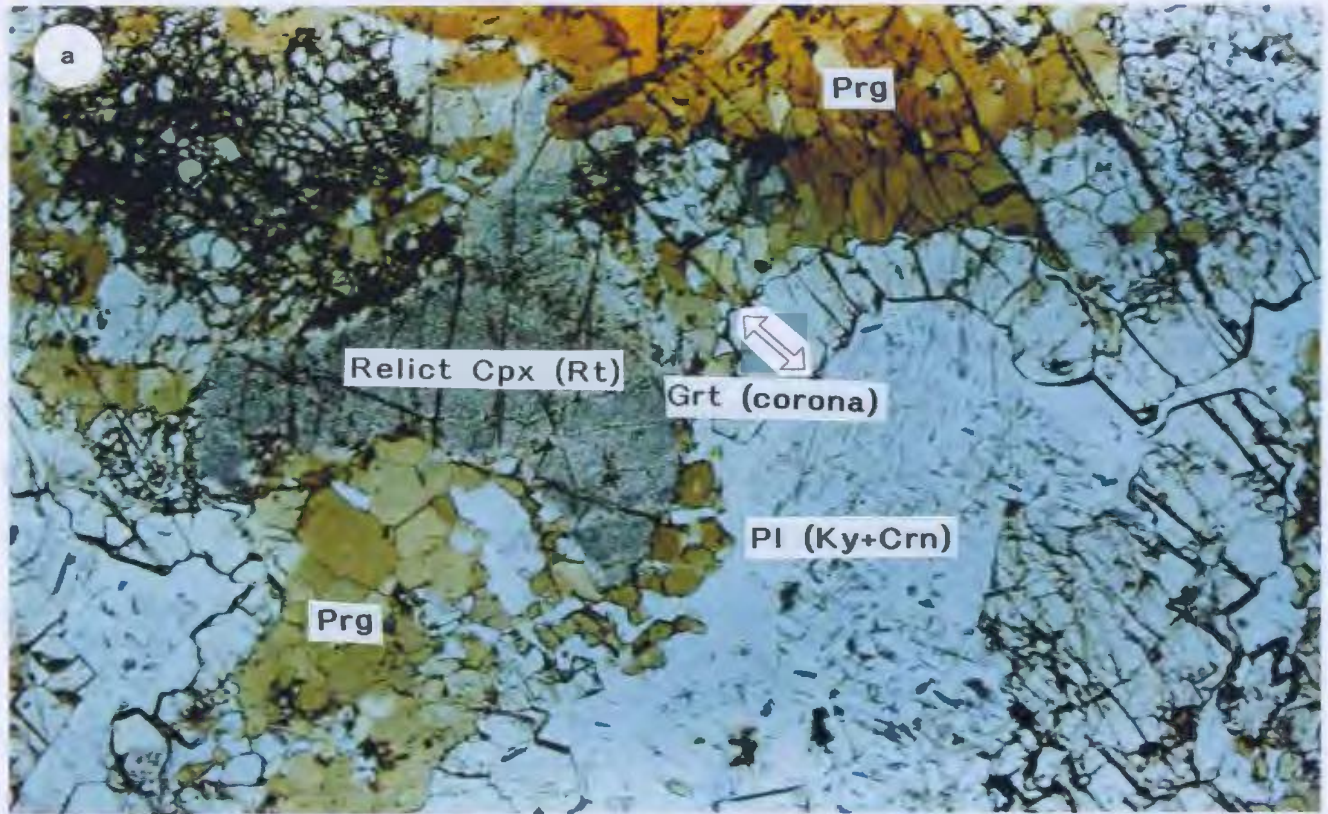


Plate A1.7 (a-d). *Coronitic metagabbro (sample 123)*: a) coronitic metagabbro showing relict plagioclase rich in spinel inclusions and orthopyroxene pseudomorphs after olivine with coronas of clinopyroxene and small plagioclase (decompressional) collars. Coronas of pargasite are present around ilmenite (5 × 3.4 mm), b) close-up of a corona assemblage with an relict olivine partially pseudomorphed by orthopyroxene c), garnet-bearing corona where areas in the assemblage locally preserve garnet-clinopyroxene contacts and others display pargasite bearing plagioclase collars (1.5 × 1 mm), d) extensively reequilibrated corona assemblage with resorbed garnet corona and wide pargasite bearing plagioclase collar (0.75 × 0.5 mm). Note the complete replacement of olivine by orthopyroxene in the last two photomicrographs.

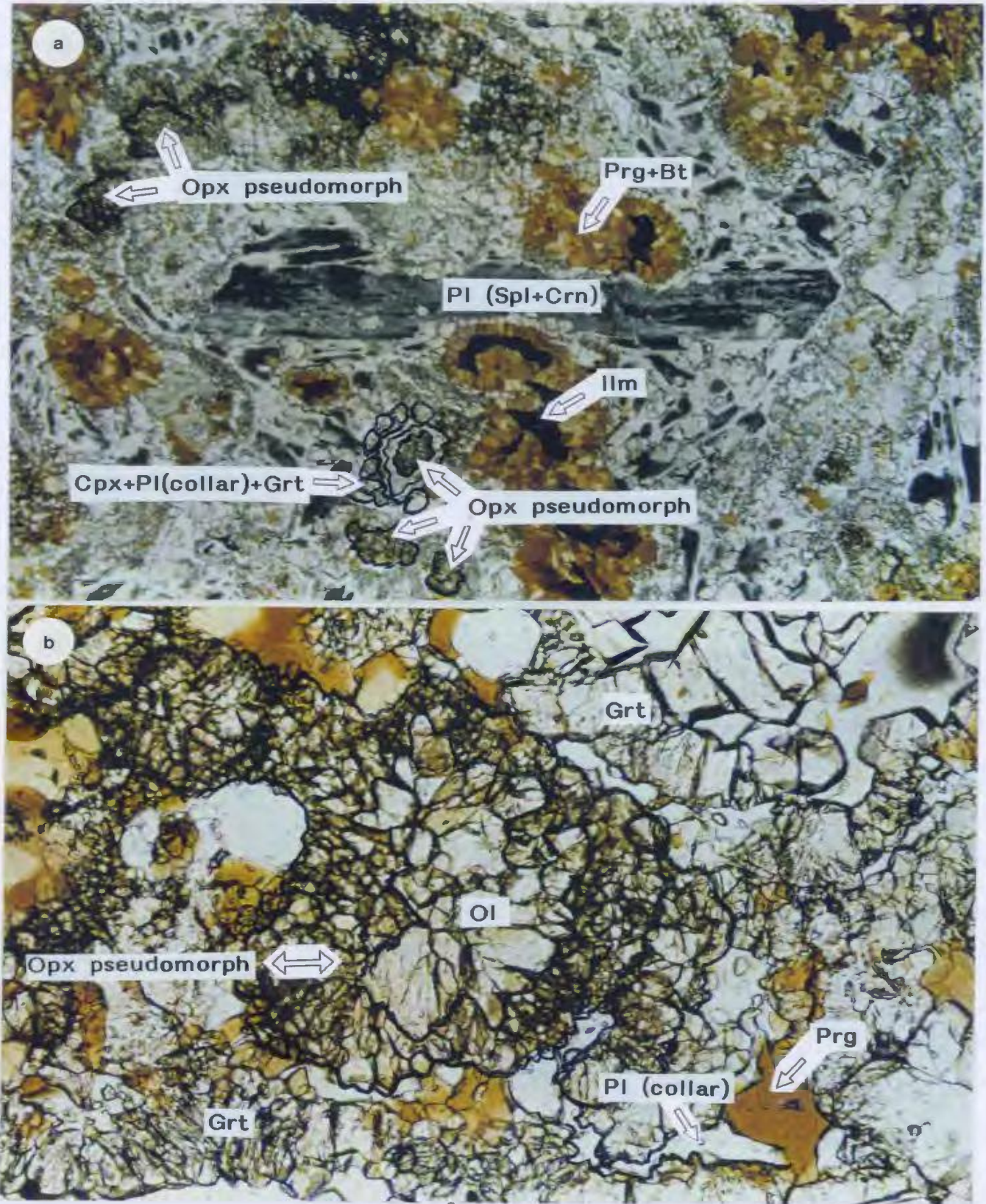


Plate A1.7 (cont.)

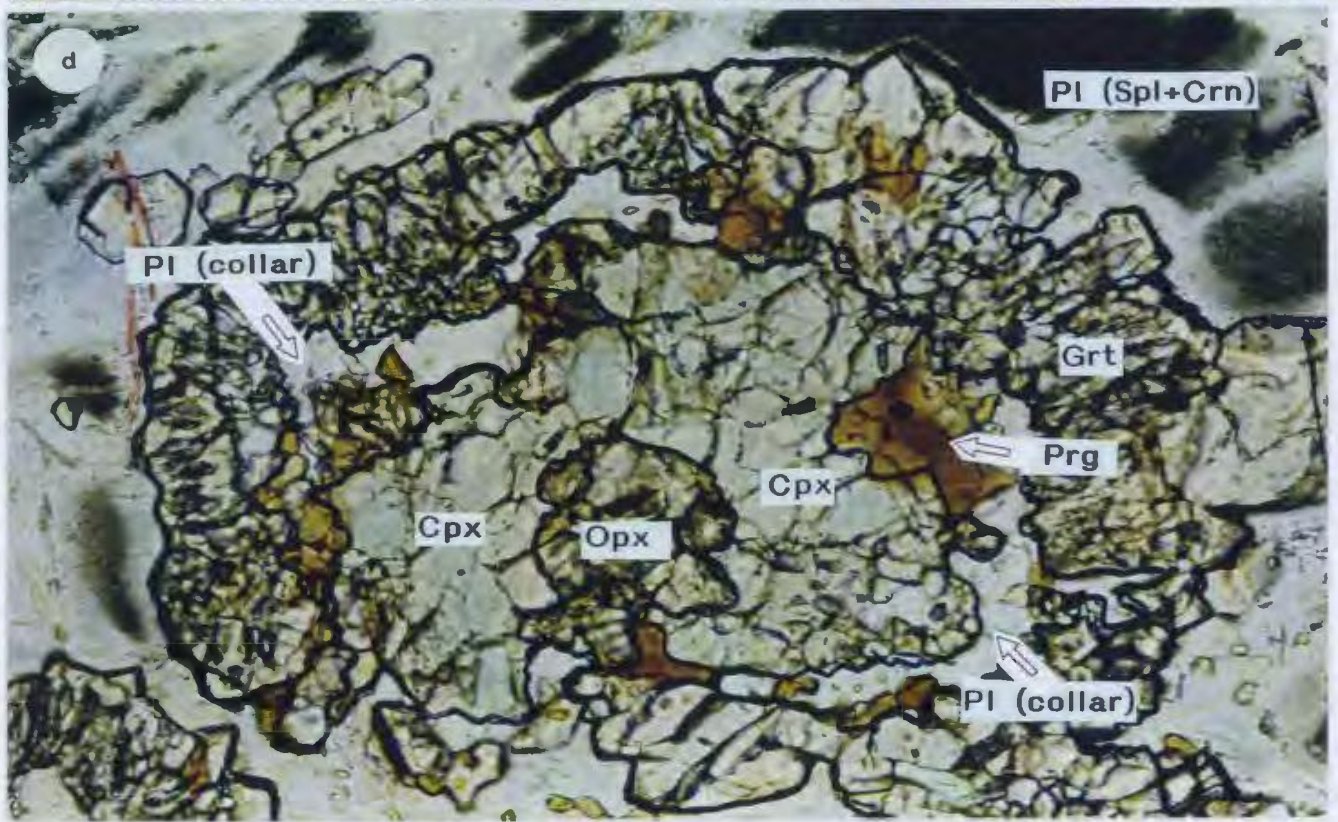
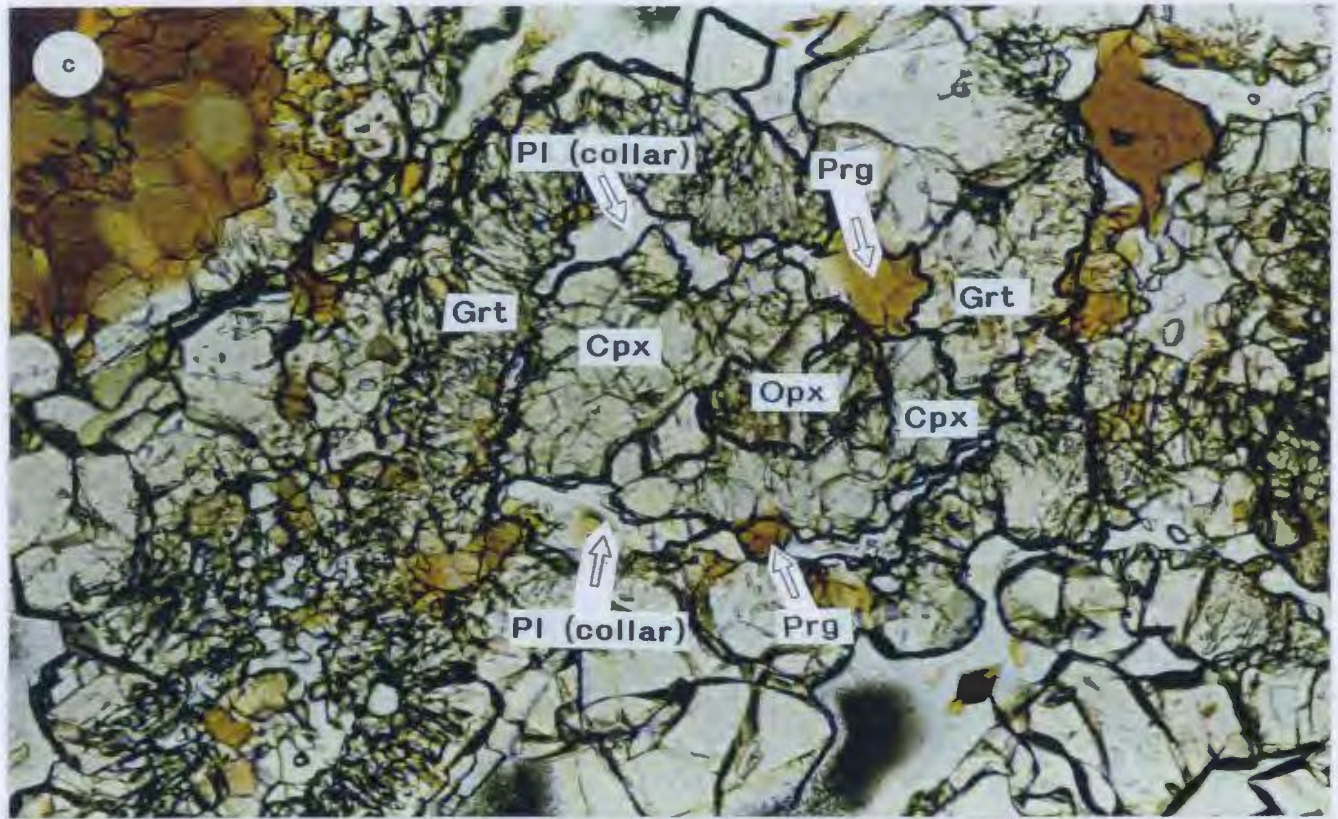


Plate A1.8 (a-b). *Transitional metagabbro (sample 85b)*: a) general texture showing garnet pseudomorphs after original plagioclase laths and major (decompressional) regeneration of plagioclase, b) garnet corona around a large plagioclase xenocryst which contains spinel and corundum inclusions (1.5 x 1 mm).

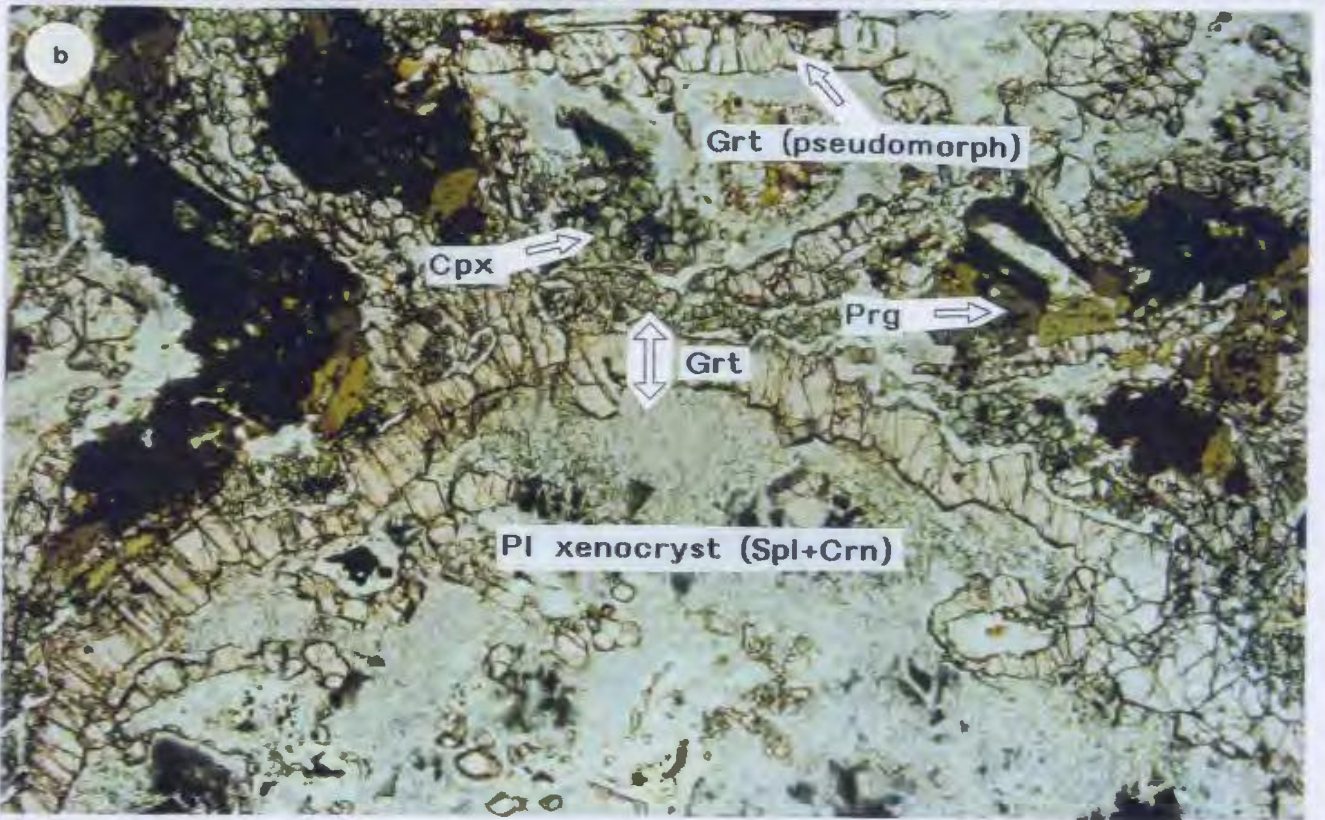
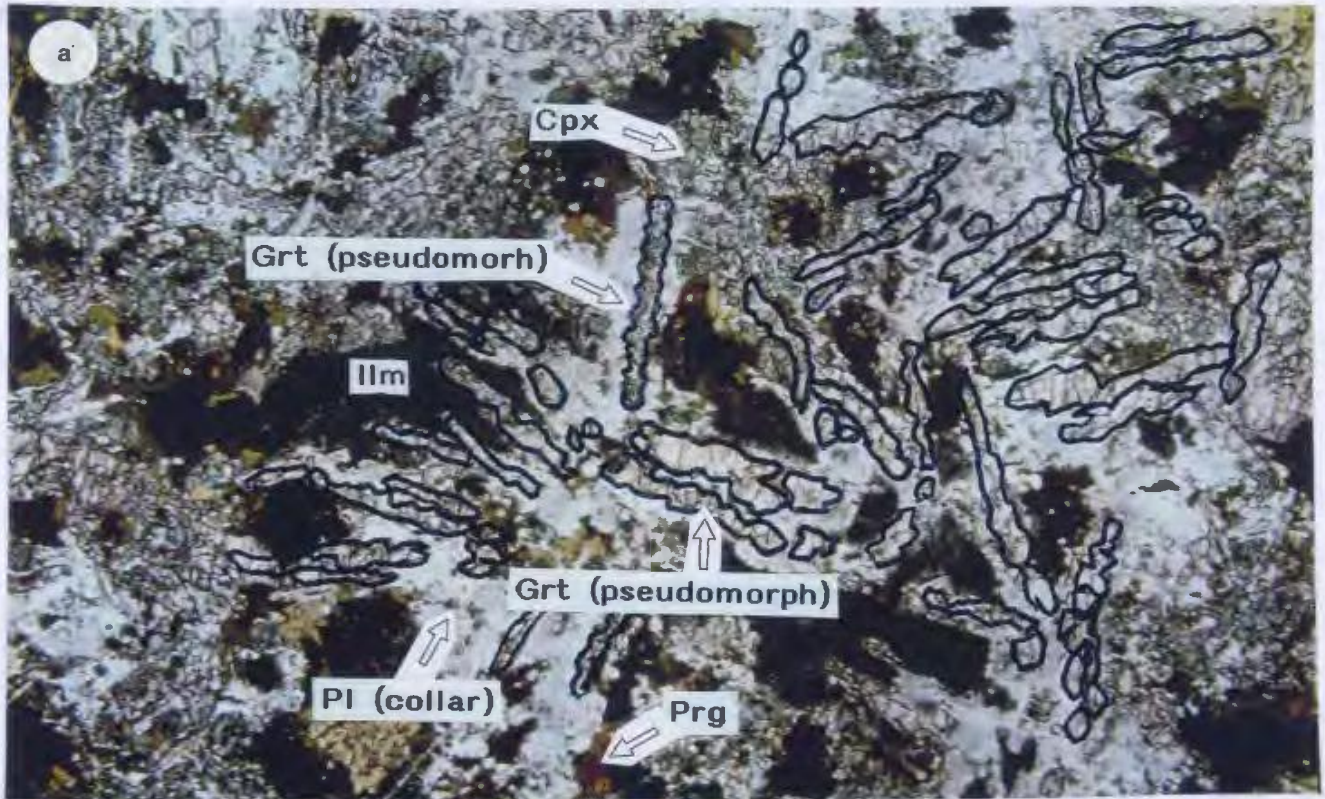


Plate A1.9 (a-b). *Eclogite (sample 21)*: Garnet pseudomorphs after plagioclase and an omphacite-rich granoblastic matrix. Note the relict "ribbon" plagioclase with abundant spinel and corundum inclusions inside the large garnet pseudomorph near the center of the image (1.5 x 1 mm), b) coronas of orthopyroxene (small), clinopyroxene and garnet between olivine and plagioclase xenocrysts in an eclogite. The plagioclase contains kyanite and corundum inclusions. (2.5 x 1.7 mm).

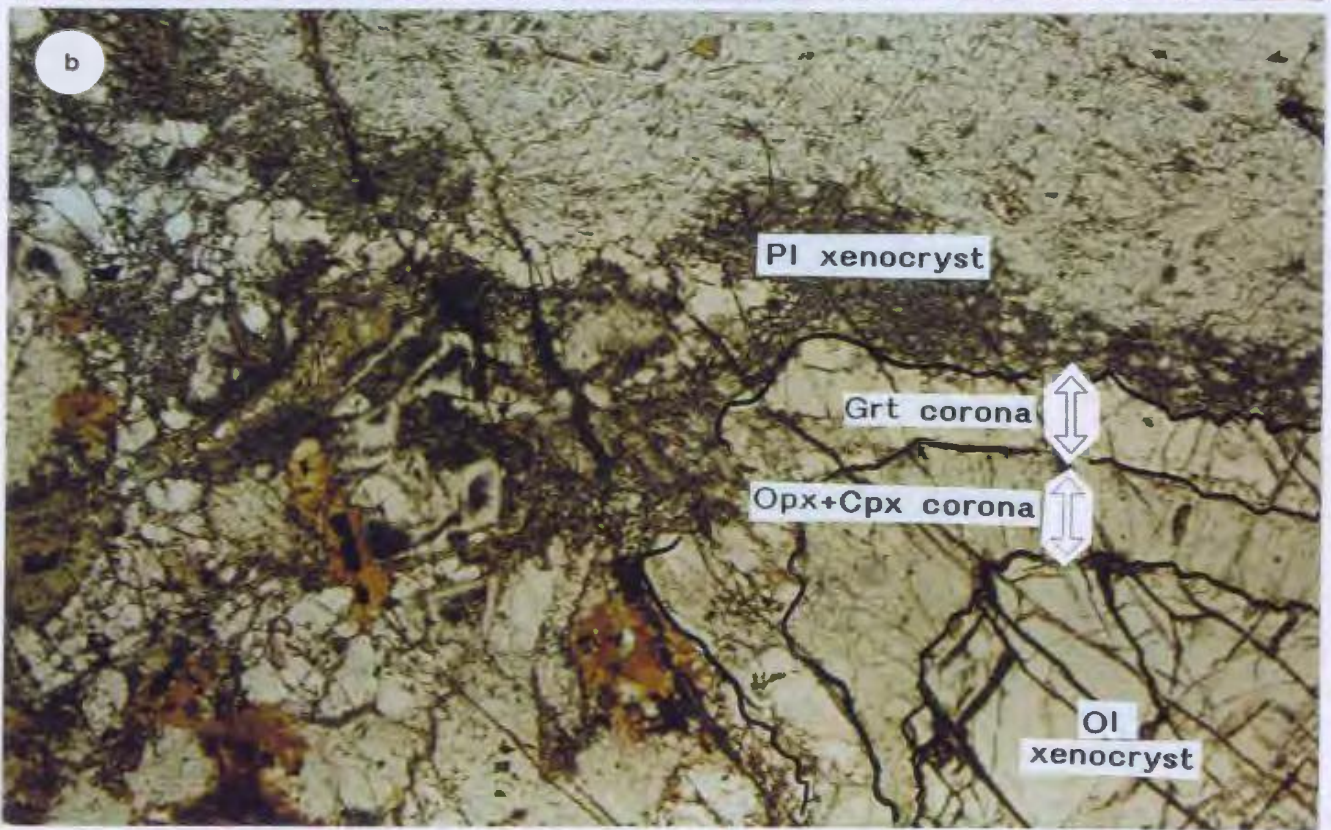
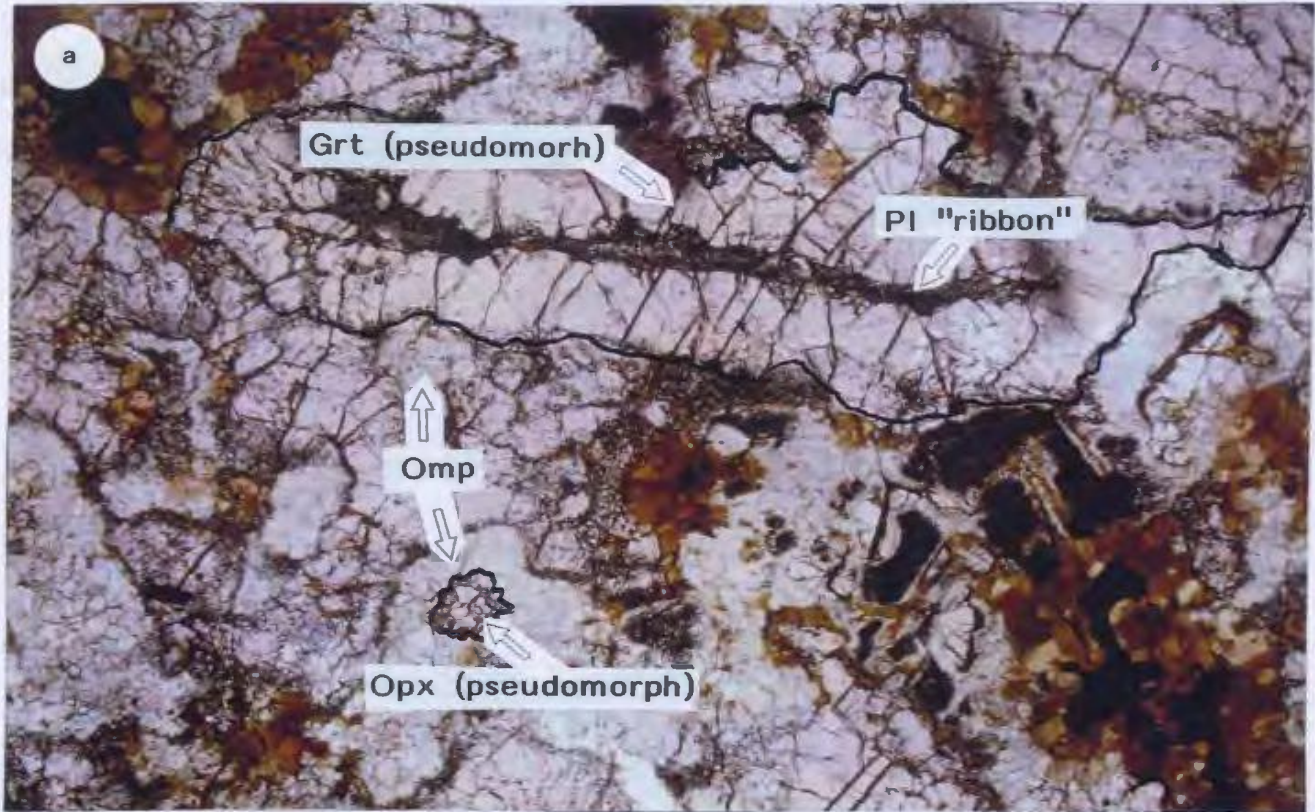


Plate A1.10 (a-b). *North Bay anorthosite (sample 316) and marginal gabbro (sample 268a):*

Photomicrographs showing the general texture of a) the North Bay anorthosite (with a garnet-pargasite-rutile metamorphic assemblage) and b) marginal gabbro showing oikophitic texture (clinopyroxene oikocryst) with spinel-rich plagioclase and pargasitic amphibole (2.5 x 1.7 mm).

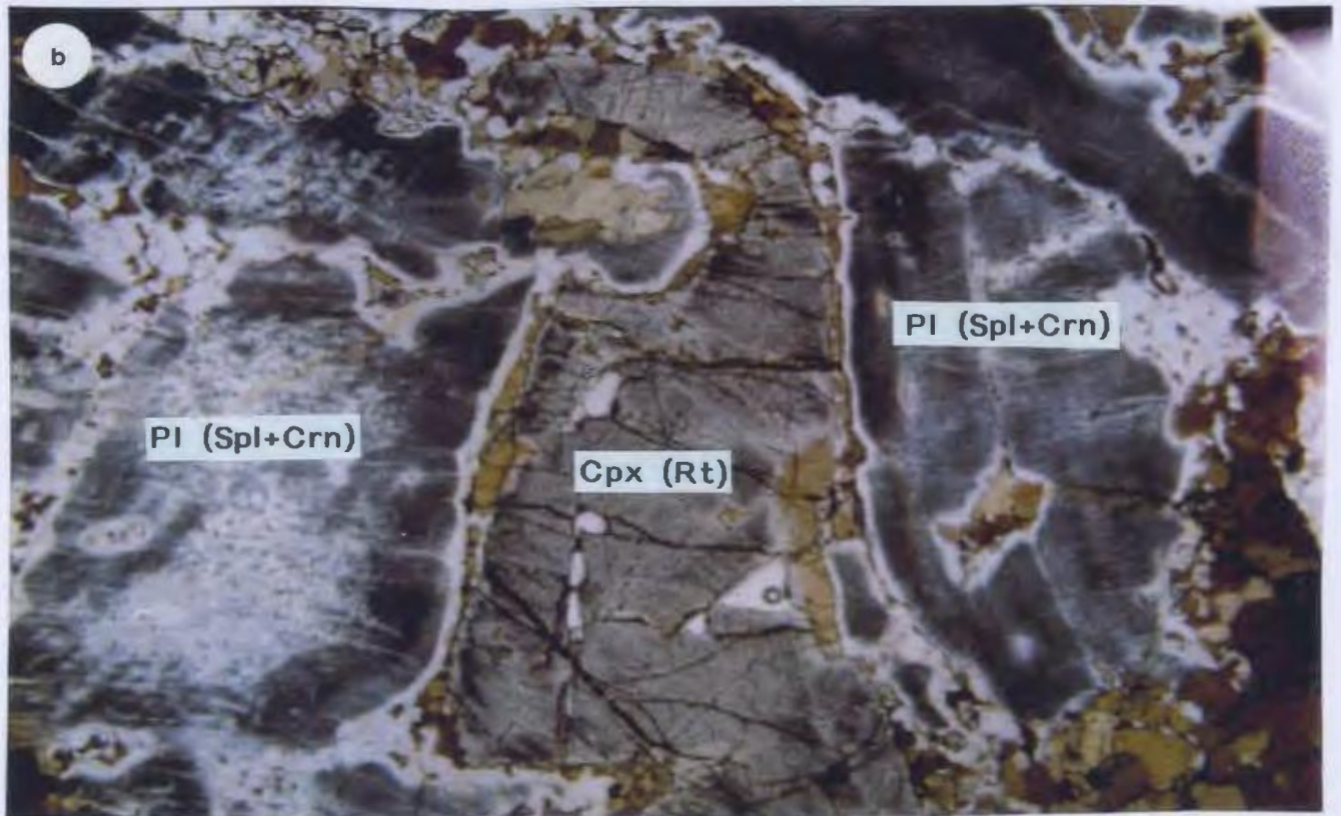
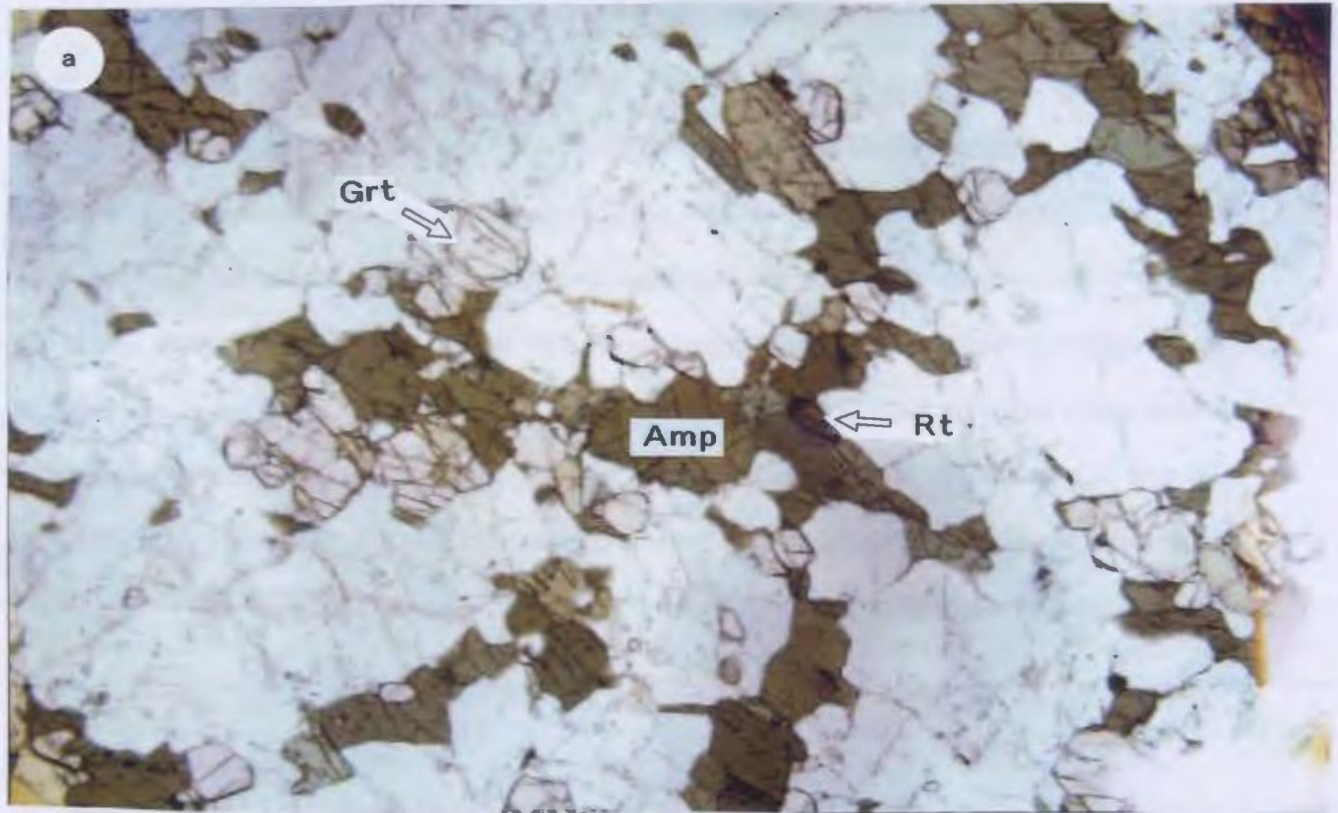


Plate A1.11 (a-d). *Migmatitic garnet amphibolite (sample 313)*: Outcrop of migmatitic-garnet amphibolite showing large poikiloblasts of garnet in close association with plagioclase-rich leucosomes. Scale card is in cm. b) garnet poikiloblast with inclusion-rich core and inclusion-free rim. The sigmoidal inclusion assemblage in the core consists of plagioclase, quartz, and ilmenite, which gives way to rutile near the inclusion-free inner rim. Note how the rutile inclusions are aligned along their long axis, suggesting entrapment against the growing face of the garnet. c) titanite-bearing garnet rim (overgrowth) around a large poikiloblast showing the transition from migmatitic assemblages in the core to amphibolite assemblages associated with the matrix (2.5 x 1.7 mm). d) close-up of titanite and plagioclase replacing garnet, rutile and quartz near the rim of a poikiloblast. Titanite does not show any sygmoidal pattern (0.75 x 0.5 mm).

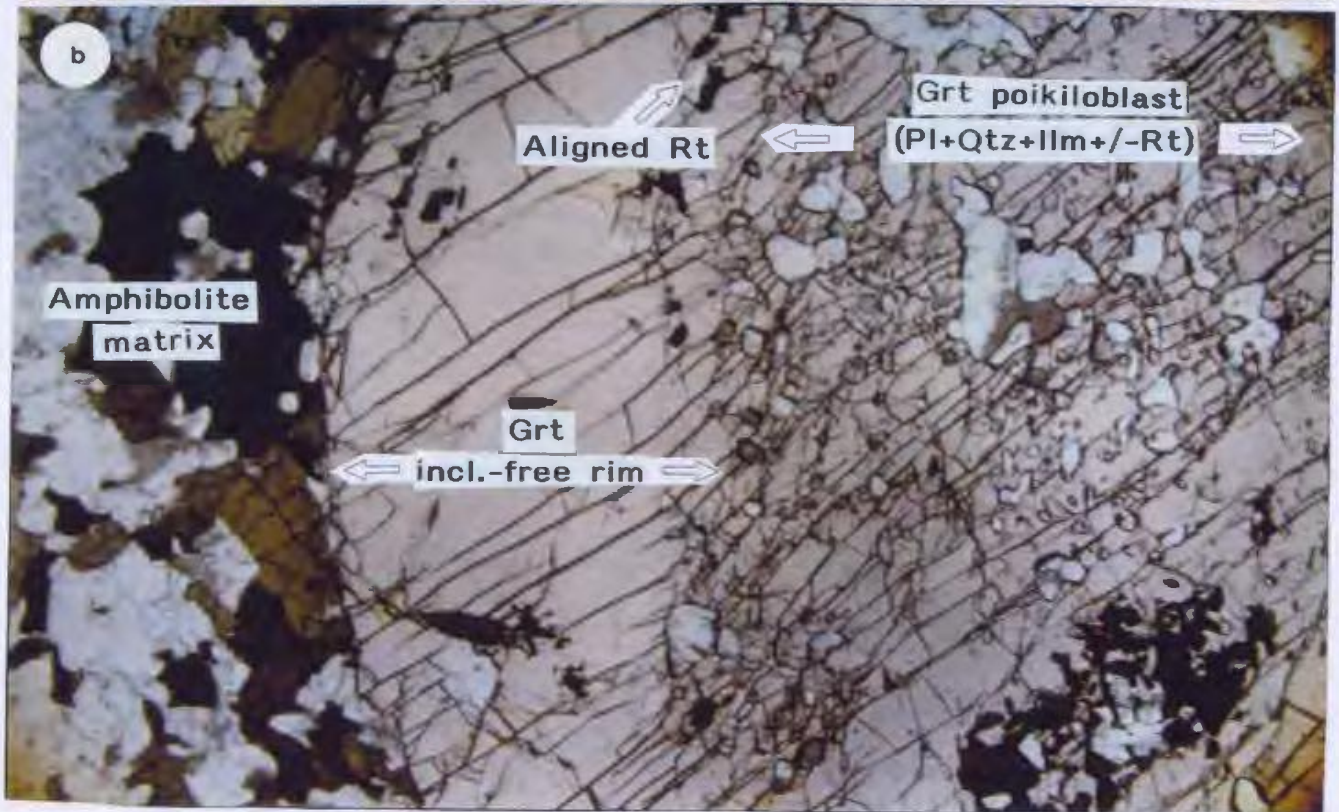
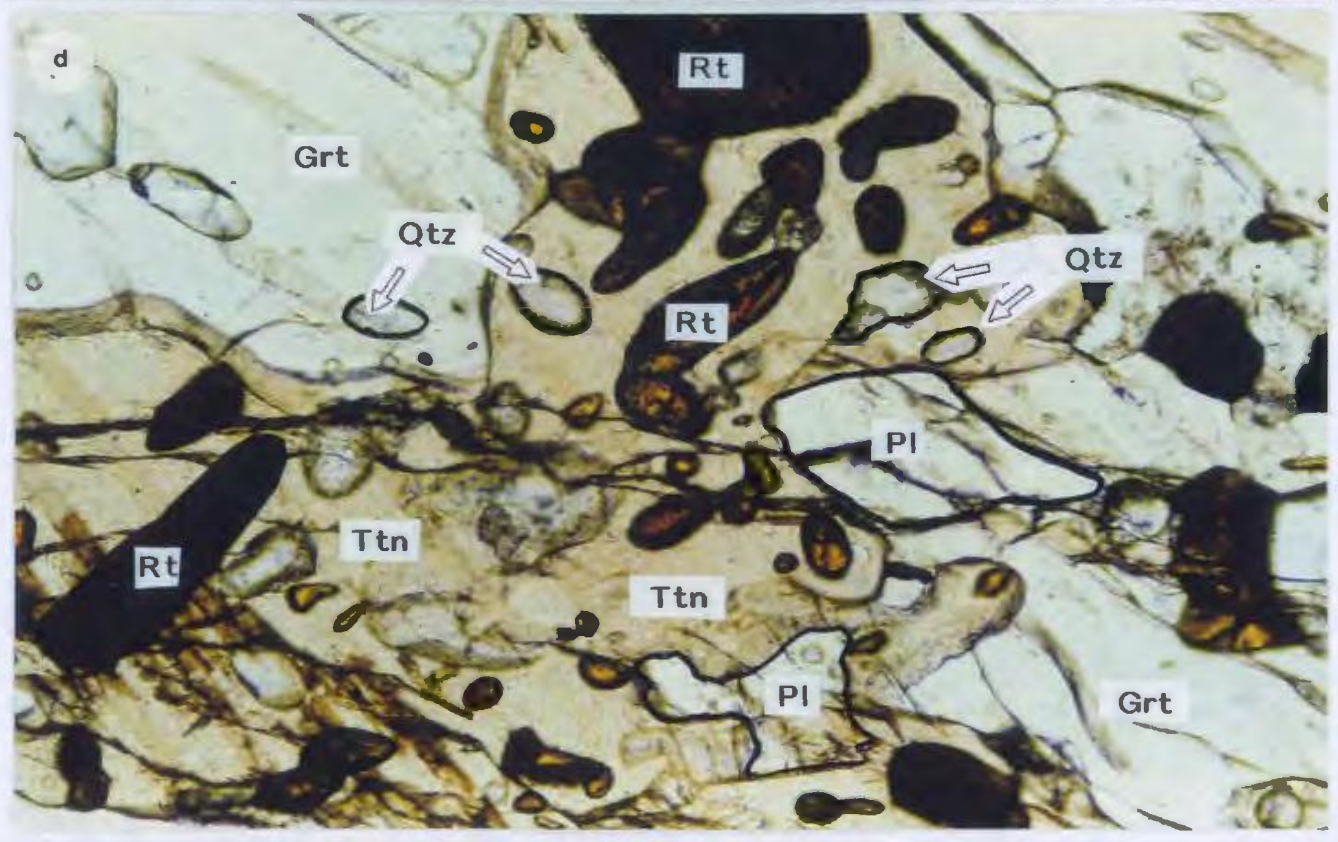
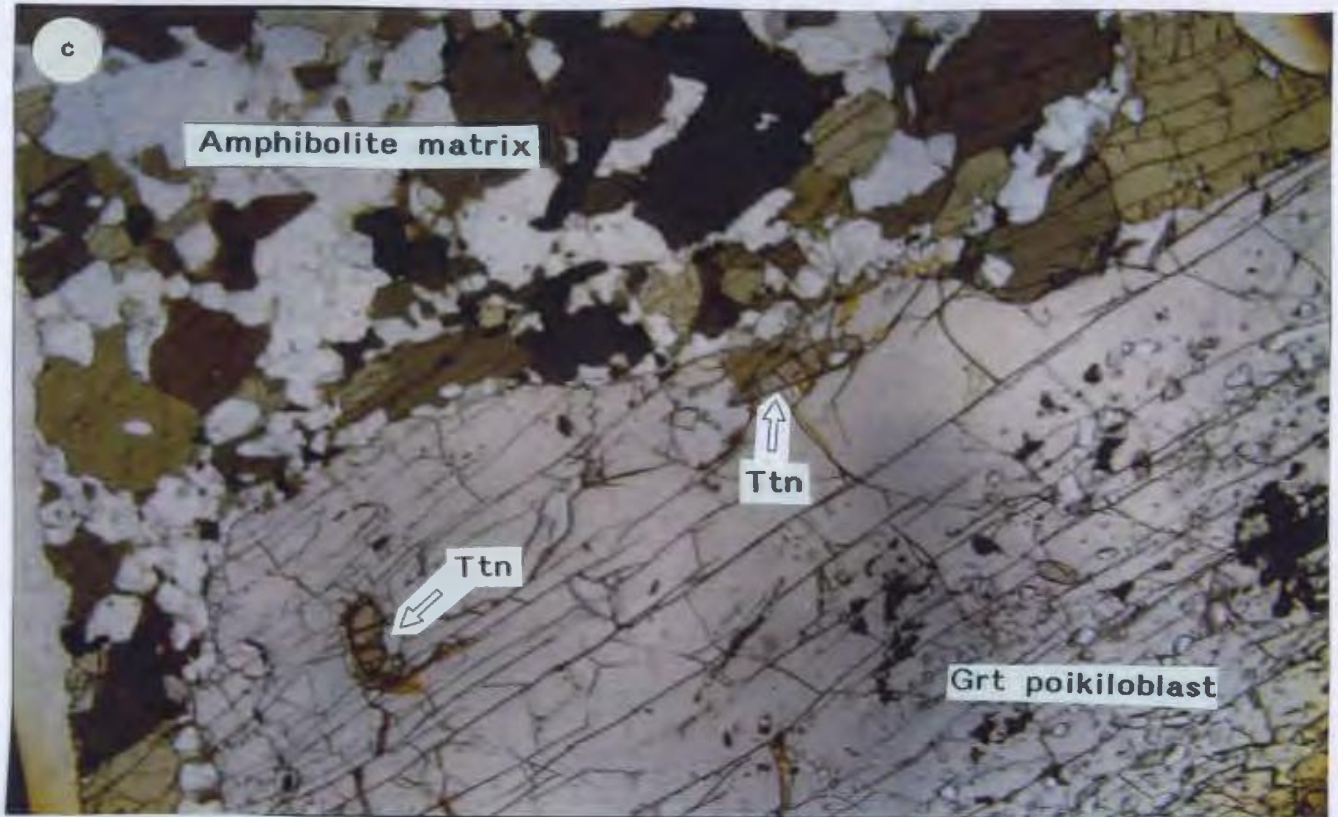


Plate A1.11 (cont.)



A.2. Cathodoluminescence (CL) microscopy*A.2.1. CL procedure*

Selected polished sections were examined by cathodoluminescence (CL). The CL-properties were examined using a Nuclide Luminoscope CL-unit mounted on a Wild-Heerburg continuous zoom binocular microscope at 10-32 times magnification. 10 times oculars and a double magnifier placed between the sample chamber and the objective give 200-640 times combined magnifications. However, working distances of more than 40 mm give an minimum field of view of 1.7 mm. The sample chamber was kept under vacuum conditions of 50-70 millitorr. Accelerating voltages varied between 10-16 kV with beam currents of 0.1-2 mA. Images were collected with an automated 35 mm camera system (although some shots were manually controlled) on 35 mm 1000 or 1600 ASA colour film. Exposure times varied from a few seconds to over 30 minutes.

A.2.2. CL activators

The emission of visible light via electron bombardment of a materials surface is known as Cathodoluminescence (CL) is caused principally by excitation of activator elements which are present in trace quantities (<0.1 wt%), although lattice defects also play an important role particularly in quartz. Typical activator elements in refractory minerals are Mn, Fe, Ti, Cr, Ga, Y, and REE's, which are incorporated during growth. Other elements, e.g. Hf and Y may enhance luminescence in certain cases. Several geologically important minerals show CL such as quartz, feldspar, zircon, apatite, and carbonates, Al_2SiO_5 silicates and even ore minerals such as sphalerite. Most studies focus on growth structures in carbonates and diagenetic from detrital minerals. In igneous and metamorphic rocks CL-studies have centred on unravelling the complex growth history of zircon and zoning of quartz and feldspar to elucidate the crystallization history of granites (e.g. Vavra 1990; Watt et al. 1997). However, CL has rarely been

applied to metamorphic rocks. Table A.1 gives a list of the minerals examined in this study, their CL properties and possible activators.

Mineral	CL colours	Textures	Activators (reference)
Plagioclase	Blue	Relict igneous crystals and recrystallized areas i.e. collars. High-P growth in granuloblastic rocks.	Ti, Al (Mariano et al. 1973; Gotze et al. 1999).
	Green-yellow	Secondary growth after garnet in amphibolite.	Mn, Fe ³⁺ (Mariano et al. 1973; Gotze et al. 1999).
Quartz	Red	High-P growth in granuloblastic rock (fast cooling).	Lattice defects and Fe ²⁺ (Zinkernagel 1978).
	Dull brown	Migmatitic growth and matrix amphibolite (slow cooling).	Lattice defects and Fe ²⁺ (Zinkernagel 1978).
Kyanite	Bright red	Inclusions in garnet and plagioclase indicative of high-P assemblages.	Cr ³⁺ (Gaal 1976).
Apatite	Bright yellow	Relict igneous crystals.	Mn (Marshall 1988; Mitchell et al. 1997)
	Violet-blue	Probable high-grade growth.	REE, (Mitchell et al. 1997; Murray and Oreskes 1997)
Zircon	Golden yellow	Zoned igneous crystals.	Dy (Mariano 1978; Marshall 1988)
	Lavender blue	Metamorphic crystals and saccharoidal growth after baddeleyite.	Dy with Hf, and Y (Oso 1976).

Table A.1. CL colours, textures revealed and possible activators in minerals examined in this study.

The following CL images (six from rocks in the Lac Espadon suite and two from the Fe-Ti gabbros in the Baie du Nord segment) show a range of textures as described in Table A.1. These exclude high magnification CL images of zircon (collected on a scanning electron microscope) which are presented in section A.3.2. The dimensions of the images are indicated in the figure captions (in brackets).

Plate A2.1 (a-b). CL images of a) plagioclase relicts and regenerated (decompressional) plagioclase from a transitional metagabbro (sample 85b). Note the brighter blue CL-colors of the regenerated plagioclase and the twinning preserved by the relicts. Purple CL-colors denote small apatite crystals (1.75 x 0.5 mm), b) xenocrystic eclogite (sample 21) showing bright red kyanite inclusions in a (blue) plagioclase xenocryst (1.5 x 0.3mm).

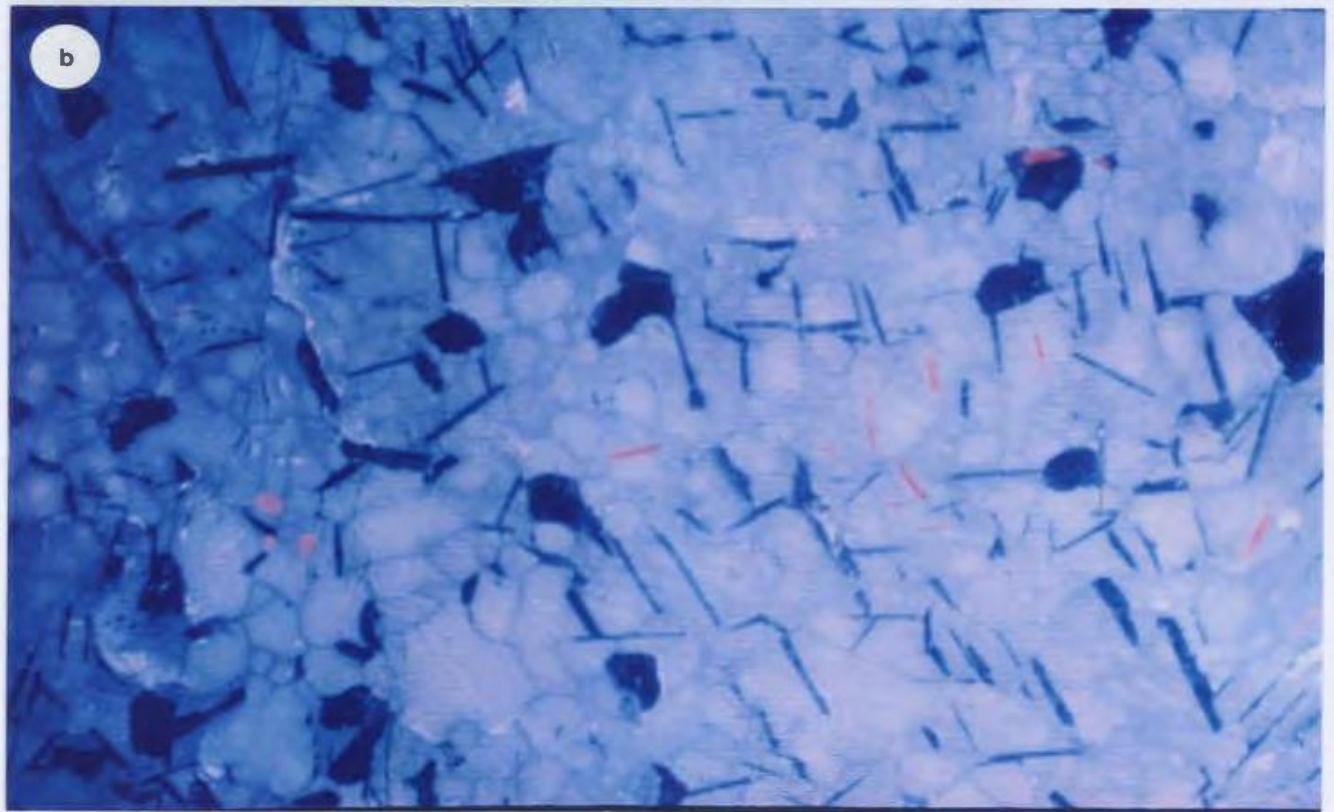
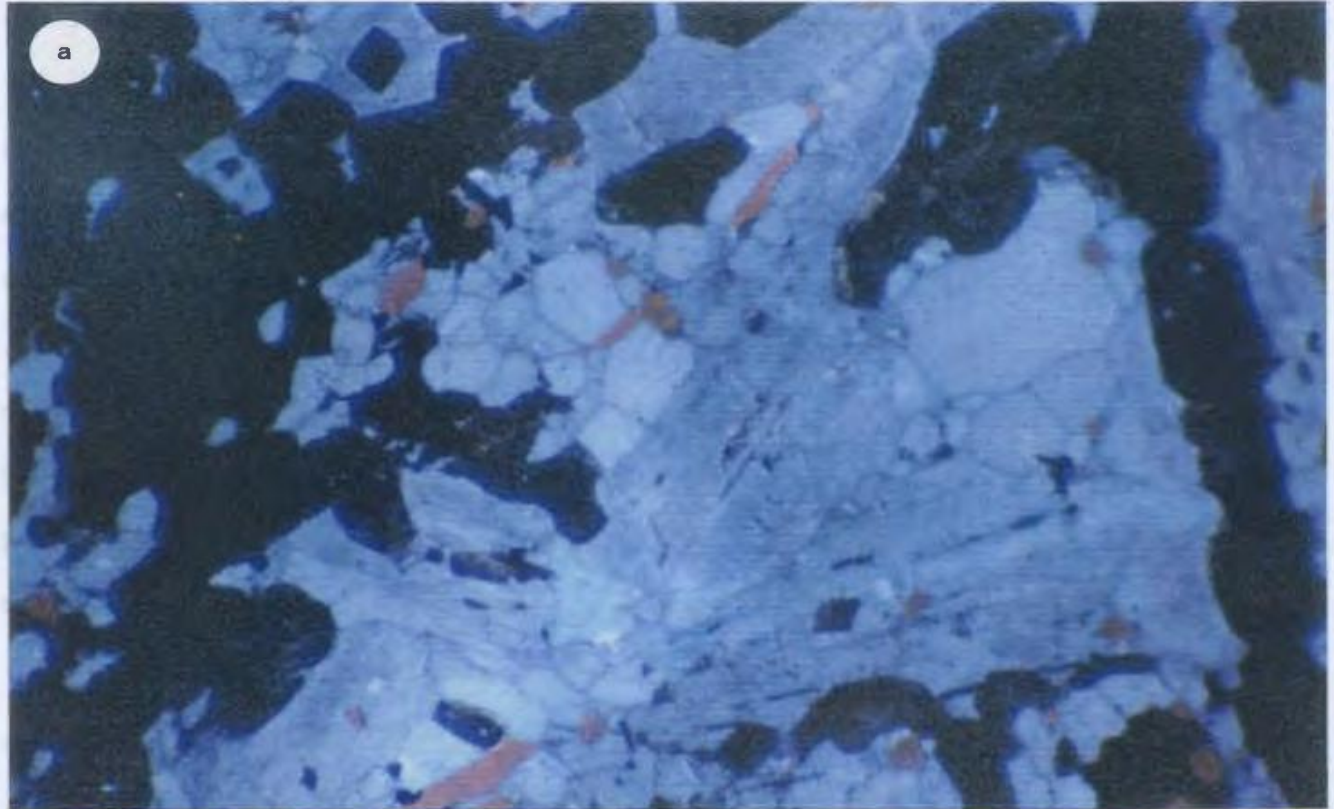


Plate A2.2 (a-f). CL images showing, a) kyanite inclusions (red) in relict plagioclase (blue) in the troctolite (sample 5a). b) kyanite inclusion (red) in relict plagioclase (blue) in hornblende (sample 3b). Note the presence of kyanite in the throughout the non-luminescent garnet corona. CL-images showing c) blue luminescent plagioclase and dull red luminescent quartz both in the matrix and in the garnet, and d) the development of secondary (yellow-green) luminescent plagioclase which appears to be overgrowing the garnet. Both c) and d) are from garnet amphibolite (sample 2b). Compare the apparent lack of quartz inclusions in the subhedral, resorbed garnet crystal, e) CL-image showing the extensive plagioclase collar as well as the relict plagioclase crystal (both blue) and large apatite megacrysts (bright yellow) in sample 9c (nelsonite) and f) CL-image showing kyanite inclusions (red) in relict plagioclase (blue) from sample 35b (olivine gabbro). Note the presence of kyanite in the non-luminescent granoblastic garnet (all images 1.5 x 1 mm).

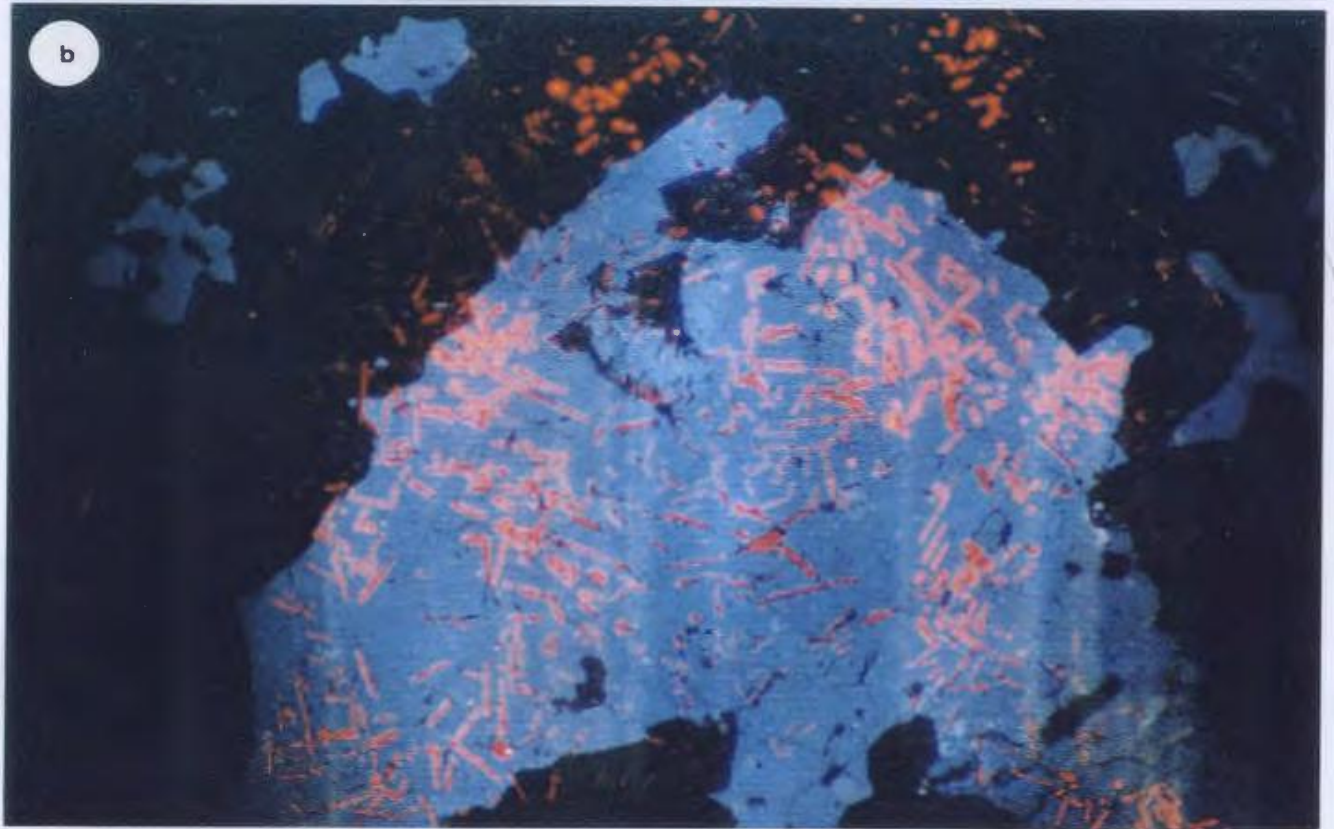


Plate A2.2 (cont.)

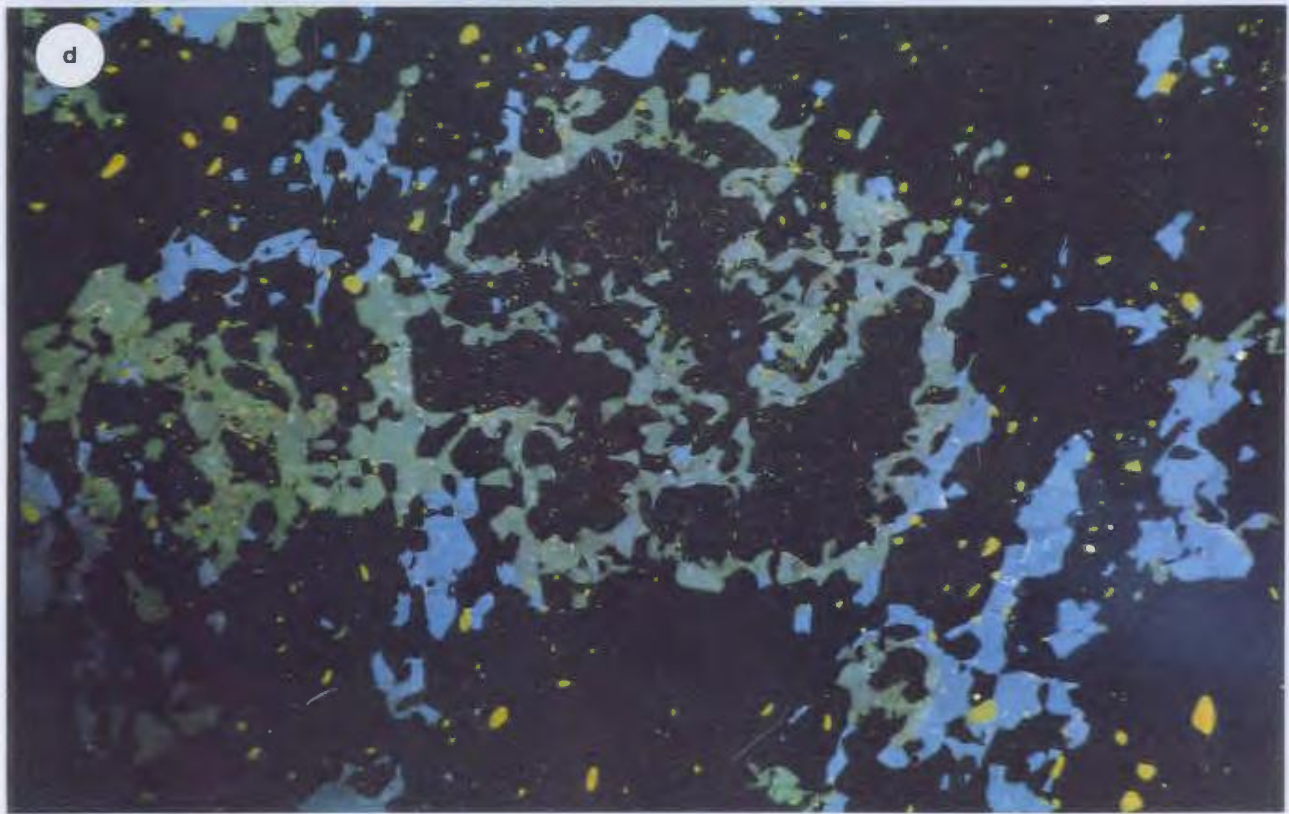
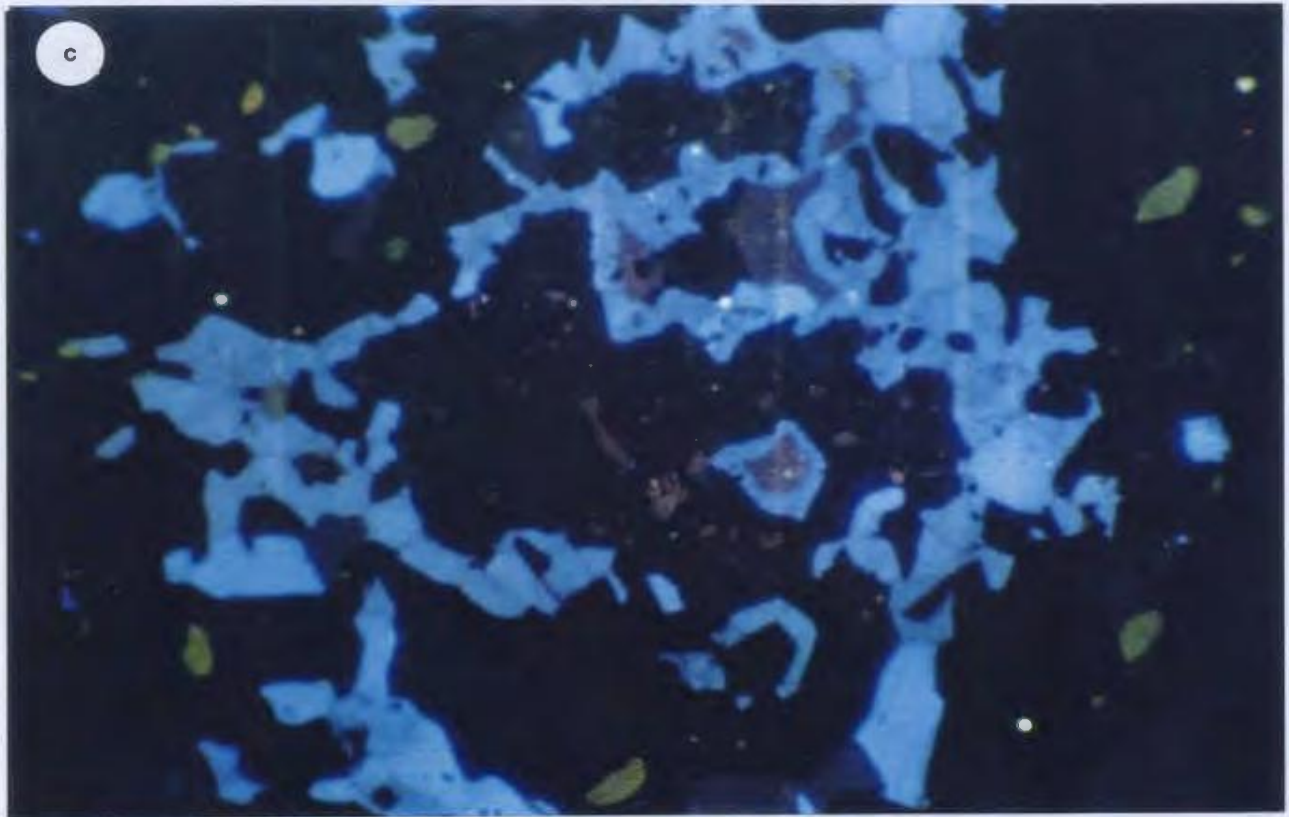
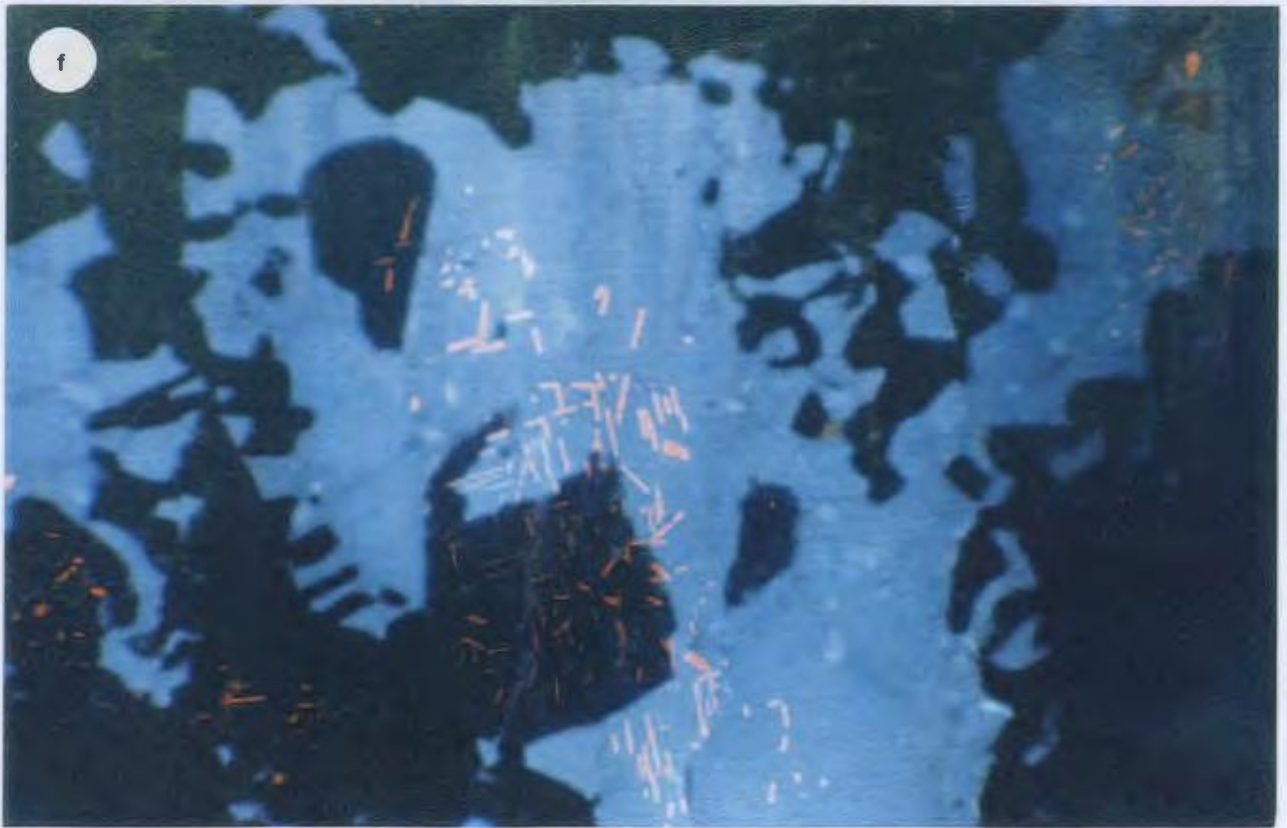
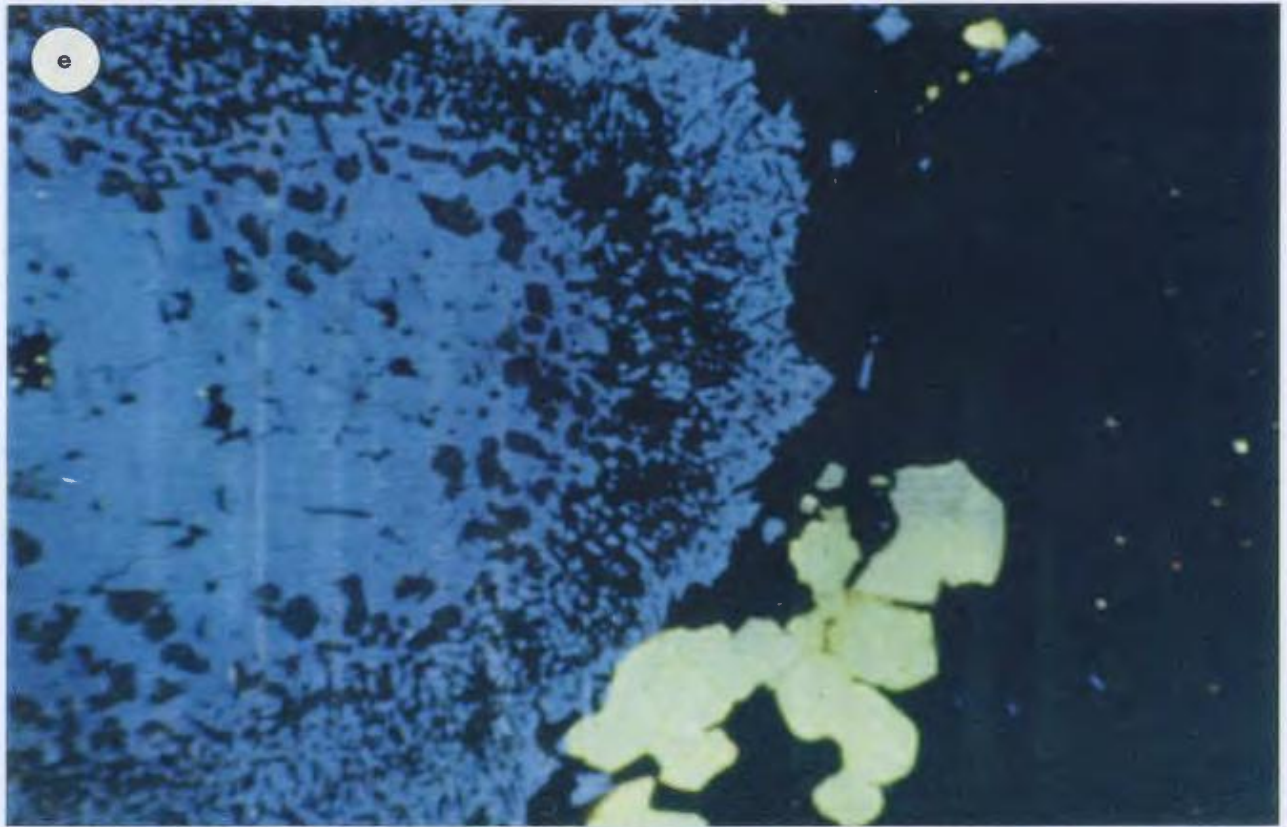


Plate A2.2 (cont.)



A.3. Accessory mineral morphology*A.3.1. Sample preparation*

Accessory mineral fractions were picked under alcohol following mineral separation procedures (see Appendix B). Populations were photographed under plane light and selected grains were mounted on scanning electron microscope (SEM) stubs using fine double-sided tape. The grain mounts were gold coated and examined using a Hitachi S-570 SEM housed in the Biology Department at Memorial University using an accelerating voltage of 20 kV and a beam current of 100 μ A. Other grains were mounted on glass slides using a quick drying epoxy resin and polished. These were examined in back-scattering mode on the same instrument using similar conditions. High magnification CL images were obtained using the SEM facility run by the Physical Studies Unit at the University of Glasgow. An accelerating voltage of 20 kV was used along with variable beam currents of 0.1-0.01 mA.

A.3.2. Accessory mineral images.

The following images are either plane light, secondary-electron (grain mounts) and back-scattering (polished grains) SEM or CL as stated in the captions. The scale bars are in μ m.

Plate A3.1 (a-g). SEM images showing a) SE-SEM b) BS-SEM and c) CL images showing an example of typical, irregular (fragmented) zircon morphology with prismatic faces and oscillatory (igneous) zoning from sample LES 1 (hornblendite). SE-SEM images of baddeleyite morphology found in samples LES 1, showing d) blocky shape and cleavage parallel to the crystal faces, and e) elongated prisms with prismatic faces. Note baddeleyite blocks were also recovered from sample BNS 1 (coronitic metagabbro), f) and g) saccharoidal zircon pseudomorphs after baddeleyite blocks and prisms. Note how the growth faces in the zircon also pseudomorph the the cleavage planes in baddeleyite.

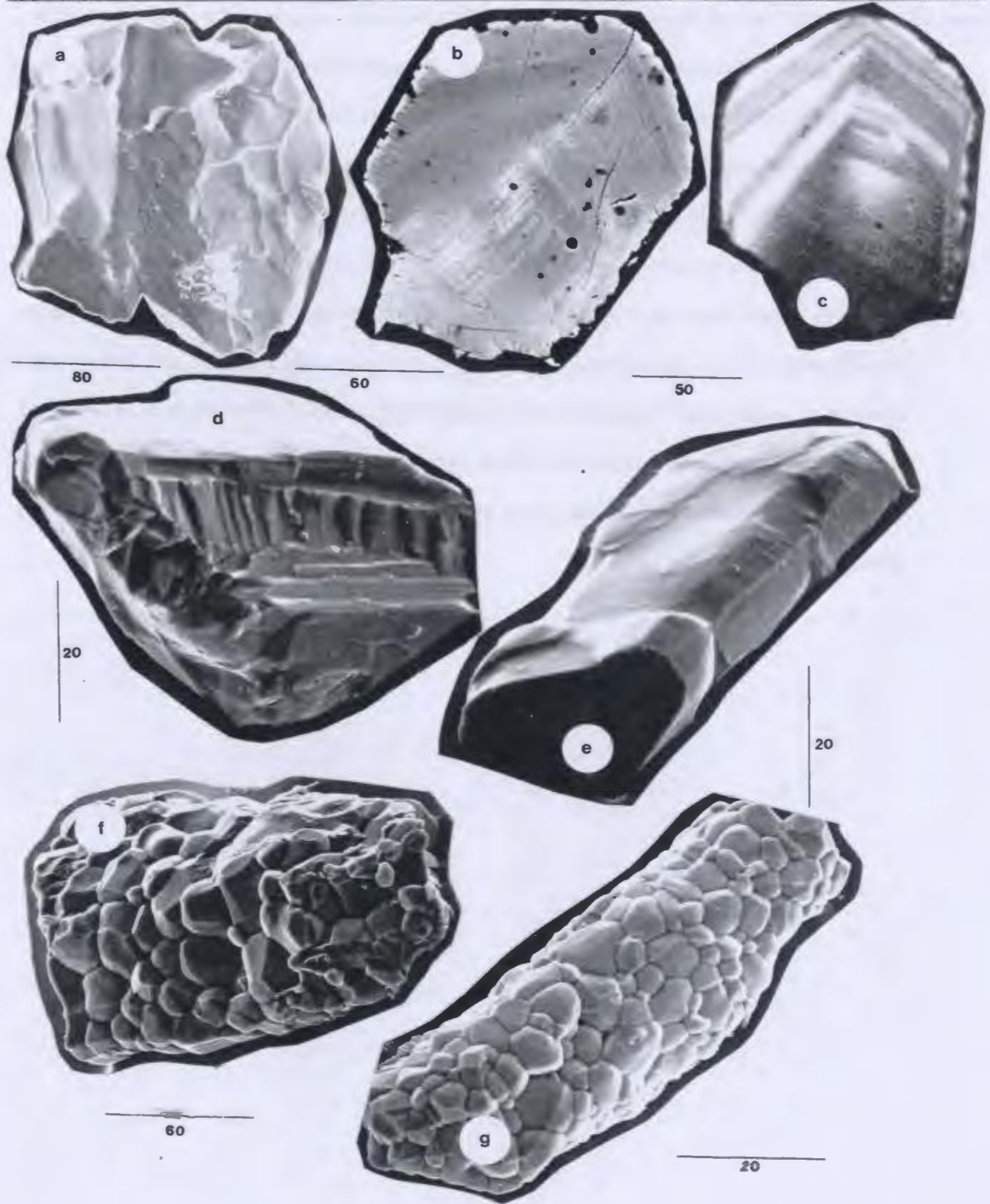


Plate A3.2 (a-h). SEM images showing a) SE-SEM and b) BS-SEM, large irregular zircon from LES 2 (olivine gabbro) with oscillatory (igneous) zoning, c) rounded overgrowths on a zircon prism from sample LES 3 (nelsonite). Note the exposed prism faces, d) CL image showing a bright, irregular (metamorphic) overgrowth on an oscillatory zoned zircon core from sample LES 3. SEM images of angular zircon fragments from sample BNS 2 (transitional metagabbro). Although the grain shows euhedral prism faces in e) SE-SEM it is clear from the CL image f) these crystals have irregularly zoned cores which are characteristic of metamorphic growth. g) SE-SEM image showing multi-faceted, equant metamorphic zircon found in samples BNS 2 and in the matrix separates of sample BNS 3 (migmatitic garnet amphibolite) and h) SE-SEM image of an elongated, zircon prism with prismatic faces and slightly rounded terminations from BNS 3. These zircon morphologies are found in both the garnet and matrix separates and are likely formed during dehydration melting.

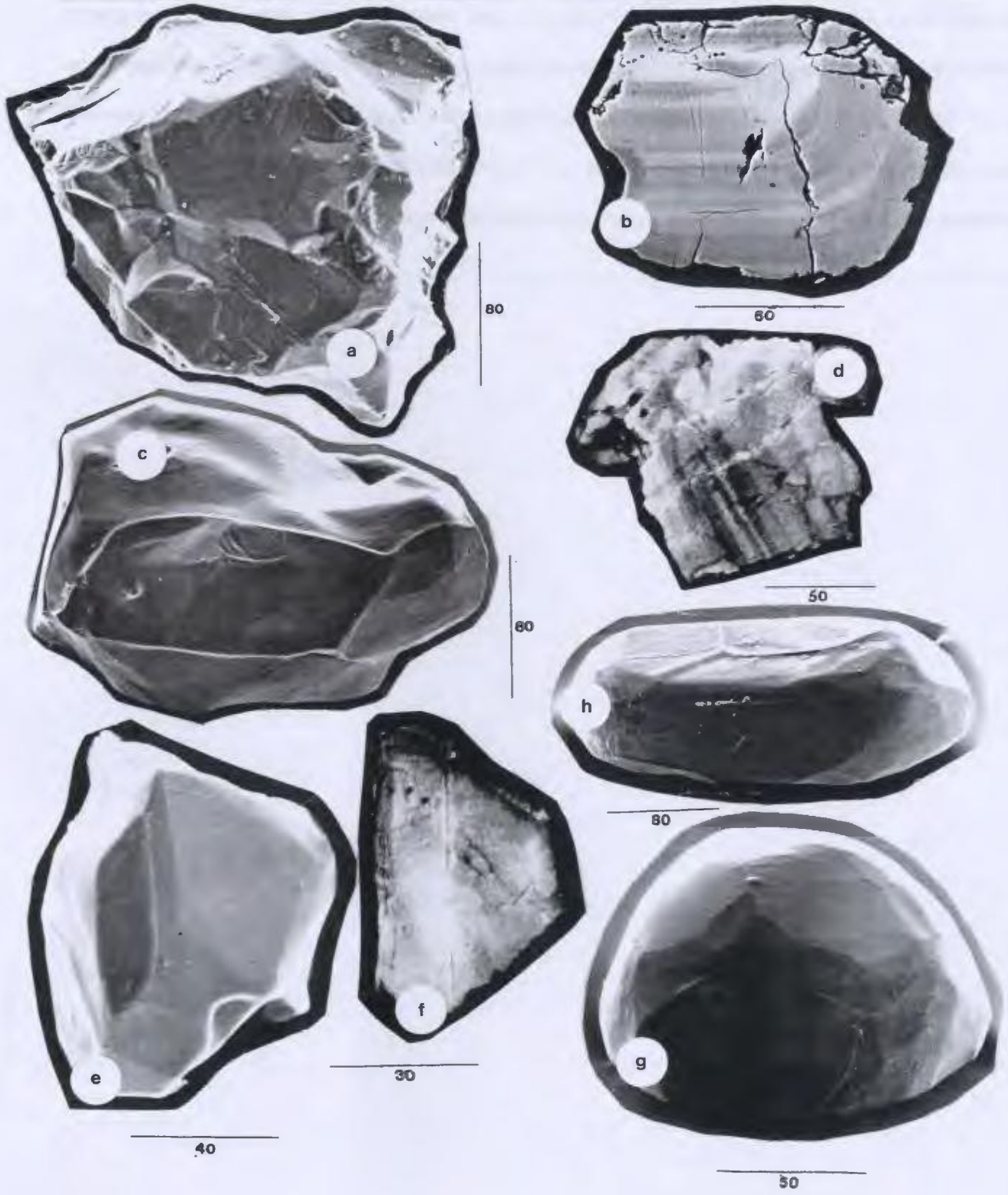
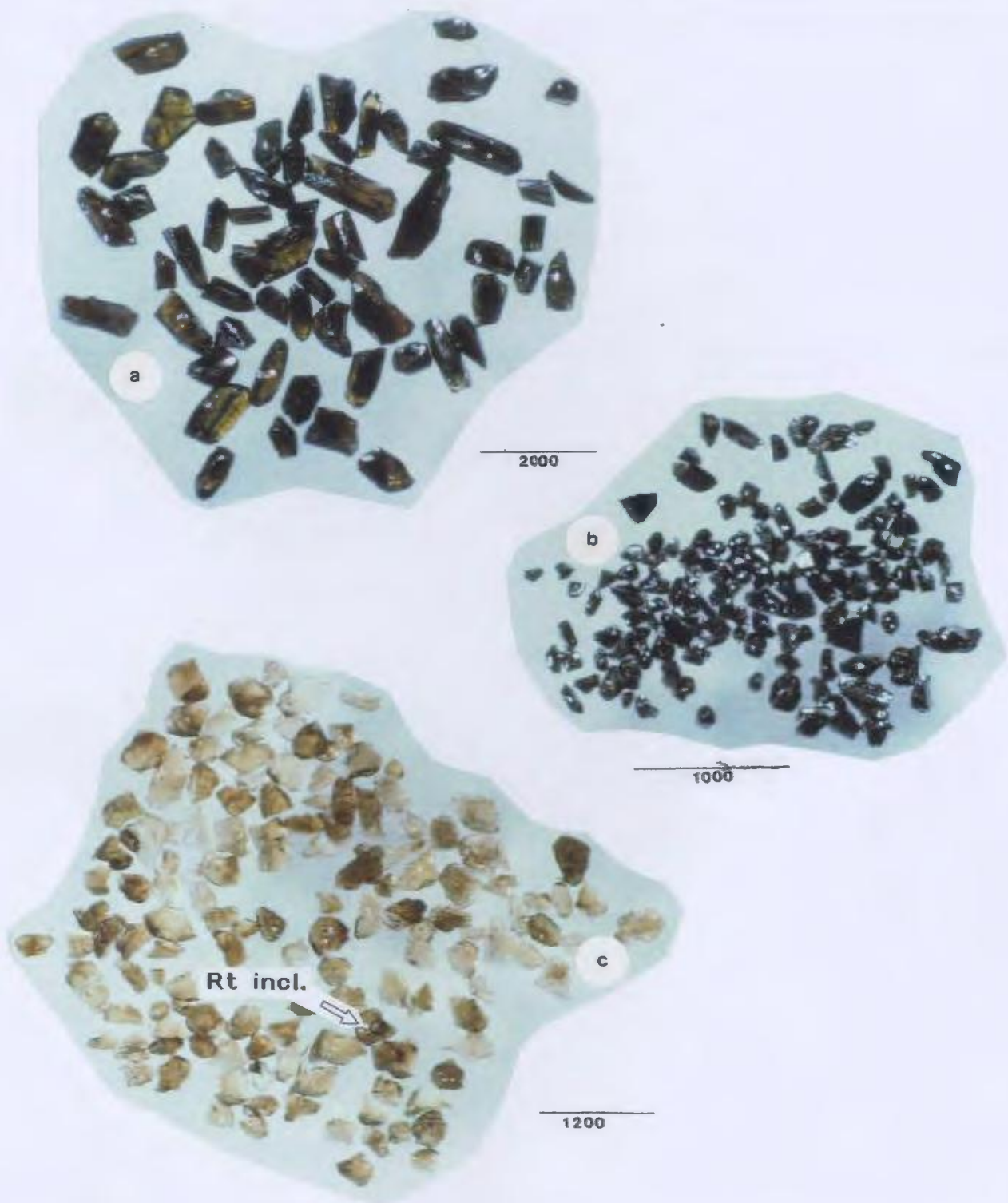


Plate A3.3 (a-c). Plane-light photomicrographs of rutile and titanite fractions from BNS 3 (migmatitic garnet amphibolite). Note the large grainsize difference between the rutile fractions (which give ages of ca. 960 and 946 respectively) and the small rutile inclusions in some titanite crystals which were removed before and after abrasion. Samples LES 1 and LES 2 (hornblendite and olivine gabbro) had similar fractions of small rutile and sample LES 4 (garnet amphibolite) contained similar populations of titanite.



Appendix B: Analytical methods

B.1. X-Ray fluorescence (XRF) analysis of major and trace element concentrations

B.1.1. Sample preparation.

The rock samples weighed between 5-10 kg depending on grain size. Where small samples of coarse grain sized samples were used (e.g. migmatitic garnet amphibolite, sample 313) slices of the rock were made using a low-speed saw and representative samples were chosen from a variety of the slices. Weathered surfaces were removed prior to rock crushing. Crushing was carried out using a jaw crusher to reduce the rock to small fragments and a puck-mill to powder the sample. A small portion (ca. 200 g) of each sample was crushed and discarded to "spike" the puck-mill before crushing the whole rock to avoid cross-contamination. Rock crushers were cleaned with water, air and alcohol between samples. The final powder was stored in a clean plastic sample vial.

B.1.2. Loss on ignition (LOI)

The loss on ignition (LOI) values were calculated by placing 2 g of fresh rock powder in a ceramic crucible. The powder and the crucible were weighed and then placed in an oven at 450 °C for 12 hours and the weight-loss measured afterwards. Some samples with high Fe-contents showed small weight increases due to oxidization and were not analyzed further.

B.1.3. Disc and pellet preparation

The trace elements were analyzed on pressed powder pellets made of 5.00 g of fresh rock powder and 0.70 g of BRP-5933 Bakelite phenolic resin. The rock powder and the resin were homogenized for 10

minutes in a roller mixer and the resulting mixed powder was pressed in a Herzog pellet-press for 5 seconds. The resulting pressed pellets were placed in an oven at 200 °C for 15 minutes.

The major elements were analyzed using fused glass pellets, except for samples where high Fe-contents would have caused melding of the sample to the platinum crucible (these samples are indicated in Table 1.1). The glass beads were made by mixing 1.5 g of dried rock powder with a flux of 6.0 g of Lithium metaborate and 1.5 g of Lithium tetraborate. The powder was then mixed and placed in a clean, dry platinum crucible with 0.02 g of Lithium Bromide solution. The glass beads were made automatically with a LECO FX 200 burner in sets of six. The burner was programmed to progressively reach temperatures of 1500 °C over 12 minutes.

B.1.4. XRF analysis

The XRF major and trace element analyses were performed using Fisons/ARL 8420+ sequential wavelength-dispersive X-ray spectrometer. This spectrometer has one goniometer, capable of holding six analyzing crystals. For trace element analysis five crystals were used, including a LiF200H crystal specially treated for heavy element sensitivity. Also, either an argon flow-proportional detector (FPC) or a scintillation (SC) detector was used with the rhodium anode end-window X-ray tube operated at 3 kw. The analytical procedure, including the calibration and matrix correction procedures, and the precision accuracy have been described in detail by Longerich (1995). The limits of detection for the major elements are 0.02% for SiO₂, 0.01% for TiO₂, 0.06% for Al₂O₃, 0.01% for total Fe and Fe₂O₃, 0.00% for MnO, 0.01% for CaO, 0.04% for Na₂O, 0.01% for K₂O and 0.01% for P₂O₅. The analysis of five standards in each run allows the determination of a precision and accuracy around 1% for concentrations above 1 wt% and 3% for concentrations below 1 wt%, for the major elements. The limits of detection for the trace elements are in brackets in ppm: Sc(6), V(6), Cr(7), Ni (5), Cu(4), Zn(3), Ca(3), Rb(0.7), Sr(1.2), Y(0.7), Zr(1.2), Nb(0.7), Ba(23), Pb(4). The precision and accuracy of the trace element analysis is below 1% for most elements, except for Zn (4%).

B.2. Trace element analysis by Inductively coupled plasma mass spectrometry (ICP-MS)***B.2.1. Sample preparation and dissolution***

Rock powders were prepared as in *section B.1.1.* above. ICP-MS analysis using Na_2O_2 sinter sample dissolution was used for the determination of the Lanthanides (REE) presented in **Table 1.2**. The high field strength elements (Zr, Nb, Hf and Ta) were also determined by ICP-MS analysis. However, there are problems with contamination (from crushing equipment), solution instability and potential memory problems with these elements (Jenner et al. 1990). For this reason the concentrations of Zr and Nb were determined by XRF only and reported in **Table 1.2**. The samples were prepared by mixing 0.2 g of fresh rock powder in a Ni crucible with 0.8 g of Na_2O_2 , and sintering the mixture in a muffle furnace at 480 °C for 1.5 hours. The crucibles were cooled and 10 ml of distilled H_2O were added until the reaction stopped. The mixture was then diluted with distilled H_2O , centrifuged and dissolved in 8N HNO_3 and oxalic acid. The solution was diluted again with distilled H_2O prior to ICP-MS analysis. This solution was later mixed with an on-line standard spike.

B.2.2. ICP-MS analysis

The analytical data were acquired with an SCIEX ELAN 250 ICP-MS modified at Memorial University and equipped with an automated sampler. Each run consisted of 56 samples distributed in 8 analytical cycles. Each cycle contains 7 samples, 4 standards and 1 calibration blank. Samples are spiked with a standard solution of Rb, Cs, Tl and U. The calibration blank was used to make a background correction, oxide interferences were corrected using the UO/U ratio in the standards. Interpolated ratios of the spike signal intensity between samples and standards were used to correct for matrix effects. Data acquisition and processing, including the calibration techniques, followed the method of Jenner et al (1990). The analytical limits of detection are all at the sub-ppm level and lie in the following ranges;

0.02 ppm for Nd, Zr[#], and Hf*.

0.01 ppm for Sm, Eu, Gd, Dy, Er, Yb and Ta*.

<0.01 ppm for Y[#], La, Ce, Pr, Tb, Ho, Tm, Lu and Th*.

([#] elements measured but only XRF results are considered).

(* elements measured but considered unreliable and not used for detailed interpretation).

The precision of the technique is generally between 3 and 10% for the REE and Y, between 10 and 15% for Zr and Hf, more than 20% for Nb and Ta and in excess of 40% for Th. The low precision for these elements is due to dissolution problems and machine memory problems (Longerich, personal communication). Duplicates of two rock samples were dissolved and analyzed separately during the same run to determine the reproducibility of the technique.

B.3. U-Pb Isotopic analysis

B.3.1. Sample Preparation

Rock samples (5-25 kg) were washed and any dirt removed with running water and a wire brush. The samples were then dried and pulverized using a hydraulic press, a jaw-crusher and a steel-plate pulverizer. Crushing equipment was dismantled and cleaned using a powerbrush, alcohol and compressed air between samples. Initial separation of light and heavy minerals was done using a Wilfley panning table. The Wilfley table was cleaned with soap and water, dilute HNO₃, alcohol and compressed air between samples. The heavy fraction and a representative fraction of the light mineral fraction were kept. Both fractions were washed with alcohol and dried. Highly magnetic minerals such as magnetite and contaminants from the crushing process were removed using an electromagnet. The remaining heavy

fraction was sieved. The heavy fraction was separated according to magnetic character using a Frantz isodynamic magnetic separator and by heavy liquid fractionation using methyl-iodide. Separation of the different accessory mineral phases such as zircon and titanite was achieved by final magnetic separation. Mineral fractions for U-Pb analysis were hand-picked from the final separates under a microscope on the basis of morphology, colour, size and crystal quality. In order to minimize discordance, due to the effects of alteration and Pb loss, most mineral fractions were air abraded (Krogh, 1982). Picked mineral fractions were washed with 4N HNO₃ (at 120 °C), H₂O and alcohol. The best grains were then selected for isotopic analysis under the microscope.

B.3.2. Sample cleaning, weighing, spiking, dissolution and U-Pb separation.

After picking, the procedure continues under clean conditions in fume-hoods with outward laminar flow of filtered air and reagents that are doubly distilled. General clean-lab sample-handling procedures were observed. The mineral fractions were washed with H₂O, leached lightly with 4N HNO₃ (100–120 °C), and washed with acetone and dried. During each wash the sample was subjected to ultrasonic agitation for 10 seconds. The mineral fractions were weighed with a high-precision balance (with an uncertainty of ca. 2-10 micrograms) and placed inside high-P Teflon dissolution bombs (Krogh, 1973) or Teflon Savillex containers. Concentrated HF and HNO₃ were then added to the samples which were then spiked with a ²⁰⁵Pb-²³⁵U tracer solution (Parrish and Krogh, 1987) according to the sample weight and the expected age and U concentration in the sample. Samples were dissolved (in 5 days) at 220 °C and then dried down and re-dissolved with 3.1N HCl. U and Pb were separated through ion-exchange chemistry following modified procedures for zircon (Krogh 1973; Dubé et al. 1996). U and Pb were separated from rutile and titanite following HBr ion-exchange chemistry (Manhès et al. 1978). Procedure blanks during the period of analysis were 1 pg U for all samples and 2-12 pg Pb for zircon and 12-20 pg Pb for rutile and titanite.

B.3.3. U-Pb isotopic analysis and age determination.

The U and Pb isotopic ratios were measured by thermal ionization mass-spectrometry (TIMS) using a Finnigan MAT 262 mass spectrometer equipped with an ion-counting secondary electron multiplier (SEM). U and Pb were loaded together with H₃PO₄ and silica gel on an outgassed single rhenium filament in a clean box. Both U and Pb were measured in static mode on the Faraday cups, ²⁰⁴Pb was measured in the axial SEM/ion counter. The SEM was calibrated with respect to the Faraday cups before and after each analysis. Small fractions (<3 mV signal of ²⁰⁵Pb or ²⁰⁷Pb in the Faraday cups) were measured in dynamic mode using the SEM (peak jumping on the SEM). These isotopic ratios were checked and calibrated against Faraday-derived data during the same run. These measurements were performed in single blocks of 10 scans each. Outliers were identified and eliminated from the final mean of the measurement using the Finnigan MAT 262 on-line software. The best signals were usually obtained between 1400-1550 °C for Pb and between 1550-1650 °C for U. The intensity of the emission was monitored on a chart recorder which for static collection allowed manual temperature adjustment of the filament during measurement to keep a stable emission. Ages have been calculated using the accepted decay constants for ²³⁵U and ²³⁸U (Jaffey et al., 1971). The ages and errors on the isotopic ratios have been calculated using unpublished software from the Royal Ontario Museum (Heaman, personal communication). The errors on the isotopic ratios are given at the 2 sigma level and are the result of propagating errors from: the amount of isotopic fractionation (0.1-0.04% a.m.u for U), total blanks in the analysis, laboratory blanks (²⁰⁶Pb/²⁰⁴Pb = 18.33; ²⁰⁷Pb/²⁰⁶Pb = 0.855; ²⁰⁸Pb/²⁰⁶Pb = 2.056), amount of initial common Pb and machine uncertainties on the measurements. The initial common Pb was corrected using the model of Stacey and Kramers (1975). The U and Pb concentrations were estimated from sample and spike weights. Linear regressions for discordia lines were calculated using the method of Davis (1982) and final age errors are given at the 95% confidence level.

B4. Electron microprobe analysis*B4.1. Sample preparation*

Polished sections were selected for analysis after detailed petrographic study using the techniques described in Appendix A. Sections were given a light polish using 0.3 μm abrasive film and cleaned with alcohol before being carbon coated and loaded into the microprobe. Selected grains (e.g. zircon and corundum) were mounted on section-glass using thin, double-sided adhesive tape and carbon coated. These were used only to assist with identification prior to U-Pb analysis and are not discussed further.

B4.2. Polished section analysis

All analyses were carried out using a Cameca SX50 electron-microprobe analyser, using an Oxford Instruments energy dispersive spectrometer (EDS) and Link analytical computer and software. EDS-analyses were used despite higher detection limits and lower precision for certain elements. The use of EDS permitted minimal calibration and set-up times, rapid multi-element analysis and reasonable precision which allowed a large number of data points to be collected. The system was optimized for major elements with a limit of detection of 0.08%. Zn was included as several wt%, can be found particularly in oxide phases. Interferences for the elements of interest were negligible. Olivine, orthopyroxene, garnet, amphibole, oxide phases (ilmenite and spinel) and clinopyroxene were analysed using a beam diameter of $1\ \mu\text{m}$ and a beam current of 20 nA with an accelerating voltage of 15 kV. Counting times used were 50 secs for olivine, orthopyroxene and garnet, 75 secs for spinel and ilmenite, and 100 secs for amphibole and clinopyroxene. For determining zoning profiles of large garnets the count times were reduced to 20-25 secs. To prevent Na-loss during analysis of plagioclase, a $3\ \mu\text{m}$ beam diameter and a beam current of 10 nA were used. Counting times for plagioclase varied between 75-150 secs. Data were analysed using the on-line ZAF correction software and mineral end-member compositions were determined using an unpublished

program (THEBA v.6.0) from the University of Montreal (J. Martignole and others, personal communication 1995). PT-estimates were carried out using carefully selected points after analytically imprecise or unreliable mineral data were rejected. The PT-estimates were calculated using the program TWEEQU v.2.01 (Berman 1991). Amphibole-garnet thermometry was carried out using v.1.01 of the program (R. Berman, personal communication 1998). The calculated temperatures were compared with other published mineral thermometers which are described in detail in Papers 2 and 3.

